University of Southampton

Faculty of Engineering, Science and Mathematics

Institute of Sound and Vibration Research

SEMI-ACTIVE DAMPING CONTROL FOR VIBRATION ISOLATION OF BASE DISTURBANCES

by

Yuyou Liu

A Thesis submitted for the degree of

Doctor of Philosophy

December 2004

UNIVERSITY OF SOUTHAMPTON

ABSTRACT

FACULTY OF ENGINEERING, SCIENCE AND MATHEMATICS

INSTITUTE OF SOUND AND VIBRATION RESEARCH

DOCTOR OF PHILOSOPHY

SEMI-ACTIVE DAMPING CONTROL FOR VIBRATION ISOLATION OF BASE DISTURBANCES

by Yuyou Liu

This thesis is concerned with semi-active damping control for vibration isolation of base disturbances. The aim is to investigate the effectiveness and suitability of semi-active damping control strategies for improving steady-state vibration isolation. A single-degree-of-freedom (SDOF) system, comprising a semi-active damper with a linear passive spring in parallel, is used to study the vibration isolation of base excitation.

The semi-active control strategies investigated include on-off skyhook control, continuous skyhook control, on-off balance control and continuous balance control. Chatter and jerk problems are investigated, which can arise in numerical simulations and possibly in practice when using semi-active control strategies. Anti-chatter and anti-jerk control strategies are proposed. These control strategies are implemented numerically in Matlab/Simulink. Harmonic, periodic and random disturbances are considered in this thesis. The vibration isolation performance is evaluated in terms of Root-Mean-Square (RMS) acceleration transmissibility.

The performance of these control strategies for the isolation of harmonic disturbances is firstly studied. The performance is compared with those of an adaptive-passive control strategy, a conventional and a skyhook passive damper. Results show that the semi-active control strategies can provide a better isolation than a conventional passive system with an equivalent damping level. The semi-active damper can

provide isolation over the whole frequency range if the on-state damping of the semi-active damper is big enough. The fraction of time when the damper is turned on or off is found to be frequency dependent.

The effects of secondary frequency, which is a harmonic or subharmonic of the fundamental frequency on switching time of the semi-active damper for isolation of the primary harmonic are examined. Upper bounds are derived for fraction of time when the switching time for the fundamental frequency may be affected by the presence of a secondary frequency. The performance of the semi-active isolation system for periodic and random disturbances, where there is more than one harmonic in the disturbance spectrum is investigated. The results for square wave and triangular wave disturbances suggest that semi-active control strategies are promising for periodic disturbance. Three special cases are considered for random disturbances when the acceleration, velocity and displacement inputs have flat spectra. The semi-active control strategies can provide some advantage in performance for random velocity and displacement disturbances with medium to high damping ratios. Only continuous skyhook control strategy can provide some benefit in isolation performance for random acceleration disturbances.

Following on from the numerical simulations, experimental work is carried out to validate the simulation results. The experimental set-up incorporates an electromagnetic device as a semi-active damper. The on-off skyhook control algorithm is chosen to be implemented using an analogue circuit. The damping of the electromagnetic semi-active damper is achieved by opening and closing the magnet-coil circuit. Numerical predictions are confirmed by experimental observation. The performance of the electromagnetic damper is limited by the achievable damping level.

TABLE OF CONTENTS

LIST OF FIGURES

LIST OF TABLES

ACKNOWLEDGEMENTS

I would like to acknowledge with deep appreciation the academic guidance, understanding and continuous encouragement provided by my supervisors, Dr Tim Waters and Professor Mike Brennan throughout this project. Their patience and inspirational guidance were extremely valuable on the successful completion of this work. Their help is far beyond what a normal supervisor could provide, and not only limited to academic aspects.

My thanks also go to Professor Brian Mace for his help at the earlier stage of the project, and Professor Stephen Elliott for his valuable suggestions at each review meeting and the final viva. I am grateful to Mr Robert Stansbridge and Mr Antony Wood for their help with the manufacture of the experimental rigs used in this thesis.

Finally, I would like to thank my wife, Gao Yan, and our parents for their understanding and support of my pursuit of the PhD degree. Thank all my friends, Li Wenjiang, Zhao Jianzhong and Cui Laiyou especially, for their encouragement and support when I was preparing for studying abroad.

CHAPTER 1

1. INTRODUCTION

1.1 BACKGROUND

The need for effective control of noise and vibration is very common in almost every dynamic system [1]. Excessive vibration and noise can cause premature structural and mechanical failure, increased maintenance requirements, human pain and discomfort. Among the various problems and issues associated with vibration, isolation of a piece of equipment from a vibrating base is a common one in the field of mechanical engineering [1-3]. For sensitive equipment where the motion is prescribed by the operating environment, then vibration reduction at source is often not feasible. The main improvements can be obtained using isolation, including the possibility of active as well as passive isolation [4]. A good general introduction to noise and vibration control is given by Bies and Hansen [5] and Beranek and Ver [6]. More specifically for vibration and shock isolation and detailed modelling of more complicated features are the definitive works by Snowdon [7] and Harris [1].

Vibration isolation can be achieved by passive, semi-active, and active means. Until about 1990, only passive control measures were generally considered for practical engineering systems, and the theory underlying these measures is well documented, for example [1]. Traditionally, engineers have solved the problem of vibration isolation by designing passive systems based on compliant materials, such as rubber, to decouple the equipment dynamics from the base dynamics [8]. Typically the base vibration has an unpredictable waveform and the passive isolators have to deal with broadband excitation spectra [4, 9]. However, the conventional passive form of isolation is generally a compromise for a single-degree-of-freedom system between (a) isolation at higher frequencies which requires low values of damping, and (b) control of vibration at resonance that requires high values of damping [2, 4, 5, 9-12]. There is inherent trade-off in performance of a passive isolation system.

Although many vibration problems are solved in a simple and reliable way with passive devices, it is clear that there are distinct performance limitations when only

passive devices are used [4, 9]. It has been established that isolation systems with parameters that can be adapted to changing excitation and response characteristics can provide better isolation performance than passive systems with fixed parameters [13, 14]. Active control systems can be used when greater performance is required and passive techniques alone cannot perform adequately (or when accomplishing a task not even possible with passive devices). Active control uses actuators to both add and dissipate energy from the system based on signals obtained from various sensors. Active control systems have demonstrated superior performance than that of the best possible passive systems. But it is also known that the active systems in general are more costly, more complex and less reliable than passive systems. The primary limitation in the application of an active system for vibration isolation is the need for external power. Thus the implementation of active vibration systems has been limited to cases in which the performance gains outweigh the disadvantages of increased cost, complexity, and weight. By recognising both the performance benefits as well as the limitations of active systems the concept of semi-active vibration control has been developed [15].

Semi-active vibration control refers to the use of devices with variable properties to control or suppress vibrations of dynamic systems. This concept involves the application of a controllable device which does not require significant external power to operate. The semi-active device is able to respond to measured feedback signals from a vibrating system to control undesired vibrations. The dynamic properties of semi-active systems can be varied with time. But they can only dissipate energy, i.e. they cannot put energy into the system. Thus the device does not use significant external power compared with fully active systems. One can expect the performance to be more limited than the fully active system.

Semi-active systems fall into three categories: variable stiffness, variable damping and variable mass. As the mass can not be changed in a short time, in most cases only the first two are considered. In the first category, the system's stiffness is adjusted to establish a non-resonance condition. In the second category, semi-active devices are operated according to semi-active damping control strategies to generate a damping force passively. It is the isolation of vibrations from the base using semi-active

damping control that is the subject of this thesis. Before considering this in detail, however, various methods for vibration control are first reviewed.

1.2 LITERATURE REVIEW

Published literature on semi-active damping control for vibration isolation discusses control strategies and devices. This can be structured for easy comprehension in the manner shown in Figure 1.1.

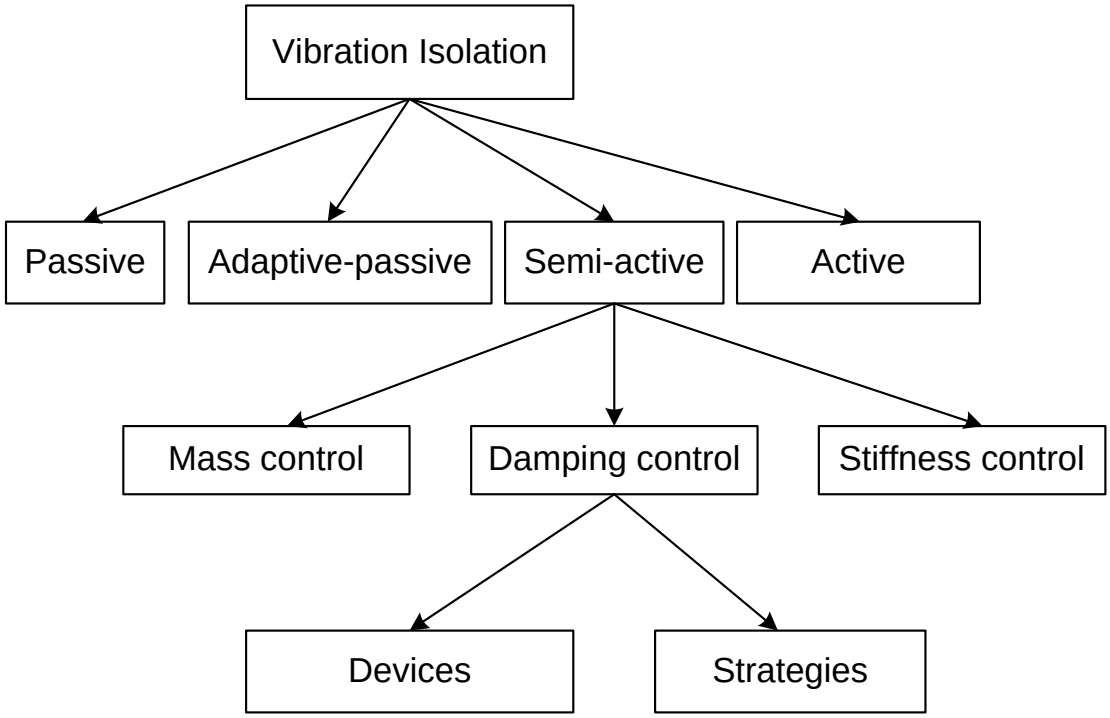

Figure 1.1 Overview of vibration isolation methods in the literature

Figure 1.1 shows that there are four established ways for vibration isolation [14]. The semi-active vibration isolation can be realised by mass control, stiffness control and damping control. Semi-active damping control for vibration isolation is the subject of this thesis. Since their inception in 1970s, semi-active dampers have found applications in many engineering areas, and have gained more and more attention these days due to their ability to attain superior performance over conventional passive dampers. In achieving this, the control algorithm by which the damper is adjusted is one of the crucial factors that ultimately determines the success or failure of a particular control strategy. The device by which variable damping is achieved is another key point to ensure the desired performance. Properties of the semi-active

damper such as the upper and the lower limits of the damping coefficients and how fast it can be switched are particularly important. This section provides an overview of the semi-active control algorithms and the devices proposed in the literature.

1.2.1 SEMI-ACTIVE CONTROL STRATEGIES

Semi-active control systems were proposed in the 1970s when patents were issued for shock absorbers which used an elastically supported mass to activate hydraulic valving (no power required) or used a solenoid valve for directing fluid flow (small amount of power required) [15]. Since then, a large amount of research on semi-active systems has actually been performed in the field of engineering for applications in automotive vibration, structural vibration and vibration isolation.

(1) Control strategies based on skyhook damping

The initial semi-active control strategy was designed to modulate the force generated by a passive device to approximate the force that would be generated by a damper connected to an inertial reference ("skyhook damper") [2, 15-17]. Thus the control strategy was named skyhook semi-active control. With the "skyhook damper" configuration, the trade-off between resonance control and high-frequency isolation, which is inherent in passive isolation, is eliminated [18]. According to this control strategy, whenever the velocity and the relative velocity are of the same sign, the semi-active damper would supply a force with the desired value of a skyhook damper. Since the damping of the semi-active skyhook control is assumed to be continuously adjustable, the control strategy is called continuous skyhook control by some authors.

Karnopp et al. studied the performance of the skyhook semi-active control strategy via computer simulations for harmonic and random disturbances [15]. The computer simulations were based on the assumption that the force provided by the semi-active damper can always be equal to the desired force, which is not always true in practice. Krasnicki also studied the vibration isolation performance of a single degree of freedom system with a prototype semi-active damper using the same skyhook semi-active control strategy [16]. The study carried out computer simulations duplicating the results in [15]. A prototype of damper consisting of a hydraulic actuator with an electrohydraulic servo-valve modulating the controlling orifice area was tested. The

system was subjected to both sinusoidal and random vibration input. The experiment results failed to validate the numerical prediction although it showed that there was some improvement in the isolation performance.

Another paper by Krasnicki [19] proposed a so called “on-off” type skyhook control strategy. It assumes either zero damping or a constant passive damping value between the semi-active damper. The on-off damper differs from the previous skyhook strategy in that the force generated by the damper is proportional to the relative velocity of the sprung and unsprung mass rather than the absolute velocity of the sprung mass. The on-off skyhook is evaluated experimentally using the prototype in [16]. The experimental results were not compared to any predictions and only showed some improvement near the resonance area compared with a conventional passive damper.

In recent years, both the continuous and on-off skyhook control strategies have been studied for their applications in vehicle suspension systems. For example, Ahmadian [20] numerically studied the behaviour of the on-off and continuous skyhook control strategy in a car primary suspension system. The study used a pure-tone input, and compared the results with the vibration isolation due to a conventional passive damper. The results showed that both on-off and continuous skyhook semi-active suspensions exhibited the ability to lower the resonance peak without worsening the isolation at higher frequencies.

In a recent paper by Yi and Song [21], the authors tried to improve the performance of the skyhook control strategy by adapting to the road surface. The proposed control law consists of a new adaptive skyhook damping algorithm and a road detection algorithm. The profiles of the road surface are detected and used to tune the gains to of the skyhook damping strategy. Simulation results showed that the performance is superior to that of the continuous skyhook control. However, this road detection algorithm is difficult to implement in practice. Sciulli and Symans [22, 23] modified the skyhook control strategy into the so called groundhook control, where the vehicle is modelled as a two degree-of-freedom system with one (unsprung) mass representing that of the tyre and one (sprung) mass that of the vehicle. The semi-active damper is connected to the unsprung mass in the model. The results show that the skyhook configuration is ideal if the primary goal is isolating the sprung mass,

while the groundhook configuration excels at isolating the unsprung mass from the input excitation [22-24].

(2) Control strategies based on balance control

Both the continuous and on-off skyhook control strategies discussed previously require a measure of the absolute velocity as well as the relative velocity. Accurate measurement of the absolute velocity may be difficult to achieve. Rakheja [25] proposed a control strategy using the directly measurable relative position and relative velocity signals. The control strategy is based on the fact that the damper force causes an increase in the magnitude of the mass acceleration whenever the forces due to the spring and the damper have the same sign. The semi-active damper has two states: on and off. The semi-active damper is switched off when the damper force and spring force have the same sign, and is switched on when the damper and spring force are in the opposite direction so that the damper force opposes the spring force. This control strategy is termed “balance control” by later authors [26].

However, this control strategy has potential for improvement. During the on-state of the damper, the instantaneous damper force is seldom exactly equal in magnitude to the instantaneous spring force. In consequence, the surplus force will still accelerate the mass. Alanoly and Sankar [27] proposed a continuous control strategy, which can be considered as a further development of the preceding control strategy in [25]. If the spring force and the damping force are in the same direction, the damping coefficient should be a minimum value, ideally zero in order to reduce the acceleration of the mass. On the other hand, if the spring force and the damper force are in opposite directions, then the damping force should be adjusted in such a way that it should be equal to the spring force in magnitude so as to produce zero acceleration. However, the desired damping force may be beyond the range that the damper can provide. A similar control strategy is discussed in [28].

Rakheja and Sanker [25] studied the vibration and shock isolation performance of the semi-active on-off balance control strategy using a orifice damper. The performance of the semi-active damper is compared with a conventional passive damper. Simulation results were provided but no physical interpretation given. Alanoly and Sanker [27] also studied the vibration isolation performance of the on-off balance

control and compared it with the performance of the continuous skyhook control. In another study by Rakheja and Sankar [29], the on-off balance control strategy was used to change the damping of a so-called Ruzicka isolator and Snowdon's [7] two inertia vibration isolation system.

Wu et al. [30] pointed out that the desired damping force may be beyond the range that the damper can supply for the continuous balance control strategy. In this case, a maximum possible damping coefficient should be applied. Furthermore, they developed a new control strategy. Instead of continuously adjusting the damping force, the damping is set at either a maximum value or a minimum value depending upon a threshold damping coefficient. The threshold damping coefficient was suggested to be 30% of the critical damping coefficient of the system for that particular case.

(3) Other semi-active control strategies

There are numerous more complicated control strategies for vibration control with semi-active dampers. Many are applied to structural vibration [31-35] and others applied to vehicular vibration [26, 36, 37]. Sadek [34, 35] gave a detailed description of the recently proposed semi-active control algorithms for use with the magnetorheological (MR) damper. The control algorithms include a linear quadratic regulator (LQR) control algorithm, a generalized LQR control algorithms and a displacement-acceleration domain algorithm. Hrovat [38] pioneered the idea of using semi-active devices for control of wind induced vibrations. Numerical simulations showed the potential of this semi-active approach for reducing wind excited structural vibrations.

Hodmann [39] numerically examined the use of different control algorithms for a semi-active suspension to improve the driving safety and ride comfort of a delivery truck, while Ahmadian et al. [40] examined the effectiveness of a semi-active suspension at improving the ride of a class 8 truck. Ahmadian found that the semi-active system yielded an improved ride as compared to the passive suspension. Additionally, he found that this result could be achieved by using controllable dampers at only four of the six damper locations. Leih [41] showed that the switching time of a controllable damper used as part of a semi-active suspension can have an appreciable effect on the vehicle ride, suspension travel, and tyre deflection. These

conclusions are based on an analysis performed on a passenger car model with a full car body and four wheel-axle assemblies.

Giua and Sanganta [42] presented a two-phase design technique for developing semi-active suspension control algorithms. In the first phase of their design technique, they computed a target active control law that can be implemented by Optimal Gain Switching, and then, in the second phase, they approximated this target by controlling the variable damping coefficient of the semi-active suspension. They showed (by way of simulation results) that the performance of the semi-active suspension is close to the performance of the ideal active suspension when considering velocity input and acceleration response. Saxon et al. [43] confirmed that ride quality and stability are the greatest advantages of using a semi-active suspension through field-testing. Leigh [44] developed a control strategy for a semi-active damper from second-order equations and compared the simulated performance with that of a full-state system, again based on a quarter car model. He also investigated the effects of high damping levels and control valve switching time on the ride performance.

Recently fuzzy logic control and neural network theory were introduced into semi-active control area. For example, Sireteanu et al [26] studied fuzzy logic control algorithms for an MR damper in the control of vibration experienced by a tractor driver. Carter [45] studied the performance of a skyhook fuzzy logic control algorithm for the vibration control of vehicle suspensions. The fuzzy logic semi-active control strategy was better able to balance the body and axle dynamics than the conventional semi-active damping control strategies that are investigated. A different study by Fang and Chen [46] applied a fuzzy control strategy to a 4-DOF vehicle model. Ursu et al. [47] examined the development of control strategies for semi-active suspension systems using artificial intelligence. The results of their study are based on a 2-DOF quarter-car model.

(4) Anti-jerk control strategies

Generally, the acceleration response of an on-off damper exhibits discontinuities at the time of switching, thus a significant jerk may be experienced by the mass of the system. Chatter, which refers to the phenomenon in which the damper switches rapidly between the on and off states, is also associated with jerk [48]. Jerk and

chatter are undesirable for some practical applications. Various methods have been proposed to overcome these problems.

Pan [49, 50] developed the method using a variable damping coefficient to smooth the on-off damper force at the time of switching. The time rate of the change of damping force and the time rate of change of acceleration were investigated and used to evaluate the smooth degree of the damping force and the acceleration. A shaping function was introduced by Ahmadian et al. [51] in a US patent to avoid the discontinuities of the semi-active damper force. The shaping function was a continuous function of the variables defining the condition functions, and it had a continuous first derivative for all values of the variables of a condition function.

Miller [52] developed a method for eliminating jerk and noise in semi-active suspensions by reducing the magnitude of force discontinuities that can result from both on-off and continuous semi-active skyhook control strategies. In the method, he introduced relative acceleration into the condition function. The semi-active damper operates as a conventional passive damper when the relative velocity carries the same sign as relative acceleration. The damping coefficient is significantly reduced (ideally zero) when the relative velocity across the damper opposes the relative acceleration.

Another method to cope with jerk and chatter problems is using sliding mode control. For example, Ursu et al. [53] carried out an investigation for using slide mode control to combat chatter. Numerical simulations were carried out on a model of a 2-DOF car suspension system. The effects of the Runge-Kutta integration step and sample time on chatter were studied. The results showed that chatter can be reduced via the proposed sliding mode control strategy.

In most numerical studies, the off-state damping coefficient of the semi-active damper is assumed to be zero. However the actual damper constant is limited by the physical parameters of the conventional damper. This means that there is both an upper bound and a lower bound. Usually the on-state damping should be much greater than the off-state damping and the off-state damping should be kept as small as possible. The effects of non-zero off-state damping were investigated in [54, 55]. The insertion of off-state damping has two effects compared to the system without off-state damping: (a) it reduces the RMS acceleration transmissibility at and around the natural

frequency; and (b) it increases the RMS acceleration transmissibility at frequencies greater than the natural frequency.

Although in most analytical studies the semi-active damper is modelled as an ideal device without any delay, it has been shown that the real-time implementation of semi-active dampers can involve as much as 50ms of time delay [56]. The time delay is defined as the time lag that exists between the sensor signal and damper response. This lag is affected by the electrical and mechanical delays that exist in any practical system. Additional time delays can reduce the benefit of a semi-active strategy [56, 57].

1.2.2 SEMI-ACTIVE DEVICES

Semi-active devices are passive devices whose properties can change with time, and over time scales, which are comparable to the period of the vibration itself. For the purpose of semi-active damping control, various energy dissipating devices have been used to obtain the desired damping. These devices include hydraulic dampers, Electrorheological (ER) and Magnetorheological (MR) dampers, semi-active friction devices and electromagnetic devices.

(1) Hydraulic dampers

Semi-active hydraulic dampers typically consist of a hydraulic piston-cylinder arrangement with a control valve mechanism. Variable damping coefficients can be achieved by the modulation of the orifice area through which the fluid flows. The control valve may take the form of a solenoid valve for on-off control or a servovalve for continuously variable control. Fluid viscous dampers have found numerous applications in the vibration isolation of aerospace and seismic response control systems.

Krasnicki [19] used a damper consisting of a hydraulic actuator in conjunction with an electro-hydraulic servovalve modulating the controlling orifice area. In the off-state the full command voltage was applied to the valve, while zero voltage was applied to the valve in the on-state. Patten, et al. [58], provided a primer on the important physical characteristics of a hydraulic semi-active vibration absorber. Karnopp [59] introduced semi-active isolators using the skyhook damper scheme. Practical

applications of skyhook dampers, namely extreme isolation for delicate manufacturing operations against seismic input and the automotive suspensions are discussed by Karnopp [24].

(2) ER and MR dampers

ER and MR dampers consist of a hydraulic cylinder containing micron-sized polarisable particles in a fluid (usually oil). Both the ER and MR materials have the ability to change from free flowing viscous fluids to a semi-solid state in a matter of milli-seconds when exposed to an electric or a magnetic field [60, 61]. These devices are mechanically reliable, since they do not contain any moving parts. More detailed information about the use of ER and MR dampers for vibration control can be found in [60, 62].

There are numerous published references on vibration control using ER and MR dampers. For example, Wu and Griffin [28] used an ER damper to reduce the severity of shocks caused by suspension seat end-stop impacts or high magnitude vibration. The ER damper was used to realise the required two-state damping. Jeon et al. [57] studied the vibration isolation performance of a MR damper under the control of the on-off skyhook control strategy. The damping constant and response time of the damper were measured. The time delay in the response of the MR damper was measured and incorporated into the control under harmonic disturbances. Experimental results show that on-off skyhook control strategy which includes the damper time delay performs less effectively than the one without the consideration of time delay.

(3) Semi-active friction devices

Semi-active friction devices use the force generated by surface friction to dissipate energy. An ideal friction damper may be considered to behave as a Coulomb element wherein the force is the product of friction coefficient and the normal force at the friction interface and the sign of the velocity of the motion. An isolation system incorporating semi-active friction controllable sliding bearing is described by Feng et al. [63]. The friction force on the sliding interface between the building and the foundation was controlled in order to limit the sliding displacement and minimise the

transmission of seismic force to the building. The simulation results showed that this type of system is effective for earthquakes with a broad range of intensity, compared to its conventional passive counterparts.

(4) Electromagnetic dampers

Electromagnetic dampers use the interaction between the movement of the coil and the magnetic field of a permanent magnet or electromagnet to provide a damping effect [64, 65]. When an electromagnetic damper coil is shorted or connected to an external resistor, the device becomes a linear mechanical damper. The damping level can be varied by changing the external resistance or the strength of the magnetic field. When the external resistance is varied, the damping coefficient is varied. In the open circuit state the coefficient vanishes, while when the coil is shorted the coefficient reaches a maximum value. Since effective resistance can be rapidly varied electronically, an electrical actuator can function as a semi-active damper in vehicle or vibration isolation suspension systems. In this thesis, an electromagnetic damper is used to achieve two-state damping required by the on-off control strategy.

In a paper by Karnopp [64], the possibility was studied for using permanent magnet linear motors as variable mechanical dampers for vehicle suspensions. Two basic electromagnetic designs were analysed, namely the moving coil and the moving magnet approach. The electromagnetic damper studied consists of a tubular coil of wire situated within a radially-oriented constant magnetic field produced by a permanent magnet. The damping coefficient is varied by changing the external resistance.

1.2.3 SUMMARY OF LITERATURE REVIEW

The technologies available to tackle vibration isolation via semi-active damping control means have been briefly reviewed in the preceding sections. The literature review concentrates on the semi-active control strategies and semi-active damping devices.

Significant research in the area of semi-active systems and controllable dampers has been carried out either numerically or experimentally by various researchers, but only in rare instances have researchers investigated both aspects. The majority of previous

research just carried out numerical simulations. They failed to provide physical interpretations to justify of the results obtained. There exists an abundance of research on the application of semi-active dampers for particular vibration control problems such as vehicle suspensions and building structural control, but relatively little research has focused on general aspects of vibration isolation [24, 37]. Although more complicated feedback control strategies offer great possibilities in many situations, it is probable that significant performance gains can be realised with basic control strategies.

The study presented in this thesis explores the feasibility, suitability and effectiveness of using relatively simple control strategies for the purpose of vibration isolation. Physical justifications are provided to enable a more complete understanding of the application of semi-active damping control for vibration isolation. Experimental work has been carried out to validate the numerical simulation results.

1.3 OBJECTIVES AND SCOPE

This thesis aims to address the application of semi-active damping in isolating sensitive equipment from the surrounding vibration environments. The primary objectives of the thesis are to:

- Evaluate the effectiveness and suitability of various basic semi-active control strategies for the purpose of vibration isolation. Compare the performance with that due to conventional and skyhook passive dampers;
- Provide physical interpretation of the results to enable a more complete understanding of the applicability of semi-active damping control for vibration isolation;
- Provide some guidelines for practical engineers when semi-active damping control can be considered as an option; and
- Implement certain control strategies using a controllable device to validate numerical simulations.

This thesis is concerned with the use of a SDOF semi-active isolation system, comprising a semi-active damper with a linear passive spring in parallel, for vibration isolation of base excitation. The base-excited SDOF system is used to study the vibration isolation performance of the semi-active dampers. Four basic control strategies based on skyhook control and balance control were studied and the effectiveness and suitability of each individual semi-active control algorithm are studied. The four control algorithms are continuous skyhook control, on-off skyhook control, on-off balance control and continuous balance control. Various base disturbances, namely harmonic, periodic and random, are considered in this study. The on-off skyhook control strategy was chosen to be implemented using an electromagnetic device and the experimental results were presented.

1.4 CONTRIBUTIONS OF THE THESIS

The contributions of this thesis are as follows:

(1) A physical interpretation for skyhook and balance semi-active control strategies are provided;

(2) Chatter and jerk problems associated with applications of the four semi-active damping control strategies are investigated and anti-jerk control strategies are proposed;

(3) The performance of the four semi-active control strategies for vibration isolation of harmonic, periodic and random disturbances has been studied with the following conclusions:
   - The superior performance of the semi-active control strategies to conventional passive damper with an equivalent damping has been confirmed by simulation and experimental results for harmonic disturbances;
   - Semi-active damping control strategies can provide better performance that the conventional passive damper for square and triangular waves;
   - An analytical solution to calculate the mean square response of a conventionally damped SDOF system and a skyhook passive SDOF system subject to random base excitation has been derived;

- The performance for isolation of random disturbances has been studied numerically for three special cases when the displacement, velocity and acceleration excitation spectrum are assumed to be flat. Semi-active control strategies are found useful for the cases when the inputs are displacement or velocity.

(4) The condition functions of the semi-active control strategies were studied to provide physical interpretations and insights;

(5) The on-off skyhook control strategy was implemented in the lab using an analogue circuit.

1.5 LAYOUT OF THE THESIS

To conduct a theoretical and experimental study on semi-active damping control for vibration isolation, a single-degree-of-freedom (SDOF) system subject to base disturbances is considered throughout this thesis.

The background of this thesis is firstly introduced in Chapter 1. An overview of different contributions in the area of semi-active damping control is presented. The advantages and limitations are briefly discussed, and the motivation behind semi-active damping control for vibration isolation is also presented in this chapter.

Chapter 2 contains information on the model development for numerical simulations of a SDOF system incorporating a semi-active damper. Four control algorithms, which are continuous skyhook control, on-off skyhook control, continuous balance control and on-off balance control, are described. Also contained in this chapter is an investigation into the chatter and jerk problems that arise in numerical simulations and possibly in practice when using semi-active dampers. An anti-jerk implementation is presented and anti-jerk control strategies are proposed. These control strategies are implemented numerically in Matlab/Simulink.

In Chapter 3 the vibration isolation performance of the four control strategies for harmonic disturbances are discussed. The performance is evaluated in terms of Root-Mean-Square (RMS) acceleration and relative displacement transmissibility. The vibration isolation performance of the semi-active dampers is compared with that due

to the conventional passive and skyhook passive dampers. Experiments are conducted to test the on-off skyhook control strategy.

Since the switching characteristics of the semi-active damper are frequency dependent, the switching for the fundamental frequency might be affected due to the presence of an extraneous frequency. Chapter 4 studies the effects of a secondary frequency on the switch state of a semi-active damper for the fundamental frequency. Upper bounds for fractions of time when the switching can be wrong are derived. A specific example of excitation with multiple harmonics is periodic disturbances in which the frequency components are integer multiples of the fundamental frequency. The effectiveness of the semi-active damper in isolating square and triangular waves is also investigated in this Chapter. Experimental work conducted to investigate the effects of a secondary frequency on the switching time of the semi-active damper for the fundamental, and the effectiveness of the on-off skyhook control algorithm in isolating square wave are also presented.

Chapter 5 discusses the effectiveness of semi-active dampers in isolating random disturbances. An analytical solution is derived for the RMS response of a SDOF system with a conventional passive and a skyhook passive damper subject to random base excitation with a constant power spectral density. The RMS responses are simulated for a SDOF system incorporating the semi-active dampers for three special cases when the spectra of displacement, velocity and acceleration are flat. Experimental work conducted on the on-off skyhook damper to verify the results of isolating random disturbances is also presented.

Finally, Chapter 6 summarises the main conclusions from this thesis and makes recommendations for future work.

This thesis also contains four appendices to support the main structure of the thesis.

CHAPTER 2

2. NONLINEAR CONTROL STRATEGIES FOR SEMI-ACTIVE DAMPING CONTROL

2.1 INTRODUCTION

Chapter 1 described how semi-active control strategies have been developed and used to control vibration. This chapter is concerned with model developments for simulations of a base-excited SDOF system with a semi-active damper. Four basic semi-active control strategies based on skyhook control and balance control will be considered. It provides detailed information for numerical simulations carried out throughout the thesis.

First, the semi-active damping concept is introduced and compared with conventional passive damping. Detailed descriptions of four semi-active control algorithms, which are continuous skyhook control, on-off skyhook control, continuous balance control, and on-off balance control, are presented in the next section followed by discussion of the numerical problems encountered when performing simulations with semi-active dampers. A phenomenon often referred to as chatter occurs with semi-active dampers at low excitation frequencies. The conditions for chatter to occur are demonstrated by studying the dynamics of the system, and a modified control scheme is suggested to avoid the chatter problem. Jerk is associated with chatter and is caused by switching between different states of the damping. A detailed description of an anti-jerk implementation is presented and anti-jerk control strategies are proposed. Finally the results are summarised.

2.2 SEMI-ACTIVE DAMPING VS. CONVENTIONAL DAMPING

Semi-active dampers are the class of device whose damping properties can be varied to reduce the vibration transmitted from the source to the receiver. Figure 2.1 shows the schematic of a SDOF system with a conventional passive, semi-active and fully active damper. In both passive and semi-active dampers, the magnitude of the damper

force is dependent on the relative velocity across the damper. However, the force versus velocity curve of each type is not identical. In passive damping, the damper has a pre-defined characteristic in units of force/velocity as shown in Figure 2.2. A change in the relative velocity across the damper, $\dot{x} - \dot{x}_0$, will change the force exerted by the damper, F_d. Referring to Figure 2.2, the magnitude and direction of the force exerted depend only on the relative velocity across the damper. In many applications, the relationship between the force and the relative velocity for the damper is nonlinear, and the gradient tends to decrease as the velocity increases [1]. However, in the passive model considered in this report, the slope of the curve is constant.

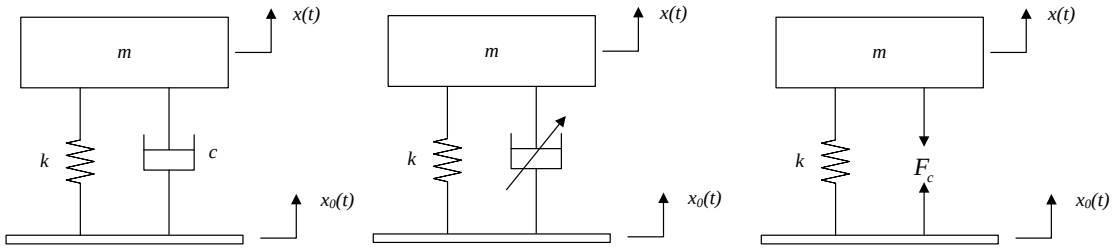

(a) (b) (c)

Figure 2.1 Schematic of a SDOF system with different type of dampers (a) conventional passive damper; (b) semi-active damper; and (c) active device

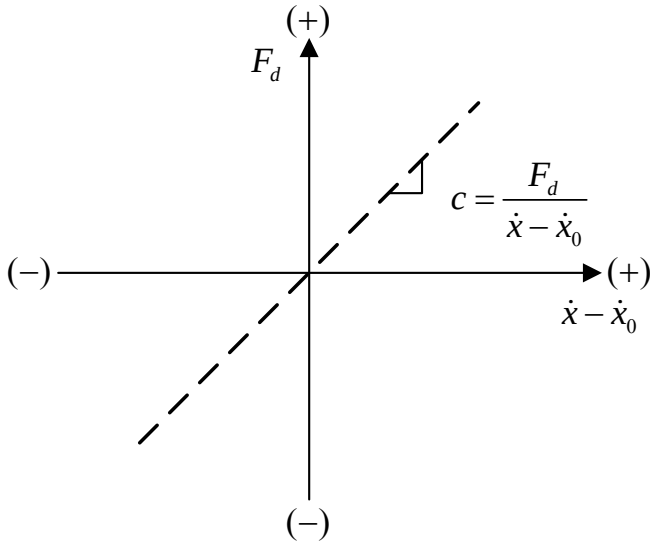

Figure 2.2 Relationship between damping force and relative velocity for a conventional passive damper

Although the direction of the damper force in semi-active dampers still depends on the relative velocity across the damper, the magnitude of the damper force is considered to be adjustable. The damping value can be adjusted by a controller that can be programmed to any type of control strategy.

Semi-active dampers may be of the on-off type or of the continuously variable type. A damper of the first type is switched, in accordance with a suitable control algorithm, between alternate on and off damping states. In its on-state, the damping coefficient is of a pre-selected relatively high magnitude. The term "damping coefficient" refers to the ratio of the damper force generated by the damper to the relative velocity across the damper, which is not necessarily a constant. In its off-state, the damping coefficient of the damper is of relatively low magnitude. This may be almost zero, but in many practical applications, a magnitude greater than zero is desired. A continuously variable semi-active damper is also switched during operations between on and off states. However, when a continuously variable damper is in its on-state, the damping coefficient and corresponding damper force may be changed over a range of magnitudes. The concept of semi-active damping is illustrated in Figure 2.3(a) and (b). The shaded part of the graph in Figure 2.3(b) represents the range of possible damping coefficients. The damping coefficient of a semi-active on-off type damper is a discontinuous function in the time domain, which can be seen in Figure 2.4 (a). The damping coefficient of a semi-active continuous type damper is a continuous function as shown in Figure 2.4 (b).

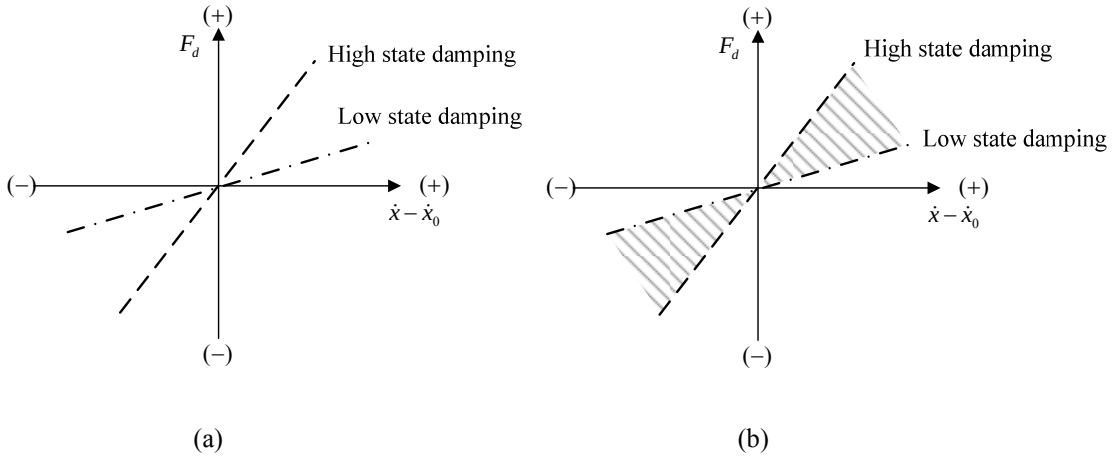

Figure 2.3 Semi-active damper concepts (a) on-off damper; (b) continuously variable damper

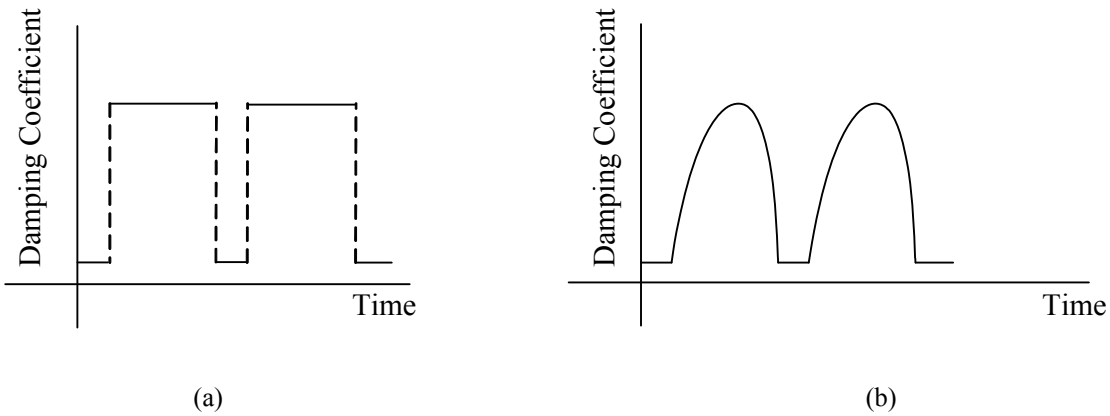

(a) (b)

Figure 2.4 Semi-active damper characteristics in time domain (a) on-off damper; (b) continuously variable damper

2.3 SEMI-ACTIVE CONTROL STRATEGIES

In the initial numerical simulations, four basic strategies are studied. The semi-active dampers investigated in this study can be classified into skyhook damping control and balance damping control. All of these can be further divided into on-off and continuously variable control strategies. As a comparison, an adaptive-passive damping control strategy is also studied.

2.3.1 SKYHOOK CONTROL

The initial semi-active system was based on skyhook semi-active control, which was first proposed by Karnopp [15] to emulate the skyhook damper. Forces were generated in a hydraulic damper by modulating its fluid-flow orifices. The name "skyhook" is derived from the fact it was a passive damper hooked to an imaginary sky. Figure 2.5 (a) shows the arrangement of a SDOF system with a skyhook damper. Considering the SDOF system with a skyhook damper in Figure 2.5(a), it can be realised using fully active control by programming the active force shown in Figure 2.5(b) as

$$F_c = c_{sky}\dot{x} + k(x - x_0) \tag{2.1}$$

where F_c is the active control force, k is the spring stiffness, and c_{sky} is the skyhook damping coefficient.

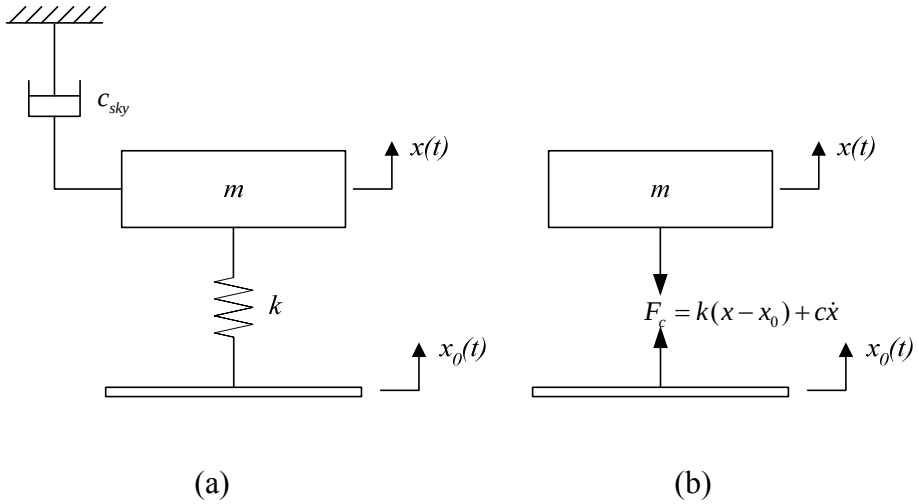

Figure 2.5 Skyhook system and its active equivalent (a) schematic of a SDOF system with a skyhook damper; (b) active system

The full active control strategy requires an actuator to provide the desired damping force. To reduce the complexity and power requirements, the semi-active continuous skyhook control algorithm was designed to modulate the force generated by a passive device to approximate the force that would be generated by a skyhook damper. The SDOF system with a semi-active damper is shown schematically in Figure 2.6. The semi-active device is installed in the place of the conventional damper, and the device is passive, but the force generated by the device is controllable. The excitation and response signals are fed into a controller to provide a desired damping force.

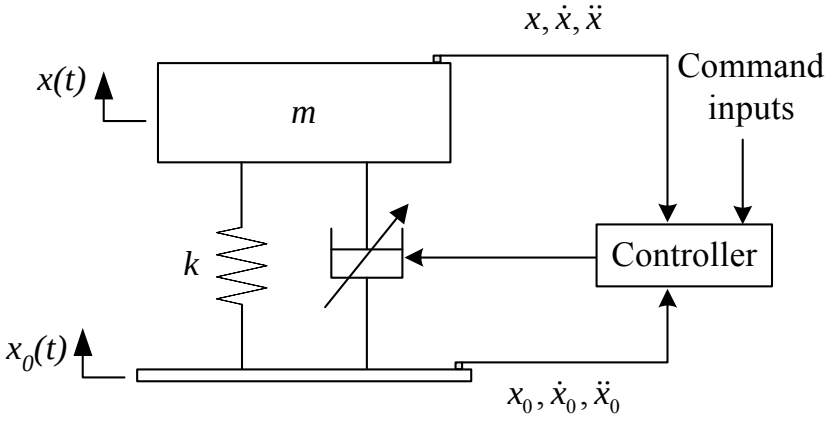

Figure 2.6 Schematic of a SDOF system with a semi-active damper

The passive device can only absorb vibration energy, so the product of the damper force, F_{sa}, and the relative velocity, $\dot{x} - \dot{x}_0$, must be greater than or equal to zero

$$F_{sa}(\dot{x}-\dot{x}_0) \geq 0 \tag{2.2}$$

i.e., the power associated with the semi-active damper force, F_{sa}, is always dissipated. Thus, if the relative velocity is increasing, $\dot{x}-\dot{x}_0 \geq 0$, F_{sa} must be positive, and if $\dot{x}-\dot{x}_0 < 0$, F_{sa} must be negative.

Defining the upwards direction as positive and downwards direction as negative, consider first the case when the mass is moving upwards separating from the base. Under the ideal skyhook configuration, the desired value of F_{sky} is

$$F_{sky} = -c_{sky}\dot{x} \tag{2.3}$$

where F_{sky} is the skyhook damper force. For the semi-active equivalent model, the damper force due to the semi-active damper is

$$F_{sa} = -c_{sa}(\dot{x}-\dot{x}_0) \tag{2.4}$$

where F_{sa} is the semi-active force, and c_{sa} is the semi-active damping coefficient required to achieve the desired skyhook damping force. In order for the semi-active equivalent model to perform like the skyhook model, the damping forces must be equal. The semi-active damping constant can thus be found by setting F_{sky} in equation (2.3) to be equal to F_{sa} in equation (2.4). The semi-active damper force can then be found for the case when both $\dot{x}$ and $\dot{x}-\dot{x}_0$ are positive, which gives

$$c_{sa} = \frac{c_{sky}\dot{x}}{\dot{x}-\dot{x}_0}, \quad \frac{\dot{x}}{\dot{x}-\dot{x}_0} \geq 0 \tag{2.5}$$

and

$$F_{sa} = \frac{c_{sky}\dot{x}}{\dot{x}-\dot{x}_0}(\dot{x}-\dot{x}_0), \quad \frac{\dot{x}}{\dot{x}-\dot{x}_0} \geq 0 \tag{2.6}$$

Next, consider the case when both $\dot{x}$ and $\dot{x}-\dot{x}_0$ are negative. Now the mass is moving downwards. The skyhook damper force would be in the positive direction, hence

$$F_{sky} = c_{sky}\dot{x} \tag{2.7}$$

Following the same procedure as the first case, equating the damper forces reveals the same semi-active damper force as the first case. Thus it can be concluded that when the product of the $\dot{x}$ and $\dot{x}-\dot{x}_0$ is positive, the semi-active damping coefficient is defined by equation (2.6) and the semi-active damper force is defined by equation (2.7).

Now consider the case when the mass is moving upwards and the mass and base are moving towards each other. The skyhook damper would again apply a force on the mass in the negative direction. In this case, the semi-active damper cannot apply a force in the same direction as the skyhook damper. For this reason, the damping should be set to zero thus minimising the force acting on the mass.

The final case to consider is the case when the mass is moving downwards and is separating from the base. Again, in this condition, the skyhook damper force and the semi-active damper force are not in the same direction. The skyhook damper force is in the positive direction, while the semi-active damper force is in the negative direction. The best that can be achieved is to set the damping in the semi-active damper to zero.

Summarising these four conditions, the well-known semi-active skyhook control algorithm is given by [15]

$$F_{sa} = \begin{cases} c_{sky}\dot{x} & \dot{x}\left(\dot{x}-\dot{x}_0\right) \geq 0 \\ 0 & \dot{x}\left(\dot{x}-\dot{x}_0\right) < 0 \end{cases} \tag{2.8}$$

Whenever it is required to supply energy to the system to produce the effect of skyhook damping, the best the device can do is to supply no force at all. Elsewhere the device provides a force proportional to the absolute velocity of the mass. The switching of the device can be controlled by the term $\dot{x}(\dot{x}-\dot{x}_0)$, which is called the

condition function. Condition function is different for different control strategies. If the product of the absolute velocity of the mass, $\dot{x}$, and the relative velocity $\dot{x}-\dot{x}_0$ between the mass and the base is positive, the damper is switched on, so that a force is generated to reduce the velocity of the mass. If this term is negative, the damper is switched off so that no force is generated. This control scheme intends to simulate closely an ideal skyhook damper. The theoretical semi-active damping required to produce the damping force, F_{sa}, is given by

$$c_{sa}=\begin{cases}\dfrac{c_{sky}\dot{x}}{\dot{x}-\dot{x}_0} & \dot{x}\left(\dot{x}-\dot{x}_0\right)\geq 0\\ 0 & \dot{x}\left(\dot{x}-\dot{x}_0\right)<0\end{cases} \tag{2.9}$$

Figure 2.7 is a three-dimensional plot of the semi-active damping coefficient required by a continuous variable skyhook damper in the above equation. It can be seen from the figure that when the relative velocity $\dot{x}-\dot{x}_0$ is very small, the required damping increases abruptly and tends to infinity, which cannot be provided by practical hardware. The damper constant, c_{sa}, is limited by the physical parameters of the semi-active damper. This means that there is both an upper bound, $c_{\max}$, and a lower bound, $c_{\min}$, on c_{sa}. Considering the limitation of the practical hardware, the damping coefficient in equation (2.9) can be rewritten as

$$c_{sa}=\begin{cases}\max\left[c_{\min},\min\left[\dfrac{c_{sky}\dot{x}}{\dot{x}-\dot{x}_0},c_{\max}\right]\right] & \dot{x}(\dot{x}-\dot{x}_0)\geq 0\\ c_{\min} & \dot{x}(\dot{x}-\dot{x}_0)<0\end{cases} \tag{2.10}$$

The control algorithm given in equation (2.8) requires a continuous modification of the damper coefficient. To simplify the operation, a simpler on-off version has been proposed [19]. The the damper force is governed by

$$F_{sa}=\begin{cases}c_{on}\left(\dot{x}-\dot{x}_0\right) & \dot{x}\left(\dot{x}-\dot{x}_0\right)\geq 0\\ 0 & \dot{x}\left(\dot{x}-\dot{x}_0\right)<0\end{cases} \tag{2.11}$$

where c_{on} is the on-state damping constant of the on-off damper.

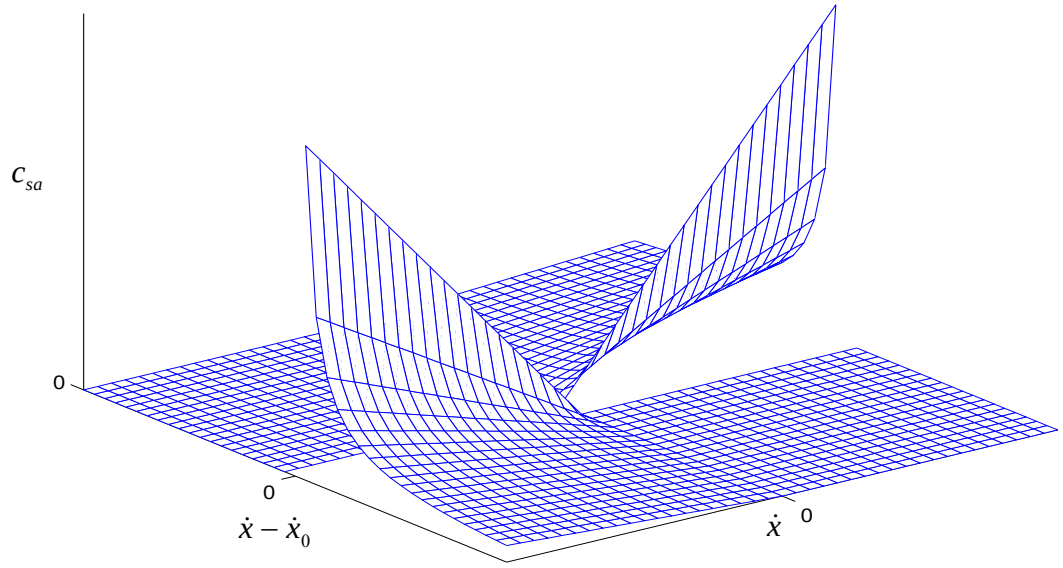

Figure 2.7 Required damping coefficient for continuous skyhook damping as a function of absolute and relative velocity (equation (2.9))

In practice, zero damping coefficients are impossible when the damper is switched off. Therefore, the damping coefficient is actually switched between a high value and a low value. Considering the non-zero off-state damping, the control algorithm in equation (2.11) can be restated as

$$c_{sa}=\begin{cases} c_{\max} & \dot{x}\left(\dot{x}-\dot{x}_0\right)\geq 0 \\ c_{\min} & \dot{x}\left(\dot{x}-\dot{x}_0\right)<0 \end{cases} \tag{2.12}$$

where $c_{\max}$ and $c_{\min}$ are the maximum and minimum coefficients of the on-off damper respectively. Usually the on-state damping $c_{\max}$ is much greater than the off-state damping $c_{\min}$, and $c_{\min}$ should as small as possible.

Figure 2.8 shows the relationship between the damper states and condition function of the skyhook control strategy. If the condition function is positive, the damper is

switched on, so that a force is generated to reduce the velocity of the mass. Otherwise, the damper is switched off. When the relative velocity across the damper is positive, the damper force acts to pull down the suspended mass; when the relative velocity is negative, the damper force acts to push up on the mass. Thus when the absolute velocity of the mass is negative, it is travelling downwards and the on-state damping is desired to push up on the mass. Once the relative velocity changes its direction while the absolute velocity is still negative, minimum damping is desired to continue pulling down on the mass. However, if the absolute velocity of the body mass is positive and the mass is travelling upwards, the on-state damping is desired to pull down on the mass, while the minimum value of damping is desired to further push the mass upwards.

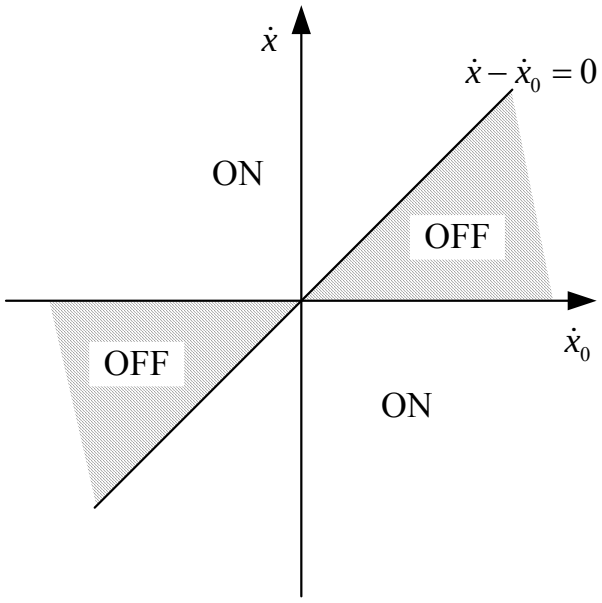

Figure 2.8 Relationship between the velocity variables and the damper states

Both the continuous skyhook control and on-off skyhook control algorithms intend to produce the effect of skyhook damping. However, there are differences between them, which can be interpreted in terms of the amplitude and phase of the damper force. The original expression for the continuous skyhook control in equation (2.8) can provide the same amplitude and phase in its on-state as those of a skyhook damper. Due to the practical limitation of physical systems, however, it can only provide the exact amplitude and phase during part of the on-state period. By comparison, on-off skyhook control can only ensure that the semi-active damping force is the same sign

of the desired skyhook damping force. The magnitude is not representative of the skyhook damper force anymore, although it is shown that it gives similar isolation performance [66].

2.3.2 BALANCE CONTROL

Considering a passive SDOF system subject to base excitation, the acceleration response of the suspended mass due to the base excitation can be expressed as

$$\ddot{x} = -\frac{1}{m}(F_k + F_d) \tag{2.13}$$

where F_k and F_d are the spring and damper forces respectively, which are given by

$$\begin{aligned} F_k &= k(x - x_0) \\ F_d &= c(\dot{x} - \dot{x}_0) \end{aligned} \tag{2.14}$$

and k and c are the spring stiffness and damping coefficients respectively. The amplitude of the acceleration of the mass due to harmonic base excitation can be expressed in terms of the spring and damper forces [25]

$$|\ddot{x}| = \frac{|F_k| + |F_d|}{m} \quad \begin{matrix} t_0 < t < t_0 + \dfrac{t}{4} \\ \\ t_0 + \dfrac{t}{2} < t < t_0 + \dfrac{3t}{4} \end{matrix} \tag{2.15}$$

$$|\ddot{x}| = \frac{|F_k| - |F_d|}{m} \quad \begin{matrix} t_0 + \dfrac{t}{4} < t < t_0 + \dfrac{t}{2} \\ \\ t_0 + \dfrac{3t}{4} < t < t_0 + t \end{matrix} \tag{2.16}$$

where t_0 is the time at which spring force is zero, and t is the period of vibration. Figure 2.9 shows the inertial force ($m\ddot{x}$), spring force and damper force of a passive SDOF system subject to harmonic base excitation. Most of the time, it is desired for the acceleration of the mass to be small, but it is evident from equation (2.15) and Figure 2.9 that the damper force tends to increase the acceleration amplitude of the mass during a part of vibration cycle. In the remaining part of a vibration cycle, the

acceleration of the mass due to the damper force may be attenuated if F_k and F_d are in the same order of quantity, which is demonstrated by equation (2.16) and Figure 2.9. Poor vibration isolation performance of heavily damped passive systems is attributed to this phenomenon. Isolation performance of passive isolators with fixed damping deteriorates at high excitation frequencies, when the magnitude of the damper force is dominant.

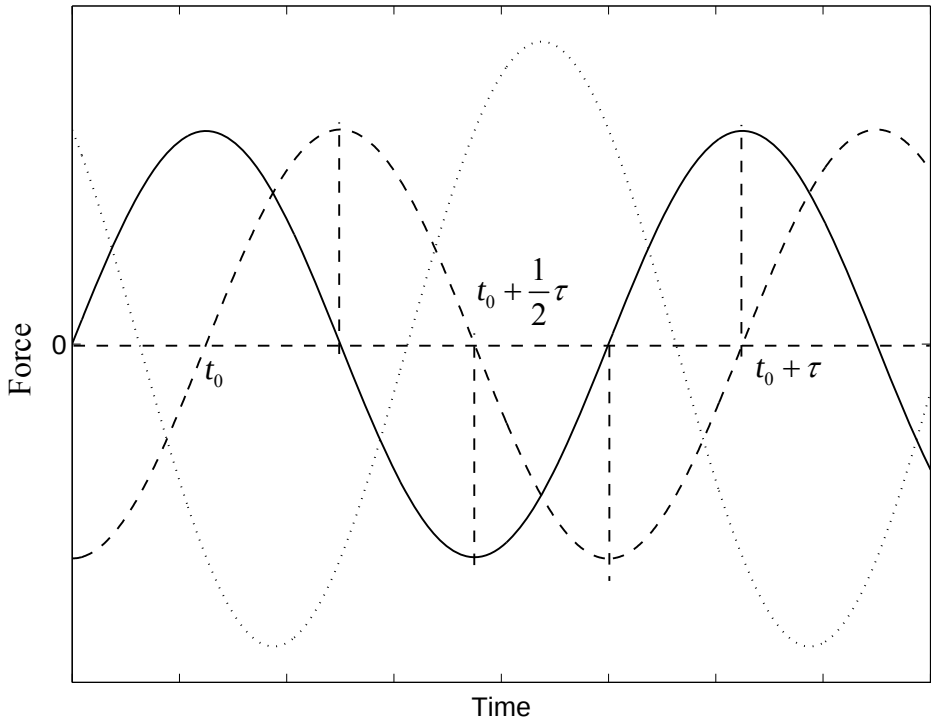

Figure 2.9 Relationship between the forces of a conventional passive SDOF system subject to a pure-tone excitation: — damping force (F_d); ---- spring force (F_k); and ····· inertial force ($m\ddot{x}$)

An on-off damping mechanism may be realised, which operates as a conventional passive damper during the part of the cycle to reduce the acceleration of the mass as demonstrated in equation (2.16) and Figure 2.9. The damping mechanism assumes zero damping during the portion of the cycle when a passive damper would normally increase the amplitude of the acceleration of the mass. In reference [25], an on-off hydraulic damper was implemented using a two position valve operated by a solenoid relay.

Based on the above discussion, the damper force will cause an increase in the acceleration of the mass whenever forces due to the spring and the damper have the same sign, or equivalently when the relative velocity and relative displacement have the same sign. A control algorithm to ensure that this does not occur is [25]

$$F_{sa} = \begin{cases} c_{on}(\dot{x} - \dot{x}_0) & (x - x_0)(\dot{x} - \dot{x}_0) \le 0 \\ 0 & (x - x_0)(\dot{x} - \dot{x}_0) > 0 \end{cases} \tag{2.17}$$

where c_{on} is the on-state damping constant of the on-off damper.

The control algorithm shows that when the damper constructively adds to the acceleration due to the spring, it is switched off. Whenever the damper force reacts with the spring force, the damper is switched on. Since the purpose of the damping force in this algorithm is to oppose the spring force, it is termed “balance control”. This control algorithm may be relatively easy to implement in some applications such as vehicle suspensions, as the relative displacement and the relative velocity can be easily measured.

The corresponding semi-active damping considering non-zero off-state damping is given by

$$c_{sa} = \begin{cases} c_{\max} & (x - x_0)(\dot{x} - \dot{x}_0) \le 0 \\ c_{\min} & (x - x_0)(\dot{x} - \dot{x}_0) > 0 \end{cases} \tag{2.18}$$

where $c_{\max}$ and $c_{\min}$ are the maximum and minimum coefficients of the on-off damper.

The control algorithm in equation (2.17) has the potential for improvement. During the on-state of the damper, the instantaneous damper force is seldom exactly equal in magnitude to the instantaneous spring force. Consequently, the surplus force will still accelerate the mass. In reference [27], a damper with a continuously variable damping force has been discussed, which can be considered as a further development of the preceding control algorithm in equation (2.17). The damping coefficient is continuously variable, depending on the relative displacement and the relative velocity

$$F_{sa} = \begin{cases} -k(x - x_0) & (x - x_0)(\dot{x} - \dot{x}_0) \le 0 \\ 0 & (x - x_0)(\dot{x} - \dot{x}_0) > 0 \end{cases} \tag{2.19}$$

This control algorithm shows that if the spring force and the damper force exerted on the mass are in the same direction, to reduce the sprung mass acceleration, the damper force should be minimum. On the other hand, if the spring force and the damper force are in anti-phase, then the damper force should be adjusted in such a way that it equals the spring force in magnitude so as to produce zero acceleration of the sprung mass. The semi-active damping required for this control algorithm is given by

$$c_{sa} = \begin{cases} \dfrac{-k(x - x_0)}{\dot{x} - \dot{x}_0} & (x - x_0)(\dot{x} - \dot{x}_0) \le 0 \\ 0 & (x - x_0)(\dot{x} - \dot{x}_0) > 0 \end{cases} \tag{2.20}$$

It can be seen from equation (2.20) that the damping coefficient tends to infinity at $\dot{x} - \dot{x} = 0$, which cannot be implemented in practice. Figure 2.10 shows a three-dimensional plot of the damping coefficient defined by equation (2.20). Similarly to equation (2.10), the damper constant c_{sa} saturates at the upper and lower bounds imposed by the physical parameters of the damper. Considering the practical hardware constraints, the damping coefficient can be rewritten as

$$c_{sa} = \begin{cases} \max\left[c_{\min}, \min\left[\dfrac{-k(x - x_0)}{\dot{x} - \dot{x}_0}, c_{\max} \right] \right] & (x - x_0)(\dot{x} - \dot{x}_0) \le 0 \\ c_{\min} & (x - x_0)(\dot{x} - \dot{x}_0) > 0 \end{cases} \tag{2.21}$$

Both on-off and continuous balance control algorithms programme the damping force so that it can oppose the spring force whenever the damping force and the spring force have the opposite sign. The two control strategies attempt to make a damper behave like a spring by varying its damping coefficient in real time. According to equation (2.17) and (2.18), since the on-off balance damper can only produce a damping force proportional to the relative velocity across the damper in its on-state, it cannot ensure the damping force is exactly equal to the spring force. Depending on the dynamics of the system and the maximum damping, $c_{\max}$, the spring force can partly be cancelled or even sometimes the spring force can be over cancelled. This might change the

static equilibrium of the system and even make the system to become unstable. The continuous balance can cancel the spring force in theory, but due to the hardware limitations, the required damping might be beyond the range the semi-active damper can provide during part of the on-state period.

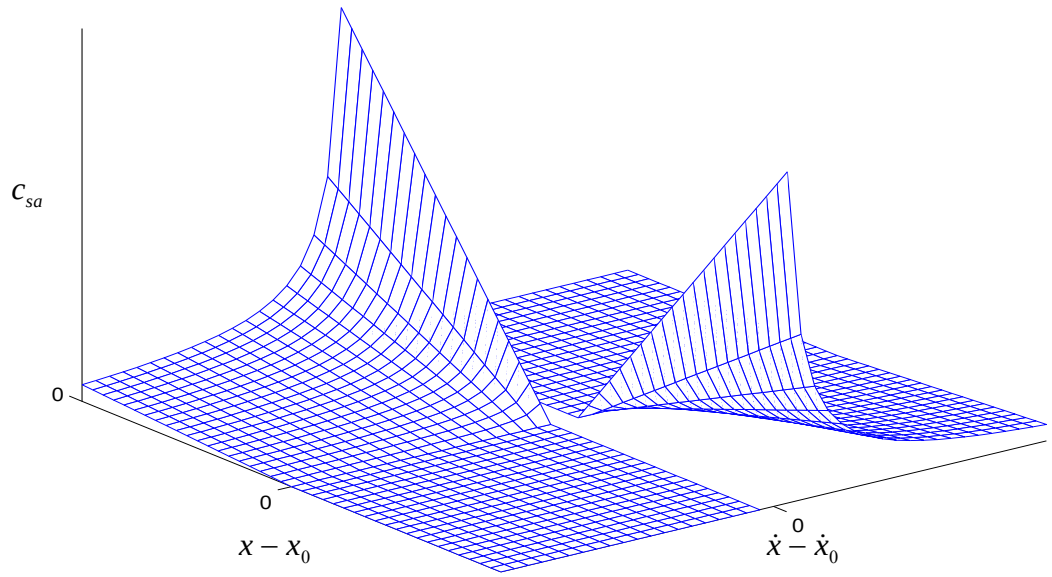

Figure 2.10 Required damping coefficient for continuous balance semi-active damping as a function of relative displacement and relative velocity (equation (2.20))

2.3.3 ADAPTIVE-PASSIVE DAMPING CONTROL

The last control algorithm considered for harmonic analysis is an adaptive damping method, which aims to adapt the damping constant according to the disturbance frequency. The idea of this control algorithm is quite straightforward. A passive SDOF system can only provide isolation in the frequency range $\omega / \omega_n > \sqrt{2}$, where ω is the excitation frequency and ω_n is the natural frequency. Increasing the damping coefficient in the frequency range $\omega / \omega_n \leq \sqrt{2}$ will reduce the resonance peak, while the isolation performance in the frequency range $\omega / \omega_n > \sqrt{2}$ will be degraded. As

illustrated in Figure 2.11, the ideal case for harmonic vibration isolation is that when $\omega/\omega_n \le \sqrt{2}$, the damping coefficient should have a big value, and when $\omega/\omega_n > \sqrt{2}$, then the damping coefficient should have a small value. To achieve this, the following control algorithm is proposed [13]

$$c_{sa} = \begin{cases} c_{\max} & \text{RMS}(\ddot{x}) \ge RMS(\ddot{x}_0) \\ c_{\min} & \text{RMS}(\ddot{x}) < RMS(\ddot{x}_0) \end{cases} \tag{2.22}$$

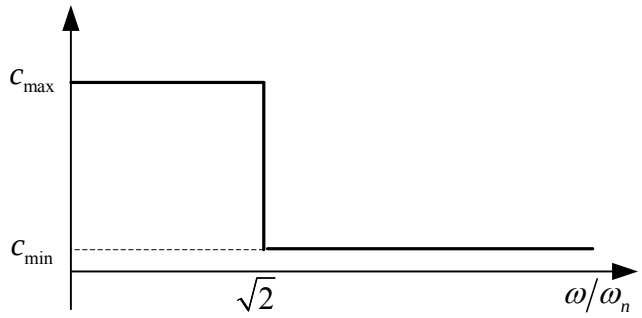

Figure 2.11 Ideal damping characteristics for vibration isolation of harmonic disturbances

The quantities $RMS(\ddot{x})$ and $RMS(\ddot{x}_0)$ are calculated over a time period much longer than the period of vibration of the system. The control algorithm uses RMS value of the response as the condition function to adjust the damping. When the RMS value of the response $\ddot{x}$ is greater than the RMS of the base acceleration, no isolation occurs and the damper is switched to its maximum value. Otherwise, the damper is switched off so that only small damping is presented in the system. For this control algorithm, the damper works in a bi-state (on-off) manner. It works as a common passive damper, switching from one value to the other. This might be the simplest way to implement a control algorithm since it does not need the damper to switch alternately between the on and off states during one period. It is very useful for vibration isolation of rotating machines such as washing machines [13]: the high damping value $c_{\max}$ is used when the drum is at low speed, i.e., during runup or rundown, while the low damping value $c_{\min}$ is used at high speeds. The disadvantage of this control algorithm is that it is only applicable to harmonic disturbances.

2.4 CHATTER OF SEMI-ACTIVE DAMPER AND ITS CURE

When performing numerical simulations with semi-active dampers the so-called chatter problem occurs under certain dynamic conditions. To observe the onset and persistence of chatter in a on-off skyhook semi-active system, consider the SDOF system shown in Figure 2.6 and assume that at some time t, the spring is compressed, the damper is off, and the base velocity, $\dot{x}_0$, is large and negative (downward). Since there is currently no damper force, the compressed spring will begin to push the mass upward, and $\dot{x}$ will become positive. With $\dot{x} > 0$ and $\dot{x} - \dot{x}_0 > 0$, the control strategy in equation (2.11) indicates that the damper will turn on to a fixed value. The damper force is tensile, and if the damper force pulling down is greater than the spring force, then the damper force will decelerate the mass and reverse its direction. The mass velocity will become negative while the relative velocity $\dot{x} - \dot{x}_0$ is still positive. The damper will turn off with the process repeating itself as long as the spring is in compression. This switching between the on-state and off-state, with $\dot{x}$ remaining near zero is called chatter.

For semi-active on-off systems, those switches due to changes in the sign of the mass velocity, $\dot{x}$, are defined as "$\dot{x}$ switches", while those due to changes in the sign of $\dot{x} - \dot{x}_0$ are called "$\dot{x} - \dot{x}_0$ switches". It is noted that only $\dot{x}$ switches are important with respect to the potential of chatter. This is because $\dot{x}$ switches are associated with a large relative velocity, $\dot{x} - \dot{x}_0$, and thus a large damper force, while $\dot{x} - \dot{x}_0$ switches are always associated with small damper forces. Also, chatter can only occur if the damper and spring force are in opposition, and if the on-state damper force is of larger magnitude than the instantaneous spring force. If the damper force is not larger than the spring force, then the damper would not change the direction of the velocity and would not initiate chatter. Figure 2.12 shows typical damping and spring forces when chatter occurs. The conditions for chatter to occur are summarised in Table 2.1. If these three conditions are met, chatter will be initiated and will continue until an $\dot{x} - \dot{x}_0$ switch takes place; or either condition (2) or (3) in Table 2.1 is no longer met.

The same phenomenon can also occur in continuously variable skyhook control at lower excitation frequencies, and has been studied in previous work by the author of

this thesis [66]. The analysis is based on an investigation into the relationship between the spring force and damping force when the relative velocity is nearly zero. Chatter occurs when the relative velocity is nearly zero and the spring force is smaller than the damping force in magnitude. Under these circumstances, the relative velocity will change from positive to negative when the damper is turned to its on-state. According to the condition function, the damper needs be turned to its off-state. But just after the damper is switched off, the relative velocity becomes positive again. The damper will be switched on accordingly. A limit cycle of oscillations exists until the conditions for chatter to occur are not met.

Table 2.1 Conditions for the chatter of the semi-active skyhook control

(1) An $\dot{x}$ switch has taken place;
(2) The damper force, F_d, if on, is of opposition sign to the spring force;
(3) The damper force is of larger amplitude than the instantaneous spring force.

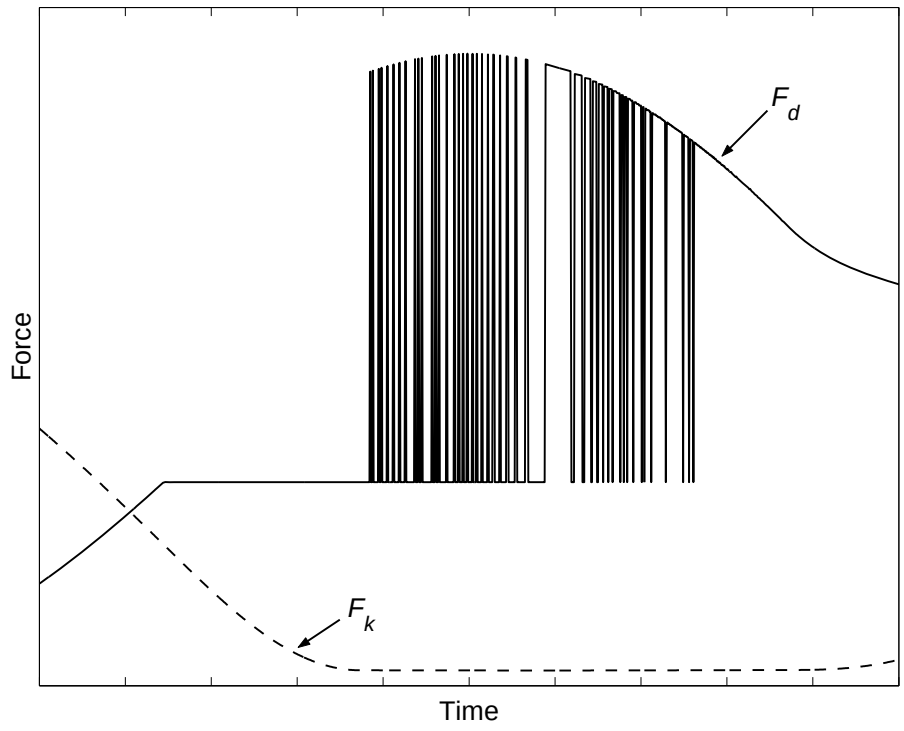

Figure 2.12 Spring force F_k (dashed line) and damping force F_d (solid line) during chatter

Following the analysis in [48], a modified logic is proposed to eliminate the chatter, which is given in Table 2.2. When $\dot{x}$ has just changed its sign, if the damper force is of different sign to the spring force, and the magnitude of the damper force is larger than that of spring force, do not switch the damper until the two conditions are not met.

Table 2.2 Modified logic for cure of chatter in the semi-active skyhook control

(1) $\dot{x}$ has just changed sign;
(2) If the damper force is of the same sign as the spring force, then switch the damper according to the switch condition. Otherwise, use (3);
(3) If the damper force magnitude, if on, is smaller than the spring force, then switch the damper according to switch function. Otherwise, use (4)
(4) Do not switch the damper until (2) or (3) are not met

2.5 JERK AND ANTI-JERK MODIFICATION

Jerk is defined as sharp changes in the acceleration response of the system. It can be seen from the discussion in section 2.4 that chatter will induce sharp changes in the damping force, thus it will result in jerk. No matter what control algorithm is used, the damper force exhibits discontinuities at the time of switching. Thus a significant change in acceleration may be experienced by the suspended mass, which is undesirable. Figures 2.13-2.16 show three-dimensional control surface plots of the damping force F_{sa} as a function of the variables in the condition function defined by equations (2.8) for continuous skyhook control, equation (2.11) for on-off skyhook control, equation (2.17) for on-off balance control, and equation (2.19) for continuous balance control. A surface discontinuity is present in the control surface at $\dot{x} - \dot{x}_0 = 0$ in Figure 2.13, a surface discontinuity in the control surface at $\dot{x} = 0$ in Figure 2.14, a surface discontinuity in the control surface at $x - x_0 = 0$ in Figure 2.15, and a surface discontinuity in the control surface at $\dot{x} - \dot{x}_0 = 0$ in Figure 2.16. All these surface discontinuities may lead to undesirable jerk.

To reduce the jerk induced by the switching of semi-active dampers, the method discussed in a US patent [51] is adopted. A shaping function, which can be a function

of $x-x_0$, $\dot{x}$, $\dot{x}-\dot{x}_0$ is introduced. The shaping function $F(x-x_0,\dot{x},\dot{x}-\dot{x}_0)$ will define the overall shape of the three-dimensional control surface. Table 2.3 lists the guidelines that should be observed in selecting the shaping function $F(x-x_0,\dot{x},\dot{x}-\dot{x}_0)$ [51].

Table 2.3 Guidelines for selecting shaping function

(1) $F(x-x_0,\dot{x},\dot{x}-\dot{x}_0)$ is a continuous function;
(2) $F(x-x_0,\dot{x},\dot{x}-\dot{x}_0)$ is equal to 0 at the points whenever a variable in the condition function will result in the occurrence of surface discontinuities ;
(3) $F(x-x_0,\dot{x},\dot{x}-\dot{x}_0)$ and the control surface both include continuous first derivatives for all values of $x-x_0$, $\dot{x}$ and $\dot{x}-\dot{x}_0$, where the conditions defined in equation 2.8, 2.11, 2.17 and 2.19 are met;
(4) $F(x-x_0,\dot{x},\dot{x}-\dot{x}_0)$ and the control surface both are devoid of discontinuities

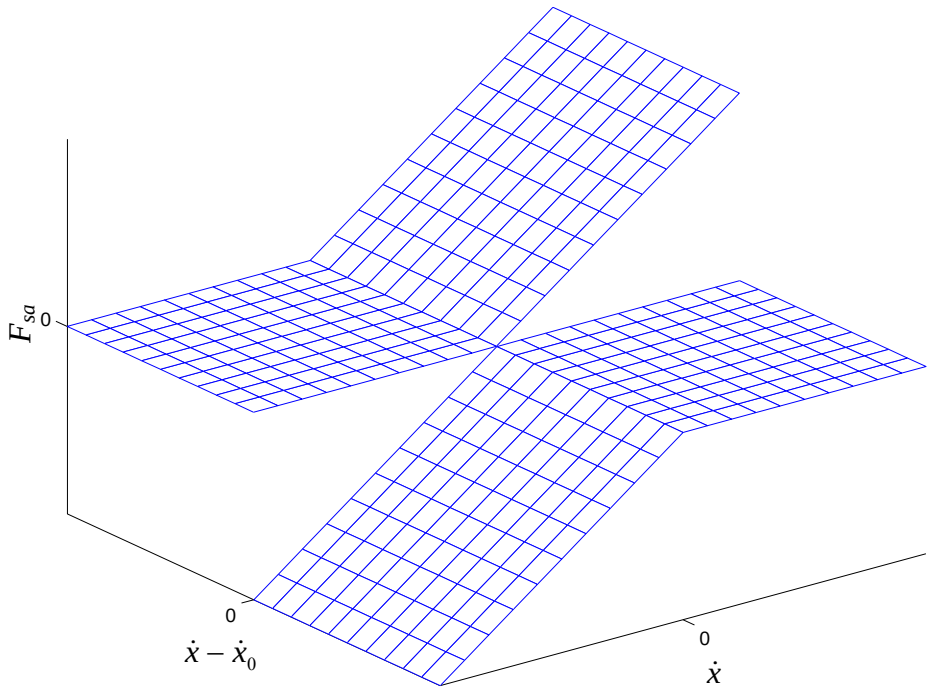

Figure 2.13 Three-dimensional control surface plot of desired force for continuous skyhook control (equation (2.8))

Three different shaping functions have been described in reference [51] for continuous skyhook control. The first one of interest has a shaping function given by

$$F(x-x_0,\dot{x},\dot{x}-\dot{x}_0)=\left|\dot{x}-\dot{x}_0\right| \tag{2.23}$$

For this shaping function the control strategy becomes:

$$F_{sa}=\begin{cases} G\cdot\left|\dot{x}-\dot{x}_0\right|\cdot\dot{x} & \dot{x}(\dot{x}-\dot{x}_0)\geq 0 \\ 0 & \dot{x}(\dot{x}-\dot{x}_0)<0 \end{cases} \tag{2.24}$$

where G is a gain factor, which has units of $N/(m/s)^2$.

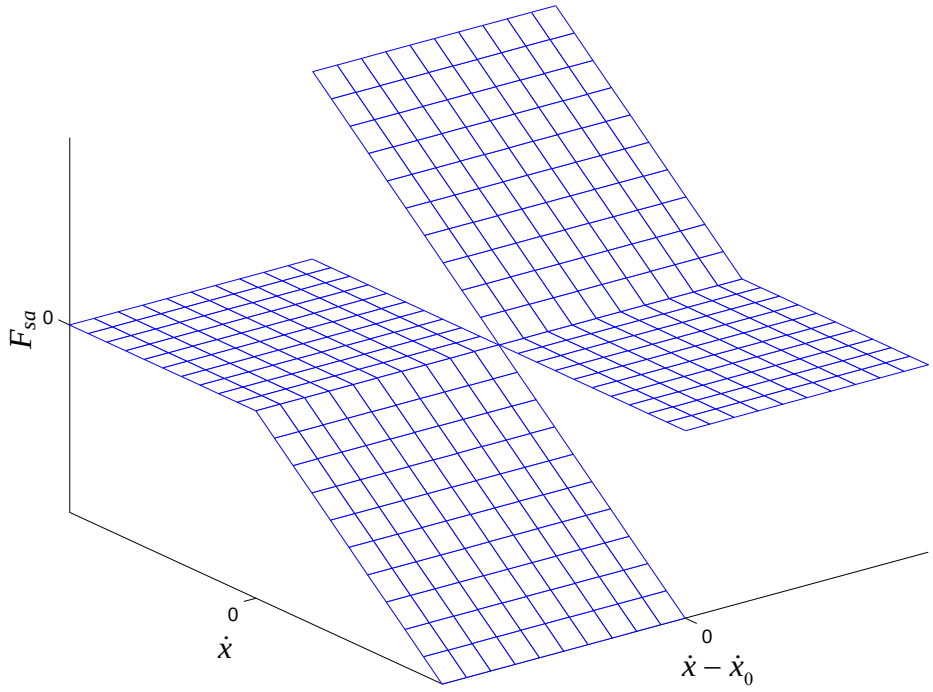

Figure 2.14 Three-dimensional control surface plot of desired force for on-off skyhook control (equation (2.11))

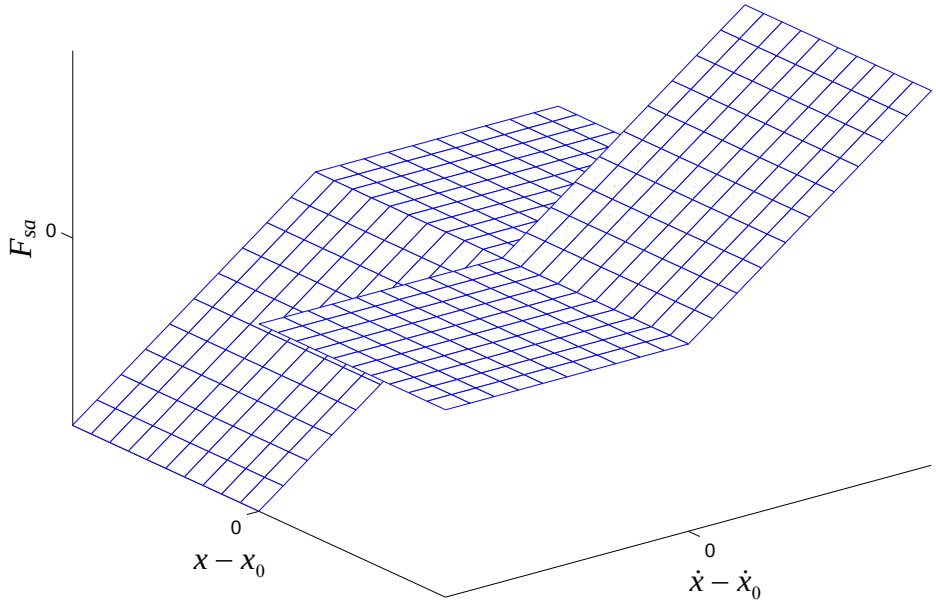

Figure 2.15 Three-dimensional control surface plot of desired force for on-off balance control (equation (2.17))

Figure 2.17 is a block diagram of the continuous skyhook control algorithm defined by equation (2.8). This control algorithm requires measurements of the velocity of the suspended mass, $\dot{x}$, and relative velocity, $\dot{x} - \dot{x}_0$ across the damper. $\dot{x}$ is scaled by a predefined damping coefficient c_{sky} to form the on-state desired damping force $c_{sky}\dot{x}$, which is the first input to the switch block. The second input to the switch block is the product of $\dot{x}$ and $\dot{x} - \dot{x}_0$, $\dot{x}(\dot{x} - \dot{x}_0)$, is tested in the switch block to decide whether the first input $c_{sky}\dot{x}$ or a zero constant force is passed through. If $\dot{x}(\dot{x} - \dot{x}_0) \geq 0$, then $c_{sky}\dot{x}$ is passed through, else, a constant zero force is passed through. Figure 2.18 is the block diagram of the proposed anti-jerk algorithm for continuous skyhook control. When compared with Figure 2.17 it can be found that the switching remains the same, but the on-state damping coefficient has been modified by the introduction of the shaping function.

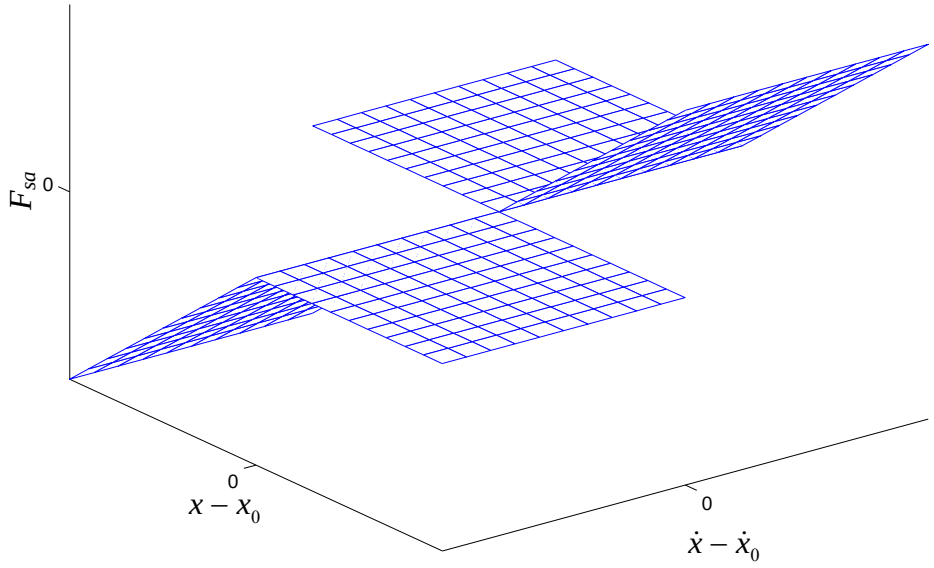

Figure 2.16 Three-dimensional control surface plot of desired force for continuous balance control (equation (2.19))

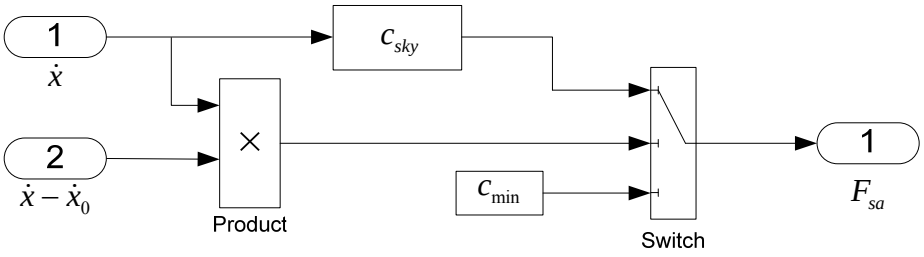

Figure 2.17 Block diagram of continuous skyhook control

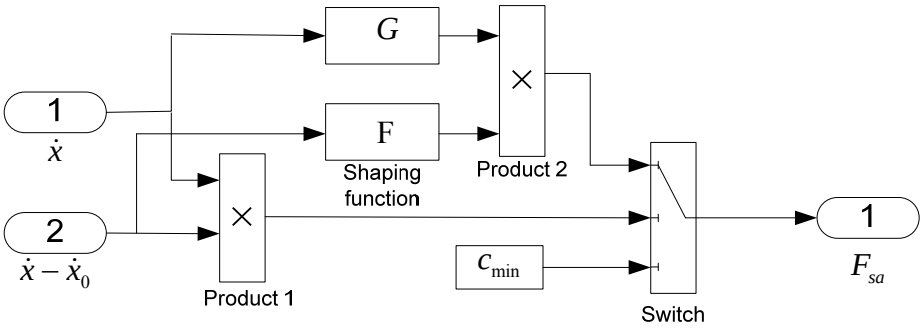

Figure 2.18 Block diagram of anti-jerk modification for continuous skyhook control

Figure 2.19 is the three-dimensional control surface plot showing the resulting control surface of the control algorithm described in equation (2.24). It can be seen that this control algorithm is devoid of any surface discontinuity at $\dot{x} - \dot{x}_0 = 0$ compared with Figure 2.13, thus it can reduce the acceleration jerk. This anti-jerk control method is used in the implementation of the semi-active control method in this thesis.

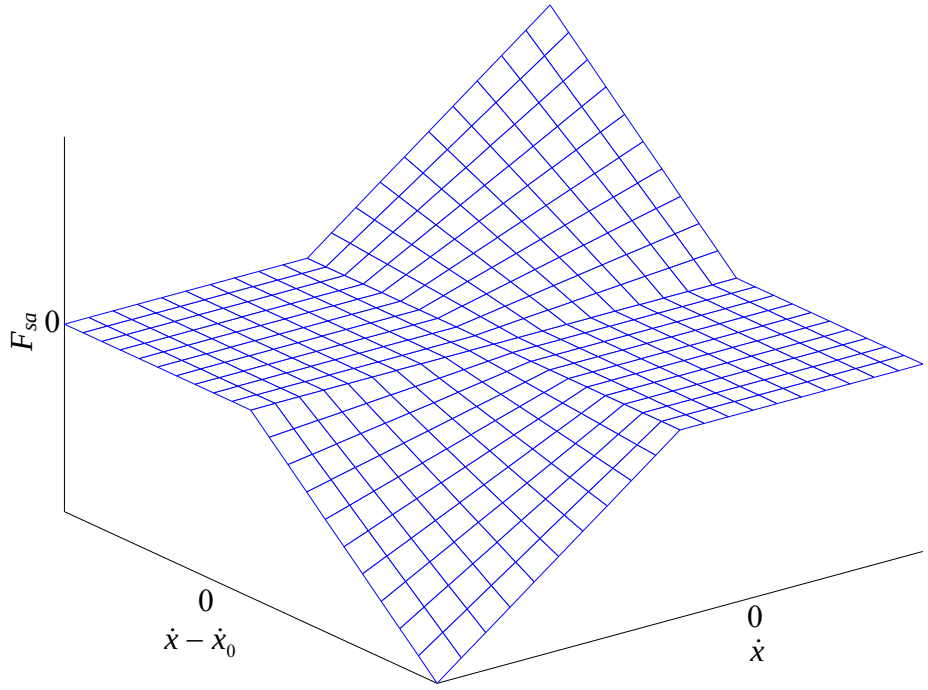

Figure 2.19 Three-dimensional control surface plot of desired damping force for continuous variable skyhook control with anti-jerk modification (equation (2.34))

2.6 CONTROLLER DEVELOPMENT

This section is concerned with the development of the semi-active control algorithms. Anti-jerk and limitations of practical hardware on achievable damping coefficient are considered. In the original control algorithms shown in Table 2.1, zero damping is assumed when the damper is switched off, which is not true in practice. When implementing the damping force required by each control algorithm in Table 2.1 using a conventional damper, which can only provide a damping force proportional to the relative velocity across it, there exists an upper and lower limit of the damping

coefficients, $c_{\max}$ and $c_{\min}$. Continuous skyhook control, on-off skyhook, continuous balance control, on-off balance control and adaptive damping control are employed. Each control algorithm is implemented using Matlab/Simulink.

2.6.1 CONTINUOUS SKYHOOK CONTROL

Recalling the anti-jerk method described in equation (2.24) which defining the damping force, and the control surface plot in Figure 2.19, the semi-active damping coefficient required can be derived as following

$$c_{sa} = \begin{cases} \dfrac{G \cdot |\dot{x} - \dot{x}_0| \cdot \dot{x}}{\dot{x} - \dot{x}_0} & \dot{x}(\dot{x} - \dot{x}_0) \geq 0 \\ 0 & \dot{x}(\dot{x} - \dot{x}_0) < 0 \end{cases} \tag{2.25}$$

Notice that the damper is switched to its on-state whenever $\dot{x}$ and $\dot{x} - \dot{x}_0$ have the same sign. When $\dot{x} - \dot{x}_0 \geq 0$, $\dot{x}$ also needs to be greater or equal to zero, thus

$$\frac{G \cdot |\dot{x} - \dot{x}_0| \cdot \dot{x}}{\dot{x} - \dot{x}_0} = G\dot{x} = G|\dot{x}| \quad \dot{x} \geq 0 \tag{2.26}$$

When $\dot{x} - \dot{x}_0 \leq 0$, $\dot{x} \leq 0$

$$\frac{G \cdot |\dot{x} - \dot{x}_0| \cdot \dot{x}}{\dot{x} - \dot{x}_0} = -G\dot{x} = G|\dot{x}| \quad \dot{x} \leq 0 \tag{2.27}$$

Following this discussion and taking into consideration the constraints of practical implementation, the following algorithm is proposed to implement the continuously variable skyhook control algorithm

$$c_{sa} = \begin{cases} \max\left[c_{\min}, \min\left[G|\dot{x}|, c_{\max} \right] \right] & \dot{x}(\dot{x} - \dot{x}_0) \geq 0 \\ c_{\min} & \dot{x}(\dot{x} - \dot{x}_0) < 0 \end{cases} \tag{2.28}$$

It can be seen from equation (2.28) that the semi-active damping coefficient c_{sa} is a function of the gain factor G, and velocity $\dot{x}$, which ensures that it has finite value and is proportional to $\dot{x}$. The maximum and minimum damping coefficients $c_{\max}$ and

$c_{\min}$ are applied as a constraint to semi-active damping. Figure 20 shows the control algorithm block diagram for the new controller defined by equation (2.28). If the product of $\dot{x}$ and $\dot{x}-\dot{x}_0$ is greater than or equal to zero, the damper force is proportional to $\dot{x}$; otherwise, the damper force has the minimum value.

2.6.2 ON-OFF SKYHOOK CONTROL

Recall that the algorithm defining the on-off skyhook damper in (2.11) is a simplified control algorithm to the continuously skyhook control. Using the anti-jerk method described in the previous section, the shaping function for this control algorithm can be chosen as

$$F(x-x_0,\dot{x},\dot{x}-\dot{x}_0)=|\dot{x}| \tag{2.29}$$

Correspondingly, the damping force is given by

$$F_{sa}=\begin{cases} G\cdot|\dot{x}|\cdot(\dot{x}-\dot{x}_0) & \dot{x}(\dot{x}-\dot{x}_0)\geq 0 \\ c_{\min}(\dot{x}-\dot{x}_0) & \dot{x}(\dot{x}-\dot{x}_0)<0 \end{cases} \tag{2.30}$$

and the damping coefficient can be written in the same form as in equation (2.28) for the continuously variable skyhook damper, i.e. this control algorithm is no longer on-off, but is continuously variable and identical to the anti-jerk control algorithm for continuous skyhook control after the anti-jerk modification. The control surface plot of equation (2.30) is the same as in Figure 2.19. One can see there are no surface discontinuities near $\dot{x}=0$ compared to Figure 2.14. The anti-jerk control algorithm block diagram for on-off skyhook controller is the same as in shown in Figure 2.20.

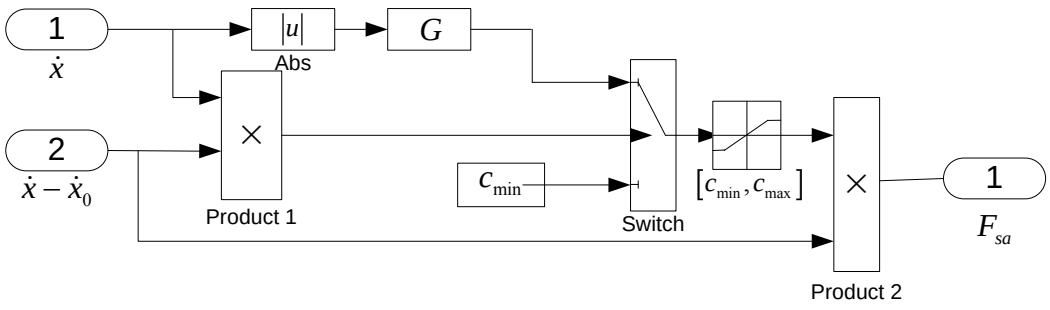

Figure 2.20 Block diagram of continuously skyhook control algorithm with anti-jerk modification

After the anti-jerk modification, both the on-off skyhook and continuous skyhook control can be implemented using the same control algorithm as described by equation (2.28). The gain factor G is introduced, which is related to c_{sky}. In the anti-jerk control algorithm, the semi-active damping force retains the same phase information as that of the desired skyhook damping force when in its on-states. However, the amplitude does not resemble that of the skyhook damping although the damping force is still related to the absolute velocity.

Although jerk might occur with the simple on-off skyhook control algorithm, it is much simpler and easier to implement since only two states of damping are assumed. Also, the effects of delays in the controller and mechanical components may suppress the occurrence of chatter. For these reasons, it is implemented numerically and studied in this thesis. Figure 2.21 shows the block diagram for on-off skyhook control algorithm without anti-jerk modification.

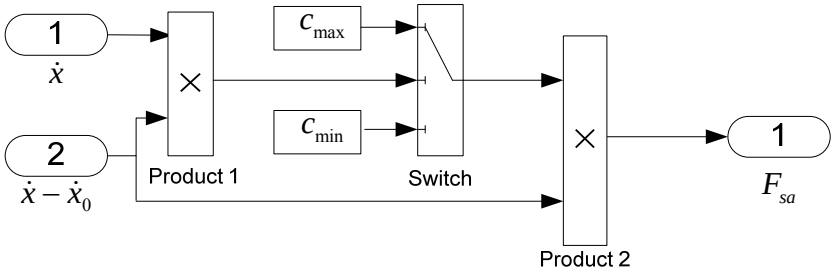

Figure 2.21 Block diagram of on-off skyhook control algorithm

2.6.3 ON-OFF BALANCE CONTROL

Recalling the on-off balance control algorithm defined by equation (2.18), the control surface exhibits discontinuities at $x-x_0=0$ as shown in Figure 2.15. The shaping function to avoid the control surface discontinuities is chosen as

$$F(x-x_0,\dot{x},\dot{x}-\dot{x}_0)=\left|x-x_0\right| \tag{2.31}$$

The damping force for this control algorithm is given by

$$F_{sa}=\begin{cases} G\cdot\left|x-x_0\right|\cdot(\dot{x}-\dot{x}_0) & (x-x_0)(\dot{x}-\dot{x}_0)\le 0 \\ c_{\min}(\dot{x}-\dot{x}_0) & (x-x_0)(\dot{x}-\dot{x}_0)>0 \end{cases} \tag{2.32}$$

Figure 2.22 shows the control surface plot of equation (2.32). The surface discontinuity at $x - x_0 = 0$ is therefore avoided by the introduction of the shaping function compared to Figure 15. The damping coefficient corresponding to equation (2.32) can be written as

$$c_{sa} = \begin{cases} \max\left[c_{\min}, \min\left[G\left|x - x_0\right|, c_{\max}\right]\right] & (x - x_0)(\dot{x} - \dot{x}_0) \le 0 \\ c_{\min} & (x - x_0)(\dot{x} - \dot{x}_0) > 0 \end{cases} \tag{2.33}$$

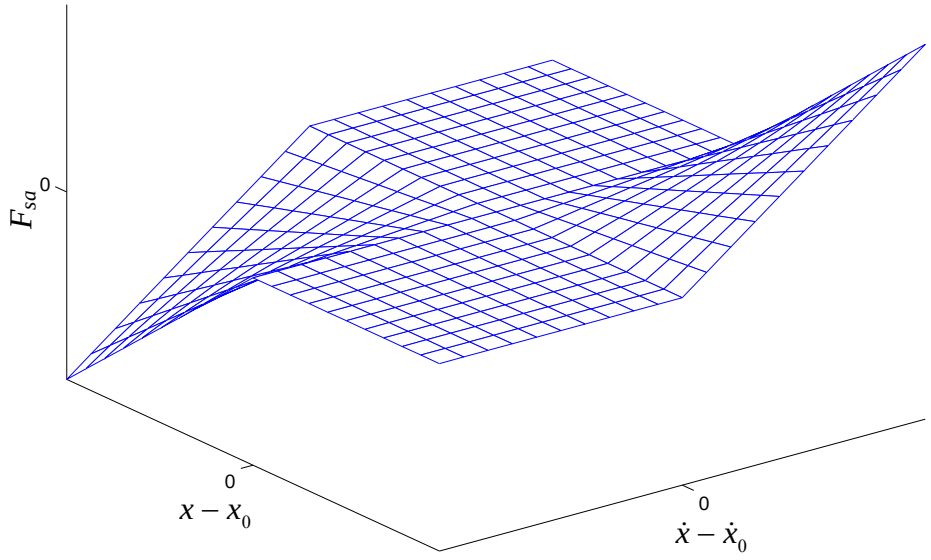

Figure 2.22 Three-dimensional control surface plot of desired damping force for on-off balance control with anti-jerk modification (equation (2.36))

As for the on-off skyhook control algorithm, the anti-jerk control algorithm defined by equation (2.33) for on-off balance control is no longer "on-off". The damping coefficient becomes continuously variable. Figure 2.23 shows the control algorithm block diagram for this controller. It will be used in the analysis of the vibration isolation performance of the semi-active damper, and it will be seen in section 3.4.4 that for the continuous balance control, the anti-jerk controller has the same form. For

the same reason given for the skyhook semi-active damper, the control algorithm described in equation (2.18) is much more simple and easy to implement since only two states of damping are assumed. It is also implemented numerically and studied in this report. The block diagram of the on-off balance control algorithm is defined by equation (2.18) is shown in Figure 2.24.

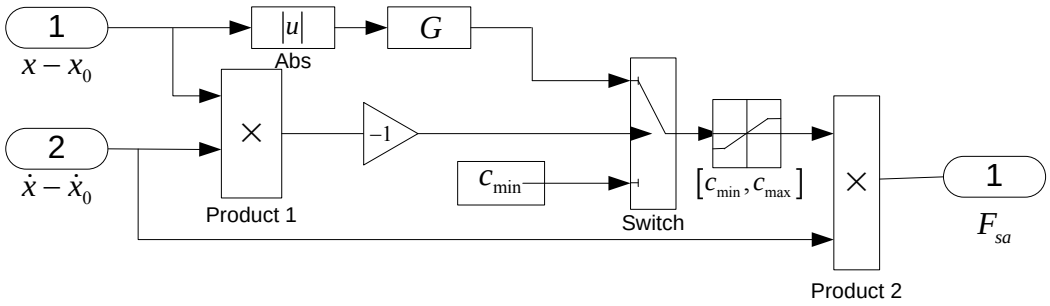

Figure 2.23 Block diagram of on-off balance control algorithm with anti-jerk modification (equation (2.36))

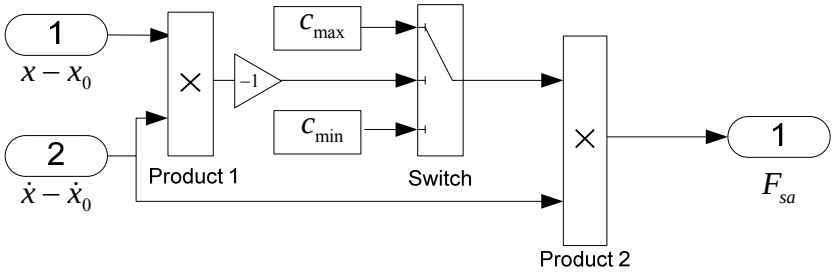

Figure 2.24 Block diagram of on-off balance algorithm without anti-jerk modification (equation (2.18))

2.6.4 CONTINUOUS BALANCE CONTROL

Recalling the algorithm defining the continuous balance control in equation (2.19), and as shown in Figure 2.16, there exists surface discontinuities at $\dot{x} - \dot{x} = 0$. When the anti-jerk control is used, the shaping function is chosen as

$$F(x - x_0, \dot{x}, \dot{x} - \dot{x}_0) = \left|\dot{x} - \dot{x}_0\right| \tag{2.34}$$

The damping force therefore can be written as

$$F_{sa} = \begin{cases} -G \cdot \left|\dot{x} - \dot{x}_0\right| \cdot (x - x_0) & (x - x_0)(\dot{x} - \dot{x}_0) \le 0 \\ c_{\min}(\dot{x} - \dot{x}_0) & (x - x_0)(\dot{x} - \dot{x}_0) > 0 \end{cases} \tag{2.35}$$

and the damping coefficient is given by

$$c_{sa} = \begin{cases} \dfrac{-G \cdot |\dot{x} - \dot{x}_0| \cdot (x - x_0)}{\dot{x} - \dot{x}_0} & (x - x_0)(\dot{x} - \dot{x}_0) \le 0 \\ c_{\min} & (x - x_0)(\dot{x} - \dot{x}_0) > 0 \end{cases} \tag{2.36}$$

The damper is switched to its on-state whenever $x - x_0$ and $\dot{x} - \dot{x}_0$ have different signs, i.e. when $\dot{x} - \dot{x}_0 \ge 0$, $x - x_0 \le 0$, we have

$$\frac{-G \cdot |\dot{x} - \dot{x}_0| \cdot (x - x_0)}{\dot{x} - \dot{x}_0} = -G(x - x_0) = G|x - x_0| (x - x_0 \le 0) \tag{2.37}$$

when $\dot{x} - \dot{x}_0 \le 0$, $x - x_0 \ge 0$

$$\frac{-G \cdot |\dot{x} - \dot{x}_0| \cdot (x - x_0)}{\dot{x} - \dot{x}_0} = G(x - x_0) = G|x - x_0| (x - x_0 \ge 0) \tag{2.38}$$

Thus the damping coefficient can be further simplified as the same form as in equation (2.33).

As with the two skyhook control algorithms, both on-off balance and continuous balance control algorithms share the same anti-jerk implementation algorithm as shown in equation (2.33). The gain factor G for balance control has the unit of $N/m^2/s$, which is different to the unit for skyhook control. The resulting semi-active damping force after anti-jerk modification has the opposite sign of the spring force when in the on-state, and it is proportional to the relative displacement, i.e. the damper is behaving in a spring-like manner.

2.6.5 ADAPTIVE-PASSIVE DAMPING CONTROL

For the adaptive damping control algorithm discussed in section 2.3.3, the damper works in a bi-state manner. It works as a common passive damper, which can be switched from one value to the other. Since the switch time can be chosen to be when the damping force equals zero, there is no jerk associated with this control algorithm.

The Matlab/Simulink model of a semi-active SDOF system is shown in Figure 2.25. Diagrams of semi-active control strategies can be used in the model to represent the semi-active damper.

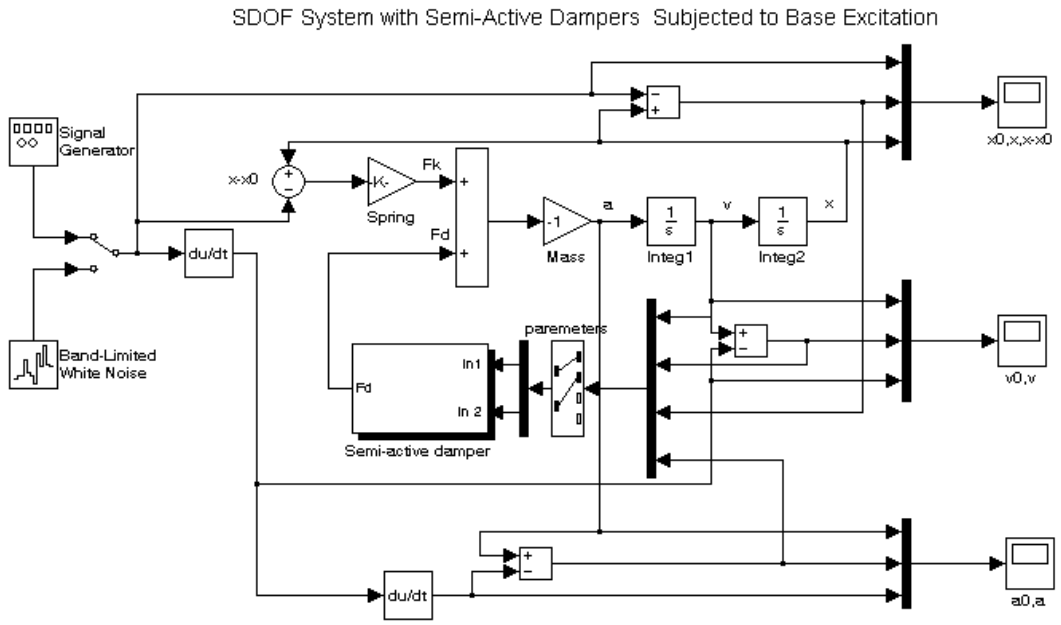

Figure 2.25 Matlab/Simulink model of a semi-active SDOF system

2.7 CONCLUSIONS

Details of four semi-active control strategies of interest and the adaptive-passive control strategy have been presented in this chapter. The original control algorithms and the theoretical semi-active damping coefficient required for the desired damping force discussed in this section are summarised in Table 2.4. Considering the constraints by the physical parameters of the conventional damper, the damping coefficient of the semi-active damper must lay in the range $[c_{\min,} c_{\max}]$. For the continuous skyhook control and continuous balance control, the denominator in the expressions of the damping equation will introduce high nonlinearity into the system.

Matlab/Simulink models for the four semi-active control algorithms are established for numerical simulations of semi-active dampers. Both chatter and jerk associated with the switches between on-state and off-states of a semi-active damper have been studied. Modified control strategies have been proposed to avoid chatter and anti-jerk control algorithms. As a summary, Table 2.5 lists the five control algorithms used in

chapter 3 to study the vibration isolation performance of semi-active dampers. The algorithms are referred to as SA-1 to SA-4, where SA denotes semi-active. It can be seen from the previous discussion that both the two skyhook semi-active dampers can be implemented by the same anti-jerk control strategy, which is referred to as SA-1 damper. A conventional on-off damper without anti-jerk is referred to as SA-2 damper. The anti-jerk implementation of the two balance control algorithms is referred to SA-3 damper. The simple on-off balance controlled damper is referred to as SA-4 damper. It should be pointed out that SA-2 and SA-4 are conventional on-off damper without anti-jerk treatment. Although they might cause jerk during operation, they are studied here since they are less complex and can provide comparison with anti-jerk control algorithms. Vibration isolation performance of a SDOF system comprising the four semi-active dampers together with the adaptive damping method is studied in the following chapters.

Table 2.4 Damping characteristics of a semi-active damper

Damper Type	Original Control Algorithm	Semi-Active Damping Required	Semi-Active Damping In Practice
Continuous skyhook	$F_{sa}=\begin{cases} c_{sky}\dot{x} & \dot{x}(\dot{x}-\dot{x}_0)\geq 0 \\ 0 & \dot{x}(\dot{x}-\dot{x}_0)<0 \end{cases}$	$c_{sa}=\begin{cases} \dfrac{c_{sky}\dot{x}}{\dot{x}-\dot{x}_0} & \dot{x}(\dot{x}-\dot{x}_0)\geq 0 \\ 0 & \dot{x}(\dot{x}-\dot{x}_0)<0 \end{cases}$	$c_{sa}=\begin{cases} \max\left[c_{\min},\min\left[\dfrac{c_{sky}\dot{x}}{\dot{x}-\dot{x}_0},c_{\max}\right]\right] & \dot{x}(\dot{x}-\dot{x}_0)\geq 0 \\ c_{\min} & \dot{x}(\dot{x}-\dot{x}_0)<0 \end{cases}$
On-off skyhook	$F_{sa}=\begin{cases} c_{on}(\dot{x}-\dot{x}_0) & \dot{x}(\dot{x}-\dot{x}_0)\geq 0 \\ 0 & \dot{x}(\dot{x}-\dot{x}_0)<0 \end{cases}$	$c_{sa}=\begin{cases} c_{on} & \dot{x}(\dot{x}-\dot{x}_0)\geq 0 \\ 0 & \dot{x}(\dot{x}-\dot{x}_0)<0 \end{cases}$	$c_{sa}=\begin{cases} c_{\max} & \dot{x}\left(\dot{x}-\dot{x}_0\right)\geq 0 \\ c_{\min} & \dot{x}\left(\dot{x}-\dot{x}_0\right)<0 \end{cases}$
On-off balance	$F_{sa}=\begin{cases} c_{on}(\dot{x}-\dot{x}_0) & (x-x_0)(\dot{x}-\dot{x}_0)\leq 0 \\ 0 & (x-x_0)(\dot{x}-\dot{x}_0)>0 \end{cases}$	$c_{sa}=\begin{cases} c_{on} & (x-x_0)(\dot{x}-\dot{x}_0)\leq 0 \\ 0 & (x-x_0)(\dot{x}-\dot{x}_0)>0 \end{cases}$	$c_{sa}=\begin{cases} c_{\max} & \left(x-x_0\right)\left(\dot{x}-\dot{x}_0\right)\leq 0 \\ c_{\min} & \left(x-x_0\right)\left(\dot{x}-\dot{x}_0\right)>0 \end{cases}$
Continuous balance	$F_{sa}=\begin{cases} -k(x-x_0) & (x-x_0)(\dot{x}-\dot{x}_0)\leq 0 \\ 0 & (x-x_0)(\dot{x}-\dot{x}_0)>0 \end{cases}$	$c_{sa}=\begin{cases} \dfrac{-k(x-x_0)}{\dot{x}-\dot{x}_0} & (x-x_0)(\dot{x}-\dot{x}_0)\leq 0 \\ 0 & (x-x_0)(\dot{x}-\dot{x}_0)>0 \end{cases}$	$c_{sa}=\begin{cases} \max\left[c_{\min},\min\left[\dfrac{-k(x-x_0)}{\dot{x}-\dot{x}_0},c_{\max}\right]\right] & (x-x_0)(\dot{x}-\dot{x}_0)\leq 0 \\ c_{\min} & (x-x_0)(\dot{x}-\dot{x}_0)>0 \end{cases}$
Adaptive damping	$F_{sa}=\begin{cases} c_{on}(\dot{x}-\dot{x}_0) & \mathrm{RMS}(\ddot{x})\geq RMS(\ddot{x}_0) \\ 0 & \mathrm{RMS}(\ddot{x})<RMS(\ddot{x}_0) \end{cases}$	$c_{sa}=\begin{cases} c_{on} & \mathrm{RMS}(\ddot{x})\geq RMS(\ddot{x}_0) \\ 0 & \mathrm{RMS}(\ddot{x})<RMS(\ddot{x}_0) \end{cases}$	$c_{sa}=\begin{cases} c_{\max} & \mathrm{RMS}(\ddot{x})\geq RMS(\ddot{x}_0) \\ c_{\min} & \mathrm{RMS}(\ddot{x})<RMS(\ddot{x}_0) \end{cases}$

Table 2.5 Anti-jerk control algorithms for semi-active damping control

Damper Type	Original Control Algorithm	Semi-Active Damping In Practice	Anti-jerk Implementation
Continuous skyhook	$F_{sa}=\begin{cases}c_{sky}\dot{x} & \dot{x}(\dot{x}-\dot{x}_0)\geq 0\\ 0 & \dot{x}(\dot{x}-\dot{x}_0)<0\end{cases}$	$c_{sa}=\begin{cases}\max\left[c_{\min},\min\left[\dfrac{c_{sky}\dot{x}}{\dot{x}-\dot{x}_0},c_{\max}\right]\right] & \dot{x}(\dot{x}-\dot{x}_0)\geq 0\\ c_{\min} & \dot{x}(\dot{x}-\dot{x}_0)<0\end{cases}$	$c_{sa}=\begin{cases}\max\left[c_{\min},\min\left[G\lvert\dot{x}\rvert,c_{\max}\right]\right] & \dot{x}(\dot{x}-\dot{x}_0)\geq 0\\ c_{\min} & \dot{x}(\dot{x}-\dot{x}_0)<0\end{cases}$ (SA-1)
On-off skyhook	$F_{sa}=\begin{cases}c_{on}(\dot{x}-\dot{x}_0) & \dot{x}(\dot{x}-\dot{x}_0)\geq 0\\ 0 & \dot{x}(\dot{x}-\dot{x}_0)<0\end{cases}$	$c_{sa}=\begin{cases}c_{\max} & \dot{x}(\dot{x}-\dot{x}_0)\geq 0\\ c_{\min} & \dot{x}(\dot{x}-\dot{x}_0)<0\end{cases}$ (SA-2)	
On-off balance	$F_{sa}=\begin{cases}c_{on}(\dot{x}-\dot{x}_0) & (x-x_0)(\dot{x}-\dot{x}_0)\leq 0\\ 0 & (x-x_0)(\dot{x}-\dot{x}_0)>0\end{cases}$	$c_{sa}=\begin{cases}c_{\max} & (x-x_0)(\dot{x}-\dot{x}_0)\leq 0\\ c_{\min} & (x-x_0)(\dot{x}-\dot{x}_0)>0\end{cases}$ (SA-4)	$c_{sa}=\begin{cases}\max\left[c_{\min},\min\left[G\lvert x-x_0\rvert,c_{\max}\right]\right] & (x-x_0)(\dot{x}-\dot{x}_0)\leq 0\\ c_{\min} & (x-x_0)(\dot{x}-\dot{x}_0)>0\end{cases}$ (SA-3)
Continuous balance	$F_{sa}=\begin{cases}-k(x-x_0) & (x-x_0)(\dot{x}-\dot{x}_0)\leq 0\\ 0 & (x-x_0)(\dot{x}-\dot{x}_0)>0\end{cases}$	$c_{sa}=\begin{cases}\max\left[c_{\min},\min\left[\dfrac{-k(x-x_0)}{\dot{x}-\dot{x}_0},c_{\max}\right]\right] & (x-x_0)(\dot{x}-\dot{x}_0)\leq 0\\ c_{\min} & (x-x_0)(\dot{x}-\dot{x}_0)>0\end{cases}$	
Adaptive damping	$F_{sa}=\begin{cases}c_{on}(\dot{x}-\dot{x}_0) & \mathrm{RMS}(\ddot{x})\geq RMS(\ddot{x}_0)\\ 0 & \mathrm{RMS}(\ddot{x})<RMS(\ddot{x}_0)\end{cases}$	$c_{sa}=\begin{cases}c_{\max} & \mathrm{RMS}(\ddot{x})\geq RMS(\ddot{x}_0)\\ c_{\min} & \mathrm{RMS}(\ddot{x})<RMS(\ddot{x}_0)\end{cases}$ (AP)	

CHAPTER 3

3. HARMONIC ANALYSIS OF SEMI-ACTIVE DAMPERS

3.1 INTRODUCTION

Chapter 2 described four basic control strategies for semi-active damping control which are based on skyhook control and balanced control. These semi-active control strategies combine a control algorithm together with a condition function. Chattering and jerk were identified as potential problems when using semi-active dampers due to abrupt changes of the damping force. Control algorithms with anti-chattering and anti-jerk implementation were proposed, and implemented in Matlab/Simulink. This chapter presents an evaluation of the performance and suitability of the four semi-active control algorithms for isolation of harmonic disturbances.

In this chapter numerical and experimental investigations of the isolation performance of the semi-active damping control strategies are described. A SDOF system incorporating a semi-active damper is used to study the isolation performance. The performance is evaluated in terms of Root-Mean-Square (RMS) acceleration transmissibility and relative displacement transmissibility. The implementation of the numerical simulations is first introduced. These are followed by an evaluation of each semi-active control algorithm. The vibration isolation performances of the semi-active system are compared with those of the conventional and skyhook passive damper systems. Experiments carried out to investigate the isolation performance of the on-off skyhook semi-active damper using an electromechanical damper are also presented. The chapter ends with comparison and critical comments on performance of the semi-active control strategies.

3.2 THE PERFORMANCE INDICES

The vibration isolation performance of a SDOF system with a semi-active damper due to harmonic excitation is evaluated in terms of the following response parameters:

Absolute Acceleration Transmissibility. Previous researchers have used displacement transmissibility to characterise isolator performance [17, 67, 68]. In practical applications, since the human body or suspended mass is sensitive to inertial forces, the characterisation in terms of acceleration may be more appropriate [4, 24]. Since the system with a semi-active damper is nonlinear with step changes in damper force, the acceleration response due to a harmonic input will not be harmonic. Thus the ratio of the RMS value of the acceleration response to the RMS value of the excitation acceleration is chosen as a performance index to evaluate the vibration isolation performance. The acceleration transmissibility is defined by

$$T_{\ddot{x}} = \frac{RMS(\ddot{x})}{RMS(\ddot{x}_0)} \qquad \text{Equation Section 3}(3.1)$$

Relative Displacement Transmissibility. The relative transmissibility is a measure of the clearance required in an isolator, which usually includes a spring and a damper in parallel. It is defined as the ratio of the RMS value of relative displacement between the mass and the base to the RMS value of the displacement of the base, and is given by

$$T_{x-x_0} = \frac{RMS(x-x_0)}{RMS(x_0)} \qquad (3.2)$$

3.3 MODEL DEVELOPMENT AND SOLUTION PROCEDURES

3.3.1 MODEL FORMULATION

The base excitation used for numerical simulations takes the form

$$\ddot{x}_0 = \ddot{X}_0 \,\mathrm{Re}(e^{i\omega t}) \qquad (3.3)$$

where ω is the excitation frequency and $\ddot{X}_0$ is the amplitude of the acceleration excitation. All the simulations are run in the time-domain with discrete frequency excitation over a range from $0.5\omega_n$ to $10\omega_n$, where ω_n is the natural frequency of the system.

The equation of motion for a base excited SDOF system with a conventional viscous damper of variable damping coefficient can be generalised as

$$m\ddot{x}(t) + c(t)\left(\dot{x}(t) - \dot{x}_0(t)\right) + k\left(x(t) - x_0(t)\right) = 0 \tag{3.4}$$

where $c(t)$ is the damping coefficient of the system, which is assumed to vary with time. The damping coefficient for different types of dampers of interest are defined as follows:

Conventional passive damper: $c(t) = c_{pass}$

Skyhook damper: $c(t) = c_{sky}$

Adaptive-passive damper: $c(t) = \begin{cases} c_{\max} & \text{RMS}(\ddot{x}) \geq RMS(\ddot{x}_0) \\ c_{\min} & \text{RMS}(\ddot{x}) < RMS(\ddot{x}_0) \end{cases}$

SA-1 damper: $c(t) = \begin{cases} \max\left[c_{\min}, \min\left[G|\dot{x}|, c_{\max} \right] \right] & \dot{x}(\dot{x} - \dot{x}_0) \geq 0 \\ c_{\min} & \dot{x}(\dot{x} - \dot{x}_0) < 0 \end{cases}$

SA-2 damper: $c(t) = \begin{cases} c_{\max} & \dot{x}\left(\dot{x} - \dot{x}_0\right) \geq 0 \\ c_{\min} & \dot{x}\left(\dot{x} - \dot{x}_0\right) < 0 \end{cases}$

SA-3 damper: $c(t) = \begin{cases} \max\left[c_{\min}, \min\left[G|x - x_0|, c_{\max} \right] \right] & (x - x_0)(\dot{x} - \dot{x}_0) \leq 0 \\ c_{\min} & (x - x_0)(\dot{x} - \dot{x}_0) > 0 \end{cases}$

SA-4 damper: $c(t) = \begin{cases} c_{\max} & \left(x - x_0\right)\left(\dot{x} - \dot{x}_0\right) \leq 0 \\ c_{\min} & \left(x - x_0\right)\left(\dot{x} - \dot{x}_0\right) > 0 \end{cases}$ (3.5)

It can be seen from equation (3.5) that the damping coefficients for the conventional and skyhook passive damper are constant. But, the damping coefficient is time varying for the adaptive-passive damper and semi-active damper.

For the conventional and skyhook passive system, analytical solutions to equation of motion based on equation (3.4) are available. However, for semi-active systems, analytical solutions are not possible since the damping coefficient of the system is time varying. Instead, numerical simulations were carried out for this study. This section describes the solution procedures deployed. The results are presented in terms of the acceleration transmissibility, as defined in equation (3.1) although it should be noted that for a nonlinear system this is not equal to the velocity or displacement transmissibility as it would be for a linear system.

Consider a SDOF system with a semi-active damper as shown in Figure 3.1. The equation of motion describing this system can be written as

$$m\ddot{x}(t)+c_{sa}(t)\left(\dot{x}(t)-\dot{x}_0(t)\right)+k\left(x(t)-x_0(t)\right)=0 \tag{3.6}$$

where c_{sa} is the damping coefficient of the semi-active damper and is defined for various control strategies as defined in equation (3.5).

Equation (3.6) is solved to establish the vibration isolation performance of harmonic disturbances. The response of the system can be obtained by directly integrating Equation (3.6). The fourth order Runge-Kutta method was chosen to integrate the differential equation.

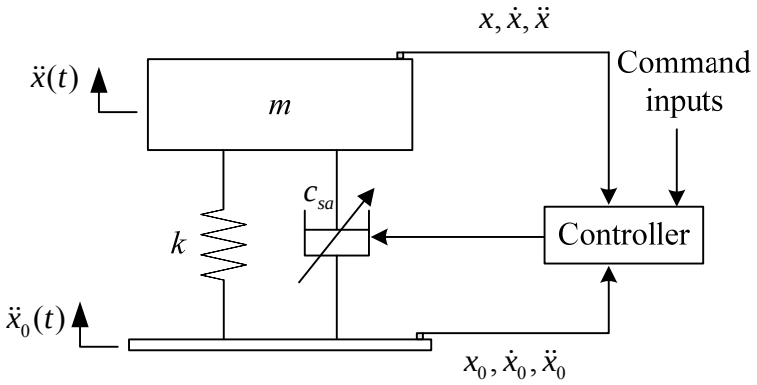

Figure 3.1 Schematic of a SDOF system with a semi-active damper

Numerical models of the semi-active SDOF systems subjected to base excitation have been established in Matlab/Simulink to carry out numerical simulations. Figure 3.2 shows the Matlab/Simulink model for the simulation. The model comprises four parts. The first one is the signal generator, which produces the excitation input into the system. The second part is the representation of the system and the third part is the semi-active controller, which produces the damper force according to different control strategies. The semi-active damper block in the model can be programmed to any control algorithm in principle. In this study, the block diagrams shown in Figures 2.10-2.14 can be inserted into this part to program a desired semi-active damping force. The last part is the displaying and the post processing the results according to the performance indices defined in section 3.2.

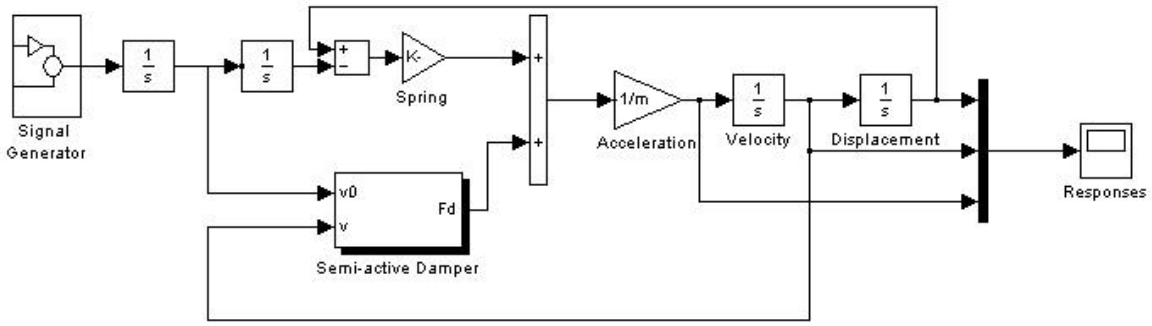

Figure 3.2 Matlab/Simulink model of a semi-active SDOF system

3.3.2 SOLUTION PROCEDURES

The organisation of the solution procedures for simulation is shown in the flow chart of Figure 3.3. As detailed in this flow chart, the procedure begins with a definition of the constants of the system parameters. Next, the initial conditions (all zero for this study) and inputs of the system are assigned. The time step for each iteration and final time of the process are now defined, setting the total number of iterations to be performed by the calculation loop of the procedure. The first part of the calculation loop determines the damping coefficient of the semi-active damper. If passive damping is applied, the damper is set to a constant, not changing within the loop. If semi-active damping is applied, the relevant control algorithm is used to calculate the current damper value based on the control algorithm applied. Once the damping values have been determined, the definition of all components of the model will be completed.

The next stage is calculating the responses of the system from the differential equation. This computation is performed using fourth order Runge-Kutta method since it does not require explicitly derivatives beyond the first [11]. For the solution of a second order differential equation, we first reduce it to two first order equations. Equation (3.6) can be rewritten as

$$\ddot{x} = \frac{1}{m}\left[(kx_0 + c\dot{x}_0) - (kx + c\dot{x})\right] = f(x, \dot{x}, t) \tag{3.7}$$

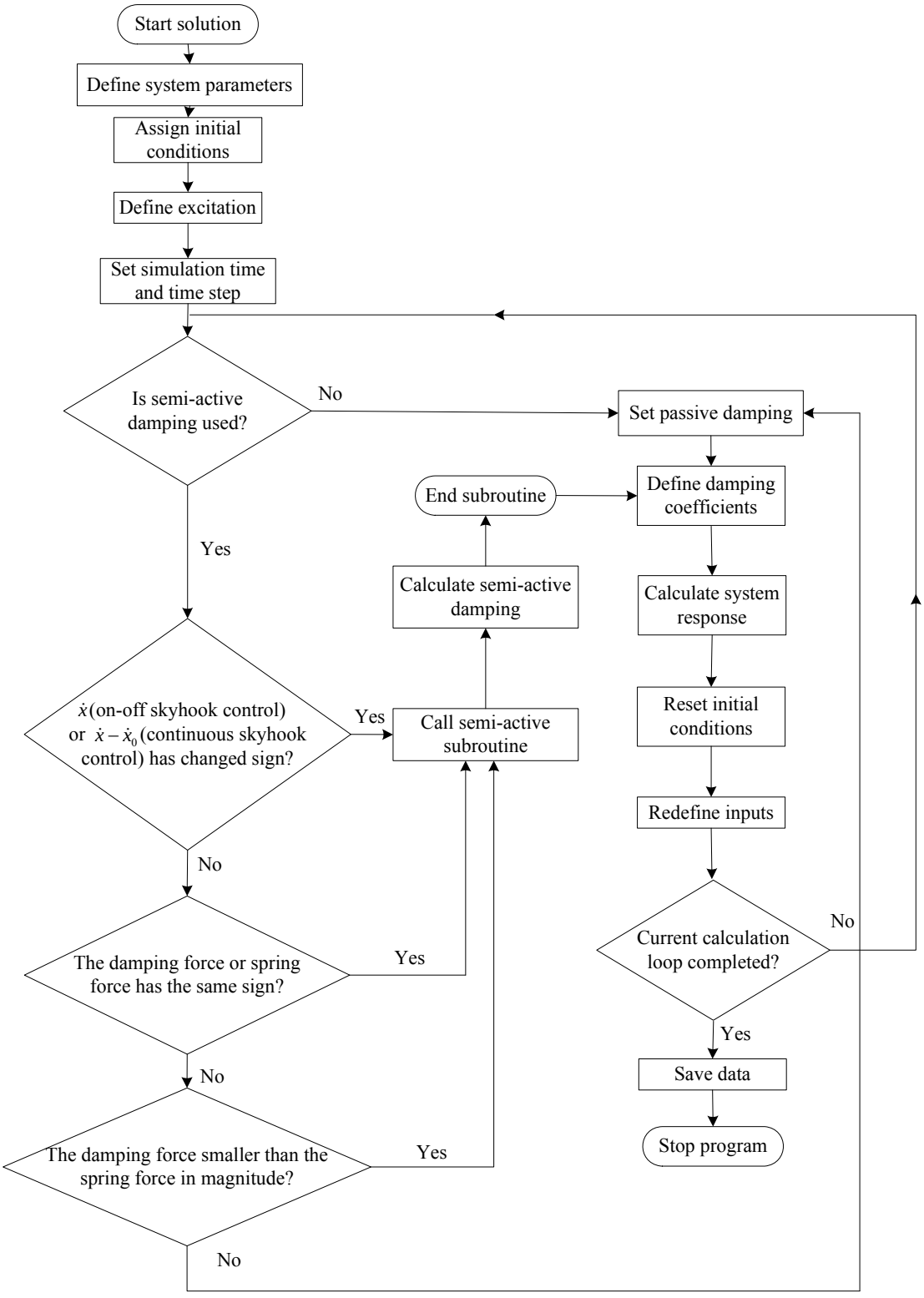

Figure 3.3 Flow chart of the solution procedure

By defining $x_1 = x$ and $x_2 = \dot{x}$, the above second order differential equation can be written as two first order equations

$$\begin{aligned} \dot{x}_1 &= x_2 \\ \dot{x}_2 &= f(x_1, x_2, t) \end{aligned} \tag{3.8}$$

By defining

$$\mathbf{x}(t) = \begin{Bmatrix} x_1 \\ x_2 \end{Bmatrix} \quad \text{and} \quad \mathbf{f}(\mathrm{t}) = \begin{Bmatrix} x_2 \\ f(x_1, x_2, t) \end{Bmatrix} \tag{3.9}$$

So

$$\dot{\mathbf{x}}(t) = \mathbf{f}(t) \tag{3.10}$$

The following recurrence formula is used to find the values of $\mathbf{x}(t)$ at different times t_i according to the fourth order Runge-Kutta method

$$\mathbf{x}(t+\tau) = \mathbf{x}(t) + \tau[\mathbf{k}_1 + 2\mathbf{k}_2 + 2\mathbf{k}_3 + \mathbf{k}_4]/6 \tag{3.11}$$

$$\begin{aligned} \mathbf{k}_1 &= \mathbf{f}(\mathbf{x}, t) \\ \mathbf{k}_2 &= \mathbf{f}(\mathbf{x} + 0.5\tau\mathbf{k}_1, t + 0.5\tau) \\ \mathbf{k}_3 &= \mathbf{f}(\mathbf{x} + 0.5\tau\mathbf{k}_2, t + 0.5\tau) \\ \mathbf{k}_4 &= \mathbf{f}(\mathbf{x} + \tau\mathbf{k}_1, t + \tau) \end{aligned} \tag{3.12}$$

where τ is the integration time step. In the simulation, τ is chosen by error and trial, which checks for the convergence of the results.

The next iteration is now ready to be calculated, continuing for a predefined number of iterations. The number of iterations for this thesis was chosen so that steady-state was reached.

It can be seen from equation (3.5) that the performance of the semi-active dampers depend on the gain factor G and the minimum and maximum damping coefficients $c_{\min}$ and $c_{\max}$. For a given system, there is a maximum value of the damping term $G|\dot{x}|$ for SA-1 damper and $G|x - x_0|$ for SA-3 damper if G is set to a constant. To make a relatively "fair" comparison between different types of dampers, a trial and error method is used to select G such that the equivalent damping ratio corresponding

to the maximum value of $G|\dot{x}|$ or $G|x-x_0|$ is equal to $0.25, 0.5, 0.707, 1$ for each control algorithm.

The results presented in this section are based on the assumption that the off-state damping, $c_{\min}=0$. However, it may not be possible to achieve a damping coefficient of zero when working with actual hardware. Therefore the semi-active damping coefficients will actually be switched to a lower value. To achieve the desired performance, the lower value of the off-state damping coefficient should be as low as physically practical. The performance of the semi-active control strategy will be slightly degraded from the ideal theoretical performance due to the non-zero off-state damping coefficient. This has been pointed out in reference [55] and will be studied in this chapter.

3.4 CONVENTIONAL AND SKYHOOK PASSIVE DAMPER

This section discusses the vibration isolation performance of a SDOF with a conventional passive and skyhook passive damper. The analytical solutions for these systems are provided and isolation characteristics are identified, which provide a benchmark against which to evaluate the performance of semi-active control strategies.

3.4.1 CONVENTIONAL PASSIVE DAMPER

A SDOF system with a conventional passive damper subjected to base excitation is shown in Figure 3.4. It consists of a spring and a viscous damper. The differential equation describing the motion of the passive system can be written as

$$m\ddot{x} + c_{pass}(\dot{x} - \dot{x}_0) + k(x - x_0) = 0 \tag{3.13}$$

where m is the mass of the system, c_{pass} is the damping coefficient, k is the stiffness of the spring, x is instantaneous displacement of the mass, and x_0 is the instantaneous displacement of the base. Defining the damping ratio $\zeta = c/2m\omega_n$, natural frequency $\omega_n = \sqrt{k/m}$, equation (3.13) becomes

$$\ddot{x} + 2\zeta\omega_n\dot{x} + \omega_n{}^2 x = 2\zeta\omega_n\dot{x}_0 + \omega_n{}^2 x_0 \tag{3.14}$$

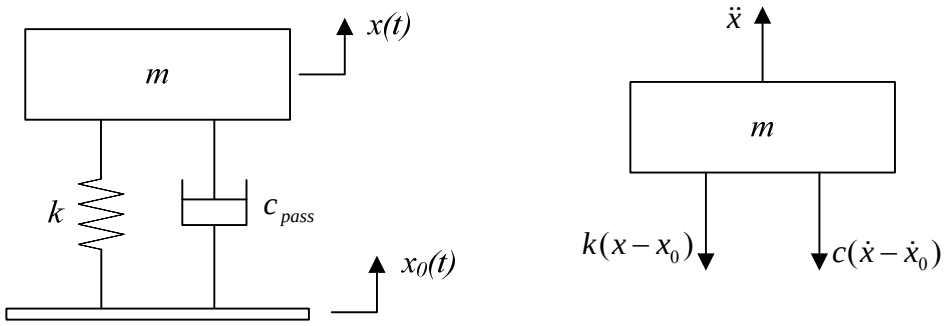

Figure 3.4 Schematic of a SDOF system with a conventional passive damper

Vibration isolation can be characterised by absolute acceleration transmissibility and relative displacement transmissibility as defined previous in Section 3.3. Since the system is linear, it does not matter whether acceleration or displacement transmissibility is used. For a conventional passive SDOF system, the absolute transmissibility is given by [11]

$$T_{\ddot{x}} = \left|\frac{\ddot{X}}{\ddot{X}_0}\right| = \frac{\sqrt{1+\left(2\zeta\dfrac{\omega}{\omega_n}\right)^2}}{\sqrt{\left[1-\left(\dfrac{\omega}{\omega_n}\right)^2\right]^2+\left[2\zeta\dfrac{\omega}{\omega_n}\right]^2}} \tag{3.15}$$

and the relative transmissibility can be expressed as

$$T_{x-x_0} = \left|\frac{X - X_0}{X_0}\right| = \frac{\left(\dfrac{\omega}{\omega_n}\right)^2}{\sqrt{\left[1-\left(\dfrac{\omega}{\omega_n}\right)^2\right]^2+\left[2\zeta\dfrac{\omega}{\omega_n}\right]^2}} \tag{3.16}$$

The acceleration and relative displacement transmissibility are shown in Figures 3.5 (a) and (b) respectively. In general, Figure 3.5(a) indicates attenuation of excitation at frequencies $\omega > \sqrt{2}\omega_n$, amplification at frequencies near resonance and almost unity at low frequencies $\omega < 0.3\omega_n$. The isolation region can be extended by decreasing the

spring stiffness, k, or by increasing the mass m. Since the mass is usually predetermined, the designer selects k to yield the desired natural frequency.

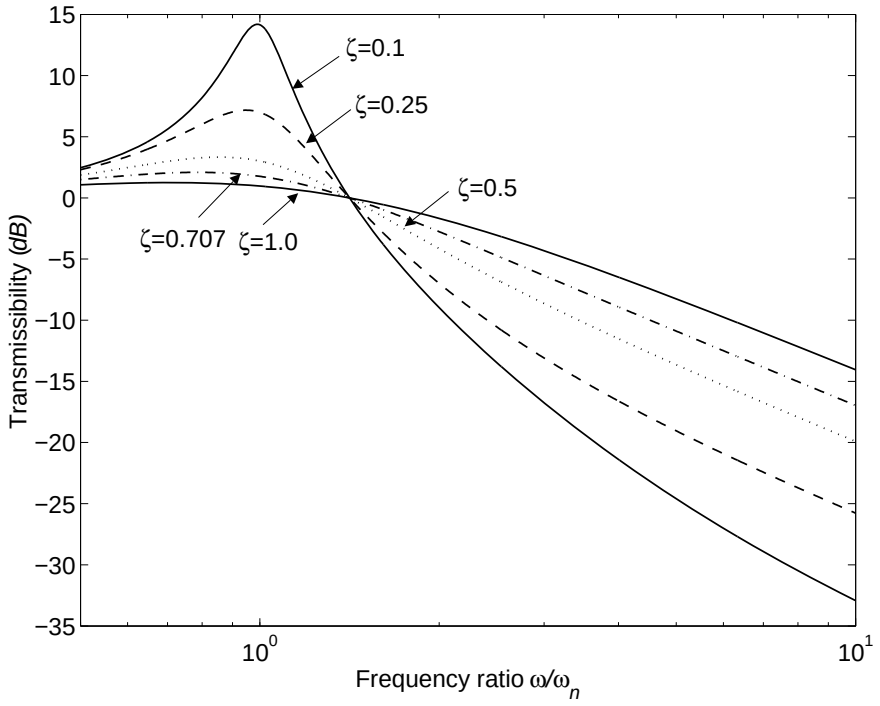

(a)

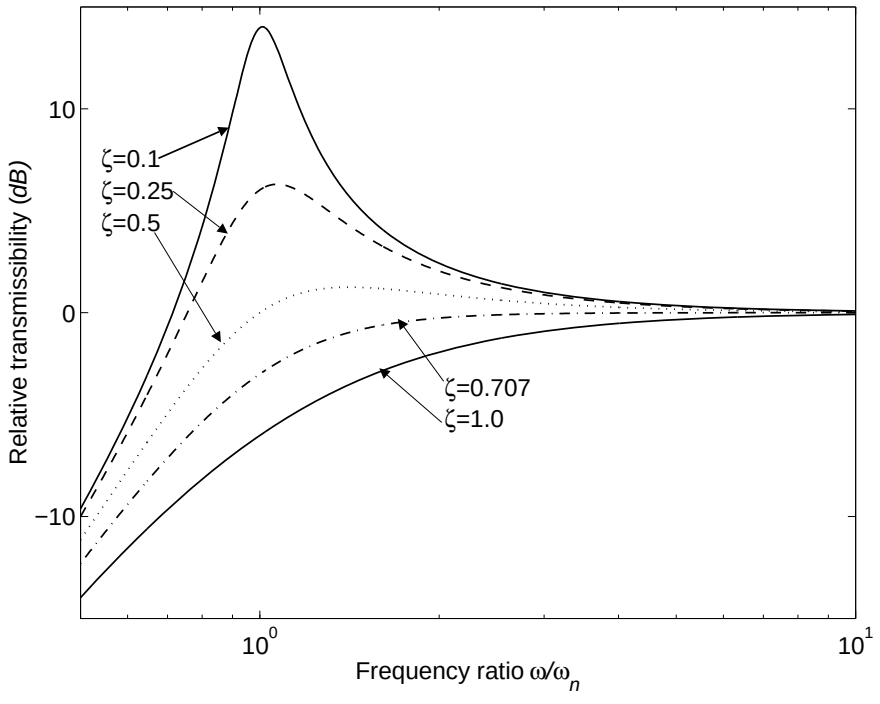

(b)

Figure 3.5 Transmissibility of a conventional passive SDOF system (a) absolute transmissibility; (b) relative transmissibility

Control of the resonant amplitude is achieved by the damper. This reduction is accompanied by decreased isolation above the resonance frequency in the isolation region. Increasing damping reduces the resonance response, but it increases transmissibility in the isolation range $\omega/\omega_n \geq \sqrt{2}$. If no damping were present, the transmissibility at resonance would be infinite. The high frequency transmissibility in this case would be asymptotic to a slope of $-40dB/\text{decade}$, giving superior isolation there. This represents the well-known compromise between better control at resonance and poor vibration isolation at high frequencies due to fixed damping. Studying the relative displacement transmissibility curves in Figure 3.5(b), it can be seen that a higher value of damping gives lower values of relative displacement transmissibility at all frequencies.

3.4.2 SKYHOOK PASSIVE DAMPER

The equation of motion for a SDOF system with a skyhook damper can be written as [15]

$$m\ddot{x} + c_{sky}\dot{x} + k(x - x_0) = 0 \tag{3.17}$$

where c_{sky} is the damping coefficient of the skyhook damper.

The above equation leads to the equation of motion of the mass as

$$\ddot{x} + 2\zeta\omega_n\dot{x} + \omega_n^2(x - x_0) = 0 \tag{3.18}$$

The transmissibility of the SDOF system with a skyhook damper is given by

$$T_{\ddot{x}} = \frac{1}{\sqrt{\left[1 - \left(\frac{\omega}{\omega_n}\right)^2\right]^2 + \left[2\zeta\frac{\omega}{\omega_n}\right]^2}} \tag{3.19}$$

and the relative transmissibility is

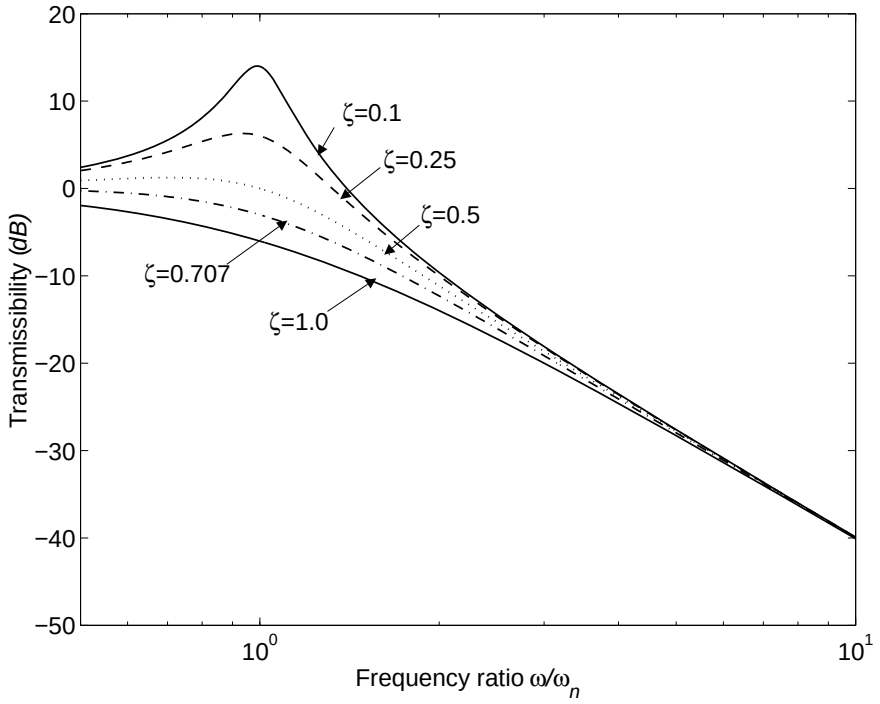

(a)

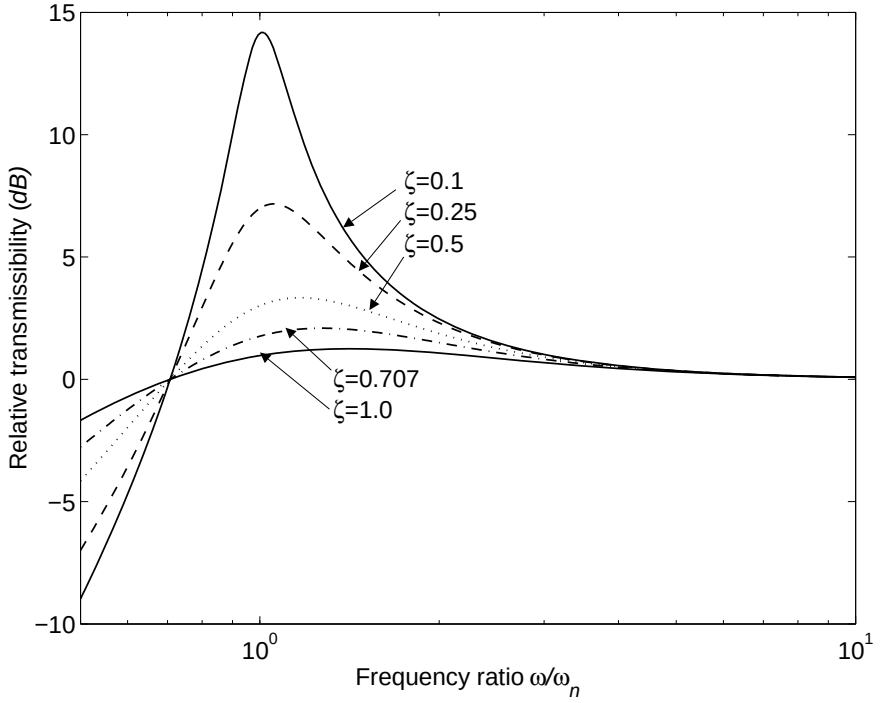

(b)

Figure 3.6 Transmissibility of a skyhook SDOF system (a) absolute transmissibility; (b) relative transmissibility

$$T_{x-x_0} = \frac{\sqrt{\left(\frac{\omega}{\omega_n}\right)^4 + \left(2\zeta\frac{\omega}{\omega_n}\right)^2}}{\sqrt{\left[1-\left(\frac{\omega}{\omega_n}\right)^2\right]^2 + \left[2\zeta\frac{\omega}{\omega_n}\right]^2}} \tag{3.20}$$

The transmissibility and relative transmissibility of a SDOF system with a skyhook damper are shown Figures 3.6 (a) and (b). From Figure 3.6 (a) it can be seen that the compromise between resonance control and isolation that is inherent in conventional passive system does not exist for the skyhook system. Increasing the damping reduces both the resonance response and the transmissibility in the isolation range. Studying the relative displacement transmissibility curves in Figure 3.6 (b), it can be seen that an increase in damping leads to smaller relative displacement transmissibility for a skyhook damper at frequencies $\omega/\omega_n = 1/\sqrt{2}$. The cross over point for the relative transmissibility curves in Figure 3.6 (b) is $1/\sqrt{2}$.

3.5 SEMI-ACTIVE DAMPERS

This section concerns the vibration isolation performance analysis of the four semi-active dampers and the adaptive-passive damper defined in equation (3.5). Numerical simulations are presented and the results are compared with those of the conventional and skyhook passive damper.

3.5.1 ADAPTIVE-PASSIVE (AP) DAMPER

Figures 3.7 (a) and (b) show the RMS acceleration and relative displacement transmissibility respectively for a SDOF system with an adaptive-passive damper. It can be seen from the two figures that the response of the AP system is identical to the passive system with the damping ratio $\zeta = \zeta_{\max}$ at frequencies $\omega/\omega_n \le \sqrt{2}$, and the response is identical to the undamped passive system at frequencies $\omega/\omega_n > \sqrt{2}$. The control of vibration at resonance is achieved by the on-state damping ratio $\zeta_{\max}$, while higher frequency isolation maintains $40dB/\text{decade}$. It retains the best performance of the undamped passive system. Studying Figure 3.7 (b) , it can be seen that the relative displacement transmissibility of the AP system is independent of the on-state damping

$\zeta_{\max}$ at frequencies $\omega/\omega_n > \sqrt{2}$, where the transmissibility is the same as a passive system with zero damping. The AP control algorithm makes the relative displacement worse beyond a frequency ratio of $\sqrt{2}$.

3.5.2 SA-1 SEMI-ACTIVE DAMPER

Figures 3.8 (a), (b) and (c) show the time history plot of the damping force, the condition function and the acceleration response with $G = 185$ for the SA-1 semi-active damper. The SA-1 control strategy is the anti-jerk implementation of the continuous skyhook control strategy, whose condition function is given in section 2.6.1. The plots in Figures 3.8 (a) to (c) correspond to the normalised frequency ratio of $\omega/\omega_n = 0.5$, 1.0 and 3.0. The system was allowed to run until steady state was reached although only the last few cycles are plotted in the figures. The plots of damping force versus time suggest that the damper is switched off for longer durations at higher frequencies. The acceleration plots show somewhat non harmonic response due to the nonlinear force generated by the semi-active damper. When $\omega/\omega_n = 3.0$ as shown in Figure 3.8(c), the acceleration plot shows significant attenuation of the base-induced acceleration disturbance.

The RMS acceleration transmissibility and RMS relative displacement transmissibility of SA-1 system to various gains G under the same maximum damping $c_{\max}$, are shown in Figures 3.9 (a) and (b). As shown in Figure 3.9 (a), increasing G improves the RMS acceleration transmissibility without worsening the high frequency isolation. For a higher G, isolation can be obtained for frequencies at and below the natural frequency of the system. Furthermore, the high frequency performance was superior to a conventional passive damper. There is no compromise between resonance control and high frequency isolation. The attenuation of base disturbances at and below resonance is achieved without reducing the spring rate, which is favourable from a static deflection point of view. However, there are limits to the performance improvement. It was noted by Karnopp [15] that as $G \to \infty$, the high frequency performance approached that of a skyhook system with $\omega_n = 0.6\sqrt{k/m}$ and $\zeta = 1.0$.

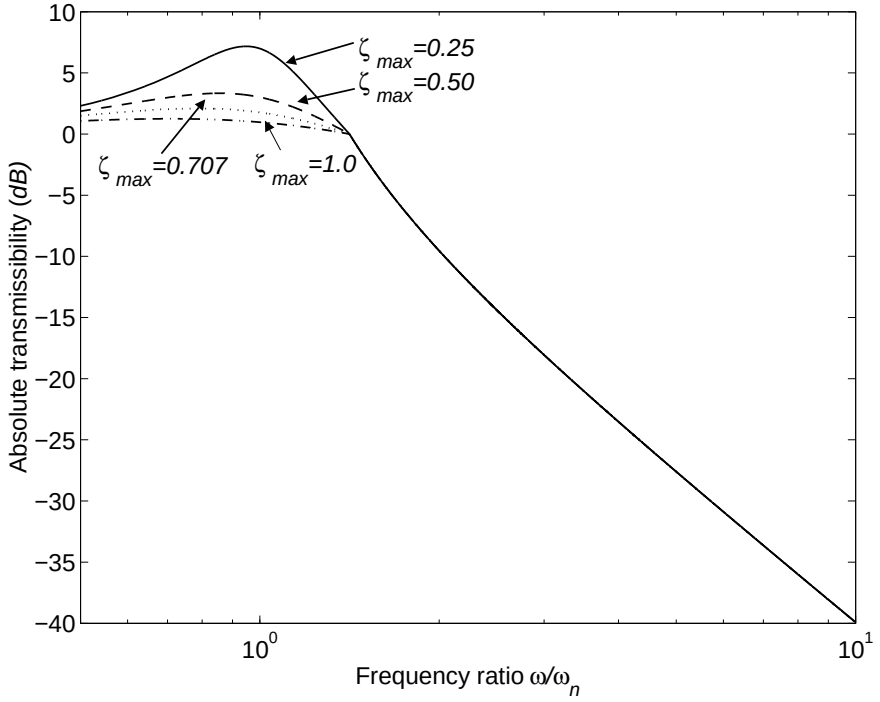

(a)

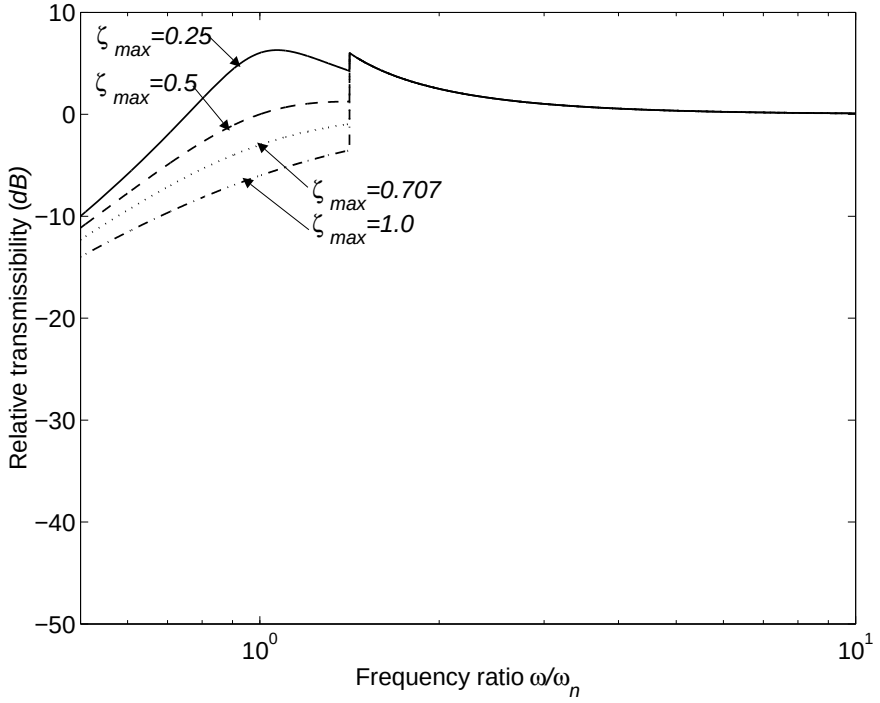

(b)

Figure 3.7 Transmissibility of an adaptive-passive damper system: (a) acceleration; (b) relative displacement

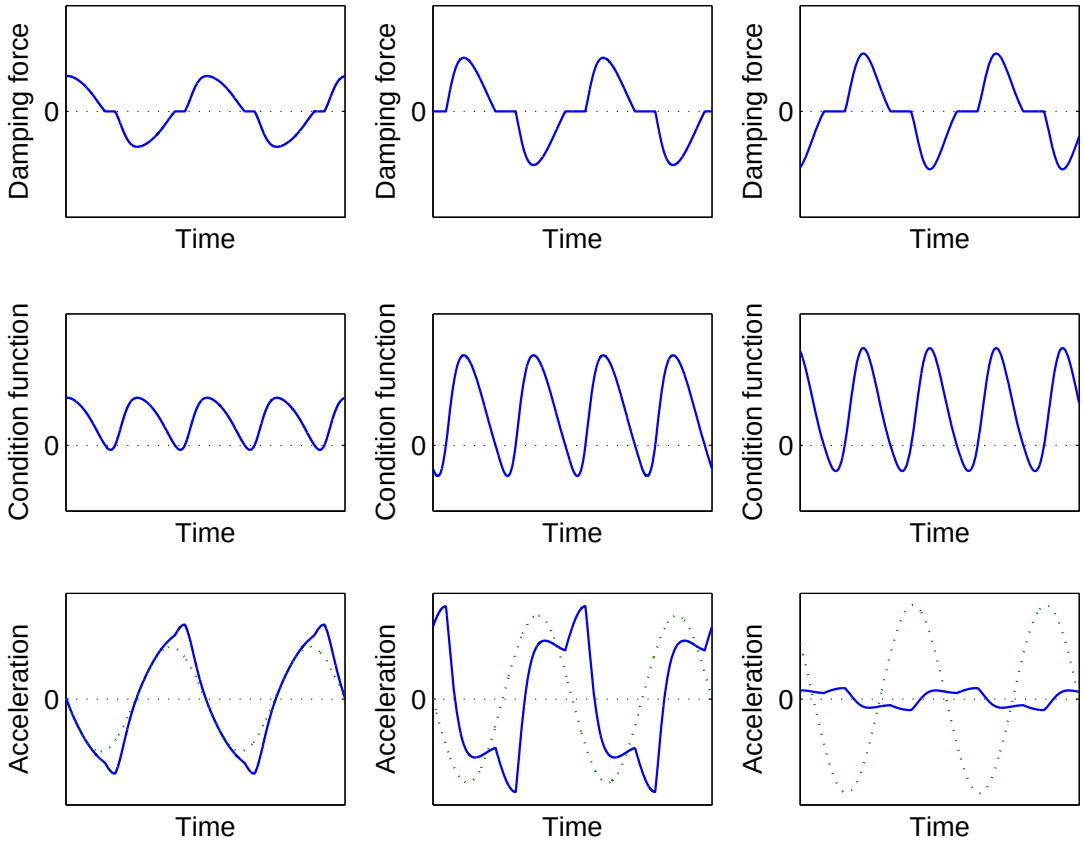

Figure 3.8 Damping force, condition function and accelerations (acceleration of the mass (solid line) and acceleration of the base (dotted line)) of a SDOF system with an SA-1 damper (a) $\omega/\omega_n = 0.5$; (b) $\omega/\omega_n = 1.0$; (c) $\omega/\omega_n = 3.0$

Studying the relative displacement transmissibility in Figure 3.9 (b) shows that increasing G improves the relative displacement transmissibility. Comparing Figure 3.9 (b) with Figure 3.6 (b) shows that there are no crossing points in Figure 3.9 (b). This is due to the fact that the damper is turned off during part of the vibration period and the amplitude of the damper force is not exactly the same as the ideal skyhook damper when it is on.

It can be seen from equation (3.5) that the performance of the SA-1 damper depends on the gain, G , as well as the minimum damping coefficient, $c_{\min}$, and the maximum damping coefficient, $c_{\max}$. The damping force attains its saturation level for longer as the gain, G , increases.

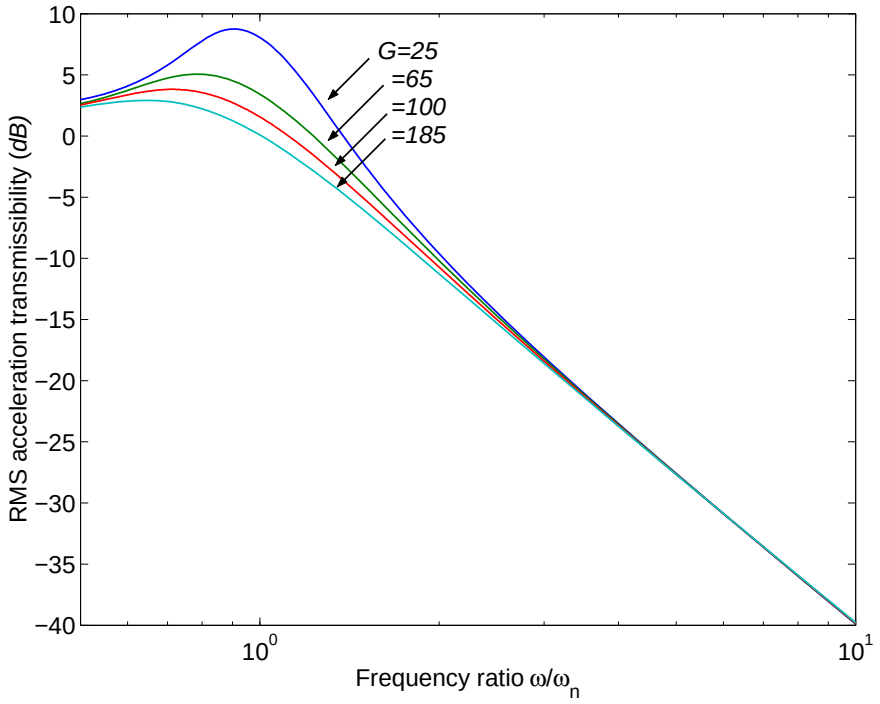

(a)

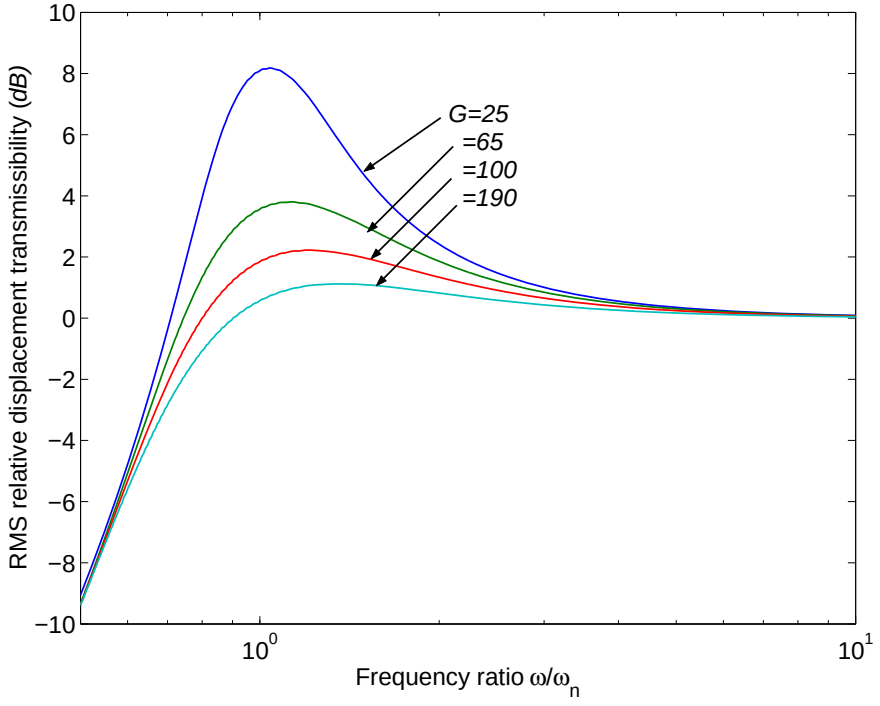

(b)

Figure 3.9 Transmissibility of a SA-1 SDOF system (a) acceleration transmissibility; (b) relative transmissibility

3.5.3 SA-2 SEMI-ACTIVE DAMPER

Figures 3.10 (a), (b) and (c) show the time histories of the condition function, the damper force and the acceleration responses for the SA-2 control algorithm with the on-state damping ratio $\zeta_{\max} = 1$. The SA-2 control strategy is the on-off skyhook control strategy, whose condition function is given in section 2.6.2. The plots in Figure 3.10 (a) to (c) correspond to the normalised frequency ratio of $\omega / \omega_n = 0.5$, 1.0 and 3.0. The acceleration response of the on-off damper consistently reveals two peaks during each vibration cycle irrespective of the excitation frequency. The two peaks are associated with the switching between high and zero values of damping ratio. With the increase of excitation frequency, the duration of the off cycle of SA-2 system increases.

The RMS acceleration and RMS relative displacement transmissibility of the SA-2 semi-active system are shown in Figures 3.11 (a) and (b). It can be seen from Figure 3.11(a) that the performance of the SDOF system with the SA-2 damper is very similar to the performance of the system with the SA-1 damper. As the on-state damping ratio $\zeta_{\max}$ increases, the performance at the frequencies near the natural frequency of the system improves but with a slightly worse isolation performance at higher frequencies. Figure 3.11(b) shows that increasing the damping reduces the RMS relative displacement transmissibility of the system at all frequencies.

Both the on-off (SA-2) and continuously variable (SA-1) skyhook control strategies exhibited the ability to lower the resonance peak without worsening isolation at higher frequencies. However, there is some difference between the performances of these two semi-active dampers. The RMS acceleration and relative displacement transmissibility of the skyhook controlled semi-active dampers are compared with those of passive and skyhook dampers. The results are shown in Figures 3.12 (a) and (b). Studying the RMS acceleration transmissibility curves in Figures 3.12 (a) and (b), it can be seen that both of semi-active dampers can provide better performance at higher frequencies than passive dampers and their performance is comparable to the skyhook damper at even higher frequencies. In the higher frequency range, the performance of SA-1 damper is better than SA-2 damper, which meets earlier expectations that it can more closely emulate the skyhook damper. However, one can

see from the Figure 3.12(a) that the SA-1 semi-active damper exhibits a higher resonance peak than the passive damper at the same damping level, which is a disadvantage of the two dampers.

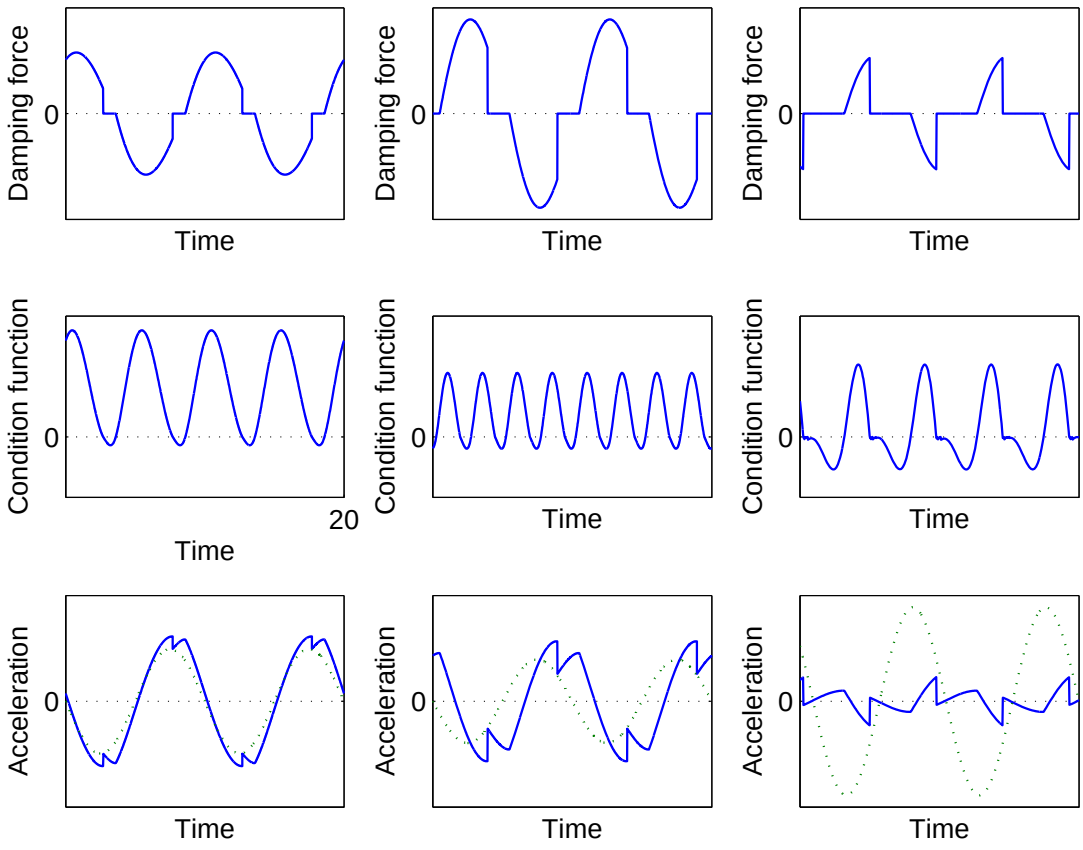

(a) (b) (c)

Figure 3.10 Damping force, condition function and acceleration (acceleration of the mass (solid line) and acceleration of the base (dotted line)) of a SDOF system with an SA-2 damper (a) $\omega/\omega_n = 0.5$; (b) $\omega/\omega_n = 1.0$; (c) $\omega/\omega_n = 3.0$

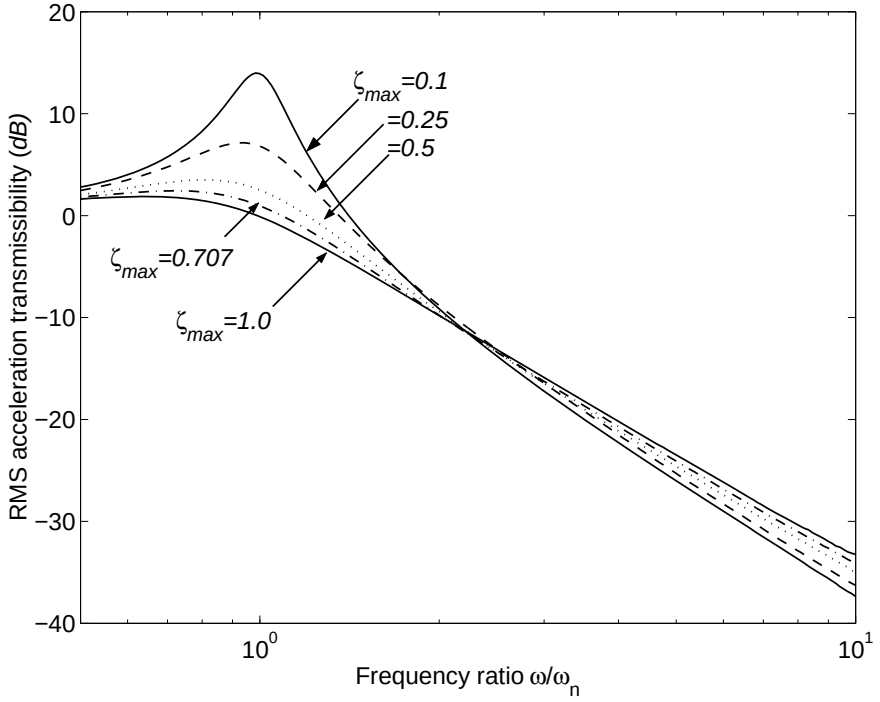

(a)

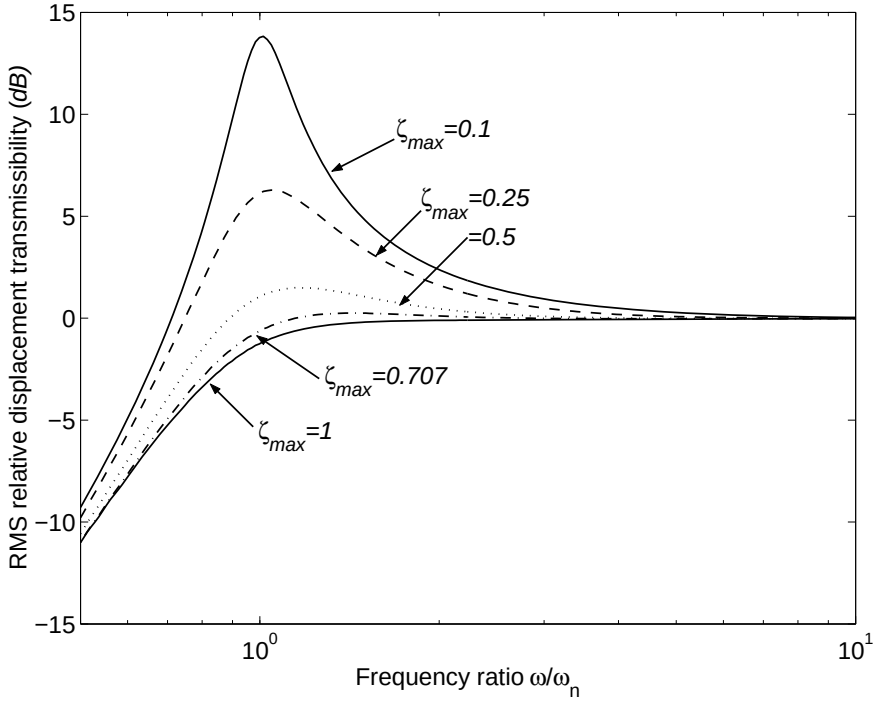

(b)

Figure 3.11 Transmissibility of a SDOF system with a SA-2 damper (a) acceleration transmissibility; (b) relative displacement transmissibility

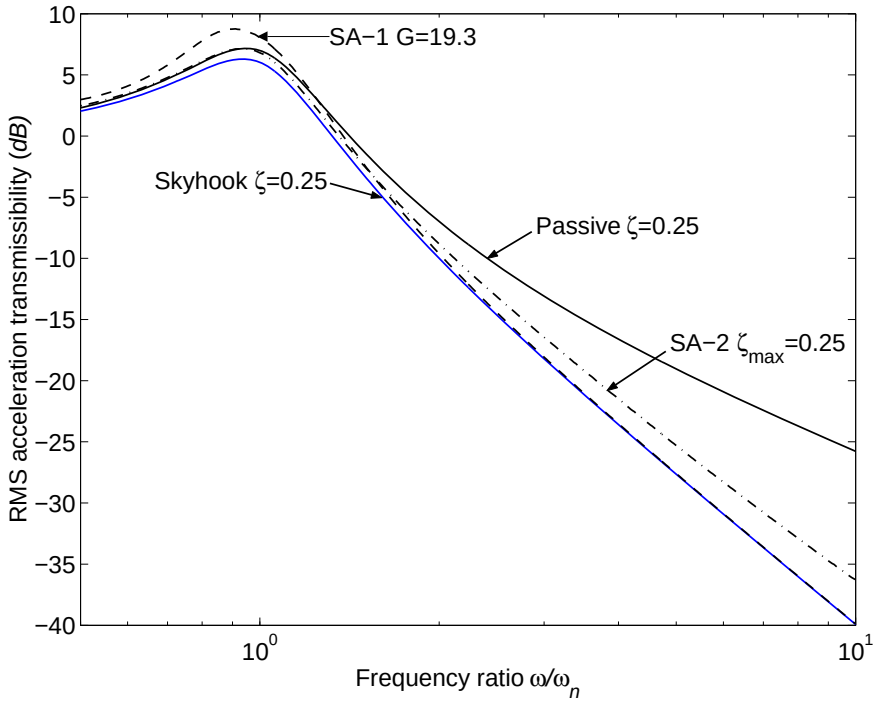

(a)

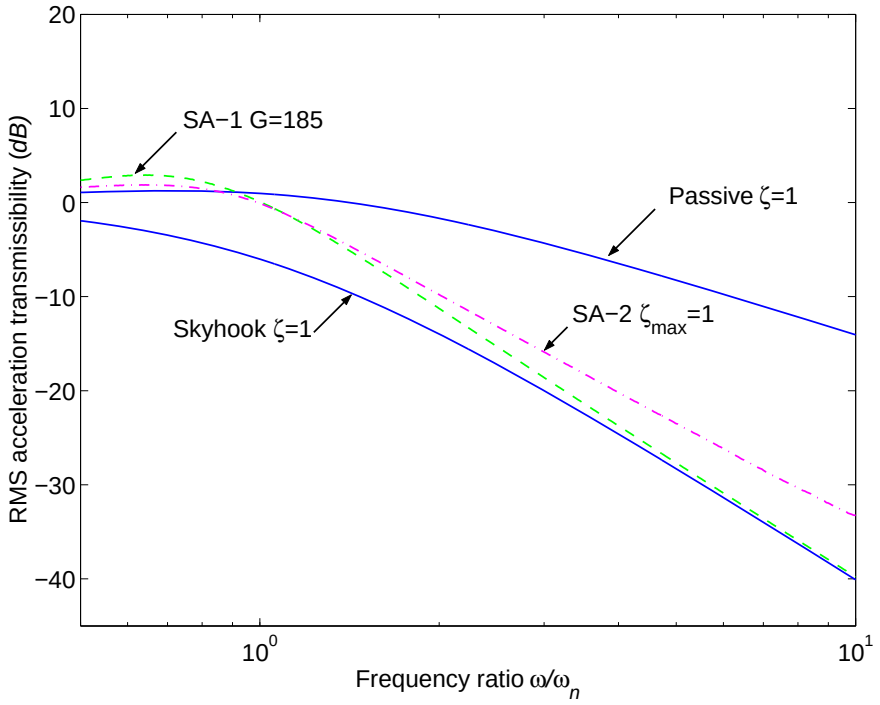

(b)

Figure 3.12 Comparison of the transmissibility of a SA-1 and a SA-2 SDOF system (a) $\zeta_{\max} = 0.25$ and (b) $\zeta_{\max} = 1.0$

3.5.4 SA-3 SEMI-ACTIVE DAMPER

Figures 3.13 (a), (b), and (c) show the steady-state response of an SA-3 system at three different frequencies for $G = 140$, which corresponds to the maximum damping ratio $\zeta_{\max} = 0.5$. The SA-3 control strategy is the anti-jerk implementation of the continuous balance control strategy, whose condition function is given in section 2.6.3. The plots in Figures 3.13 (a) to (c) correspond to the normalised frequency ratio of $\omega / \omega_n = 0.5$, 1.0 and 3.0.

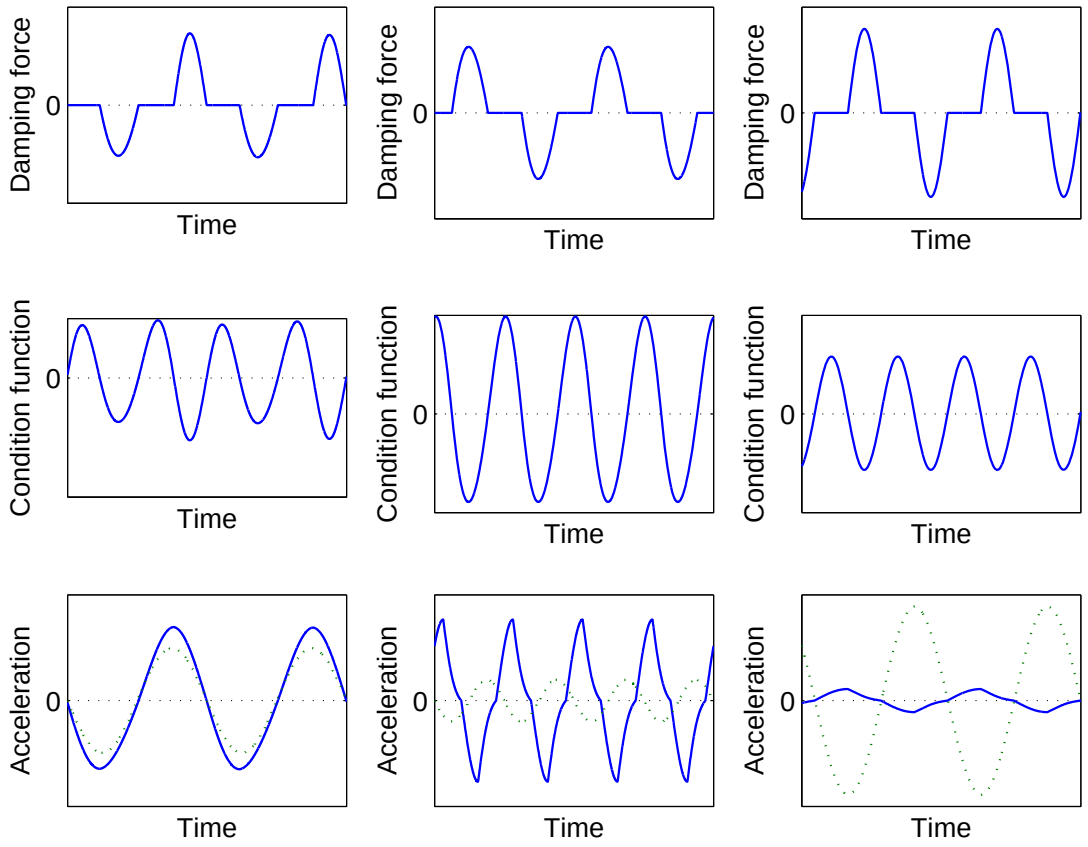

(a) (b) (c)

Figure 3.13 Damping force, condition function and accelerations (acceleration of the mass (solid line) and acceleration of the base (dotted line)) of a SDOF system with an SA-3 damper (a) $\omega/\omega_n = 0.5$; (b) $\omega/\omega_n = 1.0$; (c) $\omega/\omega_n = 3.0$

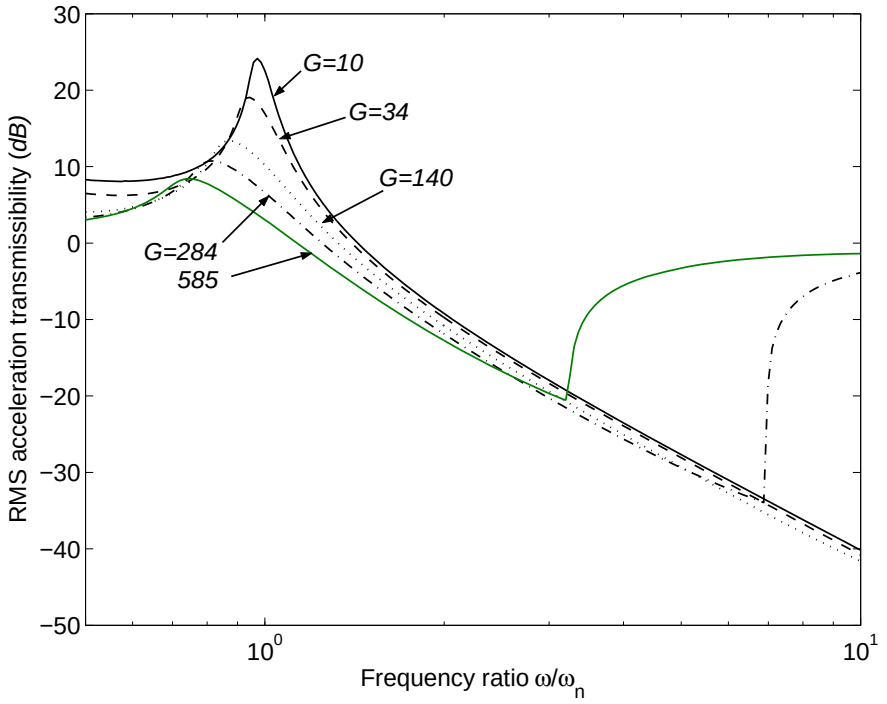

(a)

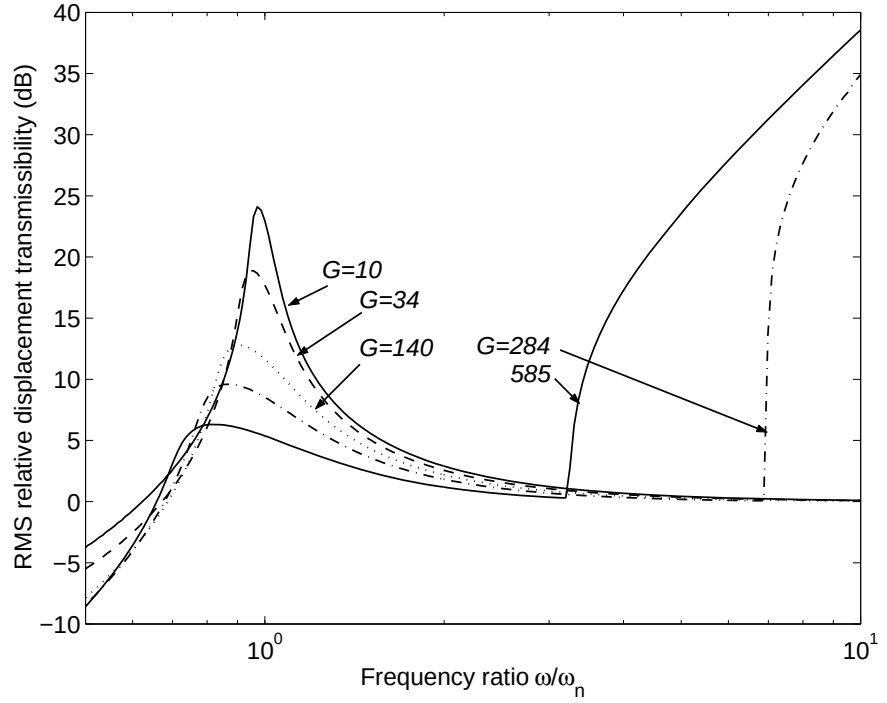

(b)

Figure 3.14 Transmissibility of a SDOF system with a SA-3 damper (a) acceleration transmissibility; (b) relative displacement transmissibility

Figures 3.14 (a) and (b) show the RMS acceleration and relative displacement transmissibility for various values of the gain G. As G is increased, the resonant

peak decreases and the isolation performance improves. At higher frequencies, the transmissibility jumps to very large values for larger G. The same trend can be found in the relative displacement transmissibility. The reason for the discontinuity of the transmissibility curves is that, although the on-state damping force has the opposite sign as the spring force and is proportional to the relative displacement, it cannot exactly oppose the spring force. At high frequencies, a large value of G can over-cancel the spring force and effectively change the stiffness of the system, which results a larger response.

3.5.5 SA-4 SEMI-ACTIVE DAMPER

The steady state response of the SA-4 system is shown in Figures 3.15 (a), (b) and (c) for three different excitation frequencies with $\zeta_{\max} = 1.0$. The SA-4 control strategy is the on-off balance control strategy, whose condition function is given in section 2.6.4. It can be seen that the damper assumes zero force whenever condition function is greater than zero, i.e. the spring and the damper forces have the same sign. The acceleration response reveals two peaks associated with the two switches of the damping level per period of vibration. The mass vibrates about a new equilibrium position although not shown in the figure. Under this circumstance, the relative displacement does not change sign, such that the switch of the semi-active damper is determined solely by the sign of relative velocity.

Figures 3.16 (a) and (b) show the acceleration transmissibility of SA-4 system with different on-state damping ratios, $\zeta_{\max}$. It can be seen from Figure 3.16(a) that with the increase of the on-state damping, the resonant responses are reduced, but the high frequency isolation performance is also degraded. Increasing the damping reduces the relative transmissibility at resonance, but the isolation performance at higher frequencies is dramatically increased due to the offset of the equilibrium position.

A comparison of the acceleration and relative transmissibility of SA-3 and SA-4 systems with conventional and skyhook passive systems is shown in Figures 3.17 (a) and (b). Compared to the conventional passive system, the SA-3 system has a far superior performance at higher frequencies. The acceleration transmissibility curves show that the SA-3 system can provide a better performance than a very lightly

damped passive system or even an undamped system at higher frequencies. However, there is a price to be paid in terms of inferior low frequency performance and relative displacement transmissibility. The SA-4 damper system can also provide better performance at higher frequencies when compared with the conventional passive damper with the same damping level. However, the performance at lower frequencies and around resonance is worse than the passive system. Both the SA-3 and SA-4 dampers were developed to minimise the RMS acceleration of the system instead of the relative displacement. It was shown from the simulations that these strategies might lead to the mass vibration about a new position, which indicates an offset of the displacement.

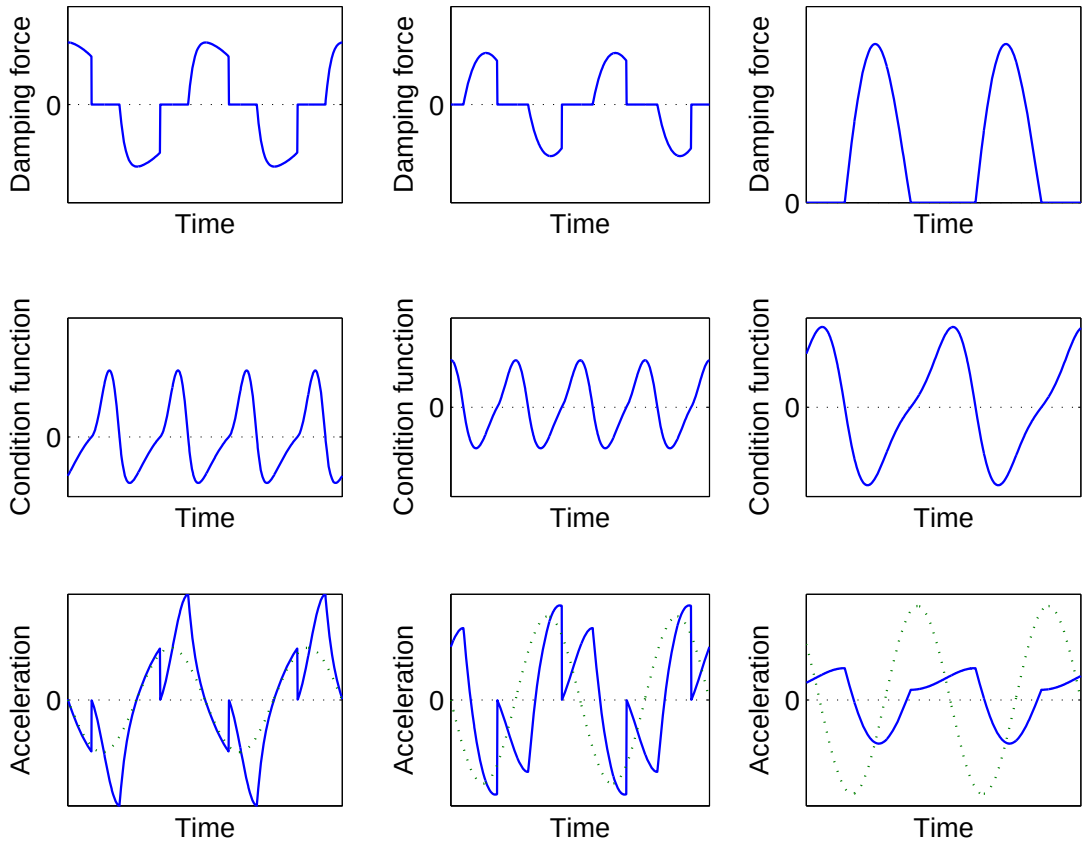

Figure 3.15 Damping force, condition function and accelerations (acceleration of the mass (solid line) and acceleration of the base (dotted line)) of a SDOF system with an SA-4 damper (a) $\omega/\omega_n = 0.5$; (b) $\omega/\omega_n = 1.0$; (c) $\omega/\omega_n = 3.0$

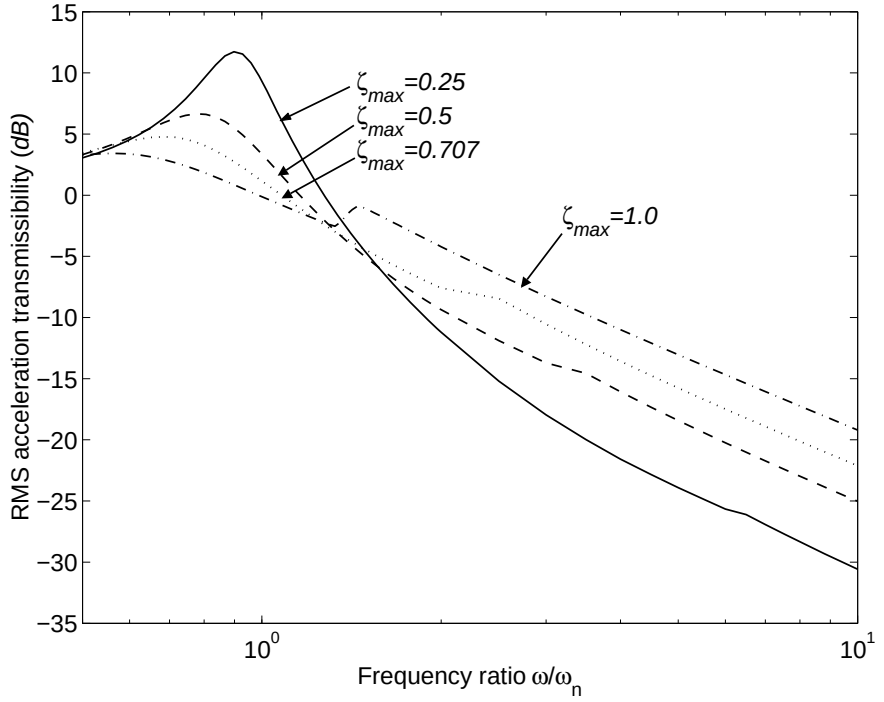

(a)

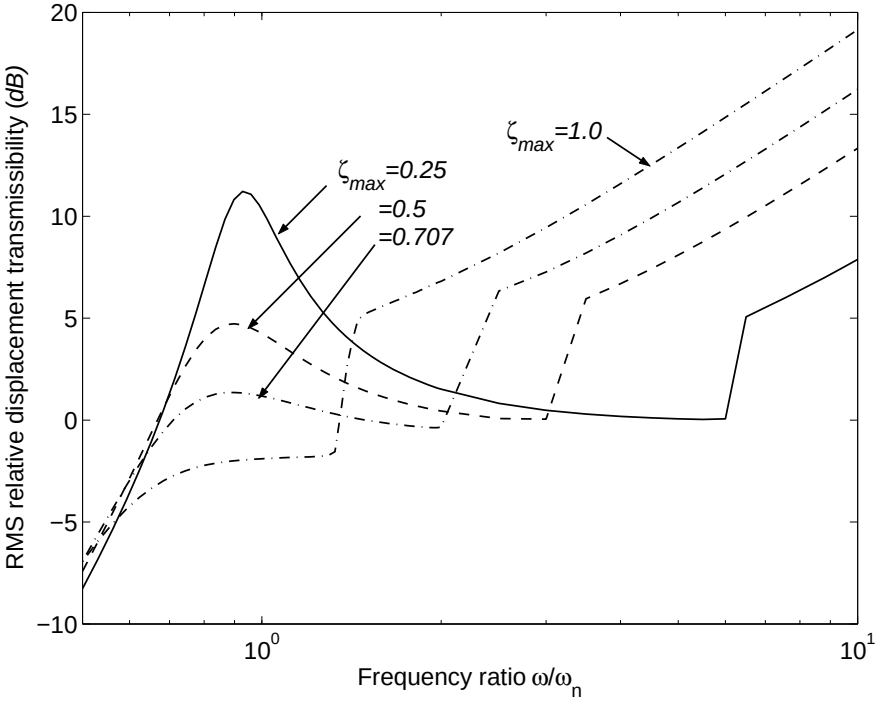

(b)

Figure 3.16 Transmissibility of a SDOF system with a SA-4 damper (a) acceleration transmissibility; (b) relative displacement transmissibility

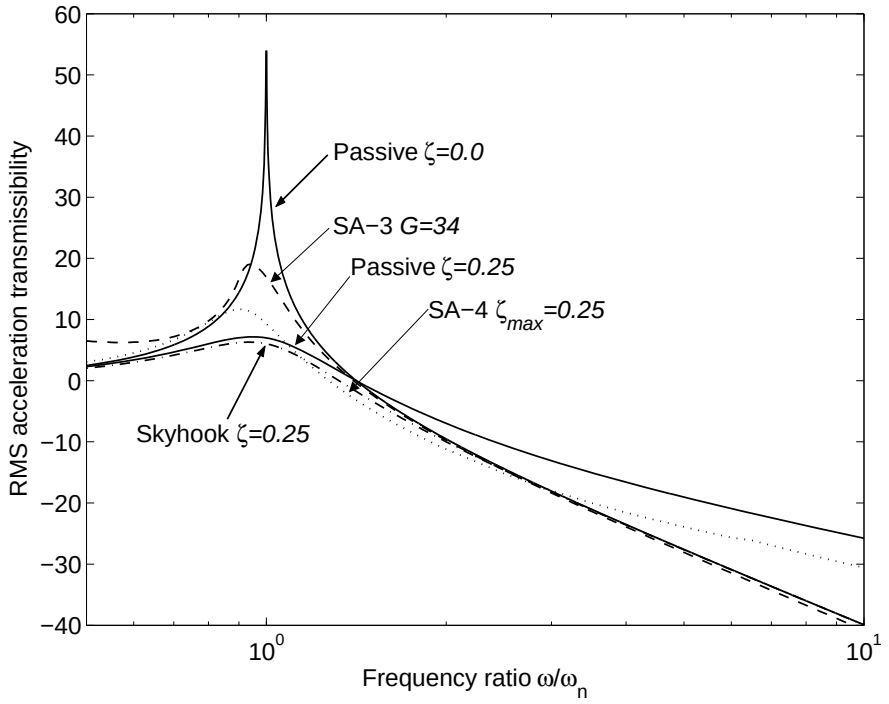

(a)

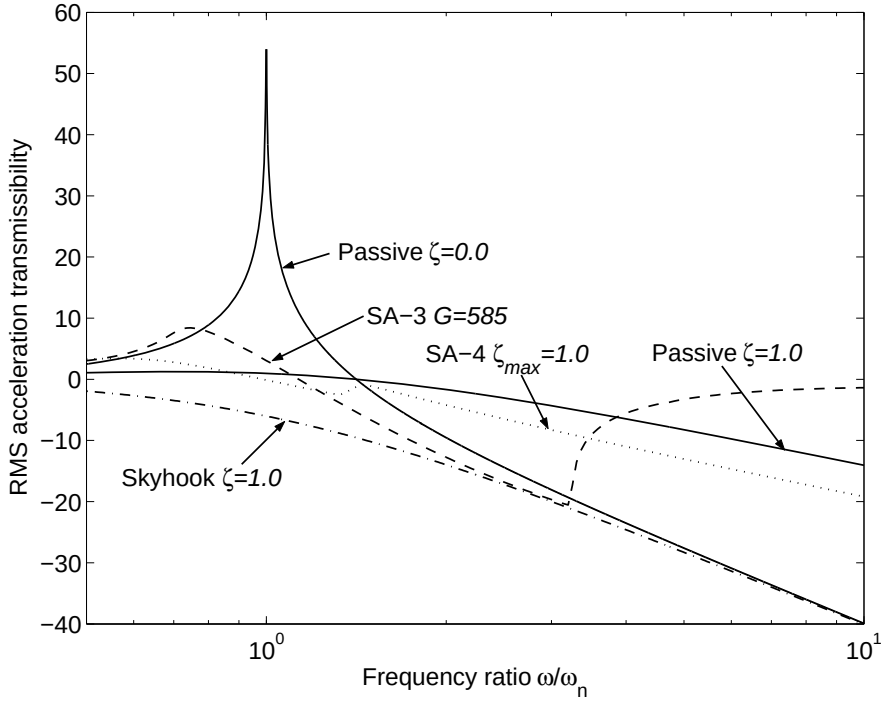

(b)

Figure 3.17 Comparison of the transmissibility of a SA-3 and a SA-4 SDOF system (a) $\zeta_{\max} = 0.25$ and (b) $\zeta_{\max} = 1.0$

3.6 DISCUSSION

Figures 3.18 (a) and (b) show a comparison of the RMS acceleration transmissibility for a SDOF system with a conventional damper, a skyhook passive damper and a semi-active damper. It can be established that:

(1) The semi-active system almost always provides a better isolation than a conventional passive system with an equivalent damping level. As the damping ratio increases, the difference between the two systems becomes more obvious;

(2) The compromise between resonance control and isolation that is inherent in a conventional passive system does not exist for the semi-active systems. The reduction in the resonance peak does not necessarily occur at the cost of reduced isolation at high frequencies. In fact, with a sufficiently large damping ratio, one can completely eliminate the resonance peak and actually achieve better isolation across the whole frequency spectrum. This is particularly useful for sensitive machinery that cannot tolerate any overshoot in power-up or power-down, and yet must have good isolation during normal operation. Conventional passive systems offer one or the other, whereas the semi-active system offers both;

(3) The performance at very low frequencies deteriorates due to the abrupt discontinuities in the damper force;

(4) The skyhook damper system nearly always provides the best performance but it is only an ideal case. SA-1 and SA-2 system provide similar performance and in terms of relative transmissibility, the SA-2 system is even better than the SA-1 system, and is much simpler; and

(5) The SA-3 system can provide superior isolation performance at higher frequencies at the cost of a large resonance peak and large relative displacement transmissibility. Both SA-3 and SA-4 systems are not good for relative displacement transmissibility reduction.

Adaptive-passive control is possibly the simplest way to implement a control algorithm for harmonic vibration isolation.

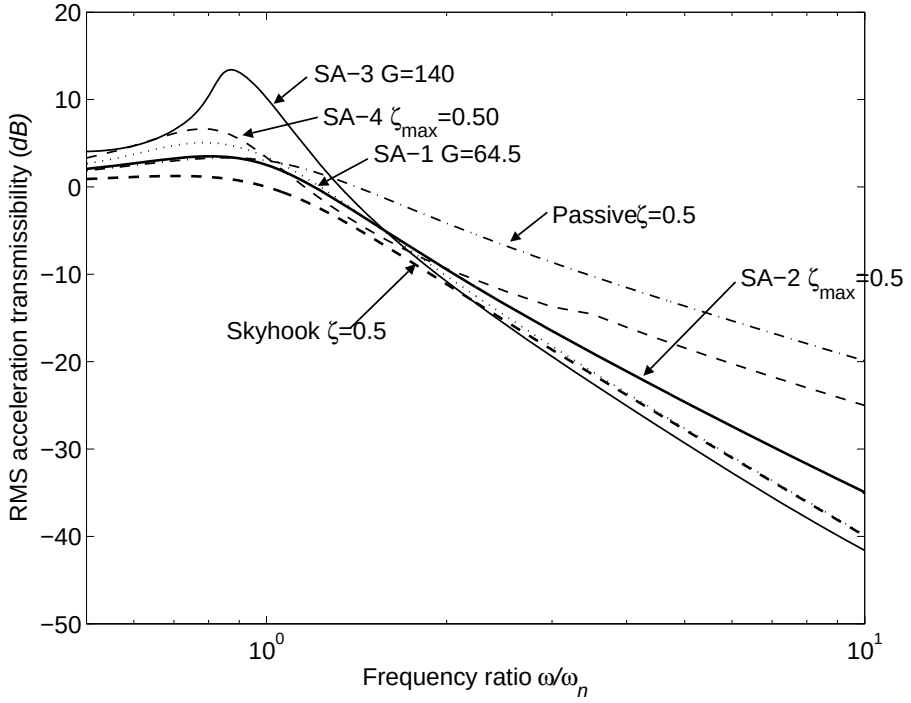

(a)

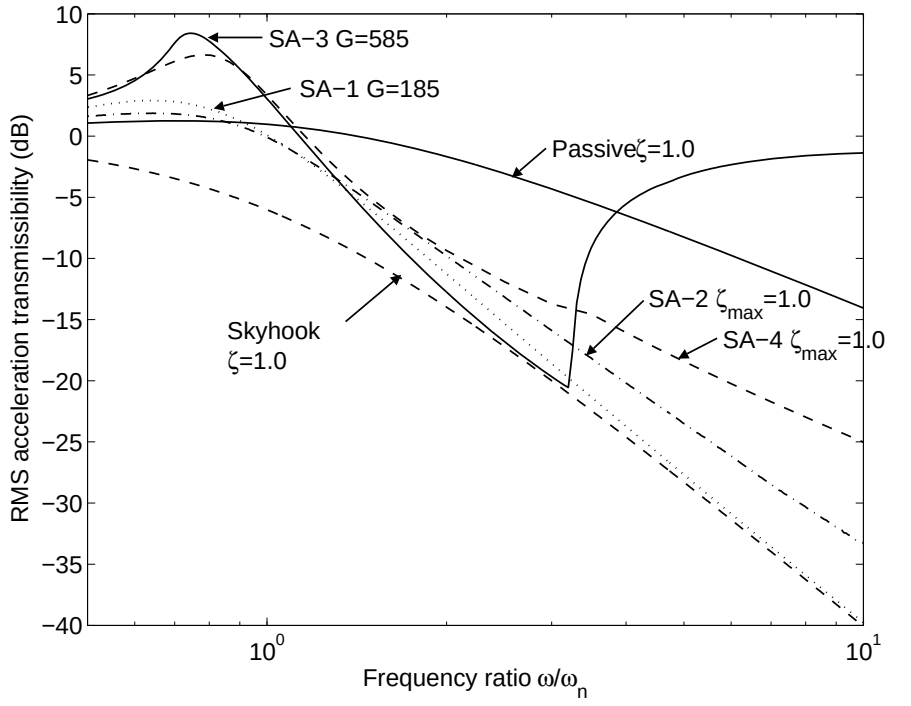

(b)

Figure 3.18 Comparison of the transmissibility of a SDOF system with different types of dampers (a) moderate damping; (b) critical damping

3.7 EXPERIMENTAL WORK

This section presents the experimental work for the evaluation of the vibration isolation performance of a semi-active base isolated system. An experiment was set up to investigate the use of an electromagnetic device as a semi-active damper for vibration isolation. The experiments were conducted with the following objectives: (1) to investigate the possibility and effectiveness of using electromagnetic damping as a semi-active damper; (2) to validate simulations of on-off skyhook control strategy.

3.7.1 INTRODUCTION

Linear electromagnetic devices consisting of coils of metal wire interacting with magnetic fields produced by a permanent magnet or an electromagnet can be used to construct electromechanical dampers. The damping coefficient can be varied rapidly by changing the external resistance connected to the coil. In the open circuit state the electromechanical damping effect vanishes, while when the coil is short circuited the damping coefficient reaches a maximum value. Since the effective resistance can be rapidly varied electrically, an electromechanical damper can function as a semi-active damper in vibration isolation systems. This principle is explained in Appendix A2.

The electromagnetic device used for the experiment is adopted from a loudspeaker since it is expected to behave like a SDOF system at low frequencies. Additional mass was added to the original system to place ω_n at desired frequency. The loudspeaker was mounted on a shaker to provide base disturbances. A photograph of the system is shown in Figure 3.19.

The on-off skyhook control strategy was chosen to be implemented due to its simplicity while retaining superior performance to that of a conventional passive damper. A analogue controller circuit board based on the on-off skyhook semi-active control algorithm was designed, tested and used in the experiment. The acceleration response of the base and the mass were the two inputs into the circuit board, which were integrated and processed according to the control algorithm. There is a digital switch installed in the circuit board, which was used to open and close the coil circuit

of the SDOF system. Detailed information about the circuit board is listed in Appendix A4.

Figure 3.19 Photograph of the experimental rig

Figure 3.20 shows the experimental setup for the semi-active vibration isolation system (a complete list of the equipment used can be found in Appendix A4). In this setup, the vibration system composed of a semi-active electromagnetic damper was mounted vertically on an electromagnetic shaker supplied with a signal from a frequency analyser. Accelerometers were attached to the mass of the system and the vibrating base, and the signals were conditioned by charge amplifiers. The acceleration signals were input into the designed controller circuit board after passing through a high pass filter with a cut-off frequency of 2Hz. The input signals were manipulated in the controller board which then produce a signal to operate the switch of the semi-active damper. The acceleration signals of the mass and the base together with the switch signal from the circuit board were measured and processed using the frequency analyser.

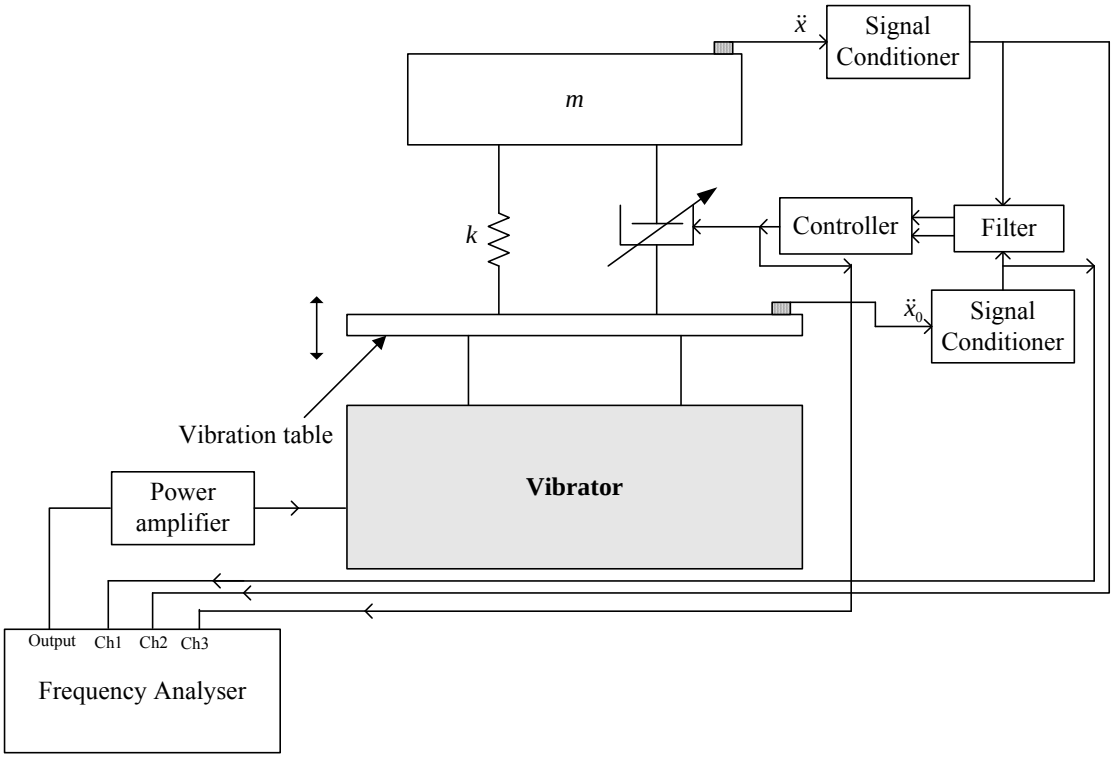

Figure 3.20 Diagram of the experimental rig

3.7.2 CHARACTERISTICS OF THE EXPERIMENTAL RIG

The first series of tests involved identifying the dynamics characteristics of the experimental rig. The frequency response of the system was measured with the electromagnetic damper in the open and short circuit state, which provided the minimum and the maximum damping ratio achievable by the system. When the switch was in the off-state, the electrical circuit was open. Thus there was no electromagnetic force exerted by the electromechanical damper. The damping coefficient of the system was a minimum and was equal to the mechanical damping of the system. The mechanical damping of the system is due to the damping in the suspension of the loudspeaker. When the switch was in the on-state, electromechanical damping was added to the system. The damping coefficient of the system was of maximum value and was equal to the sum of the mechanical damping of the system and the electromechanical damping.

A random signal in the frequency range 5-100Hz was used to excite the shaker. A frequency analyser was used to measure the frequency response. Figures 3.21 and 3.22 show the frequency responses and coherences when electromagnetic damper was

open and short circuited. Figures 3.23(a) and (b) show the magnitude and phase of the measured acceleration transmissibility between the mass and the base excitation. A comparison was made between the measured data and the numerical simulations of a passive SDOF system, where the natural frequency and the damping ratios of the model have been tuned by hand to match the measured results. The theoretical prediction curves are shown by the dotted lines in the figure. It can be seen that the system behaves as a conventional passive SDOF system when open or short circuited, and that the measurement results agree reasonably well with the numerical simulation results. However, it should be noted that there is some relatively significant difference between the phases. The system resonance response was reduced by adding electromechanical damping. It can also be seen from the measurement that the natural frequency of the system is at about 15.2 Hz. From the peak value of the acceleration transmissibility when the switch was off, the mechanical damping ratio of the system was calculated to be 0.10, and the overall damping ratio with the electromechanical damping ratio of the system was calculated to be 0.22.

3.7.3 ADAPTIVE-PASSIVE CONTROL

The second measurement was conducted to implement the adaptive-passive control algorithm using the experimental setup. Recalling the equation defining the AP damping control algorithm, the control algorithm for the current case can be defined as

$$c = \begin{cases} c_{\max} & RMS(\ddot{x}) \geq RMS(\ddot{x}_0) \\ c_{\min} & RMS(\ddot{x}) < RMS(\ddot{x}_0) \end{cases} \tag{3.21}$$

The condition function is the comparison of the RMS values of the acceleration response of the mass and the base. The RMS values of the two acceleration signals were measured using two digital volt meters. The operation of the switch was conducted by hand. Measurements were conducted in the frequency range of 8Hz-80Hz, with a frequency increment of 1Hz up to 30Hz and a frequency increment of 2Hz above 30Hz.

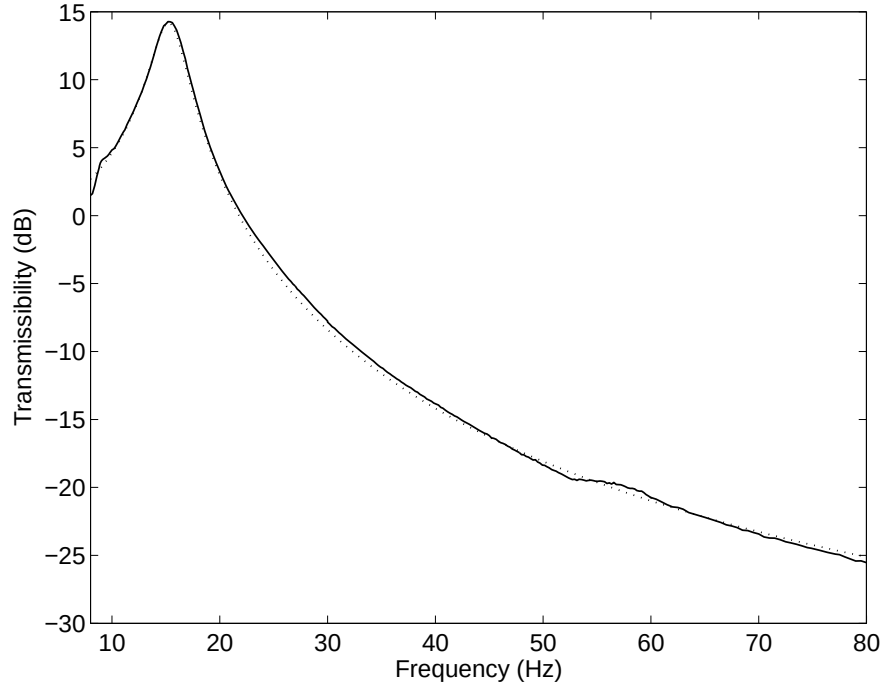

(a)

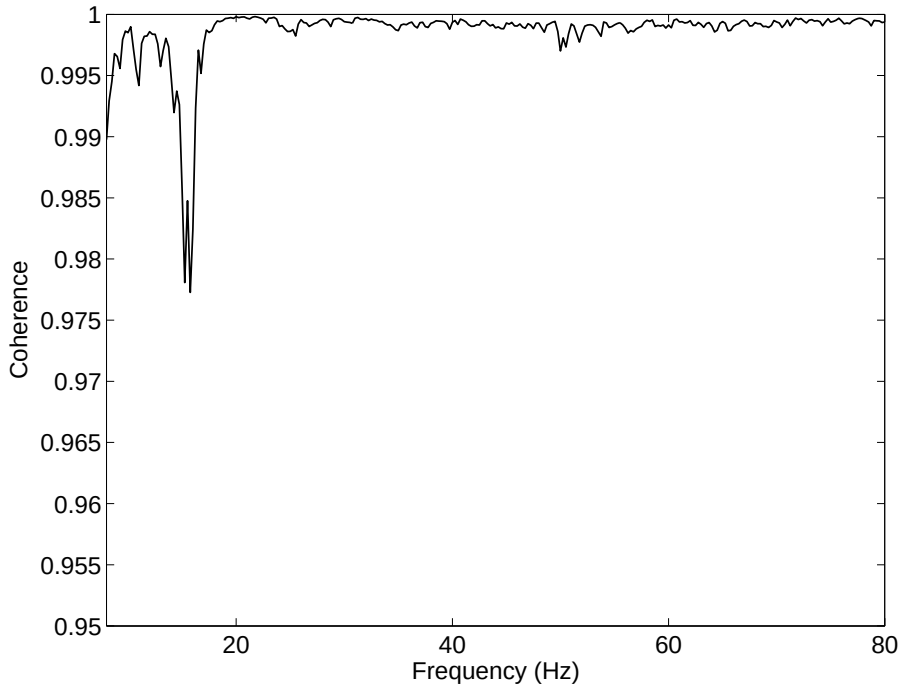

(b)

Figure 3.21 Acceleration transmissibility and coherence of the experimental rig with the electromagnetic damper in open circuit state: (a) acceleration transmissibility (—measurement results; ····· theoretical prediction); (b) coherence

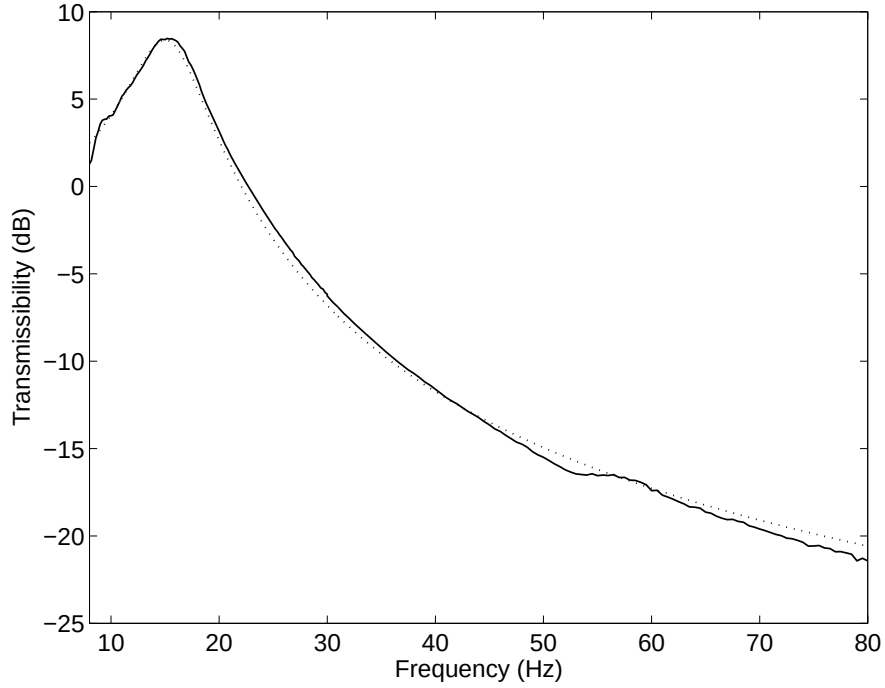

(a)

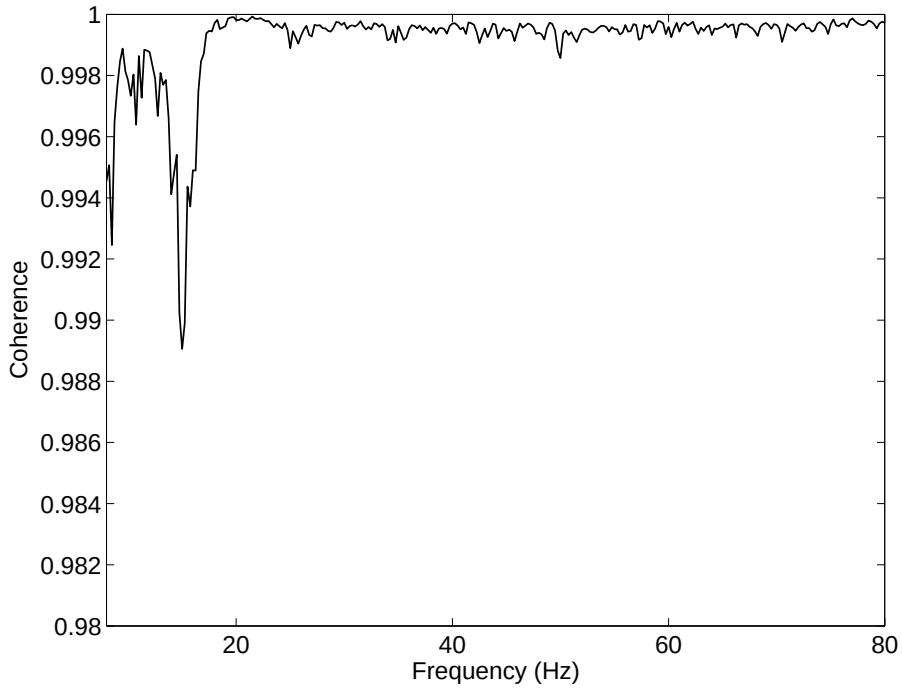

(b)

Figure 3.22 Acceleration transmissibility and coherence of the experimental rig with the electromagnetic damper in short circuit state: (a) acceleration transmissibility (—measurement results; ····· theoretical prediction); (b) coherence

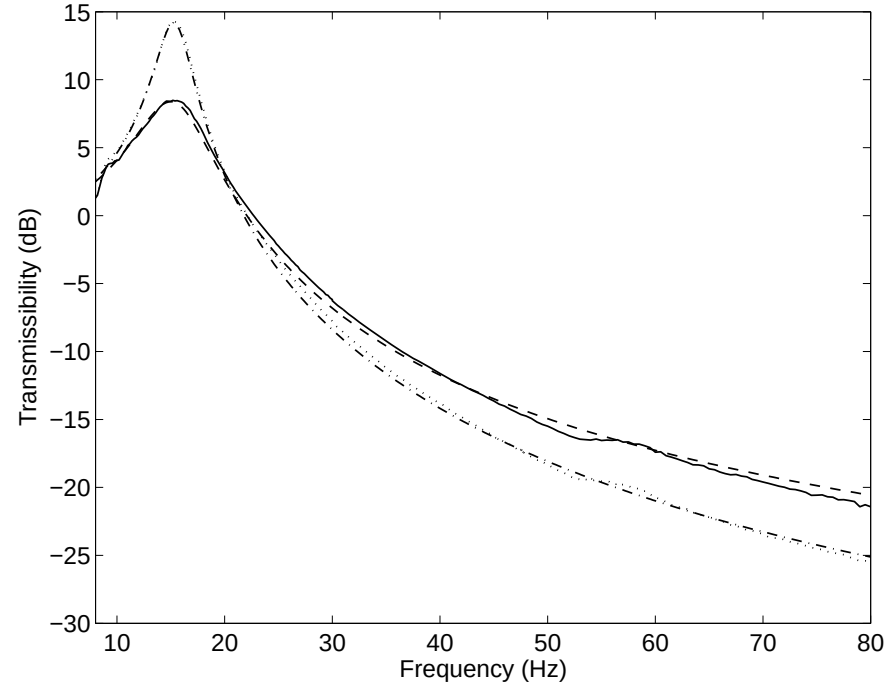

(a)

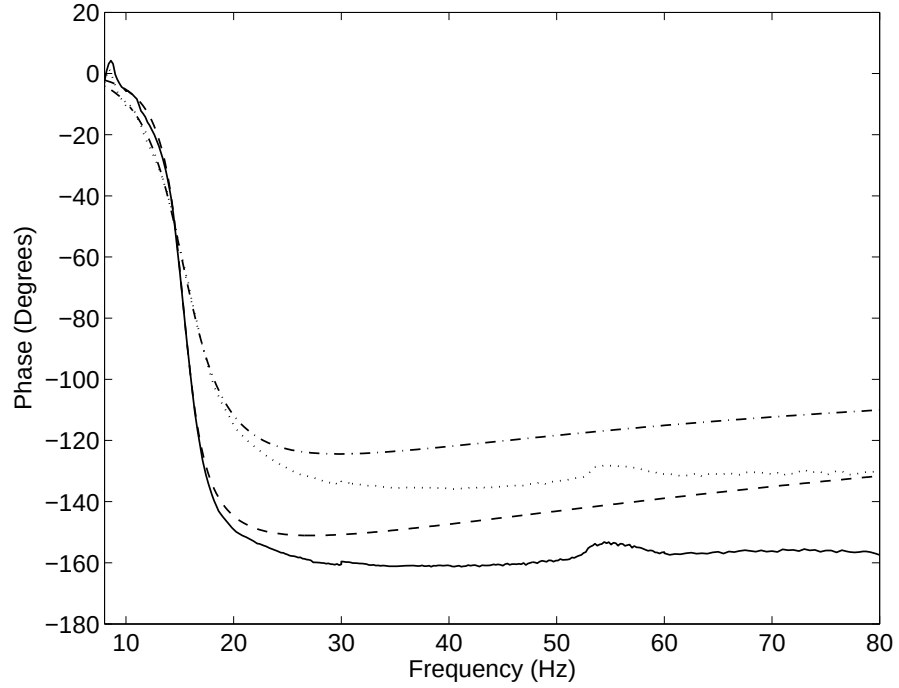

(b)

Figure 3.23 Transmissibility of the experimental rig with the electromagnetic damper in open and short circuit state: (a) acceleration transmissibility; (b) phase angle (—measurements result for open circuit; −−− theoretical prediction for open circuit; measurement result for close circuit; −·−· theoretical prediction for close circuit)

Figure 3.24 shows the result of the acceleration transmissibility with the AP semi-active control algorithm. It can be seen from the figure that the system behaves as a heavily damped system at frequencies when the excitation frequency ω is smaller than $\sqrt{2}\omega_n$, while it behaves as a lightly damped system at higher frequencies. The adaptive damping control algorithm can greatly reduce the response at resonance while retaining the higher frequency isolation performance.

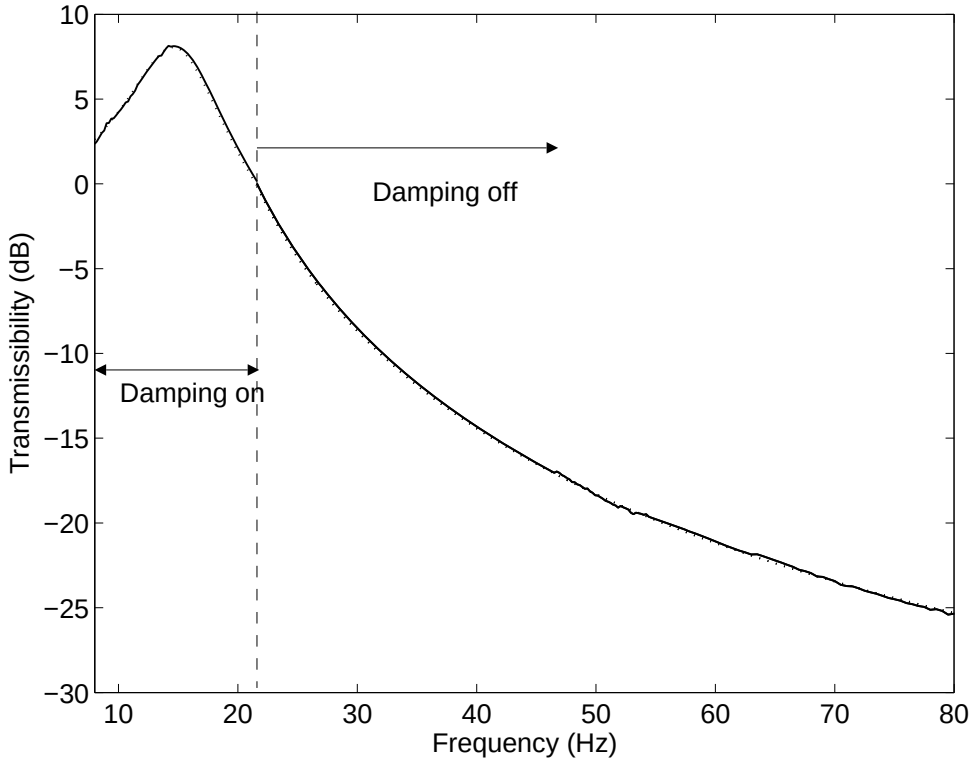

Figure 3.24 Transmissibility of the adaptive-passive system (— measured;⋯⋯ numerical simulation)

3.7.4 ON-OFF SKYHOOK CONTROL

The third series of tests was carried out to measure the RMS transmissibility of the system with the semi-active damper in operation. The controller circuit board was connected to the system. The measured acceleration signals were fed into the circuit board. A digital switch was controlled by the measured signal to open or close the circuit to provide the desired damping. The tests were carried out frequency by frequency and the steady-state RMS acceleration transmissibility was calculated.

Figure 3.25 shows the measured RMS acceleration transmissibility, compared with a theoretical prediction. As a comparison, the two passive cases are also shown for the two cases when the damping ratios are maximum and minimum as described in section 3.7.2. It can be seen from the results that the semi-active damper gives a marginally better performance than the conventional passive damper. It lowers the transmissibility near resonance when compared to the conventional passive damper with minimum damping ratio. The performance at higher frequencies is slightly better than that of the conventional passive damper with maximum damping ratio. However, the performance of the semi-active damper could be improved if the off-state damping ratio (mechanical damping) could be made much smaller, and the on-state damping ratio is larger enough. The performance of the semi-active electromagnetic damper was limited by the dynamics properties of the inductance of the suspension in the loudspeaker and also the inductance of the circuit.

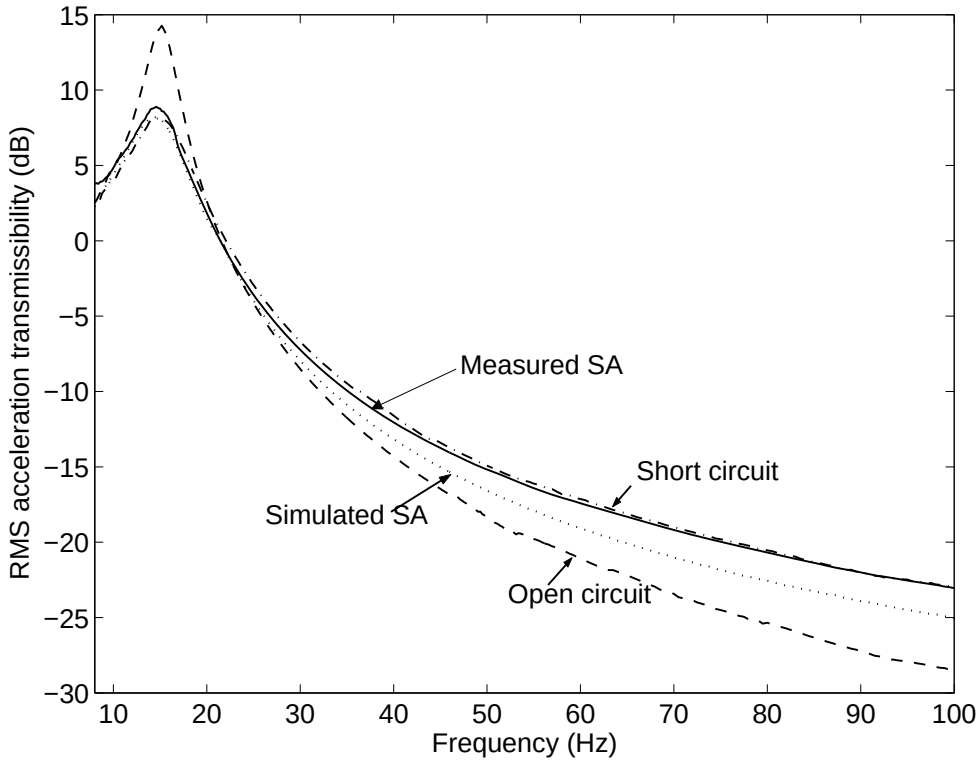

Figure 3.25 RMS transmissibility of the SDOF system with the semi-active damper in operation

In order to understand the results fully, it is necessary to look at some of the time traces and therefore verify that the semi-active damper is behaving as intended. Figures 3.26 to 3.28 show the time traces for the acceleration response and the voltage to operate the damper when subjected to a pure-tone excitation below resonance (10 Hz), near resonance (15Hz) and above resonance (30Hz) respectively. The input wave form was used to synchronise the start time for the simulations and measurements. It can be seen from the figures that the measured acceleration responses for the semi-active system are reasonably close to those predicted. The semi-active damper can provide somewhat better performance by switching the damper on and off alternately during one vibration cycle. Figures 3.26 to 3.28 also show that the semi-active damper switches on and off twice in one vibration period irrespective of the excitation frequency. The jerk presented in the simulated response curves does not appear in the measured data. This is because there are some time delays in the electromagnetic damper which help to suppress the jerk.

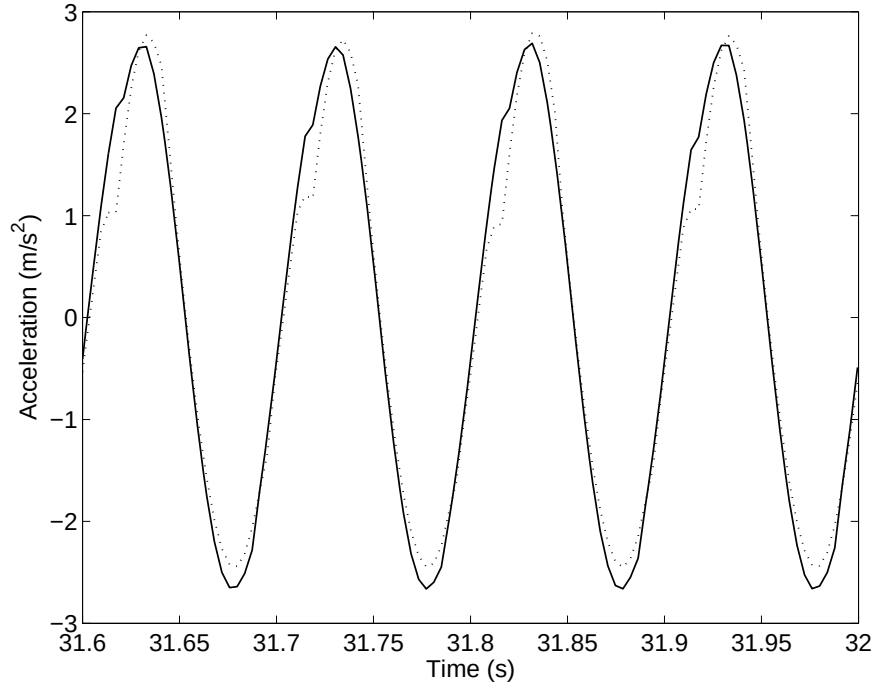

(a)

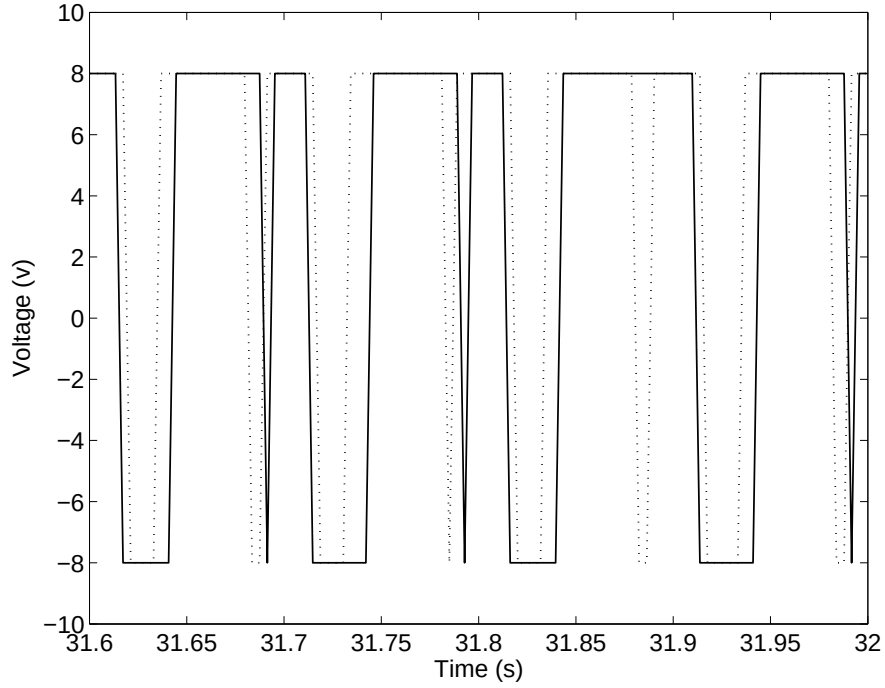

(b)

Figure 3.26 Measured acceleration responses and voltage across the digital switch at 10Hz (a) acceleration; (b) voltage (— measured; ····· numerical simulation)

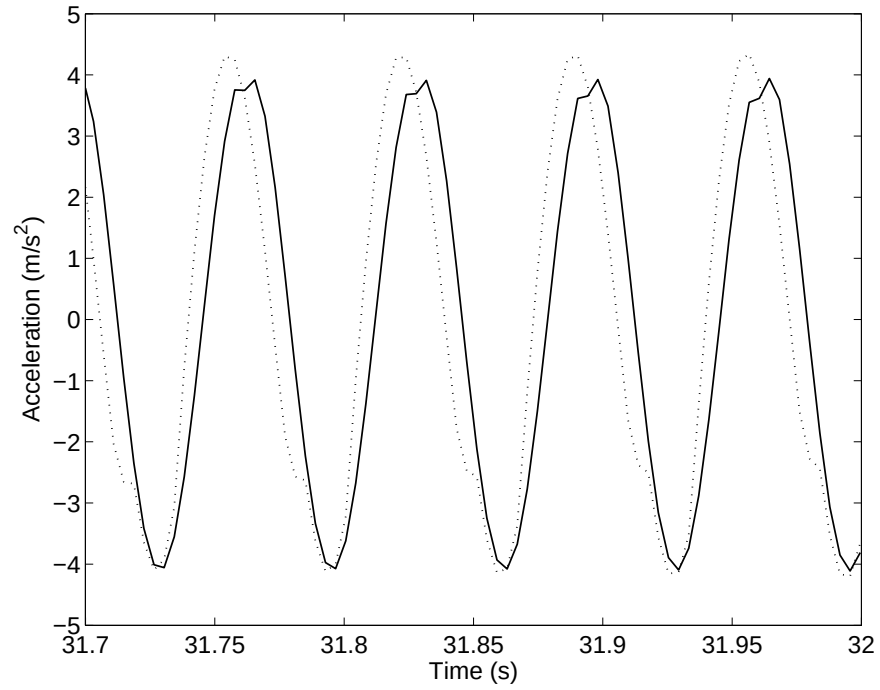

(a)

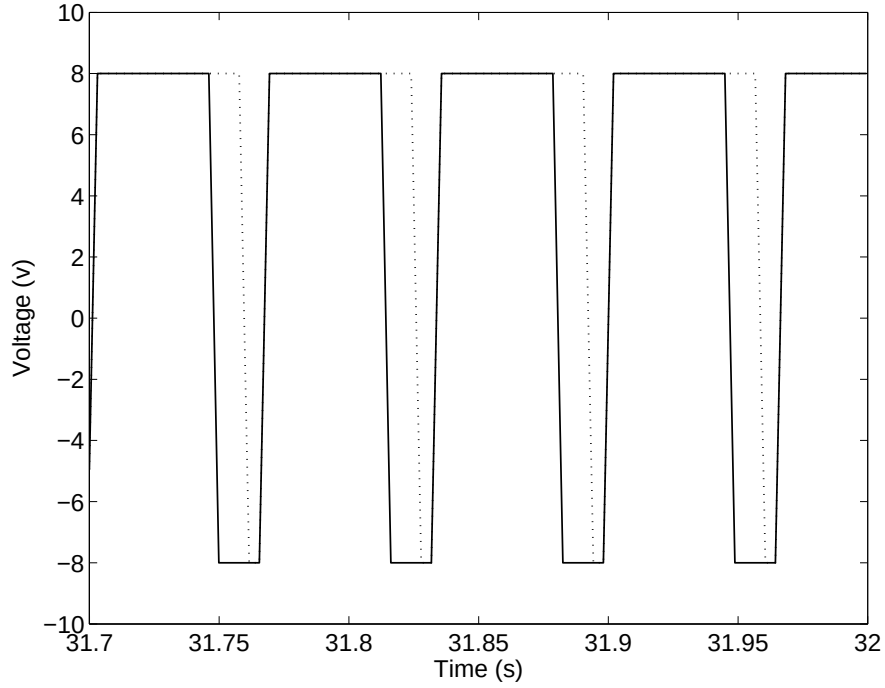

(b)

Figure 3.27 Measured acceleration responses and voltage across the digital switch at 15Hz (a) acceleration; (b) voltage (— measured; ····· numerical simulation)

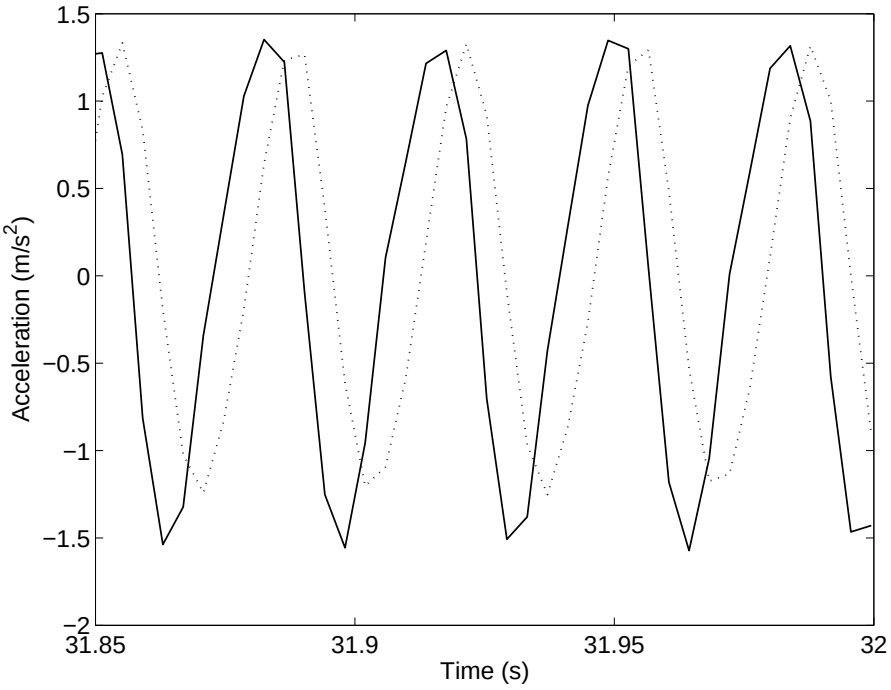

(a)

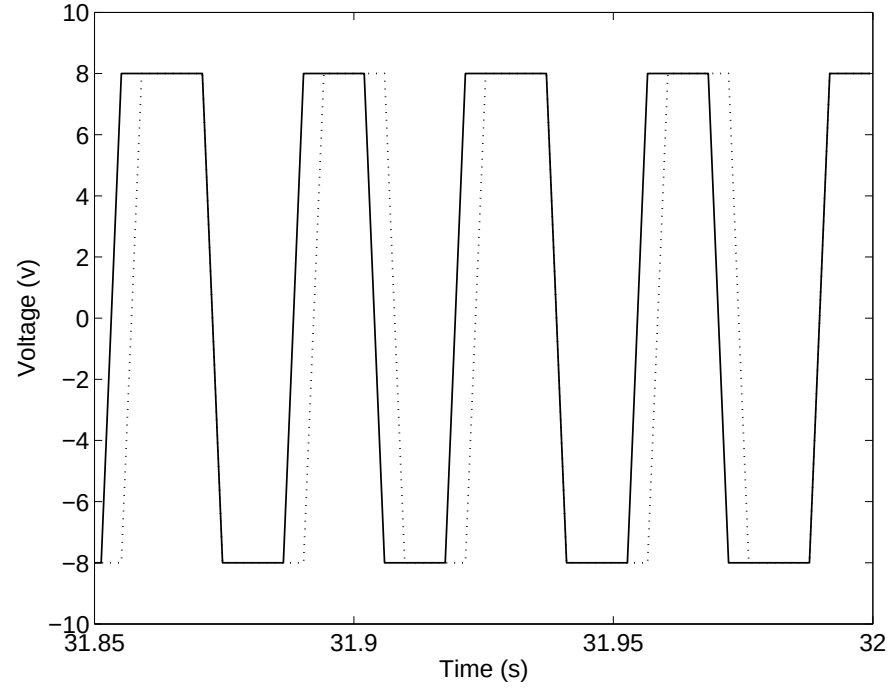

(b)

Figure 3.28 Measured acceleration responses and voltage across the digital switch at 30Hz (a) acceleration; (b) voltage (— measured; ····· numerical simulation)

3.7.5 FRACTION OF ON-STATE TIME

The waveforms in section 3.7.4 suggest that the duration for which the damper is on is a function of frequency. This can be further analysed by evaluating the fraction of time for which the damper is on, and this is shown in Figure 3.29. Results from numerical simulations of a semi-active system and results obtained by studying the expression of the condition function using a conventional passive system are also shown as a comparison.

It can be seen from the figure that the fraction of time when the damper is on is frequency dependent. With increasing frequency, the duration of the on-state also increases. At frequencies near resonance, the damper is on almost all the time. At higher frequencies, both the analytical solution for a conventional passive system and numerical solution for a semi-active system indicate that the damper is on for 50% of the whole period. There are good physical reasons for this and they are discussed in section 4.1.

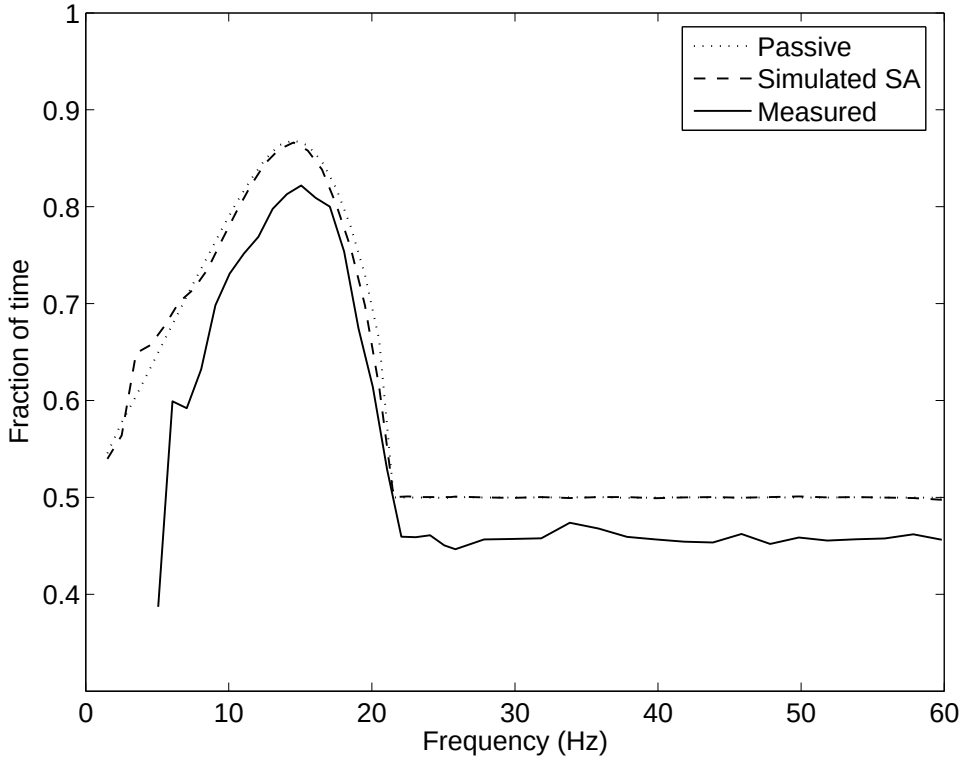

Figure 3.29 Comparison of measured and simulated results for the fraction of time when the condition function is on

3.8 CONCLUSIONS

This chapter investigated the performance of four semi-active damping control strategies for isolation of harmonic disturbances through numerical simulations and experimental tests.

Numerical simulations were carried out in Matlab/Simulink to study the vibration isolation performance of the semi-active damping control strategies. The isolation performance was evaluated in terms of root-mean-square (RMS) transmissibility of acceleration and relative displacement. The performances of the semi-active damping control algorithms are compared with that of a conventional and skyhook passive damper. The results showed that semi-active damping control can reduce the response at resonance without worsening higher frequency isolation performance.

An experiment was set up to investigate the use of an electromagnetic device as a semi-active damper for vibration isolation and verify the simulations. The on-off skyhook control algorithm was chosen to be implemented in the laboratory because of its simplicity and effectiveness. Four series of test were conducted to investigate the dynamic characteristics of the electromagnetic damper. The measurement results showed that by opening and closing the circuit of the coil system, the damping of the system can be effectively changed. Thus, it can be used as a semi-active damper for vibration isolation.

The measurement results agreed with the theoretical prediction reasonably well. By varying the damping of the system a few times during one vibration period, the acceleration response of the mass can be reduced. The measured result showed that the semi-active damper gives a marginally better performance than the conventional passive damper. This performance was limited by the dynamic properties of the suspension in the loudspeaker. Better performance could be achieved if the off-state damping ratio could be made much smaller and the on-state damping much larger.

The measurement results also showed that the fraction of time when the damper is on is frequency dependent. This means that the switching of the damper may be compromised if more than one frequency present at the same time, in the case of general periodic excitations for example. This is the subject of the next chapter.

CHAPTER 4

4. ISOLATION OF PERIODIC DISTURBANCES

4.1 INTRODUCTION

In the previous chapter, the performance of semi-active damping control strategies in isolating harmonic disturbances has been presented. The results show that semi-active damping systems can provide better performance than a conventional passively damped system, especially at higher frequencies. However, in practice, disturbances may comprise a number of harmonics. The purpose of this chapter is to study the effectiveness of semi-active damping control strategies in isolating disturbances with more than one frequency component.

A semi-active damper is switched on and off within an operating cycle according to the condition function to suppress the responses of the system. This means that switching time is an important issue for the success of a semi-active damper. Both the theoretical and experimental results in Chapter 3 show that the switching of a semi-active damper is frequency dependent. If only one frequency is present in the excitation, a semi-active damper will be switched to suppress the response of the system due to the excitation at that particular frequency. One can expect that switching times may be less favourable for suppressing that particular frequency due to the presence of extraneous frequency components.

The effects of multiple harmonics on the switching and performance of a semi-active damper will be investigated. For simplicity, only the on-off skyhook semi-active damper is considered in this chapter, which is relatively simple to implement whilst maintaining better isolation performance than a conventional passive damper. A specific example of multiple harmonic excitation is periodic disturbances in which the frequency components are integer multiples of the fundamental frequency. Periodic disturbances are commonly met in practice, for example the vibration of a cam-follower system. The effectiveness of the semi-active damper in isolating periodic disturbances will also be studied.

Chapter 4 consists of four sections. Following the introduction section 4.2 describes the effect on the switching time of the damper of introducing a secondary frequency in addition to a fundamental frequency. The secondary frequencies are limited to be harmonics or subharmonics of the fundamental frequency. Section 4.3 discusses the effectiveness of the on-off skyhook damper in isolating two commonly met periodic disturbances. Experimental work carried out to study the effects of multiple harmonics on the switching time is also presented. The chapter ends with some conclusions and comments on the effectiveness of using semi-active damping control for isolating periodic disturbances.

4.2 EFFECTS OF MULTIPLE FREQUENCIES ON SWITCHING OF A SEMI-ACTIVE DAMPER

Recalling from the previous chapter that the switching of a semi-active skyhook damper is controlled by the product of the absolute velocity and the relative velocity, then the instances at which a semi-active damper is required to switch will depend on the frequencies present in the disturbance. If only one frequency is present in the excitation, the damper will be switched according to the signs of the condition function arising from that particular frequency. However, the switching of a semi-active damper may be compromised for both frequencies if there is a second frequency also present in the excitation. This section investigates the effects of a disturbance with multiple frequencies on switching times of semi-active dampers. The frequency dependent characteristics of the switching of an on-off skyhook semi-active damper are first illustrated. The effect of a second frequency on the switching times ideally required to attenuate the first frequency is studied in detail. General conclusions on the effects of multiple frequencies on the switching of the semi-active damper are then presented.

4.2.1 FREQUENCY DEPENDENCE OF THE SWITCHING FUNCTION FOR A SEMI-ACTIVE SKYHOOK DAMPER

Recall that the on-off skyhook control algorithm is defined by

$$c_{sa} = \begin{cases} c_{\max} & \dot{x}(\dot{x} - \dot{x}_0) \geq 0 \\ c_{\min} & \dot{x}(\dot{x} - \dot{x}_0) < 0 \end{cases} \qquad \text{Equation Section 4}(4.1)$$

When the semi-active damper is subjected to a pure-tone excitation, the percentages of the time when the damper is switched on and off are frequency dependent. This can be demonstrated using a conventional passive SDOF system by studying the phase relationship between the two variables of the condition function, namely the velocity and relative velocity. If the velocity response and the velocity of the base excitation in the frequency domain are denoted by $\dot{\mathrm{X}}$ and $\dot{\mathrm{X}}_0$, then one has the following transfer function relating $\dot{\mathrm{X}}$ and $\dot{\mathrm{X}}_0$

$$\frac{\dot{\mathrm{X}}}{\dot{\mathrm{X}}_0} = \frac{1 + i2\zeta \dfrac{\omega}{\omega_n}}{1 - \left(\dfrac{\omega}{\omega_n}\right)^2 + i2\zeta \dfrac{\omega}{\omega_n}} \tag{4.2}$$

Using equation (4.2), one can get

$$\frac{\dot{\mathrm{X}}}{\dot{\mathrm{X}} - \dot{\mathrm{X}}_0} = \frac{1 + i2\zeta \left(\dfrac{\omega}{\omega_n}\right)}{\left(\dfrac{\omega}{\omega_n}\right)^2} \tag{4.3}$$

The phase angle between the velocity and relative velocity can be expressed as

$$\angle \frac{\dot{\mathrm{X}}}{\dot{\mathrm{X}} - \dot{\mathrm{X}}_0} = \tan^{-1}\left(2\zeta \frac{\omega}{\omega_n}\right) \tag{4.4}$$

The result in equation (4.4) is shown in Figure 4.1 for various damping ratios, and the fraction of time when the velocity and relative velocity have same sign is shown in Figure 4.2. From Figures 4.1 and 4.2 one can see that for low frequency excitation, the phase angle between the velocity and relative velocity is very small, and the absolute velocity and relative velocity are nearly in phase. As the excitation frequency increases, the phase difference increases and approaches 90^o as $\omega / \omega_n \to \infty$. It must be emphasised that this is an approximate interpretation of what happens because a conventional passive system is considered instead of a semi-active system. In a conventional passive system, $\dot{x}$ and $\dot{x}_0 - \dot{x}_0$ are harmonic to harmonic excitation.

However, although, $\dot{x}$ and $\dot{x}_0 - \dot{x}_0$ are non-harmonic responses to harmonic excitations due to the non-linearity of the on-off skyhook semi-active damper, the results are reasonably representative according to the experimental results in section 3.7.5.

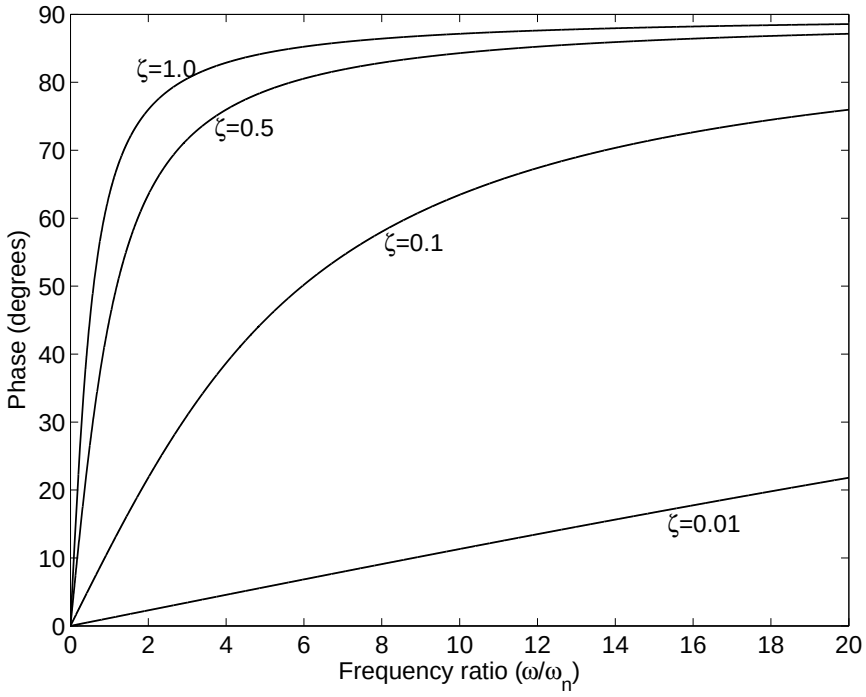

Figure 4.1 Phase angle between absolute velocity and relative velocity for a base excited passive SDOF system

Assuming that the waveforms of the velocity and relative velocity for the passive and semi-active systems are not too dissimilar, one can draw qualitative conclusions regarding the duration of the on-cycle. For an on-off skyhook semi-active system, one would expect the damper to be on most of the time at low frequencies since $\dot{x}$ and $\dot{x} - \dot{x}_0$ have the same sign most of the time. As the excitation frequency increases, the damper would be on less of the time. It can be expected that the fraction of time when the damper is on will approach 0.5 at higher frequencies. The actual frequency dependent characteristics of a semi-active damper are illustrated through numerical simulations in the next section.

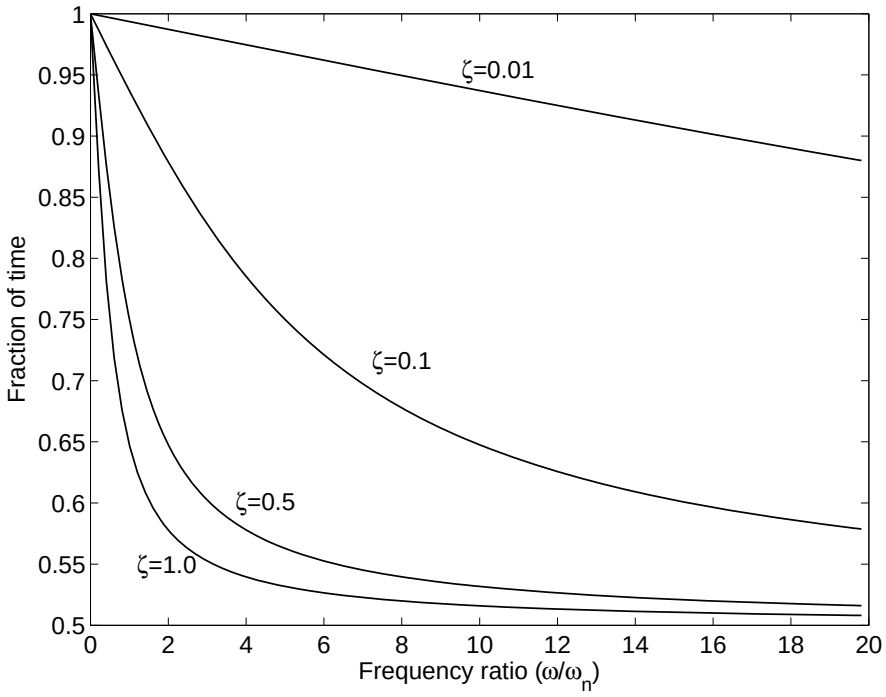

Figure 4.2 Fraction of the time when velocity and relative velocity have the same sign

4.2.2 SIMULATION OF EFFECT OF MULTIPLE FREQUENCIES ON SWITCHING OF SDOF SEMI-ACTIVE SKYHOOK DAMPER

The interpretation in section 4.2.1 shows that when only one frequency is present in the excitation, the percentage of time that a semi-active damper is switched on is frequency dependent. It can be seen from Figure 4.2 that this observation is especially true for the frequency range $0 \le \omega / \omega_n \le 3$, say, for moderate to high damping values $\zeta > 0.5$. When another frequency is also present in the excitation, the switching times may no longer be ideal for the first frequency. Numerical simulations have been carried out on a SDOF system with a semi-active on-off skyhook damper subject to base excitation to investigate the effects of an extraneous frequency component on the switching for the fundamental frequency of interest. An example of the results is shown in Figure 4.3, in which the fundamental frequency is chosen to be at the natural frequency. The figure shows the time percentages for which the semi-active damper is in the same state with and without the presence of other frequency components. The on-state damping ratio of the semi-active on-off skyhook damper is 0.5, and the off-state damping ratio is zero. The disturbance is generated by superposing unit amplitudes of the various harmonics.

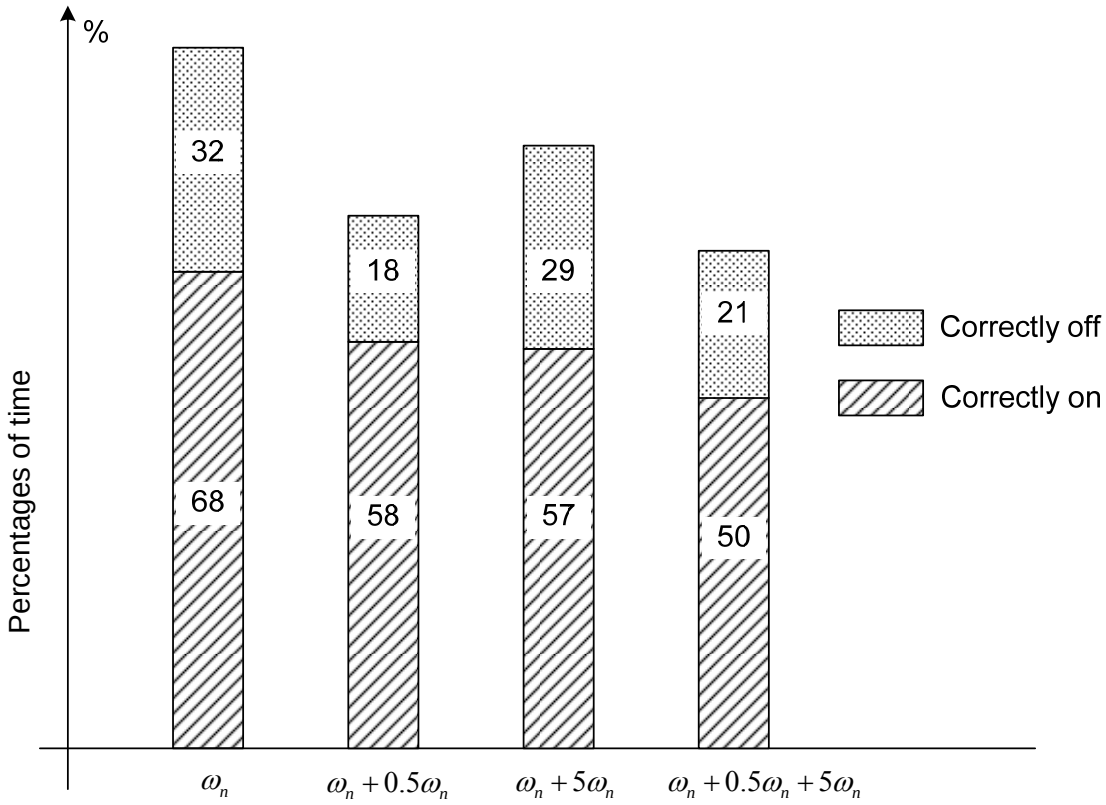

Figure 4.3 Effect of multiple input frequencies on the switching characteristics of an on-off semi-active skyhook damper (correctly on: fraction of time when the damper is on as required by the fundamental frequency; correctly off: fraction of time when the damper is off as required by the fundamental frequency)

One can see from the first column in Figure 4.3 that when only frequency, ω_n, is applied to the system, the percentage of time when the damper is in the on-state is 68% and the off-state is 32%. This is consistent with the corresponding result for a passive SDOF system in Figure 4.2 ($\zeta = 0.5$, frequency ratio $= 1$, which shows that the fraction of time when the velocity and relative velocity have same sign is 72%). This again indicates that the behaviour of the condition function is not significantly affected by the nonlinearity in the system.

For the combinations of different frequencies, the percentage of time when the switching state is the same as when only one frequency component is present is shown. It can be seen that with the addition of an excitation at a frequency of 0.5 times the natural frequency of the system (2nd column), the switching characteristics are far from the ideal for isolating the ω_n component. The percentage of time when the damper is correctly on to isolate the excitation at just ω_n drops from 68% to 58%

and the time when it is correctly off drops from 32% to 18%. When an excitation at a frequency of five times the natural frequency of the system is added (3rd column), the switch characteristics for an excitation at about ω_n are not significantly affected. The percentages of time when the damper are correctly on and off drop to 57% and 29% respectively. When both an excitation at a frequency of 0.5 times and five times the natural frequency of the system is added (4th column), the switch characteristics for an excitation at about ω_n are significantly affected. The percentage of time when the damper is correctly on to isolate the excitation at just ω_n drops to 50% and the time when it is correctly off drops to 21%. As can be seen from the 2nd and 3rd columns, this is mainly due to the presence of the excitation at 0.5 times the natural frequency of the system.

It can be expected that changes in the switching times due to extraneous frequency components may adversely affect the response of the system at the primary frequencies of interest, which is crucial to the application of semi-active damping control. The effect of extraneous frequency components on switching times will be studied firstly in the following section, and the consequences of this on isolation performance will be studied afterwards.

4.2.3 ANALYSIS OF EFFECT OF MULTIPLE FREQUENCIES ON SWITCHING TIME

The simulation results in section 4.2.2 show that switching times of the semi-active damper may be adversely affected by extraneous frequency components. The analysis in this section seeks to establish when this effect can be expected to be most pronounced. Later, general results are applied to a conventional passive SDOF system to study the skyhook condition function.

Assume that the velocity response of a system comprises two harmonics, $y_1(t)$ and $y_2(t)$, at frequencies ω_1 and ω_2, and amplitudes Y_1 and Y_2 respectively. $y_1(t)$ and $y_2(t)$ are synchronised to be in phase at the initial time. In the following context ω_1 is named fundamental frequency, and ω_2 is named secondary frequency. A "velocity switch" will occur when $y_1(t) + y_2(t) = 0$, whereas without the second frequency

component, the switch would have occurred at $y_1(t) = 0$. Therefore, the signs of $y_1(t)$ and $y_1(t) + y_2(t)$ can be compared to determine the effects on the switching times of $y_1(t)$ by the addition of $y_2(t)$. In order to achieve a good performance in isolating disturbance $y_1(t)$ in the presence of $y_2(t)$ it is desirable for the switch to be largely unaffected by the presence of $y_2(t)$.

Two special cases when $\omega_2 = n\omega_1$ and $\omega_1 = n\omega_2$, ($n = 1, 2, 3, ...$) are considered, i.e. when ω_2 is a harmonic or subharmonic of ω_1. In each case, there are two different situations when comparing the amplitudes of $y_1(t)$ and $y_2(t)$, i.e. $Y_1 \le Y_2$ and $Y_1 \ge Y_2$.

(1) Case I: $\omega_2 = n\omega_1$, ($n = 1, 2, 3, ...$) *, i.e. harmonics of the fundamental frequency*

Figures 4.4(a) and (b) illustrate how the sign of $y_1(t)$ will be affected by the addition of $y_2(t)$ for the case when $\omega_2 = n\omega_1$. Figure 4.4(a) shows the time histories of $y_1(t)$ and $-y_2(t)$ for the case when $Y_1 \le Y_2$ and $\omega_2 = 4\omega_1$, and Figure 4.4(b) shows the time histories for $Y_1 \ge Y_2$ and $\omega_2 = 7\omega_1$. In both Figure 4.4(a) and (b), if only $y_1(t)$ is present, then the sign of $y_1(t)$ changes at the points when $y_1(t) = 0$. However, the sign of $y_1(t) + y_2(t)$ changes at points when $y_1(t) = -y_2(t)$, i.e. the crossing points of $y_1(t)$ and $-y_2(t)$. Thus, the sign of $y_1(t)$ and $y_1(t) + y_2(t)$ is different during some parts of a cycle.

For the first case when $Y_1 \le Y_2$ (as shown in Figure 4.4(a)), the addition of $y_2(t)$ causes the switching to be alternately right and wrong for isolating $y_1(t)$. There are n segments per fundamental period when it is right and n segments when it is wrong. It can be observed from the figure that the portion of 'right' switching time when $y_1(t)$ and $y_1(t) + y_2(t)$ have the same sign is bigger than that the portion when $y_1(t)$ and $y_1(t) + y_2(t)$ have the opposite sign. As n increases, the portion of 'right' switching time will decrease until it reaches the limiting case when $\omega_1 << \omega_2$ and $Y_1 << Y_2$. Under this circumstance, the portion of 'right' and 'wrong' switching time will be

equal. So the upper bound when the sign of $y_1(t)+y_2(t)$ and $y_1(t)$ is different is $1/2$ of the period.

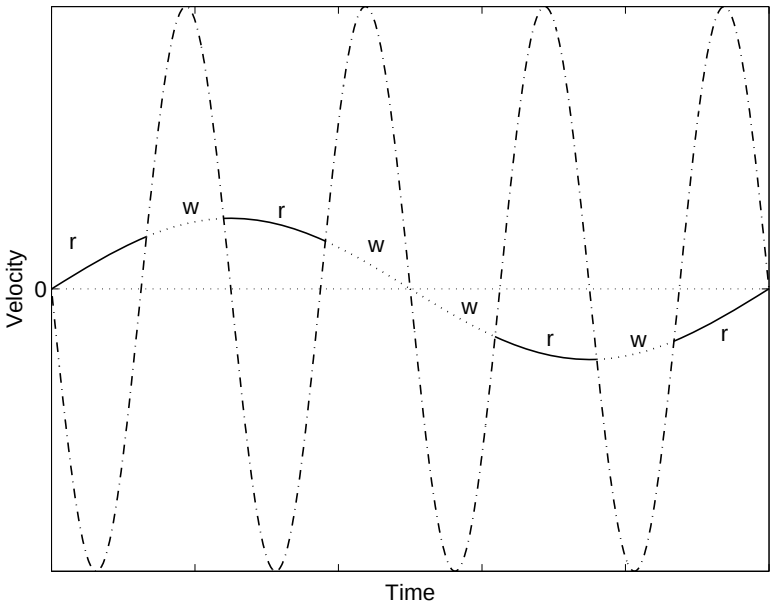

(a)

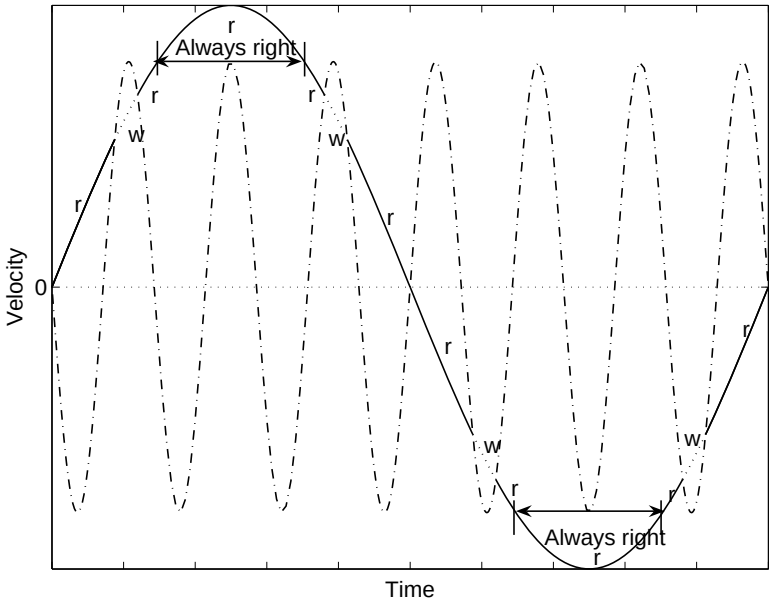

(b)

Figure 4.4 Effect of a secondary frequency on the damper state for the fundamental frequency (a) $\omega_2 = 4\omega_1$ and $Y_1 \le Y_2$ (b) $\omega_2 = 7\omega_1$ and $Y_1 \ge Y_2$ ($-\ y_1(t)$ when it has the same sign as $y_1(t)+y_2(t)$; ---- $y_1(t)$ when it has the opposite sign from $y_1(t)+y_2(t)$; $-\cdot-\cdot-y_2(t)$) ('r' - right, and 'w' - wrong).

For the second case when $Y_1 \geq Y_2$ (as shown in Figure 4.4b), there are two segments of time when the sign of $y_1(t)$ is always right, i.e. when the instantaneous velocity $|y_1(t)| \geq Y_2$. The two segments are equal due to the symmetry of the waveforms of $y_1(t)$ and $y_2(t)$. The fraction of the fundamental period that these two segments together comprise can be written as

$$T_{r,I} = \frac{4}{2\pi}\cos^{-1}\left(\frac{Y_2}{Y_1}\right) = \frac{2}{\pi}\cos^{-1}\left(\frac{Y_2}{Y_1}\right) \tag{4.5}$$

It can be seen from equation (4.5) that when $Y_2 = Y_1$, the fraction of time when the sign of $y_1(t)$ is guaranteed to be right becomes zero. In the remaining time, the switching time for $y_1(t)$ is alternately right and wrong. Let the fraction of time when the switching time of $y_1(t)$ is possibly affected by the presence of $y_2(t)$ be denoted by $T_{pw,I}$. Then $T_{pw,I}$ can be written as

$$T_{pw,I} = 1 - T_{r,I} = 1 - \frac{2}{\pi}\cos^{-1}\left(\frac{Y_2}{Y_1}\right) = \frac{2}{\pi}\sin^{-1}\left(\frac{Y_2}{Y_1}\right) \tag{4.6}$$

One can also see from Figure 4.4 (b) that in the segments where the sign of $y_1(t)$ may be affected by $y_2(t)$ the portion of 'right' time is larger than that the portion of 'wrong' time. With the increase of ω_2, the portion of 'right' switching time will decrease until it reaches the worst case when $\omega_2 >> \omega_1$. Under this circumstance, the 'right' portions and 'wrong' portions are equal, i.e. the damper has the wrong state for a duration of half of $T_{pw,I}$. Let this fraction of time be denoted by $T_{w,I}$. Then from equation (4.6), $T_{w,I}$ can be written as

$$T_{w,I} = \frac{1}{\pi}\sin^{-1}\left(\frac{Y_2}{Y_1}\right) \tag{4.7}$$

(2) Case II: $\omega_2 = \omega_1 / n, (n = 1, 2, 3, ...)$,i.e. subharmonics of the fundamental frequency

The same procedure can be used to find the upper bounds for the fraction of time when $y_1(t) + y_2(t)$ has the opposite sign from $y_1(t)$ for the case when ω_2 is subharmonics of ω_1. Figures 4.5(a) and (b) illustrate how the sign of $y_1(t)$ will be affected by the addition of $y_2(t)$ when $\omega_2 = \omega_1 / n$. Figure 4.5(a) shows the time histories of $y_1(t)$ and $-y_2(t)$ for the case when $Y_1 \le Y_2$ and $\omega_2 = \omega_1 / 2$, and Figure 4.5(b) shows the time histories for $Y_1 \ge Y_2$ and $\omega_2 = \omega_1 / 3$.

For the first case when $Y_1 \le Y_2$ (as shown in Figure 4.5(a)), it can be seen the switching time for $y_1(t)$ is 'right' for at least half of the fundamental period. In the other half of the period, the sign of $y_1(t)$ may be wrong. The worst case is that all of the other half will be 'wrong', which is expected to happen when Y_2 is much bigger than Y_1. So the upper bound for the fraction of time when the sign of $y_1(t) + y_2(t)$ is different to that of $y_1(t)$ is $1/2$.

For the second case when $Y_1 \ge Y_2$ (as shown in Figure 4.5(b)), the sign of $y_1(t)$ is always right in the first half of its period. In the second half of its period the sign of $y_1(t)$ is always right when the instantaneous velocity $|y_1(t)| \ge Y_2$. So the total fraction of time when the sign of $y_1(t)$ is always right can be written as

$$T_{r,II} = \frac{1}{2} + \frac{2}{2\pi}\cos^{-1}\left(\frac{Y_2}{Y_1}\right) = \frac{1}{2} + \frac{1}{\pi}\cos^{-1}\left(\frac{Y_2}{Y_1}\right) \tag{4.8}$$

It can be seen from equation (4.8) that when $Y_2 = Y_1$, the fraction of time when the sign of $y_1(t)$ is always right becomes $1/2$. In the remaining time, switching time for $y_1(t)$ is wrong. If this fraction of time is denoted by $T_{w,II}$, then $T_{w,II}$ can be written as

$$T_{w,II} = 1 - T_{r,II} = \frac{1}{2} - \frac{1}{\pi}\cos^{-1}\left(\frac{Y_2}{Y_1}\right) = \frac{1}{\pi}\sin^{-1}\left(\frac{Y_2}{Y_1}\right) \tag{4.9}$$

The upper bounds for fraction of time when $y_1(t)$ has the opposite sign from $y_1(t)+y_2(t)$ for the two cases when $\omega_2 = n\omega_1$ and $\omega_2 = \omega_1/n$ are summarised in Table 4.1. It can be seen from the table that when the amplitude of the second harmonic $y_2(t)$ is bigger than that of the $y_1(t)$, the upper bound is $1/2$. The upper bound is independent of whether the secondary frequency is a subharmonic or harmonic of the fundamental frequency. The derived upper bounds for the case $\omega_2 = n\omega_1$ are shown graphically in Figure 4.6 as a function of the amplitude ratio Y_2/Y_1. It should be noted here that the results in Table 4.1 and Figure 4.6 only provide an upper bound for the fraction of time when the sign of $y_1(t)+y_2(t)$ is different from that of $y_1(t)$. The actual fraction of time when the sign of $y_1(t)+y_2(t)$ is different from that of $y_1(t)$ might be anywhere under the upper bound curve.

Table 4.1 Upper bounds for fraction of time when the sign of the sum of two harmonic velocities $y_1(t)+y_2(t)$, is different from that of $y_1(t)$ alone

Frequency / Amplitude	Harmonics $\omega_2 = n\omega_1$	Subharmonics $\omega_2 = \omega_1/n$
$Y_1 \le Y_2$	$\frac{1}{2}$	$\frac{1}{2}$
$Y_1 \ge Y_2$	$\frac{1}{\pi}\sin^{-1}\frac{Y_2}{Y_1}$	$\frac{1}{\pi}\sin^{-1}\frac{Y_2}{Y_1}$

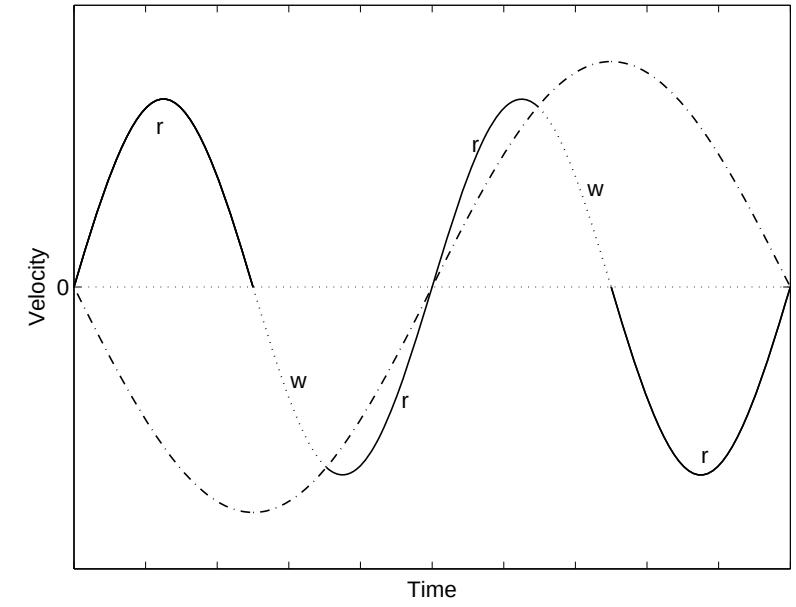

(a)

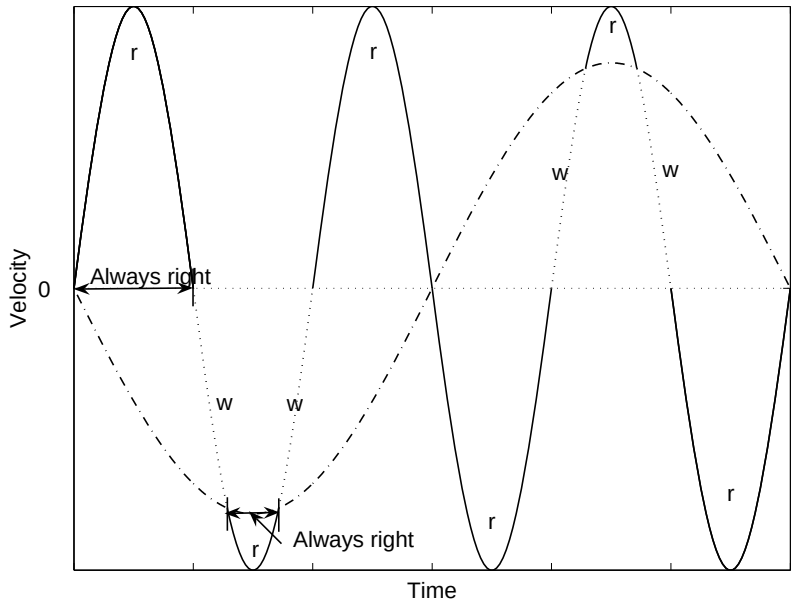

(b)

Figure 4.5 Effect of a secondary frequency on the damper state for the fundamental frequency (a) $\omega_2 = \omega_1/2$ and $Y_1 \le Y_2$ (b) $\omega_2 = \omega_1/3$ and $Y_1 \ge Y_2$ (– $y_1(t)$ when it has the same sign as $y_1(t) + y_2(t)$; ---- $y_1(t)$ when it has the opposite sign from $y_1(t) + y_2(t)$; –·–· $-y_2(t)$) ('r' - right, and 'w' - wrong).

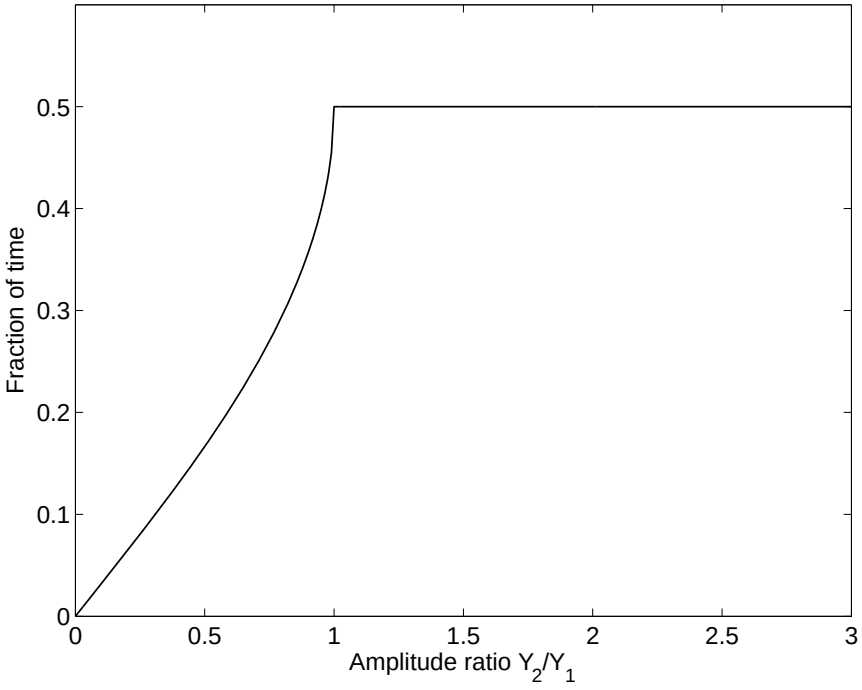

Figure 4.6 Upper bound for the fraction of time when $y_1(t)$ has the opposite sign to $y_1(t)+y_2(t)$

4.2.4 EFFECT OF MULTIPLE HARMONICS ON THE SKYHOOK CONDITION FUNCTION WHEN APPLIED TO A PASSIVE SDOF SYSTEM

In section 4.2.3, the effects of multiple harmonics on the switching time of the condition function in equation (4.1) were investigated using two harmonics, $y_1(t)$ and $y_2(t)$. Upper bounds for the fraction of time when the sign of $y_1(t)+y_2(t)$ is different from that of $y_1(t)$ were derived. This section applies this understanding to the case where $y_1(t)$ and $y_2(t)$ arise from the velocity and relative velocity responses of a passive SDOF system to different input frequencies, which will give some understanding of real semi-active systems.

The condition function for the on-off skyhook semi-active damper in equation (4.1) is composed of two parts: the velocity $\dot{x}$; and the relative velocity $\dot{x}-\dot{x}_0$. Changes in the sign of the condition function are caused by either changes in the sign of the velocity or the sign of the relative velocity. The following analysis uses the physical behaviour of the pure passive system. Assume the two velocity inputs are

$$\dot{x}_{01} = |\dot{x}_{01}| \mathrm{Re}\left(e^{i\omega_1 t}\right); \quad \dot{x}_{02} = |\dot{x}_{02}| \mathrm{Re}\left(e^{i\omega_2 t}\right) \tag{4.10}$$

Correspondingly, the two velocity responses can be written as

$$\dot{x}_1 = |\dot{x}_{01}| \mathrm{Re}\left(H(\omega_1) e^{i\omega_1 t}\right); \quad \dot{x}_2 = |\dot{x}_{02}| \mathrm{Re}\left(H(\omega_2) e^{i\omega_2 t}\right) \tag{4.11}$$

where $H(\omega)$ is the transfer function between the output and input, and defined by

$$H(\omega) = \frac{1 + i2\zeta\omega}{1 - \dfrac{\omega^2}{\omega_n{}^2} + i2\zeta\omega} \tag{4.12}$$

So the amplitudes of $\dot{x}_1$ and $\dot{x}_2$ can be written as

$$|\dot{x}_1| = |\dot{x}_{01}||H(\omega_1)|; \quad |\dot{x}_2| = |\dot{x}_{02}||H(\omega_2)| \tag{4.13}$$

Using the analysis in Table 4.1 of section 4.2.3, the upper bound for the fraction of time when the switching times arising from excitation $\dot{x}_{01} + \dot{x}_{02}$ have the wrong sign from those for excitation $\dot{x}_{01}$ is given by

$$\begin{cases} \dfrac{1}{2} & (|\dot{x}_1| \le |\dot{x}_2|) \\ \dfrac{1}{\pi} \sin^{-1}\left(\dfrac{|\dot{x}_{02}||H(\omega_2)|}{|\dot{x}_{01}||H(\omega_1)|}\right) & (|\dot{x}_1| \ge |\dot{x}_2|) \end{cases} \tag{4.14}$$

The results of equation (4.14) are shown for various damping ratios in Figures 4.7 (a) and (b). In the figure, the damping ratio of the system is set to 0.5 and 1.0, and ω_1 is assumed to be varying from 0.1 to 10 times the natural frequency of the system. ω_2 is chosen to be a subharmonic $(1/10, 1/9, ..., 1/2)$ or harmonic $(2, 3, ..., 9, 10)$ of ω_1. The amplitude of the second input harmonic is equal to that of the first one.

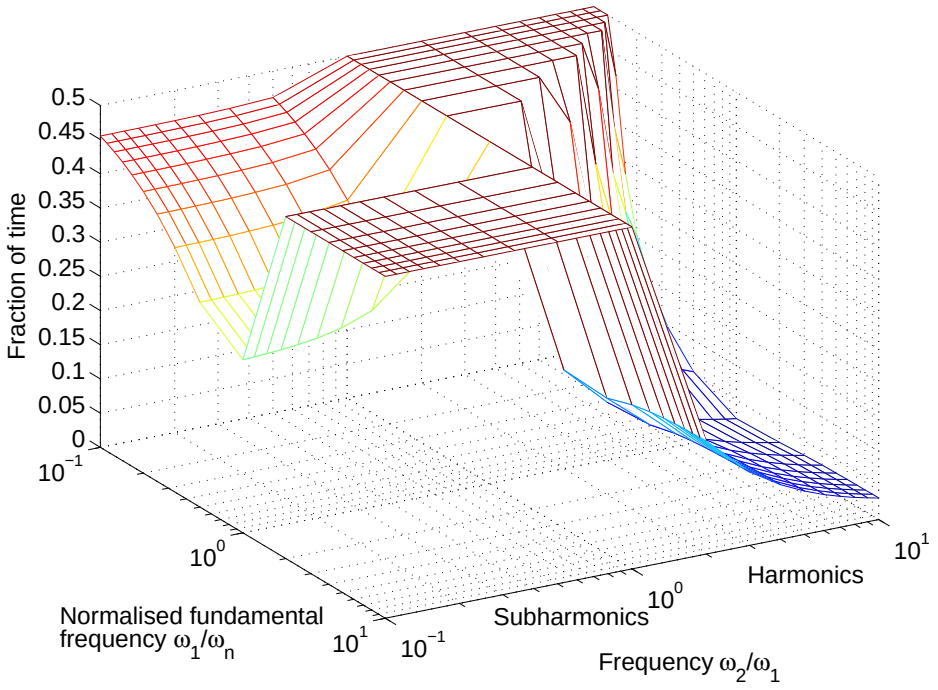

(a)

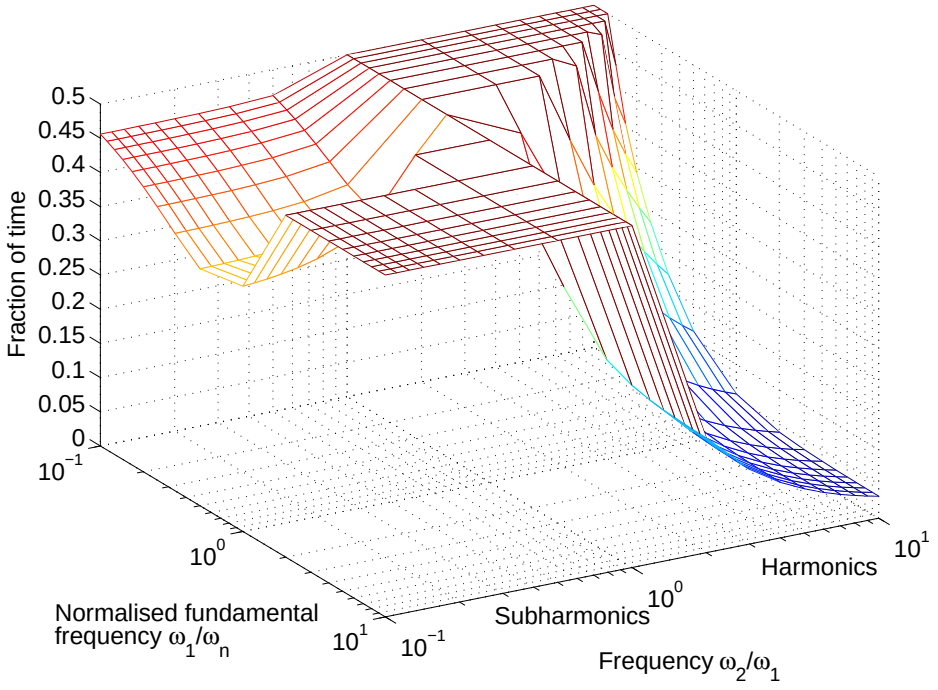

(b)

Figure 4.7 Upper bound for fraction of time when the velocity switch has incorrect state (a) $\zeta = 0.5$; (b) $\zeta = 1.0$

It can be seen from Figures 4.7 (a) and (b) that the addition of the subharmonic ($\omega_2/\omega_1 < 1$) may have a significant effect on the velocity switch for the first frequency

for all excitation frequencies. The fraction of time when the damper has the wrong state can be as large as $1/2$. Harmonics ($\omega_2/\omega_1 > 1$), however, will have less effect on the velocity switch provided that the excitation frequency is above resonance. The larger the damping ratio is, the wider the frequency range over which a secondary harmonic will significantly affect the switching state of the fundamental frequency. The reason for this is that the transmissibility curve for large damping ratio is smoother than that for smaller damping ratio. This implies that the components of response at different frequencies are not so different compared to the case when the damping ratio is small.

The same procedure can be applied to study the effect of multiple harmonics on the relative velocity switch. The relative velocity for only one excitation at individual frequencies, ω_1 and ω_2 can be expressed as follows:

$$\dot{x}_1 - \dot{x}_{01} = |\dot{x}_{01}|\,\mathrm{Re}\left((H(\omega_1)-1)e^{i\omega_1 t}\right); \quad \dot{x}_2 - \dot{x}_{02} = |\dot{x}_{02}|\,\mathrm{Re}\left((H(\omega_2)-1)e^{i\omega_2 t}\right) \quad (4.15)$$

where H_1 and H_2 have the same meaning as in equations (4.11). The amplitudes of $\dot{x}_1 - \dot{x}_{01}$ and $\dot{x}_2 - \dot{x}_{02}$ can be further written as

$$|\dot{x}_1 - \dot{x}_{01}| = |\dot{x}_{01}||H(\omega_1)-1|; \quad |\dot{x}_2 - \dot{x}_{02}| = |\dot{x}_{02}||H(\omega_2)-1| \quad (4.16)$$

The upper bound for the fraction of time when the relative velocity switch is wrong is given by

$$\begin{cases} \dfrac{1}{2} & (|\dot{x}_1 - \dot{x}_{01}| \le |\dot{x}_2 - \dot{x}_{02}|) \\ \dfrac{1}{\pi}\sin^{-1}\left(\dfrac{|\dot{x}_{02}||H(\omega_2)-1|}{|\dot{x}_{01}||H(\omega_1)-1|}\right) & (|\dot{x}_1 - \dot{x}_{01}| \ge |\dot{x}_2 - \dot{x}_{02}|) \end{cases} \quad (4.17)$$

The results of equation (4.17) are shown graphically in Figures 4.8(a) and (b). In the figure, the damping ratio of the system is set to 0.5 and 1.0, and ω_1 is assumed to be varying from 0.1 to 10 times the natural frequency of the system. ω_2 is chosen to be a subharmonic ($1/10, 1/9, ..., 1/2$) or harmonic ($2, 3, ..., 9, 10$) of ω_1. The amplitude of the second input harmonic is equal to that of the first one. One can see from the figure

that the effect on relative velocity switching of the presence of harmonics of the fundamental frequency is significant but subharmonics have little effect. This is true except for the case when the fundamental frequency is close to resonance ($\omega_1 \approx \omega_n$) and the damping is very small.

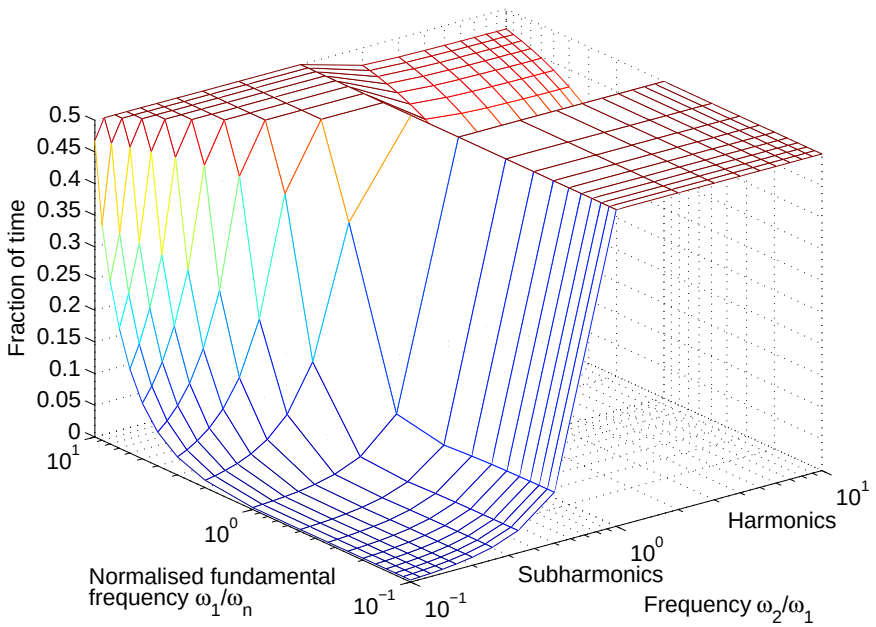

(a)

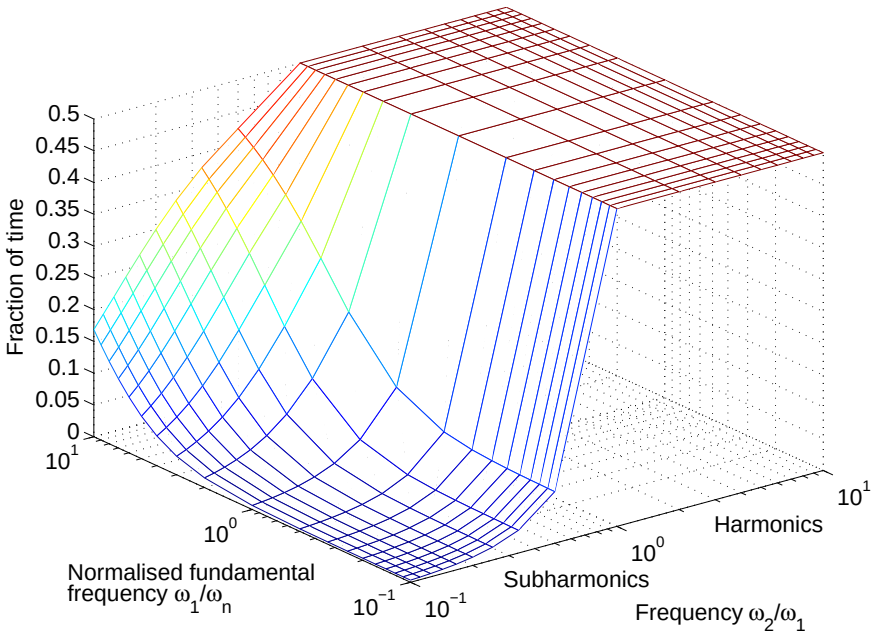

(b)

Figure 4.8 Upper bound for fraction of time when the relative velocity switch has incorrect state (a) $\zeta = 0.5$; (b) $\zeta = 1.0$

The conclusions from section 4.2.4 indicate that the time for which the damper has the wrong state due to an extraneous frequency is amplitude dependent. For the actual system, the velocity responses depend on the properties of the excitation and also the characteristics of the system. Thus the effects are also frequency dependent. When the secondary frequency is a subharmonic of the fundamental frequency, the effects will be most on the velocity switch. Whilst when the secondary frequency is a harmonic of the fundamental frequency, the effects will be mostly on the relative velocity switch. If both harmonics and subharmonics are present then the total effects on the switching time will be decided by both the velocity and relative velocity switch.

This general conclusion can be used to explain the simulation results of section 4.2.2 as shown in Figure 4.3 to some extent. With the addition of a secondary frequency $\omega_2 = 0.5\omega_n$ and/or $\omega_2 = 5\omega_n$ to $\omega_1 = \omega_n$, both the velocity switch and relative velocity switch are affected. Thus the fractions of time when the damper is correctly on and off are affected.

4.2.5 EXPERIMENTAL STUDY OF THE EFFECT OF MULTIPLE HARMONICS ON THE ON SWITCHING TIME OF A SEMI-ACTIVE ON-OFF SKYHOOK DAMPER

Experimental work was carried out to study the effect of a secondary frequency on the switching of fundamental frequency using the experimental set-up for semi-active vibration isolation detailed in section 3.7 of the previous chapter. The fundamental frequency was chosen as 10Hz, 15Hz and 30 Hz in turn to represent the whole working frequency range of the experimental setup. Due to the limitation of the working frequency range of the experimental rig the secondary frequency was varied from 5Hz to 60 Hz in steps of 2Hz for each primary frequency instead of only looking at harmonics or subharmonics. The two harmonics were of equal amplitude. The system was run to reach steady state, and the acceleration response of the system, the acceleration of the base and the voltage across the digital switch were measured.

The natural frequency of the system was identified to be about 15Hz in section 3.7. Measured time histories for excitation at combinations of frequencies 10Hz and 15Hz, 10Hz and 30Hz, and 15Hz and 30Hz are shown in Figures 4.9, 4.10 and 4.11 respectively. Figures 4.9(a), 4.10(a) and 4.11(a) show the response time histories for

each frequency combination. It can be seen from Figure 4.11(a) that the 30Hz harmonic does not affect the10Hz harmonic waveform very much. The shape of the response curve looks more like a harmonic. Figures 4.9(b), 4.10(b) and 4.11(b) show the measured voltage across the digital switch. The time histories for each individual frequency in the frequency combination are also shown in the figure as a comparison. It can be seen that the switching time for an excitation at the fundamental frequency has been affected by the presence of the extraneous frequency. There are times when the damper is switched off when the fundamental frequency component wants it to be on, and vice versa.

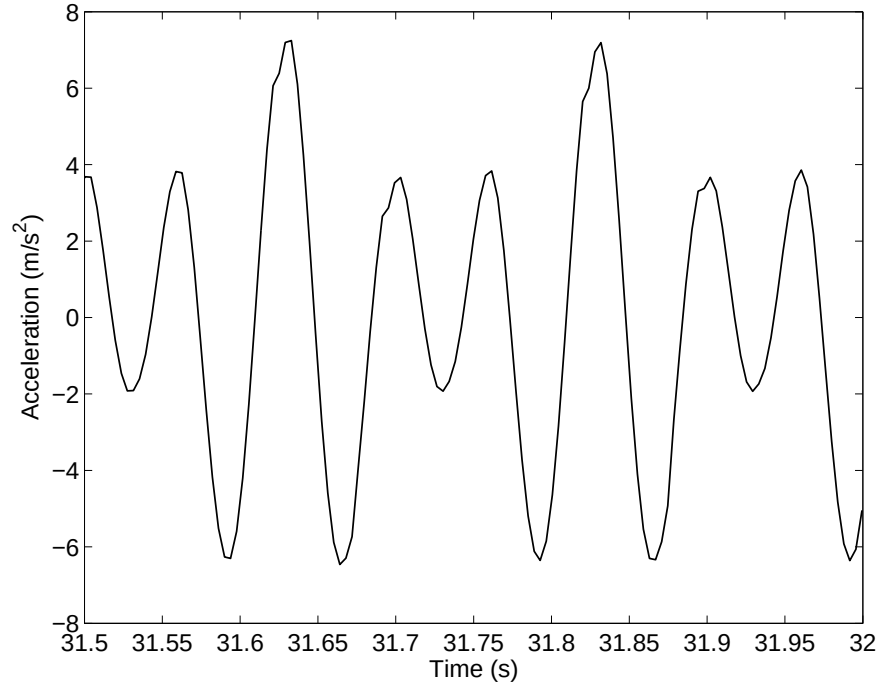

(a)

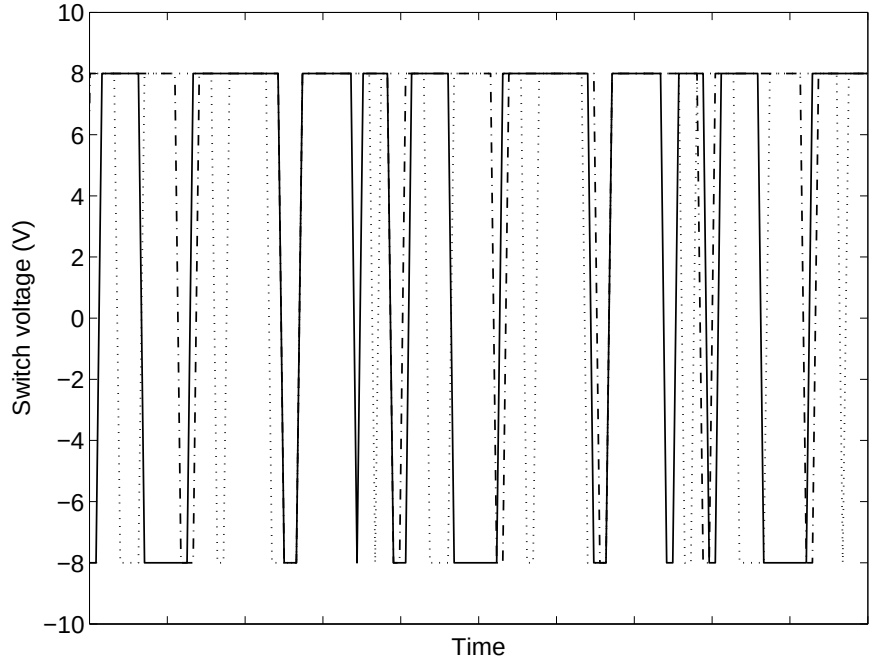

(b)

Figure 4.9 Time histories showing the effect of a 15Hz frequency on the switching of the damper to a 10Hz frequency (a) acceleration response (b) measured voltage across the digital switch (− 10Hz and 15Hz; ····· 10Hz only; −·−·− 15Hz only)

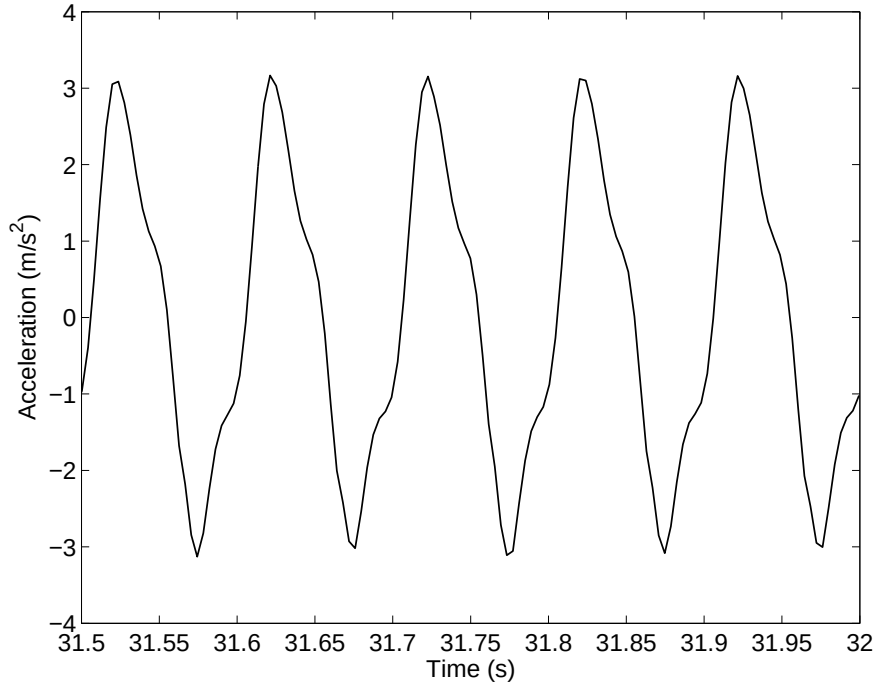

(a)

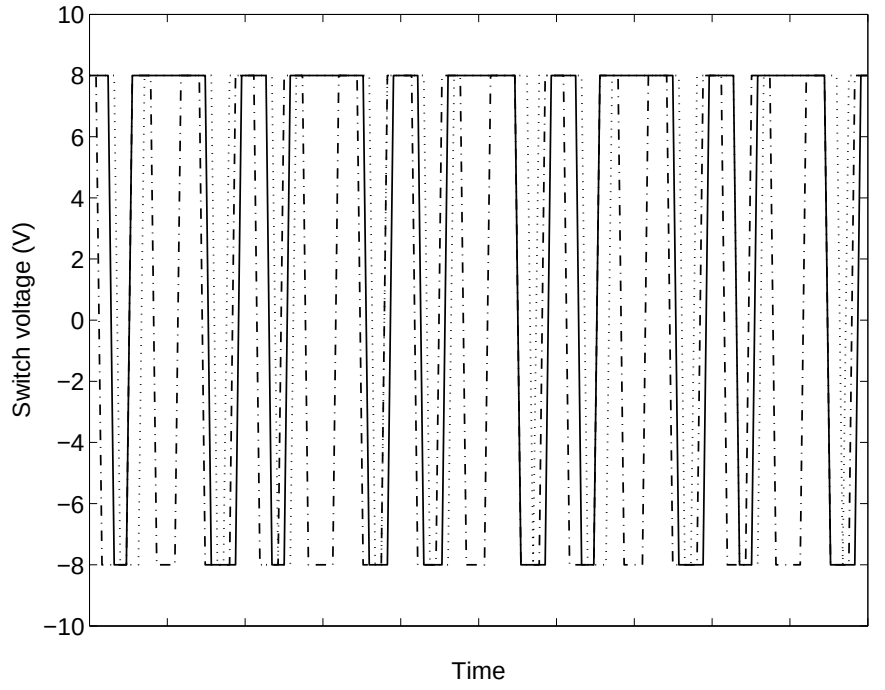

(b)

Figure 4.10 Time histories showing the effect of a 30Hz frequency on the switching of the damper to a 10Hz frequency (a) acceleration response (b) measured voltage across the digital switch (− 10Hz and 15Hz; ····· 10Hz only; −·−·− 15Hz only)

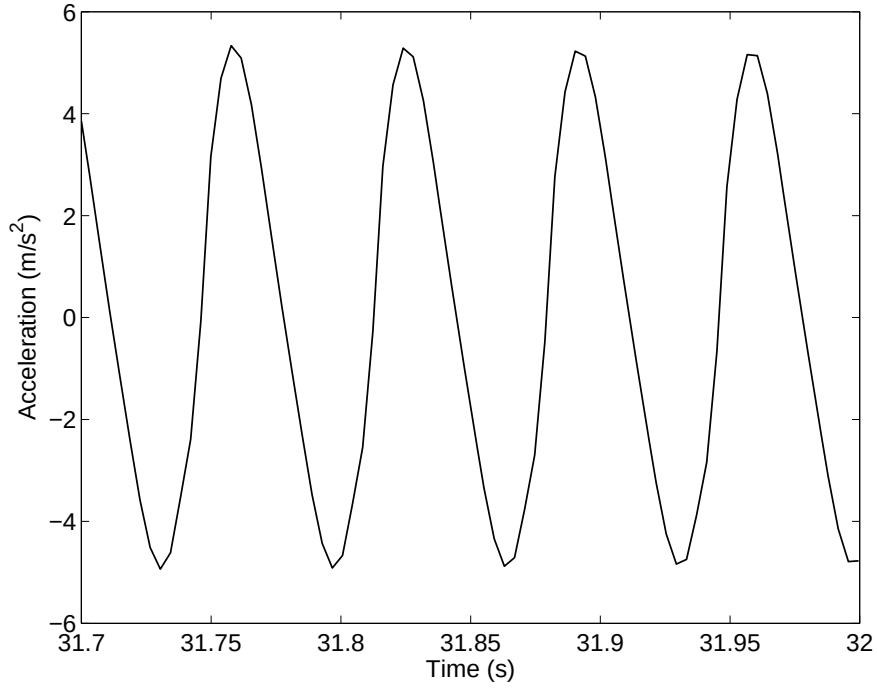

(a)

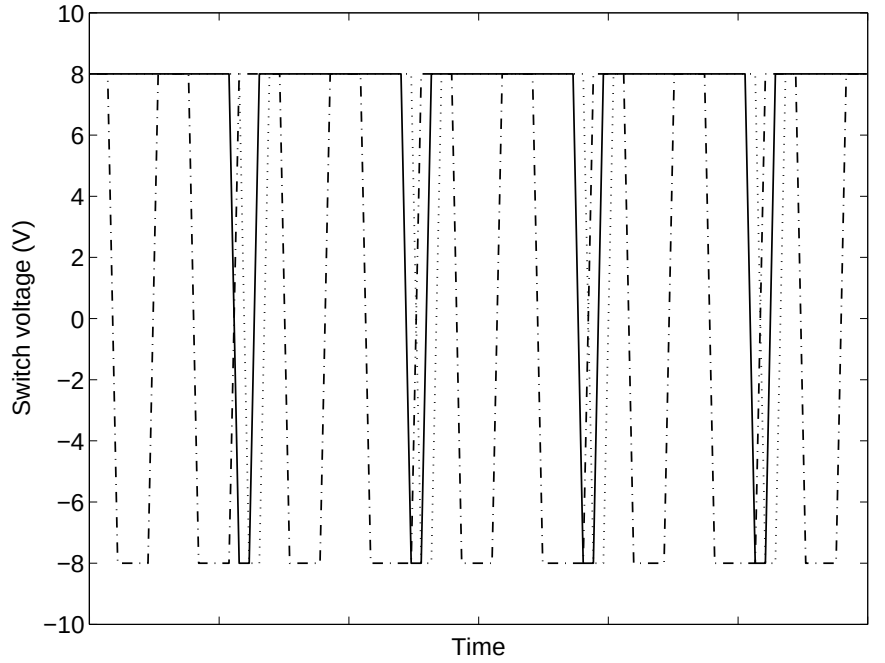

(b)

Figure 4.11 Time histories showing the effect of a 30Hz frequency on the switching of the damper to a 15Hz frequency (a) acceleration response (b) measured voltage across the digital switch (− 10Hz and 15Hz; ····· 10Hz only; −·−·− 15Hz only)

The switching time of the semi-active damper in one vibration period can be divided into four parts by comparing the on and off-state of the excitation at the combination of the excitation at secondary frequency and fundamental frequency and the fundamental frequency: (1) the fraction when the damper is on and the excitation at the primary frequency also required it to be on; (2) the fraction when the damper is on while the excitation at primary frequency requires it to be off; (3) the fraction when the damper is off and the excitation at the primary frequency also required it to be off; (4) the fraction when the damper is off while the excitation at the primary frequency requires it to be on.

Figures 4.12 to 4.14 show these four fractions for the primary frequencies of 10 Hz, 15Hz and 30 Hz respectively. It can be seen from Figures 4.12 to 4.14 that the switching times associated with just the fundamental frequency were more or less affected by the presence of the secondary frequency except when these two frequencies are equal to each other. For all the cases, the frequencies of the secondary harmonic in the range up to 30Hz have greater effects than others. By the presence of the extraneous harmonic near the resonance frequency, the switching of the damper for the primary harmonic will be greatly affected. For example, as shown in Figure 4.14, the fraction of the on-state time for the fundamental frequency at 30Hz is 0.48 and the off-state time is 0.52. However, with the presence of an extraneous frequency at 15Hz, the damper is switched on for 86% of the period, of which only a fraction of 0.40 is correct according to the requirement by the harmonics at 30Hz. The remaining fraction of 0.46 is completely opposite to the requirement.

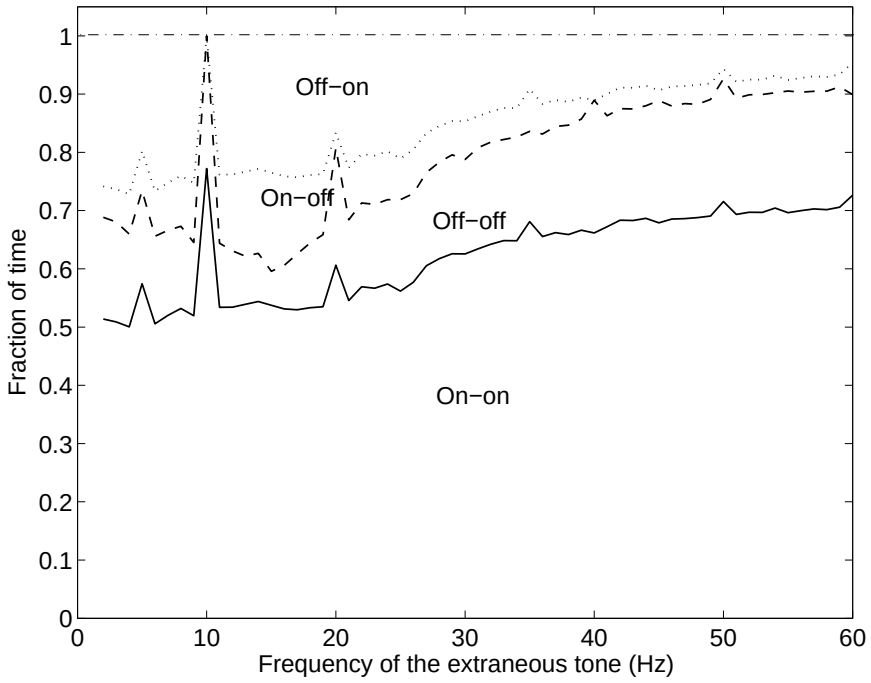

Figure 4.12 Fractions of times for different switch states of the damper with the presence of an extraneous tone in addition to a 10Hz tone

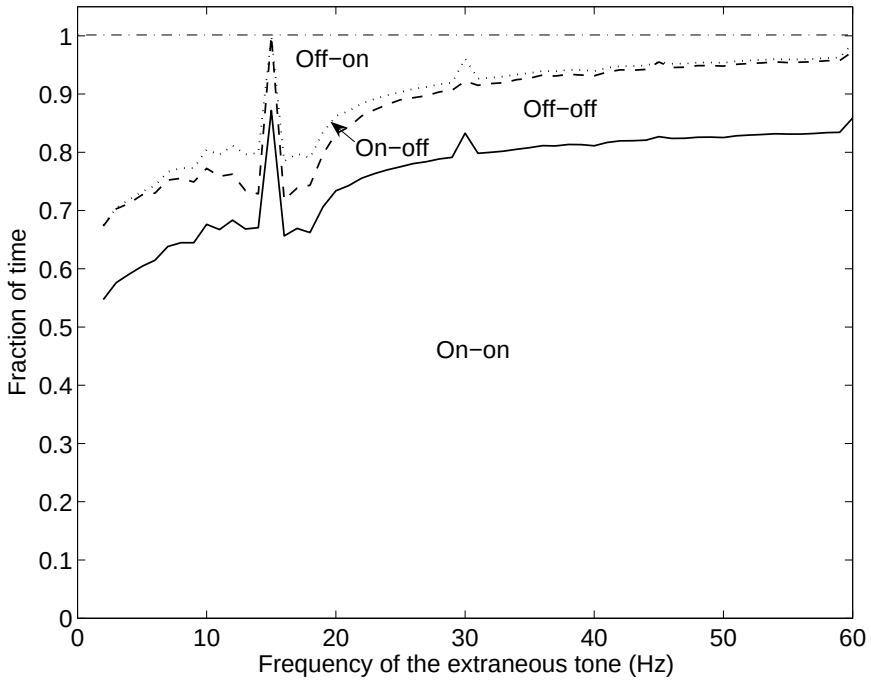

Figure 4.13 Fractions of times for different switch states of the damper with the presence of an extraneous tone in addition to a 15Hz tone

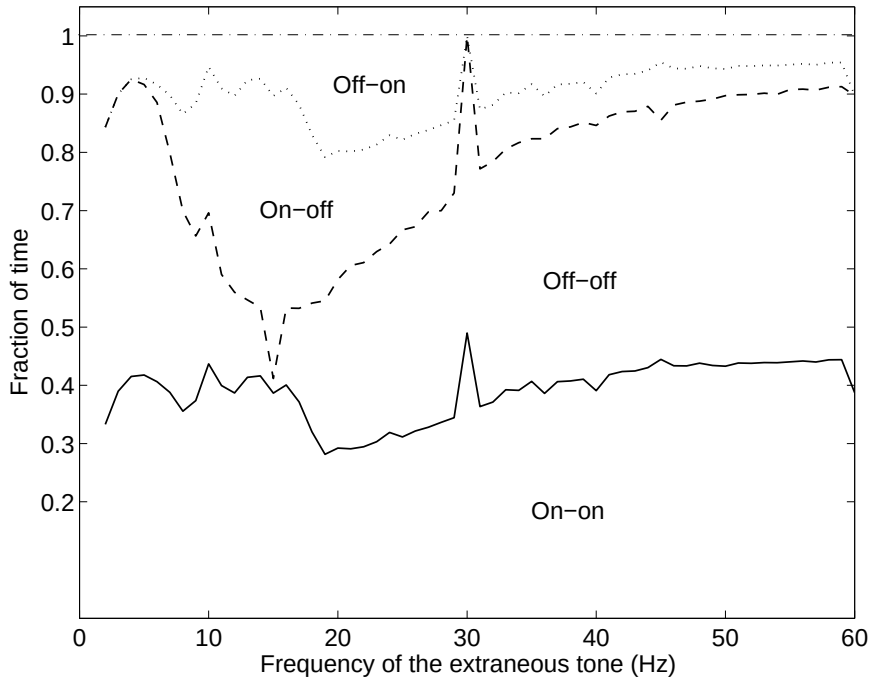

Figure 4.14 Fractions of times for difference switching states of the damper with the presence of an extraneous frequency in addition to a frequency at 30Hz

4.3 PERFORMANCE OF THE SEMI-ACTIVE DAMPER IN ISOLATING PERIODIC DISTURBANCES

In this section the vibration isolation performance of the semi-active skyhook damper for periodic disturbances is discussed. Two periodic waveforms which are commonly studied in the literature are used as the excitation. The simulation results are compared with the performance due to conventional and skyhook passive dampers. Experimental work conducted using one of the periodic waveforms to investigate the isolation performance of the semi-active damper is also presented.

4.3.1 FOURIER ANALYSIS

Although harmonic motion is simpler to analyse, the motion of many vibratory systems is not harmonic. However, in many cases the vibrations are periodic. For example, a wing panel adjacent to a propeller may vibrate periodically at a fundamental frequency equal to the cyclic rate at which propeller blades pass the panel and also at multiples of this blade-pass frequency. Any periodic function of time

can be represented by a Fourier series as an infinite sum of sine and cosine terms. If $x(t)$ is a periodic function with period τ, its Fourier series representation is given by

$$x(t) = \frac{a_0}{2} + \sum_{n=1}^{\infty} (a_n \cos n\omega t + b_n \sin n\omega t) \tag{4.18}$$

where $\omega = 2\pi / \tau$ is the fundamental frequency. a_0, a_n and b_n are constant coefficients, and are given by

$$a_0 = \frac{\omega}{\pi} \int_0^{\tau} x(t) dt \tag{4.19}$$

$$a_n = \frac{\omega}{\pi} \int_0^{\tau} x(t) \cos n\omega t dt \tag{4.20}$$

$$b_n = \frac{\omega}{\pi} \int_0^{\tau} x(t) \sin n\omega t dt \tag{4.21}$$

Although the series in equation (4.18) is an infinite sum, we can approximate most periodic functions with only the first few harmonics.

4.3.2 EFFECTIVENESS OF THE SEMI-ACTIVE DAMPER IN ISOLATING PERIODIC DISTURBANCES

Figure 4.15 shows a schematic of a semi-active system subject to periodic excitation. To study the effectiveness of the semi-active damper in isolating periodic disturbances, two commonly met periodic wave forms are chosen, which are shown in Figures 4.16 (a) and (b). The Fourier series expansion of the square wave function shown in Figure 4.16(a) can be written as

$$\ddot{x}_{01}(t) = -\frac{4A}{\pi} \sum_{n=1}^{\infty} \frac{1}{(2n-1)} \sin(2n-1)\omega_0 t \tag{4.22}$$

The Fourier series expansion of the triangular wave function shown in Figure 4.16(b) can be written as

$$\ddot{x}_{02}(t) = \frac{8A}{\pi^2} \sum_{n=1}^{\infty} \frac{(-1)^{n-1}}{(2n-1)^2} \sin(2n-1)\omega_0 t \tag{4.23}$$

where A is the amplitude and ω_0 is the fundamental frequency of the Fourier series.

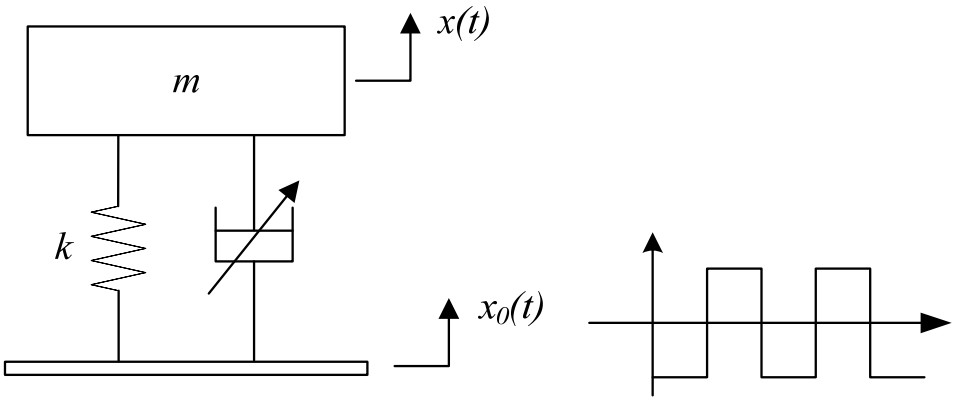

Figure 4.15 Schematic of a semi-active system subject to periodic excitation

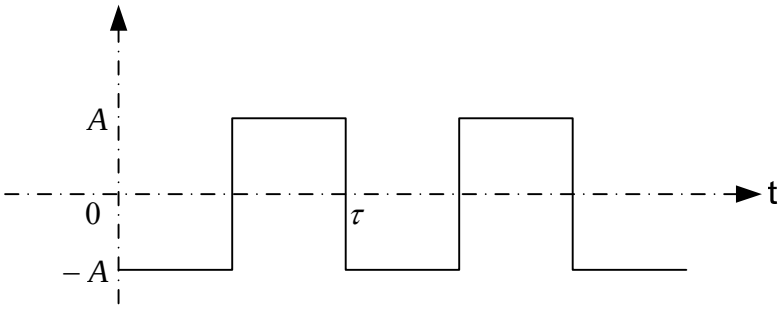

(a)

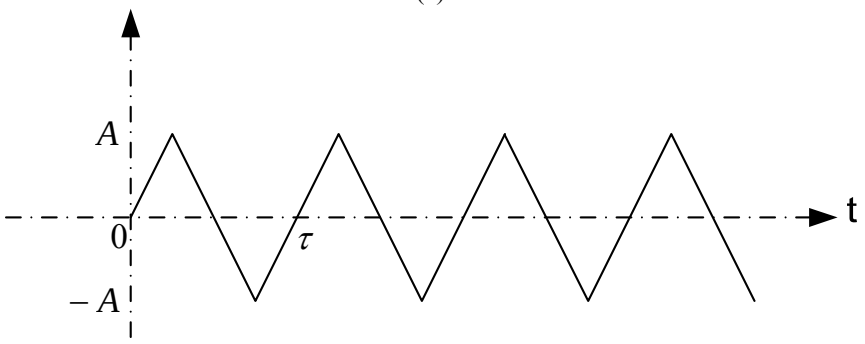

(b)

Figure 4.16 Wave forms of two periodic functions (a) square wave (b) triangular wave

It is required to compare the isolation performance of the semi-active damper in isolating periodic disturbances with that of conventional passive dampers. For this purpose, the following RMS acceleration transmissibility is defined

$$a_{TR}(\bar{\omega}) = \frac{RMS(\ddot{x})}{RMS(\ddot{x}_0)} \tag{4.24}$$

where $\bar{\omega}$ is the fundamental frequency of the periodic disturbance.

Numerical simulations were carried out to calculate the RMS acceleration transmissibility. Only the first three harmonics in equations (4.22) and (4.23) are used to represent the periodic functions. The fundamental frequencies of the periodic function are chosen to vary from 0.1 to 10 times the natural frequency of the system.

Figures 4.17 and 4.19 show the acceleration transmissibility of the semi-active system to the square wave and triangular wave as shown in Figure 4.16 (a) and (b) respectively with various damping ratios. Both Figures 4.17 and 4.19 show that the isolation performance at frequencies near resonance improves with the increase of damping while retaining the higher frequencies performance. For both the two periodic excitations there are some clear peaks present at the frequency range lower than the natural frequency of the system. These are due to the odd harmonics in the periodic excitations. For this particular case, when the fundamental frequency is $1/3$ or $1/5$ of the resonance frequency, then the 2^{nd} and 3^{rd} term of the odd series will be at the resonance frequency, which will induce a much greater response than at the fundamental frequency.

Figures 4.18(a) to (c) and 4.20(a) to (c) compare the isolation performance of the semi-active damper at three different damping levels with those due to a conventional and a skyhook passive damper. It can be seen from both Figures 4.19 and Figures 4.20 that if the damping ratio of the system is very small, for example, as shown in Figure 4.19(a) and Figure 4.20(a) then the performance of the semi-active system, conventional passive system and the skyhook system are almost the same. With the increase of damping, the difference between the passive and semi-active becomes more apparent. The performance improvement of the semi-active system over the conventional passive system is mainly in the frequency range beyond the natural frequency of the system. The higher the damping is, the greater the improvement in the performance. The skyhook system can always provide the best performance; however, the performance of semi-active system is comparable. The results indicate that semi-active damping control is promising for periodic disturbances.

It can be seen from Figure 4.19 and Figure 4.20 that the isolation performance of the on-off skyhook damper does not have apparent deterioration due to the presence of the three frequency components in the periodic function although it is concluded from

section 4.2 that the extraneous multiple harmonics will affect the switching time of the damper for the fundamental frequency. But this is not contrary to the previous conclusion. This is because higher order harmonics of the periodic functions occur with descending amplitudes. The amplitude of the harmonic with the fundamental frequency is dominant.

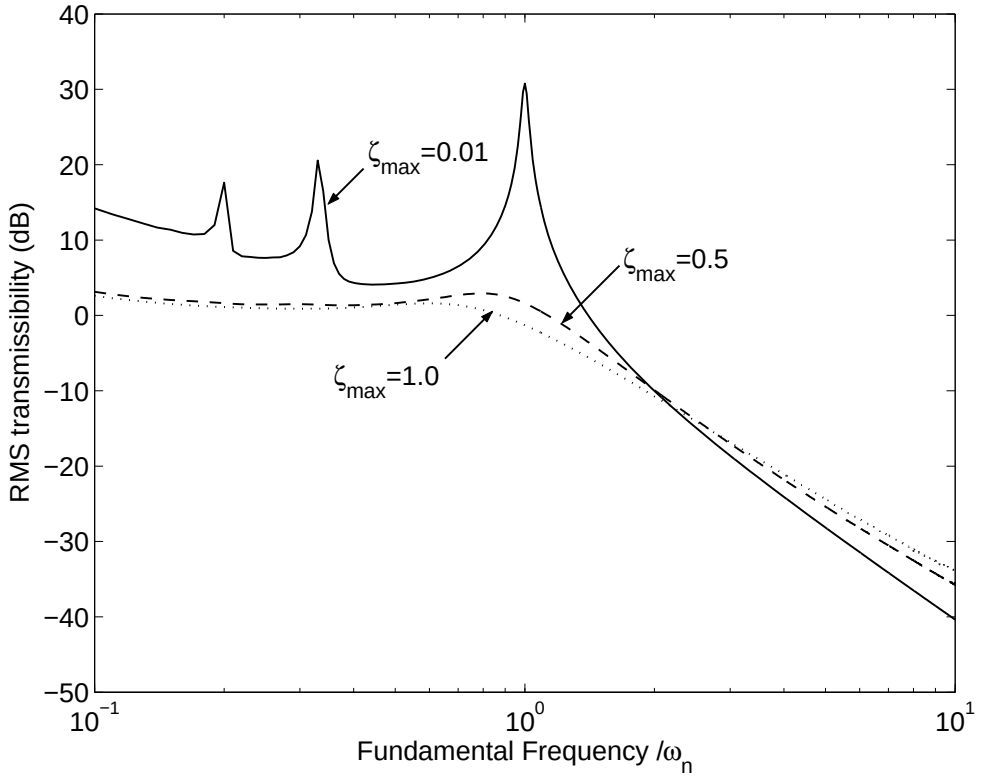

Figure 4.17 Acceleration transmissibility of a SDOF system with an on-off semi-active skyhook damper to square wave excitation in Figure 4.16(a)

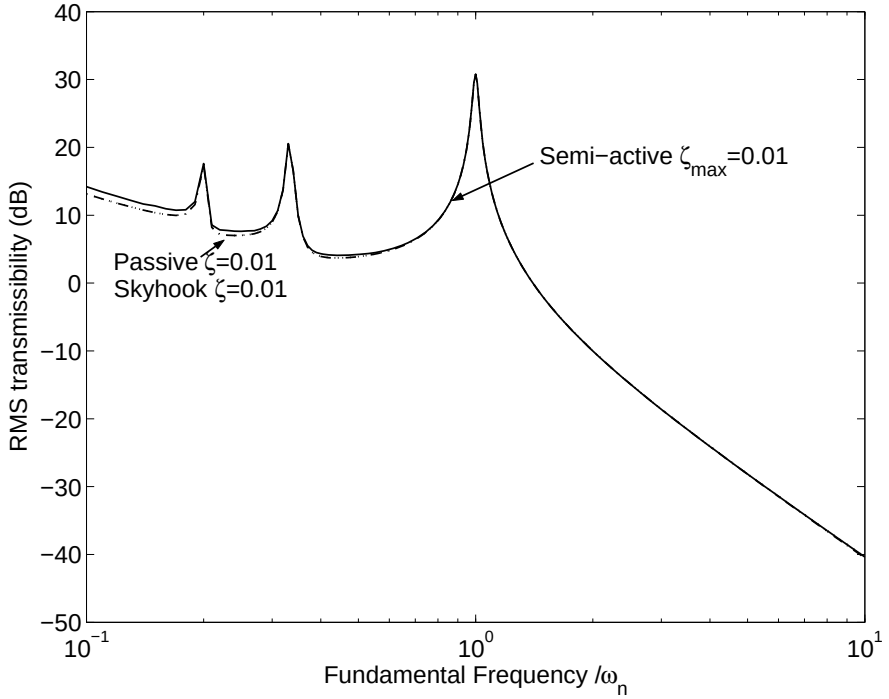

(a) Acceleration transmissibility of the semi-active damper when $\zeta_{\max} = 0.01$

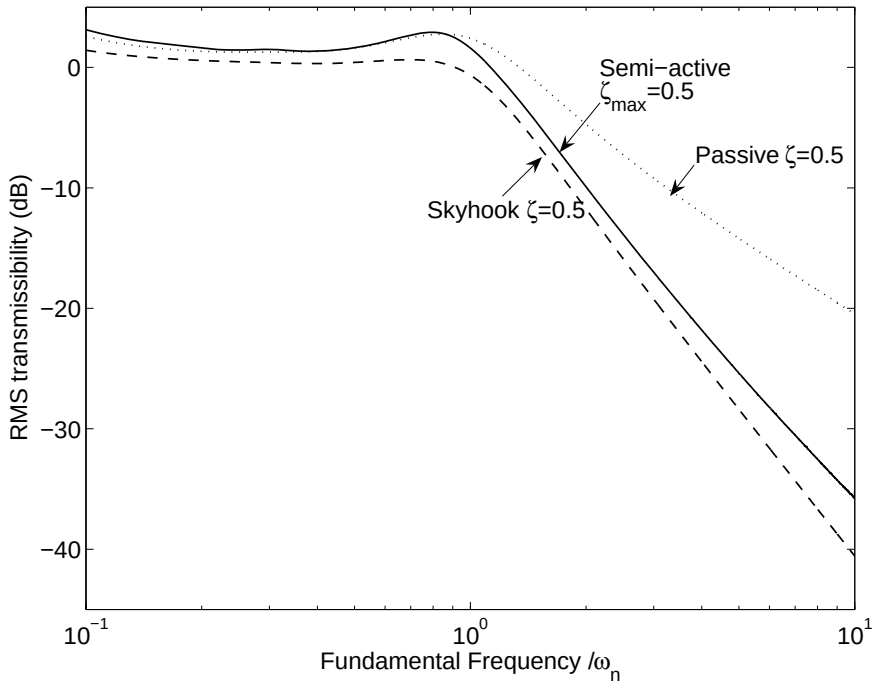

(b) Acceleration transmissibility of the semi-active damper when $\zeta_{\max} = 0.5$

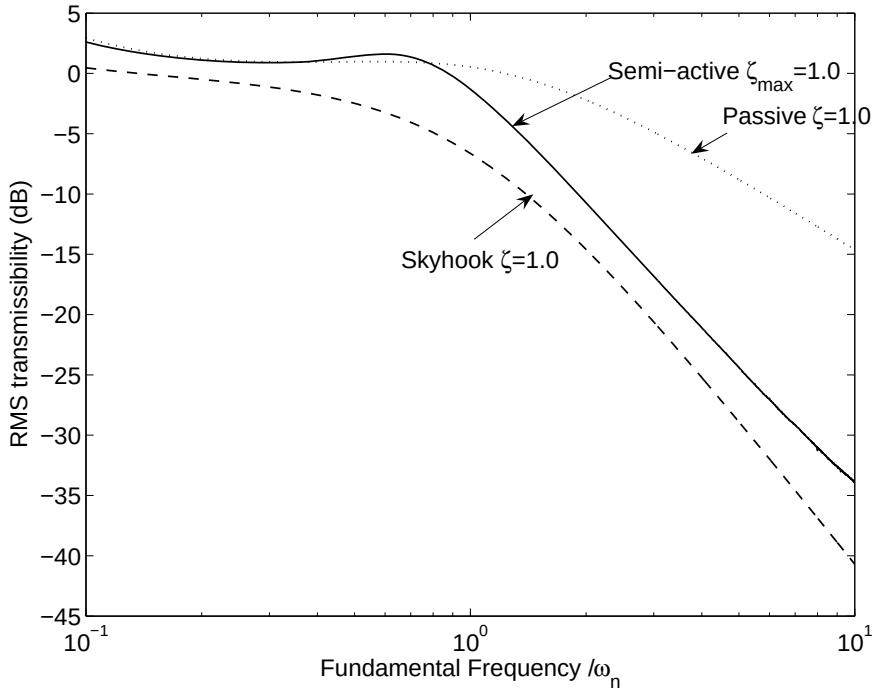

(c) Acceleration transmissibility of the semi-active damper when $\zeta_{\max} = 1.0$

Figure 4.18 Comparison of acceleration transmissibility of a semi-active damper with those due to a conventional and skyhook passive damper for square wave excitation (a) $\zeta_{\max} = 0.01$ (b) $\zeta_{\max} = 0.5$ (c) $\zeta_{\max} = 1.0$

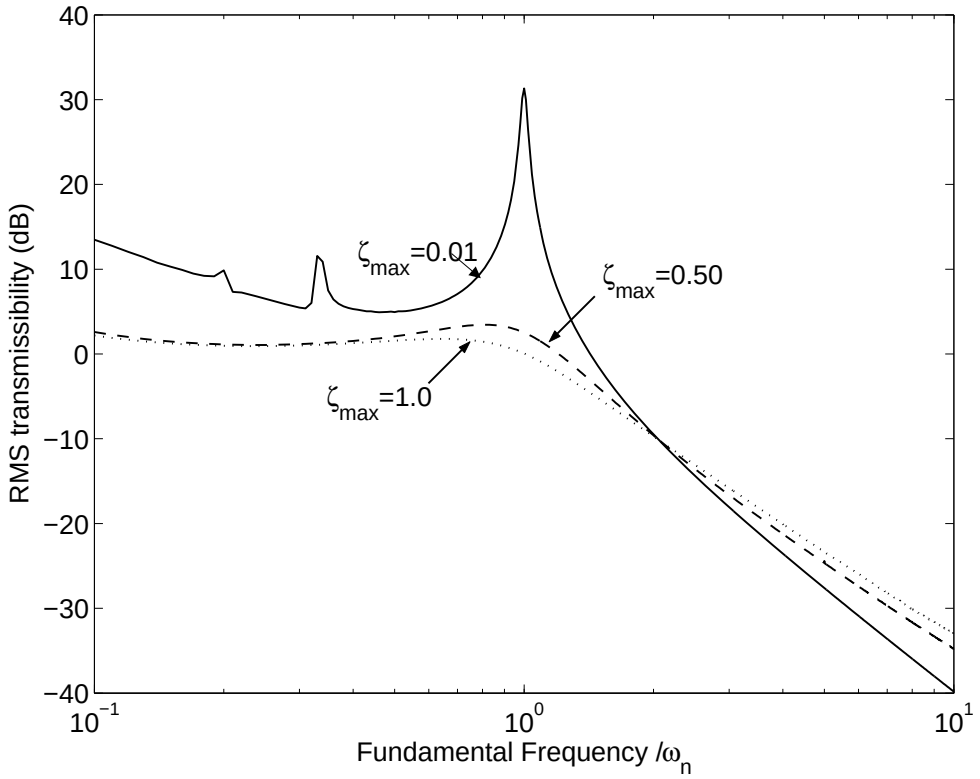

Figure 4.19Acceleration transmissibility of a SDOF system with an on-off semi-active skyhook damper to triangular wave excitation in Figure 4.16(b)

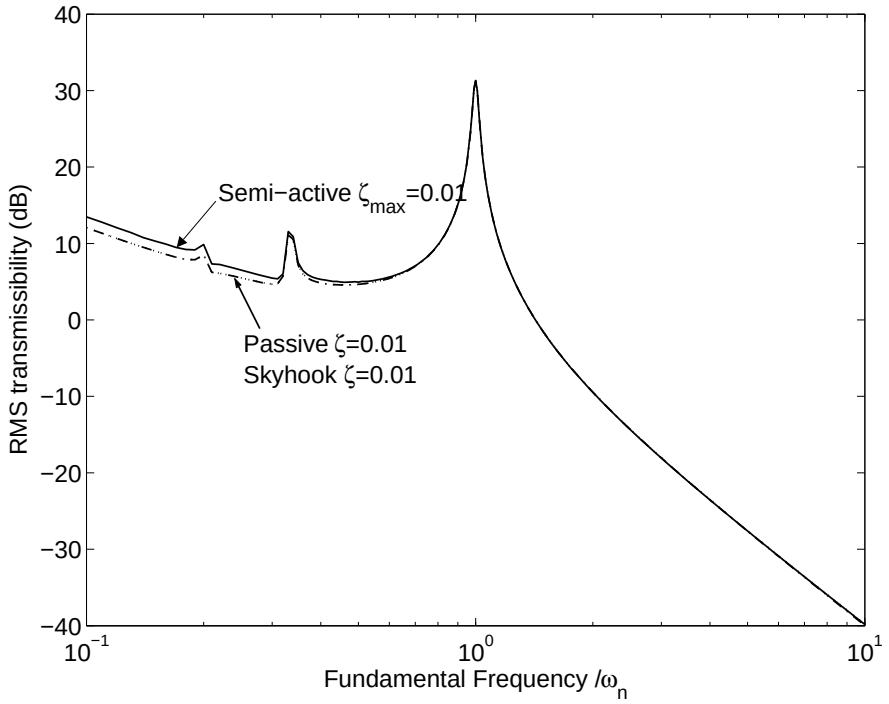

(a) Acceleration transmissibility of the semi-active damper when $\zeta_{\max} = 0.01$

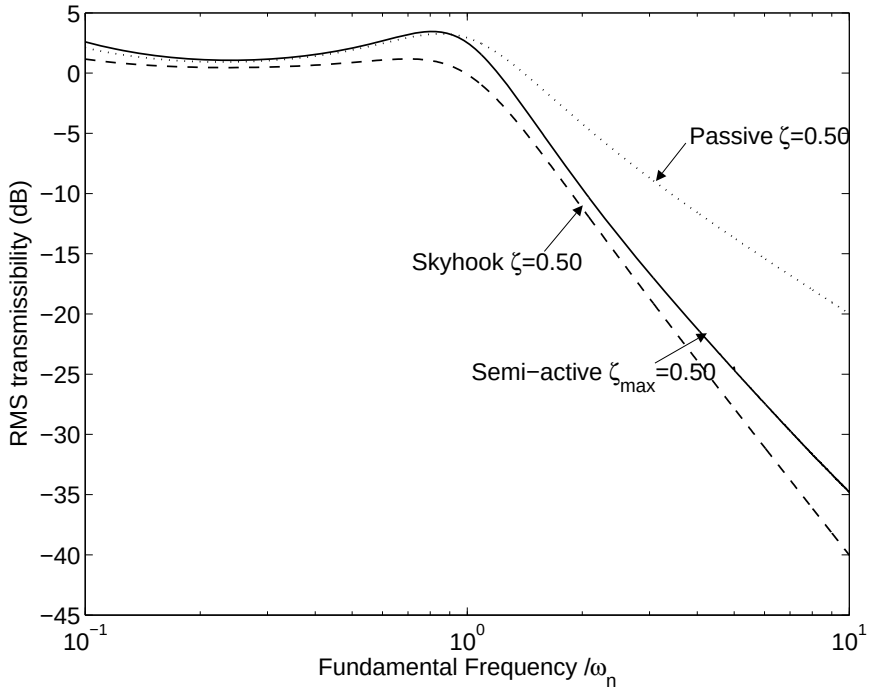

(b) Acceleration transmissibility of the semi-active damper when $\zeta_{\max} = 0.5$

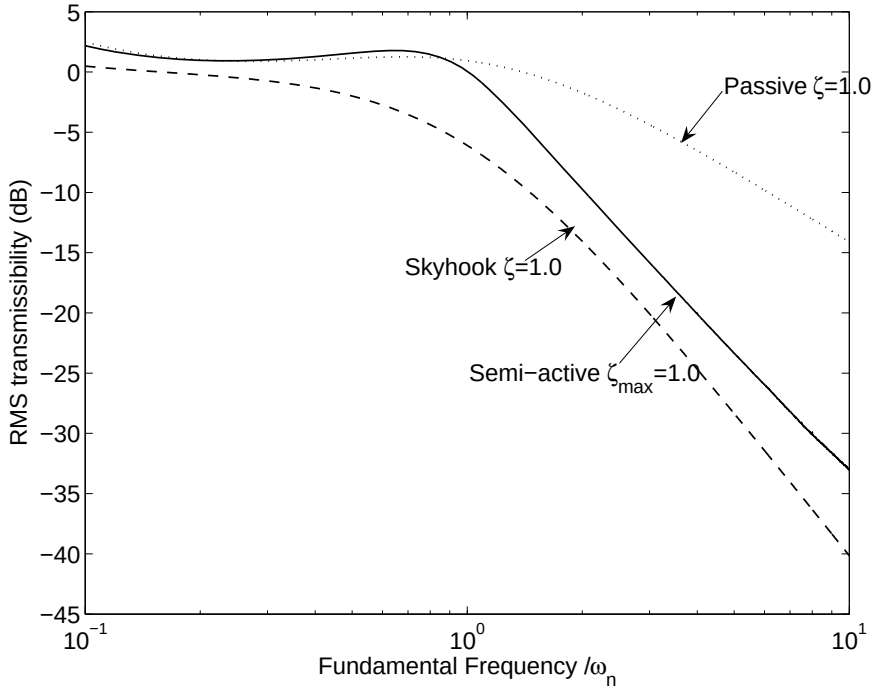

(c) Acceleration transmissibility of the semi-active damper when $\zeta_{\max} = 1.0$

Figure 4.20 Comparison of acceleration transmissibility of a semi-active damper to with those due to a conventional and skyhook passive damper for triangular wave excitation (a) $\zeta_{\max} = 0.01$ (b) $\zeta_{\max} = 0.5$ (c) $\zeta_{\max} = 1.0$

4.3.4 EXPERIMENTAL WORK

Experimental work was also conducted to investigate the isolation performance of the on-off skyhook damper in isolating periodic disturbances using the same experimental setup as detailed in section 3.7. A square wave from a signal generator was used in the experiment. The fundamental frequency of the square wave was chosen from 5 Hz to 60 Hz, and the time traces at each discrete frequency were measured to obtain the RMS acceleration transmissibility according to equation (4.24).

Figures 4.21 (a) to (c) show the acceleration response of the system and the voltage across the switch when the fundamental frequency of the square wave is chosen to be 10Hz, 15Hz and 30 Hz respectively. The figures show that the acceleration response is obviously mainly at the fundamental frequency. This is because the amplitude of the harmonic at the fundamental frequency is largest. The switching of the damper is consistent with just the fundamental frequency. It switches on and off twice a period.

The RMS acceleration transmissibility of the semi-active system was evaluated and plotted in Figure 4.22. The two measured curves when the circuit is open and short circuited are also plotted in the figure. From Figure 4.22 it can be seen that the latter are very similar in the frequency range beyond 20Hz. This is because ζ_{on} and ζ_{off} are similar for the experimental setup. The semi-active damper can provide as much as about 6dB improvement over the system with open circuit in the resonance area. The improvement at higher frequencies over the system with short circuit does not appear to be very much. Only a marginal benefit can be gained in the frequency range above 30Hz using semi-active damping control. This is due to the fact that the maximum damping ratio (0.22) of the experimental setup does not have a large enough effect and the minimum damping ratio (0.10) is not small enough. However, a greater improvement of the performance may be obtained if the on-state damping is much bigger than the off-state damping.

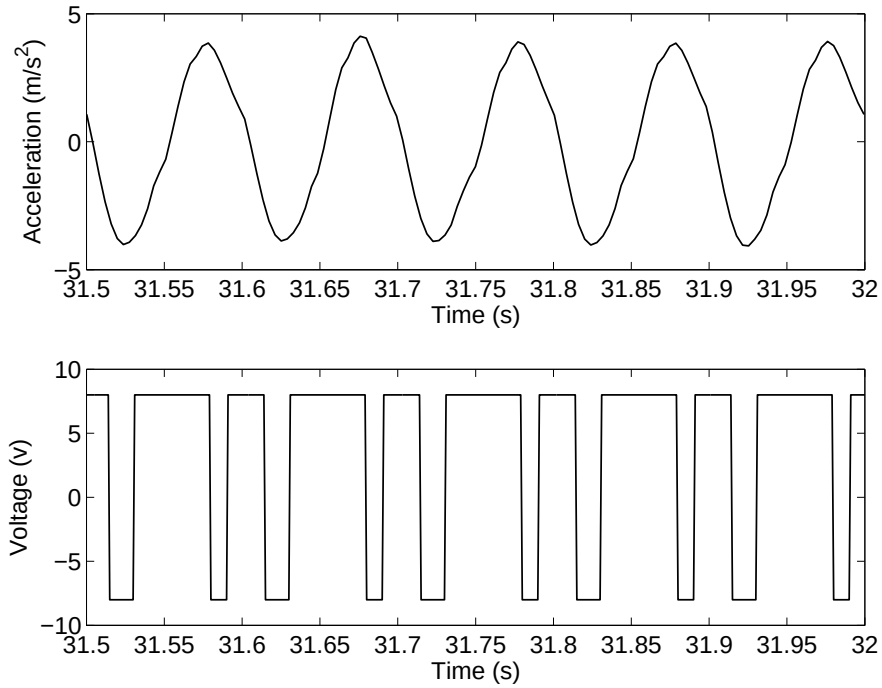

(a) Time histories at 10Hz

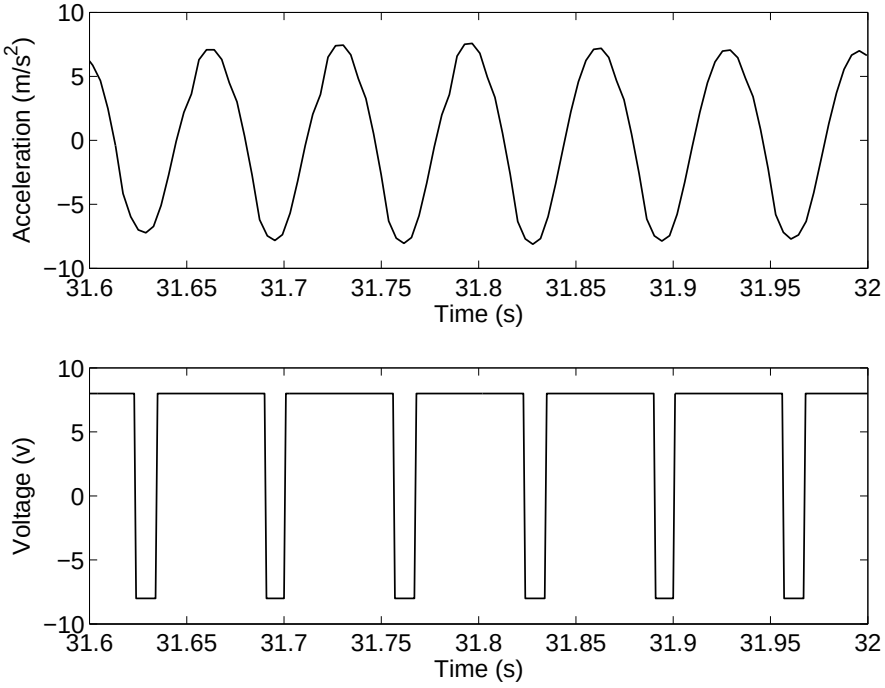

(b) Time histories at 15Hz

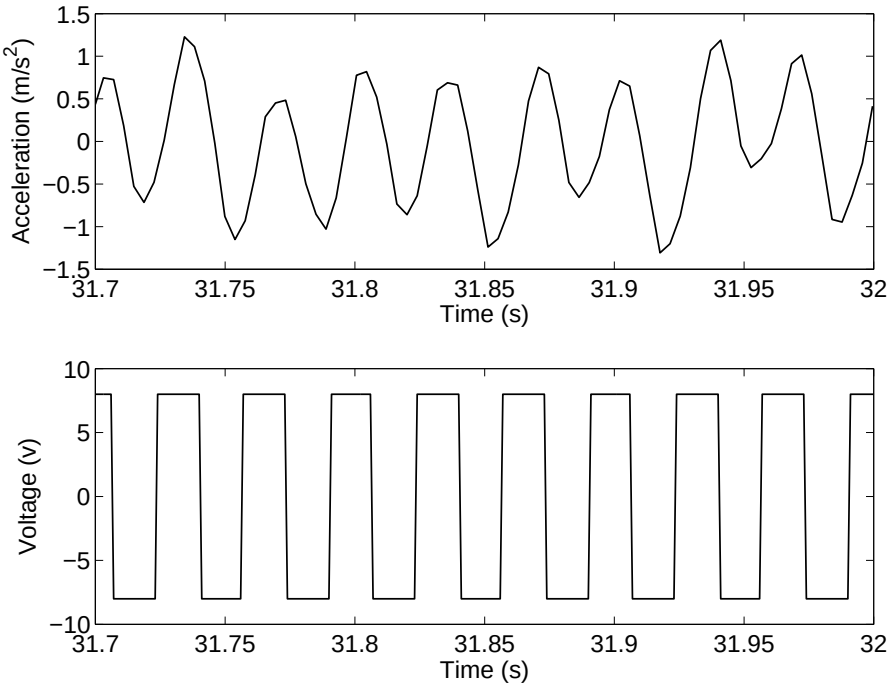

(c) Time histories at 30Hz

Figure 4.21 Measured time histories of the semi-active system subjected to a square wave at (a) 10Hz; (b) 15 Hz; and (c) 30Hz

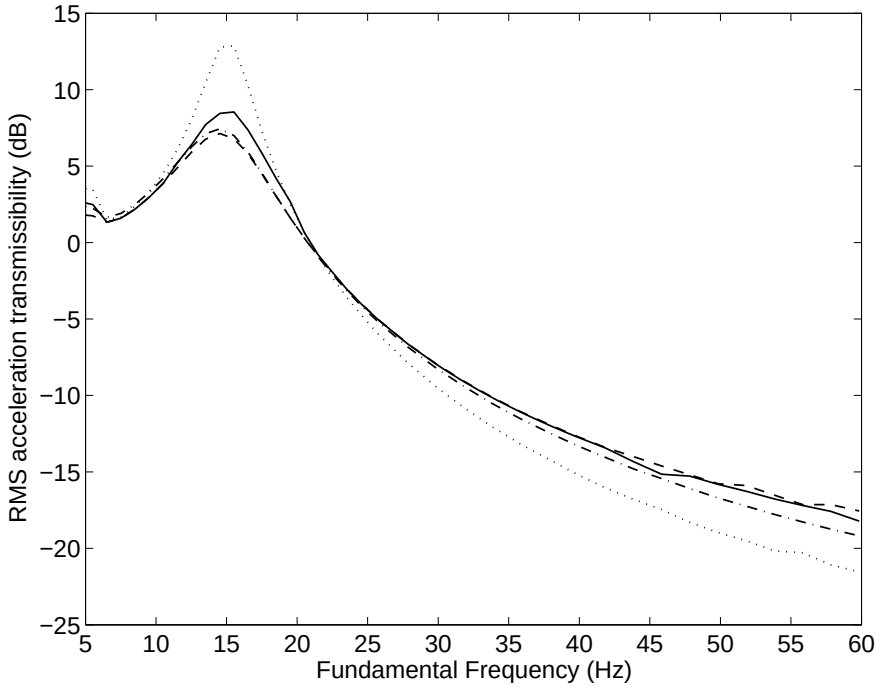

Figure 4.22 Measured RMS acceleration transmissibility of the semi-active system to square wave excitation (− measured SA; --- measured short circuit; ····· measured open circuit; −·−·− simulated SA)

4.4 CONCLUSIONS

This chapter has studied the vibration isolation performance of semi-active damping control for periodic disturbances. The effect of a secondary frequency which is a harmonic or subharmonic of the fundamental frequency on the switching of the semi-active damper was studied. Since the switching of a semi-active damper to harmonic excitation is frequency dependent, the addition of harmonics or subharmonics to the fundamental frequency in the excitation will affect the switching of the semi-active damper for the fundamental frequency. The study shows that for a SDOF system with an on-off skyhook semi-active damper, both the velocity switch and the relative velocity switch will be greatly affected due to the addition of a secondary frequency. The addition of harmonics of the fundamental frequency will largely affect the relative velocity switch, while addition of subharmonics will largely affect the velocity switch.

The vibration isolation performance of the semi-active system to periodic excitation was studied numerically and experimentally. The results are compared with the performance of the conventional passive and skyhook system. The numerical results show that the semi-active damper can provide better isolation performance than the conventional passive damper and the performance is comparable to that of a skyhook damper. Measurement results show a marginal improvement on the performance using the semi-active electromagnetic damper. However, the performance is limited by the achievable damping of the experimental rig.

The conclusions of this chapter indicate that the effects of multiple harmonics on the switching time depend on the amplitude and frequency of the harmonics. For the two periodic disturbances studied in this chapter, the frequency components are integer multiples of the natural frequency of the system, and the first harmonic is dominant in amplitude. However, greater improvement in the performance may be expected if the on-state damping can be made large and the off-state damping can be made very small. Semi-active damping control is promising for isolating periodic disturbances.

For the random excitations, there are many frequency components present at the same time with random amplitudes and phases, so the semi-active damper might fail to

work properly. The vibration isolation performance of semi-active damping control for random disturbances will be studied in the next chapter.

CHAPTER 5

5. ISOLATION OF RANDOM DISTURBANCES

5.1 INTRODUCTION

Chapters 3 and 4 investigated the vibration isolation performance of semi-active active damping control strategies for harmonic and periodic disturbances. The results show that semi-active dampers can provide superior performance than the conventional passive damper with same damping level. However, in some practical cases, the excitation is random. For random excitation there are many frequency components present at the same time with random amplitude and phase. The semi-active damper may not work as well as for other excitations. This chapter studies the effectiveness of using semi-active damping for isolation of random disturbances.

Following the introduction, the relationship between the Fourier integral and spectral densities is described. From this relationship an analytical solution is derived for the RMS response of a single degree of freedom (SDOF) system with a conventional and a skyhook passive damper subject to random base excitation with a constant power spectral density. The root-mean-square (RMS) responses are numerically simulated for a SDOF system with semi-active dampers for three special cases when the spectra of displacement, velocity and acceleration are flat. The results are compared with those of the conventional and skyhook passive damping and interpreted physically. Experimental work to verify the numerical simulation results is also presented, and finally conclusions are drawn.

5.2 RESPONSE OF A PASSIVE SDOF SYSTEM TO A RANDOM BASE EXCITATION

5.2.1 USING POWER SPECTRAL DENSITIE (PSD) TO CHARACTERISTIC RANDOM VIBRATION

In reference [69], the mean square response for a SDOF system to random *force* excitation has been derived and an analytical solution is given. In this section, the

mean square response of a SDOF system subject to random *base* excitation is investigated and an analytical solution is derived.

The Fourier integral is used to obtain a frequency domain description of a periodic function by representing it as an infinite series of harmonic components. Transient or aperiodic functions can be described in a similar manner, but their aperiodicity requires that their frequency domain descriptions be in terms of continuous spectra rather than discrete spectra. The pair of Fourier integrals used to relate a real-time function, $y(t)$,with its corresponding frequency domain representation $Y(i\omega)$ are given by the Fourier transform [69]

$$Y\left(i\omega\right)=\frac{1}{2\pi}\int_{-\infty}^{\infty}y(t)e^{-i\omega t}dt \qquad \text{Equation Section 5}(5.1)$$

and the inverse Fourier transform [69]

$$y(t)=\int_{-\infty}^{\infty}Y(i\omega)e^{i\omega t}d\omega \tag{5.2}$$

Any time history $y(t)$ of finite length can be described in terms of a Fourier spectrum. The Fourier integral in equation (5.2) is finite only if $y(t)$ is zero at $\pm\infty$ [12]. The equation relating the mean square value of $y(t)$ to its power spectral density function can be written as

$$\overline{y^2(t)}=\int_{-\infty}^{\infty}S_y(\omega)d\omega \tag{5.3}$$

where in equation (5.3)

$$S_y(\omega)=\lim_{T\to\infty}\pi E\left[\frac{\left|Y_T(i\omega)\right|^2}{T}\right] \tag{5.4}$$

$S_y(\omega)$ is the power spectral density of $y(t)$. Equation (5.3) can be simply interpreted as follows. If a random variable is thought of as a summation of an infinite number of infinitely small, randomly phased, sinusoidal components of continuously distributed

frequencies, $S(\omega)$ can then be interpreted as the mean square value of these components having angular frequencies within one radian/second bandwidth centered on the angular frequency ω. Thus for a continuous frequency distribution from $-\infty$ to $+\infty$, the mean square value of the random variable $y(t)$ is equal to the integral of its power spectral density $S_y(\omega)$ over the entire frequency range. Equation (5.4) can be used to determine the power spectral density of the response of a system to random excitations.

5.2.2 APPLICATION OF FLAT INPUT PSDS TO A SDOF SYSTEM

For the SDOF system subject to random base excitation as shown in Figure 5.1, the equation of motion can be written as

$$m\ddot{x}(t) + c\dot{x}(t) + kx(t) = c\dot{x}_0(t) + kx_0(t) \tag{5.5}$$

where $x_0(t)$ is the base displacement excitation and $x(t)$ is the system displacement response. The relationship between the power spectral densities of $x_0(t)$ and $x(t)$ can be written as [69]

$$S_x(\omega) = |H(\omega)|^2 S_{x_0}(\omega) \tag{5.6}$$

where $S_x(\omega)$ and $S_{x_0}(\omega)$ are the power spectral densities of $x_0(t)$ and $x(t)$ respectively. $H(\omega)$ is the transfer function between the displacement response and the displacement excitation.

Equation (5.6) states that the power spectral density of the displacement response is equal to the power spectral density of the base excitation multiplied by the square of the modulus of the transfer function between the base and the vibrating mass.

If the modulus of the transfer function and the power spectral density of the displacement base excitation are known for a given system, the mean square response can be written as

$$\overline{x^2(t)} = \int_{-\infty}^{\infty} |H(i\omega)|^2 S_{x_0}(\omega) d\omega \tag{5.7}$$

For a displacement excitation having a constant spectral density ('white noise'), S_{x_0} is a constant, the mean square displacement response can be obtained as

$$\begin{aligned}\overline{x^2(t)} &= \int_{-\infty}^{\infty} S_x(\omega)d\omega \\ &= \int_{-\infty}^{\infty} |H(\omega)|^2 S_{x_0}(\omega)d\omega \\ &= S_0 \int_{-\infty}^{\infty} |H(\omega)|^2 d\omega\end{aligned} \tag{5.8}$$

where S_0 is the constant spectral density.

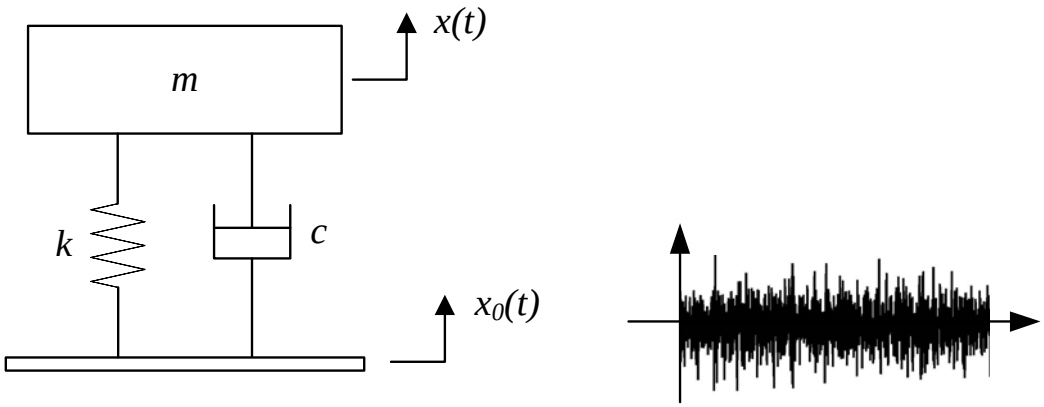

Figure 5.1 Schematic of a passive SDOF system subject to base excitation

5.2.3 MEAN SQUARE REPONSE OF A CONVENTIONAL PASSIVE SDOF SYSTEM

For the conventional passive SDOF system in Figure 5.1, the transfer function is given by

$$H(\omega) = \frac{k + ic\omega}{k - m\omega^2 + ic\omega} \tag{5.9}$$

Substituting equation (5.9) into equation (5.8) gives

$$\begin{aligned}\overline{x^2(t)_{con}} &= S_{x_0}\int_{-\infty}^{\infty}\left|\frac{ic\omega+k}{-m\omega^2+ic\omega+k}\right|^2 d\omega \\ &= S_{x_0}\int_{-\infty}^{\infty}\frac{k^2+(c\omega)^2}{(k-m\omega^2)^2+(c\omega)^2}d\omega \\ &= \frac{\pi(c^2+mk)}{cm}\end{aligned} \tag{5.10}$$

If written in terms of ω_n and ζ, one has

$$\overline{x^2(t)_{con}} = S_{x_0}\pi\omega_n\frac{(4\zeta^2+1)}{2\zeta} \tag{5.11}$$

where $\omega_n = \sqrt{k/m}$ is the natural frequency of the system, and $\zeta = c/2m\omega_n$ is the damping ratio. The analytical result in equation (5.10) has been derived on the assumption that the spectral density of the displacement excitation is a constant from frequency $-\infty$ to ∞. Crandall and Mark [70] have shown that for forced vibration this 'infinite' result is a close approximation to practical situations providing that the bandwidth of the excitation is wide in comparison with the bandwidth of the system ($2\zeta\omega_n$). The time history of the response takes the form of a randomly modulated "sine" wave, whose period is $2\pi/\omega_n$ and the modulation "period" is proportional to $1/(\zeta\omega_n)$. Therefore for small damping the typical periods in the modulation are very long [70]. The same is true for the base excitation system studied in this section.

5.2.4 MEAN SQUARE RESPONSE OF A SKYHOOK PASSIVE SDOF SYSTEM

For a SDOF system with a skyhook damper as shown in Figure 5.2, the transfer function can be written as

$$H(\omega) = \frac{k}{k-m\omega^2+ic\omega} \tag{5.12}$$

Using equation (5.8), the mean square response can be written as

$$\begin{aligned}\overline{x^2(t)}_{sky} &= S_{x_0}\int_{-\infty}^{\infty}\left|\frac{k}{-m\omega^2+ic\omega+k}\right|^2 d\omega \\ &= S_{x_0}\int_{-\infty}^{\infty}\frac{k^2}{(k-m\omega^2)^2+(c\omega)^2}d\omega \\ &= \frac{\pi k}{c}S_{x_0}\end{aligned} \tag{5.13}$$

If written in the form of ω_n and ζ, one has

$$\overline{x^2(t)}_{sky} = \pi\omega_n S_{x_0}\frac{1}{2\zeta} \tag{5.14}$$

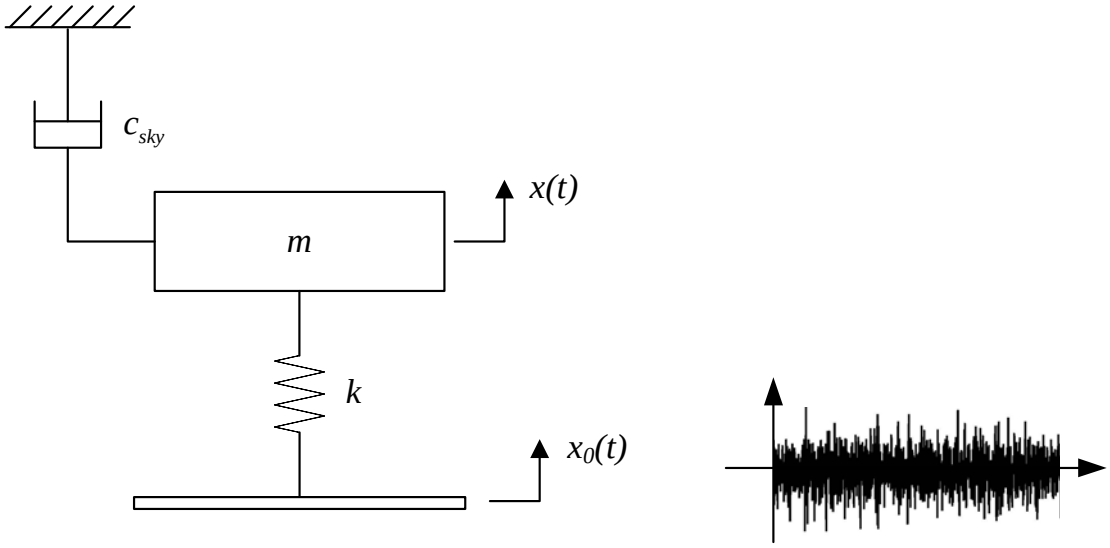

Figure 5.2 Schematic of a skyhook SDOF system subject to base excitation

5.2.5 COMPARISON OF MEAN SQUARE RESPONSES OF A CONVENTIONAL AND SKYHOOK PASSIVE SDOF SYSTEM

Figure 5.3 shows the MS response as a function of damping ratio for a SDOF system with a conventional and a skyhook passive damper subject to a random base excitation with a unity spectrum. It can be seen that the MS response of the conventional SDOF system decreases initially with increasing damping ratio, and reaches a minimum value when $\zeta = 0.5$. After that point, the RMS response rises up gradually. The damping ratio $\zeta = 0.5$ when the MS response is minimum can also be derived from equation (5.11). Equation (5.11) can be rewritten as

$$\overline{x^2(t)}_{con} = S_{x_0}\pi\omega_n(2\zeta + \frac{1}{2\zeta}) \tag{5.15}$$

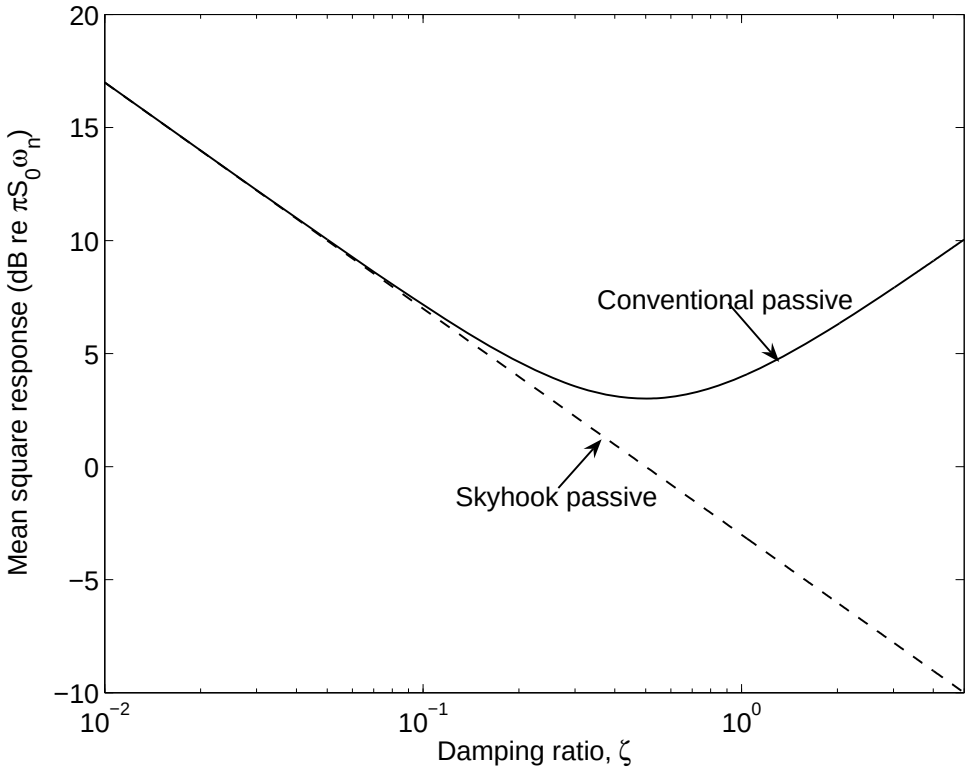

Figure 5.3 Mean square response of a SDOF system with a conventional and a skyhook passive damper subject to random base excitation

According to the limitation theory, the minimum value of equation (5.15) happens when

$$2\zeta = \frac{1}{2\zeta} \quad (\zeta>0) \tag{5.16}$$

i.e. when $\zeta = 0.5$.

It can also be derived from equation (5.11) that for small damping ratio ζ, the mean square response tends to $\pi S_{x_0}\omega_n/2\zeta$. The slope of the curve is -3dB per doubling of ζ. For large value of ζ the mean square response tends to $2\pi S_{x_0}\omega_n\zeta$. The slope of the curve is 3dB per doubling of ζ.

As for the skyhook system, one can see from Figure 5.3 that the MS response decreases monotonically with increase in damping ratio. It can also be seen from the figure that with the increase of the damping ratio, the difference between the MS response of the conventional and skyhook passive systems increases. It can be derived from equation (5.14) that the gradient of the mean square response is -3dB per doubling of ζ.

If one takes the ratio of the mean square response of a conventional SDOF system to that of a skyhook passive system as defined in equation (5.11) and (5.14), one gets

$$\frac{\overline{x^2(t)_{con}}}{\overline{x^2(t)_{sky}}} = 4\zeta^2 + 1 \tag{5.17}$$

Equation (5.17) tends to 1 for smaller damping ratios, i.e. $\overline{x^2(t)_{con}}$ and $\overline{x^2(t)_{sky}}$ are almost the same, which was clearly shown in Figure 5.3 that the two curves are very close. For large damping ratios, equation (5.17) tends to $4\zeta^2$. The difference of the two mean square response tends to 6dB per doubling of ζ.

The frequency dependence of a random excitation may be such that it appears generally flat in the frequency range of interest when viewed as displacement, velocity, acceleration or none of these. The three special cases when the displacement, velocity and acceleration excitation spectra are assumed to be flat will be studied in this section, and the results will be compared with those of the conventional and skyhook passive systems.

Since the skyhook semi-active dampers considered attempt to emulate skyhook damping, the performance of the conventional passive and skyhook systems provide lower and the upper bounds between which the semi-active may perform. The semi-active damper can only be expected to provide an intermediate level of performance. Table 5.1 lists the transfer functions between the response (displacement, velocity and acceleration) and the excitation for a conventionally damped SDOF system. Table 5.2 shows the corresponding transfer functions for a SDOF system with passive skyhook damping. The transfer functions in the two tables can be substituted into equation (5.8) to obtain the RMS response due to a particular type of excitation.

Table 5.1 Transfer functions of a conventional SDOF system

Response / Excitation	Displacement	Velocity	Acceleration
Displacement	$\frac{ic\omega+k}{-m\omega^2+ic\omega+k}$	$\frac{i\omega(ic\omega+k)}{-m\omega^2+ic\omega+k}$	$\frac{-\omega^2(ic\omega+k)}{-m\omega^2+ic\omega+k}$
Velocity	$\frac{ic\omega+k}{i\omega(-m\omega^2+ic\omega+k)}$	$\frac{ic\omega+k}{-m\omega^2+ic\omega+k}$	$\frac{i\omega(ic\omega+k)}{-m\omega^2+ic\omega+k}$
Acceleration	$\frac{ic\omega+k}{-\omega^2(-m\omega^2+ic\omega+k)}$	$\frac{ic\omega+k}{i\omega(-m\omega^2+ic\omega+k)}$	$\frac{ic\omega+k}{-m\omega^2+ic\omega+k}$

Table 5.2 Transfer functions of a skyhook passive SDOF system

Response / Excitation	Displacement	Velocity	Acceleration
Displacement	$\frac{k}{-m\omega^2+ic\omega+k}$	$\frac{ik\omega}{-m\omega^2+ic\omega+k}$	$\frac{-k\omega^2}{-m\omega^2+ic\omega+k}$
Velocity	$\frac{k}{i\omega(-m\omega^2+ic\omega+k)}$	$\frac{k}{-m\omega^2+ic\omega+k}$	$\frac{ik\omega}{-m\omega^2+ic\omega+k}$
Acceleration	$\frac{k}{-\omega^2(-m\omega^2+ic\omega+k)}$	$\frac{k}{i\omega(-m\omega^2+ic\omega+k)}$	$\frac{k}{-m\omega^2+ic\omega+k}$

The three cases in the sub-diagonal elements of Tables 5.1 and 5.2 represent displacement response due to velocity excitation, and displacement and velocity responses due to acceleration excitation. It can be seen that the transfer functions for these three cases tend to infinity as the frequency ratio tends to zero. From equation (5.8), the RMS responses of the system are unbounded because the integral tends to infinity at low frequency. These three cases will not be considered. The three diagonal cells in the table are the cases where both the response and the excitation are the same quantity. The three cases in the super-diagonal elements and the diagonal elements will be studied in the following section for both passive and semi-active systems.

5.3 EFFECTIVENESS OF SEMI-ACTIVE DAMPERS FOR ISOLATION OF RANDOM DISTURBANCES

Figure 5.4 shows the schematic of a SDOF system with a semi-active damper subject to random disturbances. This section studies the performance of the three semi-active dampers as shown in Table 5.3 for random disturbances through numerical simulations. The performance of the three semi-active control strategies is compared with those of the conventional and skyhook passive damping for base isolation. Physical interpretation is presented to explain the comparison of results. In the simulation, the models established in Chapter 2 are used. The random excitation is formulated by passing a Gaussian random signal through a 10th order Butterworth low-pass filter with a cut-off frequency of ten times the natural frequency of the system. Thus the random excitation has a power spectral density which is flat up to ten times the natural frequency of the system. The RMS responses of the system are calculated up to ten times the natural frequency of the system.

Table 5.3 Damping characteristics of the semi-active dampers studied

Damper Type	Semi-Active Damping
Continuous skyhook (SA-1)	$c_{sa}=\begin{cases}\max\left[c_{\min},\min\left[G\lvert\dot{x}\rvert,c_{\max}\right]\right] & \dot{x}(\dot{x}-\dot{x}_0)\geq 0\\ c_{\min} & \dot{x}(\dot{x}-\dot{x}_0)<0\end{cases}$
On-off skyhook (SA-2)	$c_{sa}=\begin{cases}c_{\max} & \dot{x}(\dot{x}-\dot{x}_0)\geq 0\\ c_{\min} & \dot{x}(\dot{x}-\dot{x}_0)<0\end{cases}$
On-off balance (SA-3)	$c_{sa}=\begin{cases}c_{\max} & (x-x_0)(\dot{x}-\dot{x}_0)\leq 0\\ c_{\min} & (x-x_0)(\dot{x}-\dot{x}_0)>0\end{cases}$

5.3.1 ACCELERATION TRANSMISSIBILITY SIMULATIONS

Numerical simulations have been carried out to investigate the acceleration transmissibility of a SDOF system with a semi-active damper subject to random acceleration of the base. Figure 5.5 compares the RMS transmissibility of the SA-2 (on-off skyhook) semi-active damper to random and harmonic acceleration disturbances with the maximum damping ratio of the semi-active system, $\zeta_{\max}$, set to 0.5. For harmonic disturbances, the transmissibility curve is obtained by running the

simulation at each discrete frequency. One can see from the figure that the RMS transmissibility for random disturbances is worse than the harmonic cases over the whole frequency range. The study in section 4.2 of the effect of multiple harmonics on the switching of the semi-active damper suggests this is because the semi-active damper cannot handle many harmonic components simultaneously.

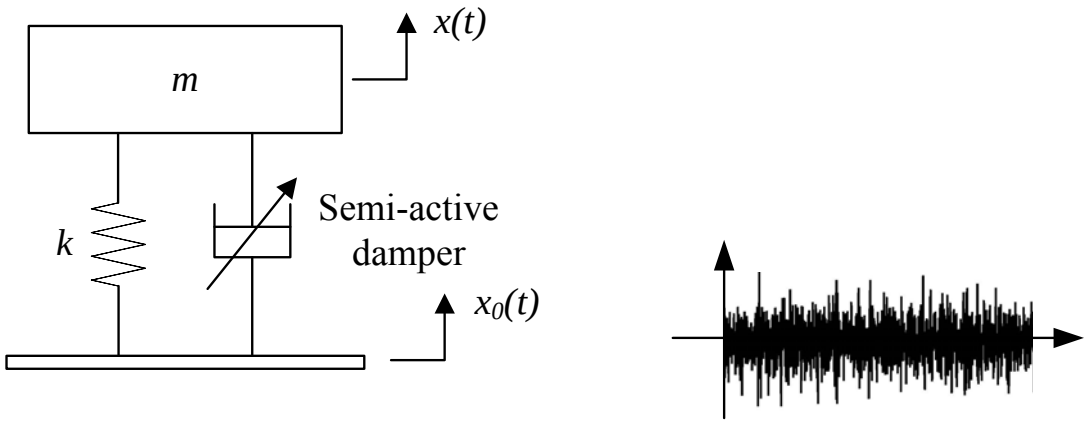

Figure 5.4 Schematic of a semi-active SDOF system subject to base excitation

When the semi-active system is subject to random disturbances, many frequency components are applied to the system simultaneously. The semi-active damper cannot ensure that the switch time for every frequency is right. Referring back to Figure 5.5, for lower frequencies ($\omega \le 0.5\omega_n$), for example $\omega_1 = 0.5\omega_n$, it can be expected from the conclusions in the previous chapter that both the velocity and the relative velocity switches will be greatly affected. But since this frequency range is not damping controlled, the transmissibility is not affected very much. For the frequency range near resonance, the lower frequency will largely affect the velocity switch and the higher frequency will largely affect the relative velocity switch, thus the transmissibility near resonance will be greatly increased. As for the higher frequencies, the best the semi-active damper can do is turned off for half of the time to provide the desired performance. But due to the addition of multiple harmonics at lower frequencies, the semi-active damper will be turned on for quite a lot of time. Thus the transmissibility at higher frequencies will also be very high due to the addition of the damping.

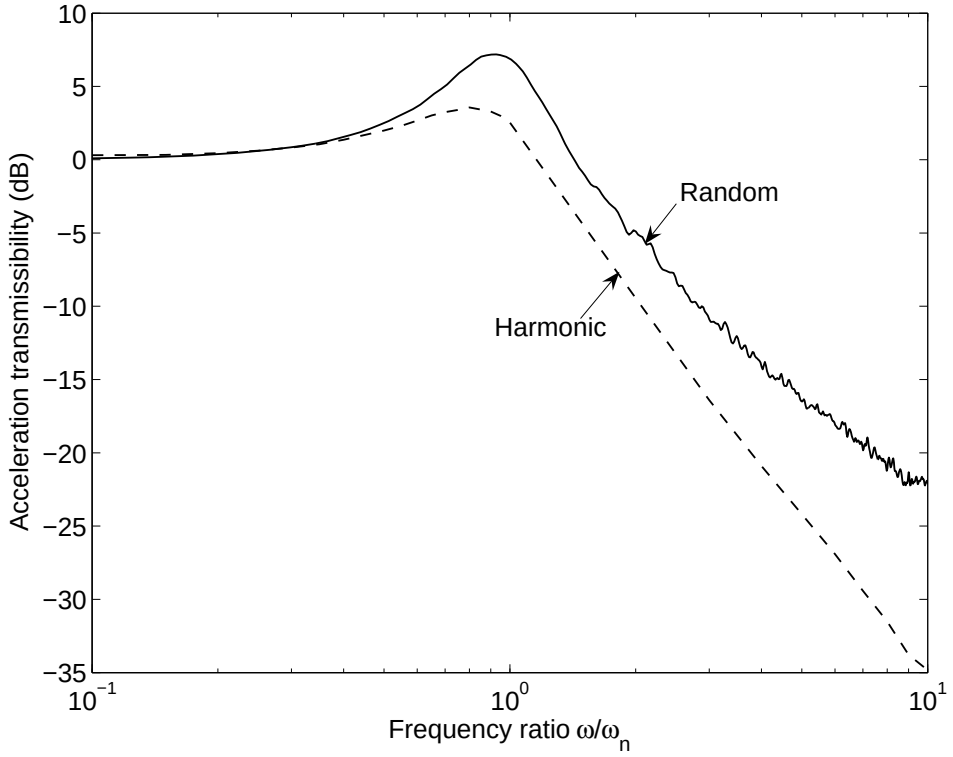

Figure 5.5 RMS transmissibility of a SA-2 damper to harmonic and random disturbances for white acceleration input spectrum

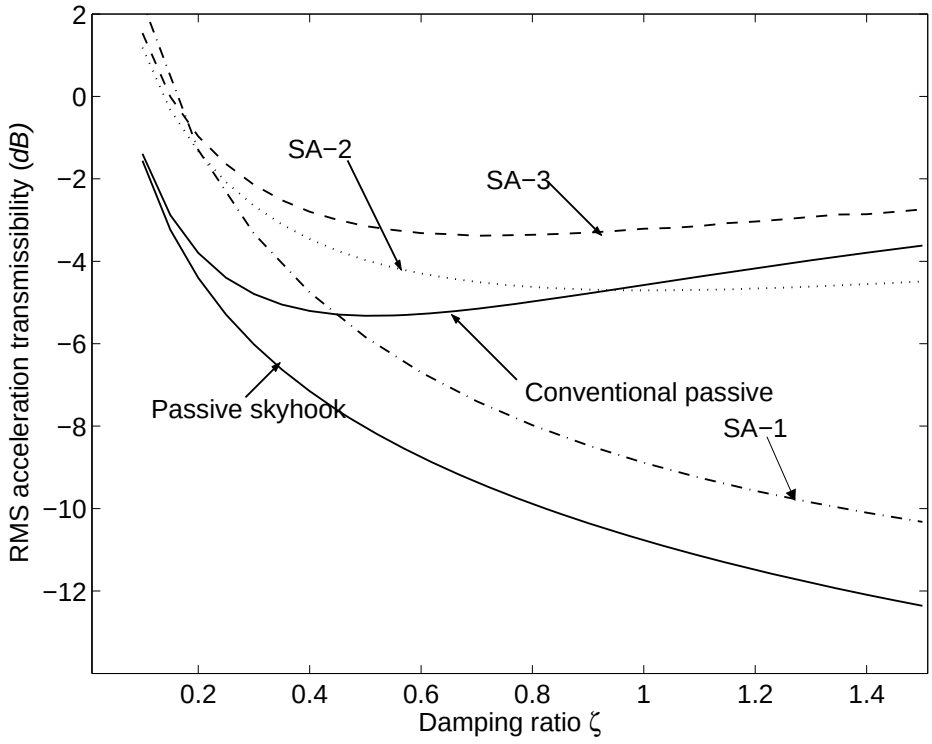

Figure 5.6 RMS acceleration transmissibility of semi-active dampers to white acceleration input

Figure 5.6 shows the RMS acceleration transmissibility of the three semi-active dampers to random acceleration excitation as functions of the damping ratio. As a comparison, the RMS response of both conventional and skyhook passive systems are also shown. It can be seen from the figure that at lower to moderate damping ratios, the performance of the semi-active damper is worse than the conventional passive system for all the three control strategies. For high damping ratios ($\zeta \geq 1.0$) some modest benefit is apparent for the SA-2 damper. SA-1 and SA-3 dampers are still worse. The results in Figure 5.6 suggest that semi-active dampers fail to isolate random acceleration excitations effectively.

5.3.2 RANDOM VELOCITY AND DISPLACEMENT EXCITATION

The other two special cases when considering random disturbances are random velocity and displacement inputs with flat spectra. The former is often considered when looking at the isolation of vehicles from road disturbances. The simulation results for a semi-active damper with random velocity excitation are shown in Figures 5.7 and 5.8. Figure 5.7 is looking at the velocity response and Figure 5.8 looks at the acceleration response. It can be seen from Figure 5.7 that with the increase of the damping ratio, both the SA-1 and SA-2 damper can provide some improvement in the response over conventional passive damping. When the damping ratio is 1.5, the improvement for both of the two semi-active dampers is about *6dB*. At lower frequencies, the SA-3 damper is even worse than the conventional passive case, but at higher frequencies, it is slightly better.

Figure 5.8 shows that the improvement of the semi-active damping over conventional passive damping is more pronounced if one looks at the acceleration response due to the velocity input. With the increase of damping ratio, there is significant benefit from both SA-1 and SA-2 semi-active damping control strategies. When the damping ratio ζ=1.5, the performance improvement for SA-1 is 10dB, for SA-2 13dB. The SA-3 damper only has 3dB improvement at ζ=1.5. Similar conclusions are reached by Karnopp to address the superiority of continuous variable skyhook damping control to conventional passive damper in reference [15], in which he studied the acceleration response spectrum due to random velocity excitation with a flat spectrum.

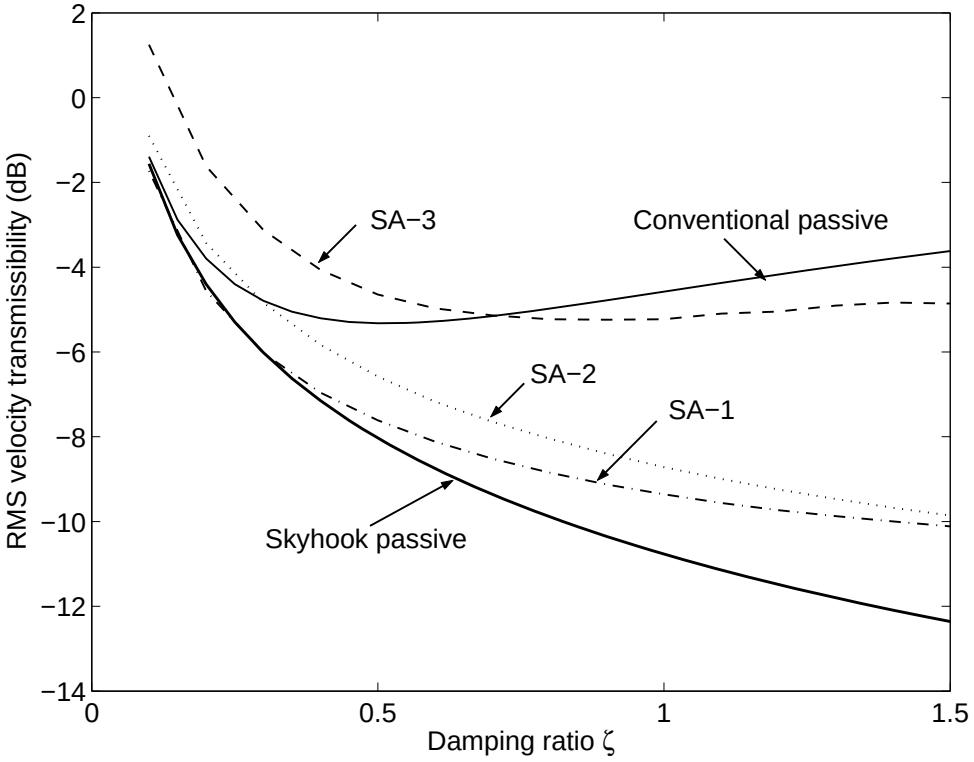

Figure 5.7 RMS velocity transmissibility to random velocity excitation

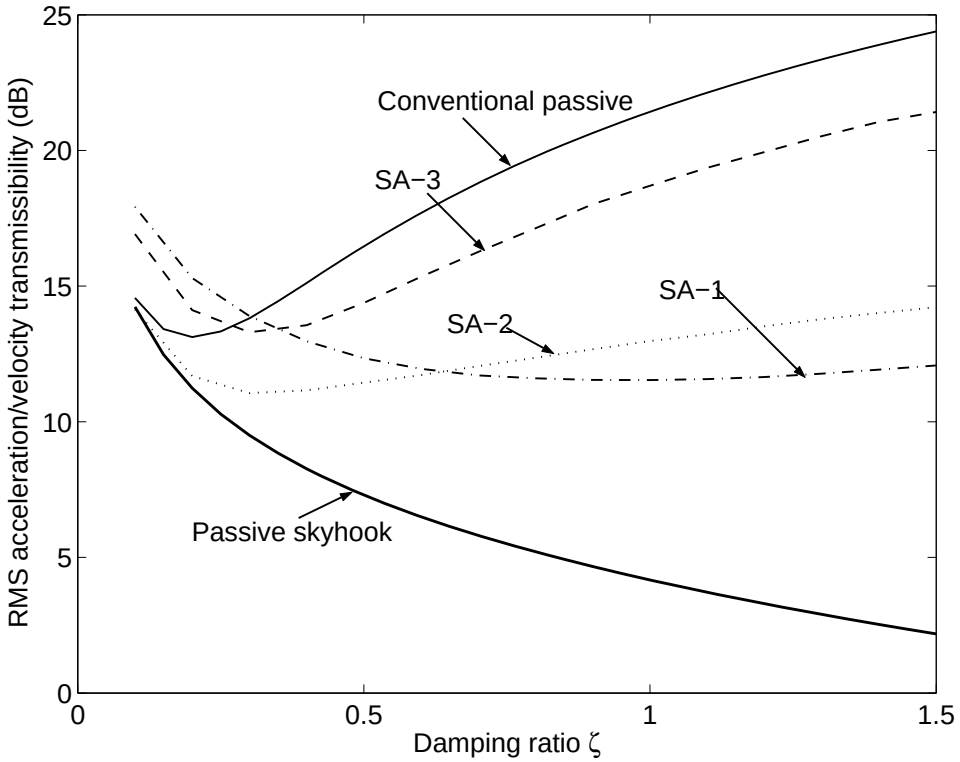

Figure 5.8 RMS acceleration transmissibility to random velocity excitation

The RMS transmissibility of displacement, velocity and acceleration response to random *displacement* excitation are shown in Figure 5.9-5.11 respectively. Figure 5.9 shows that all of the three semi-active strategies can provide some improvement for the displacement response when the damping ratio is greater than 0.5. Figures 5.10 and 5.11 show that SA-3 semi-active damper can hardly provide any improvement on the performance, and at lower damping ratio, it is even worse than conventional passive damping. For the displacement and velocity responses due to the random displacement excitation, both SA-1 and SA-2 dampers can provide significant improvement with high damping ratio. Only the SA-1 semi-active damper can provide significant improvement on the acceleration performance to random displacement excitation.

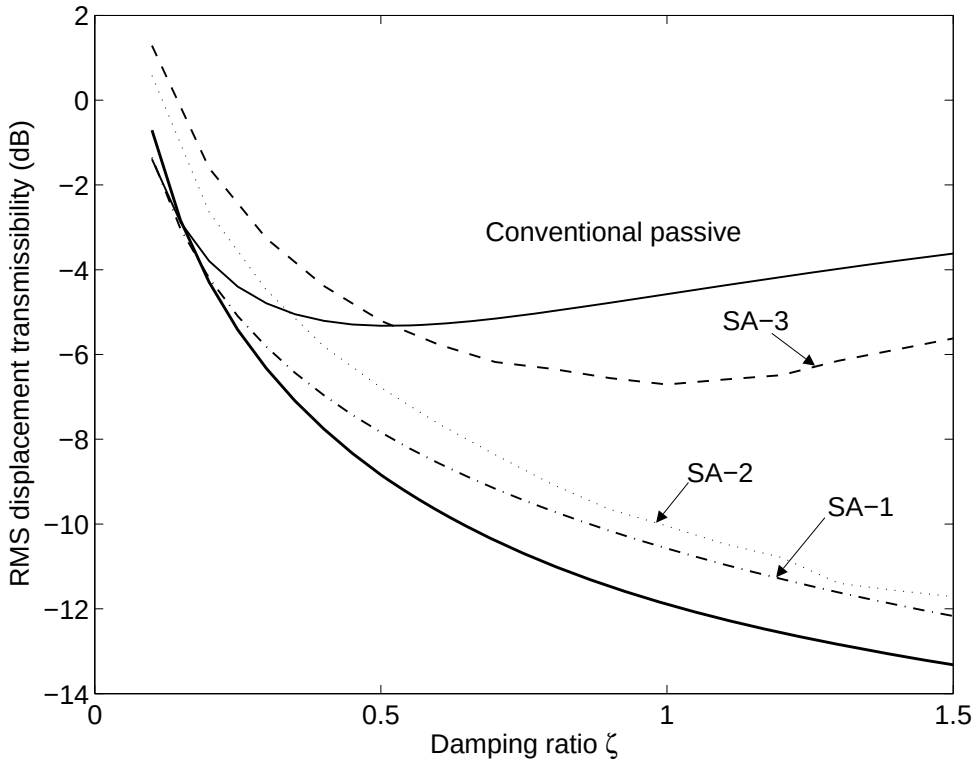

Figure 5.9 RMS displacement transmissibility to random displacement excitation

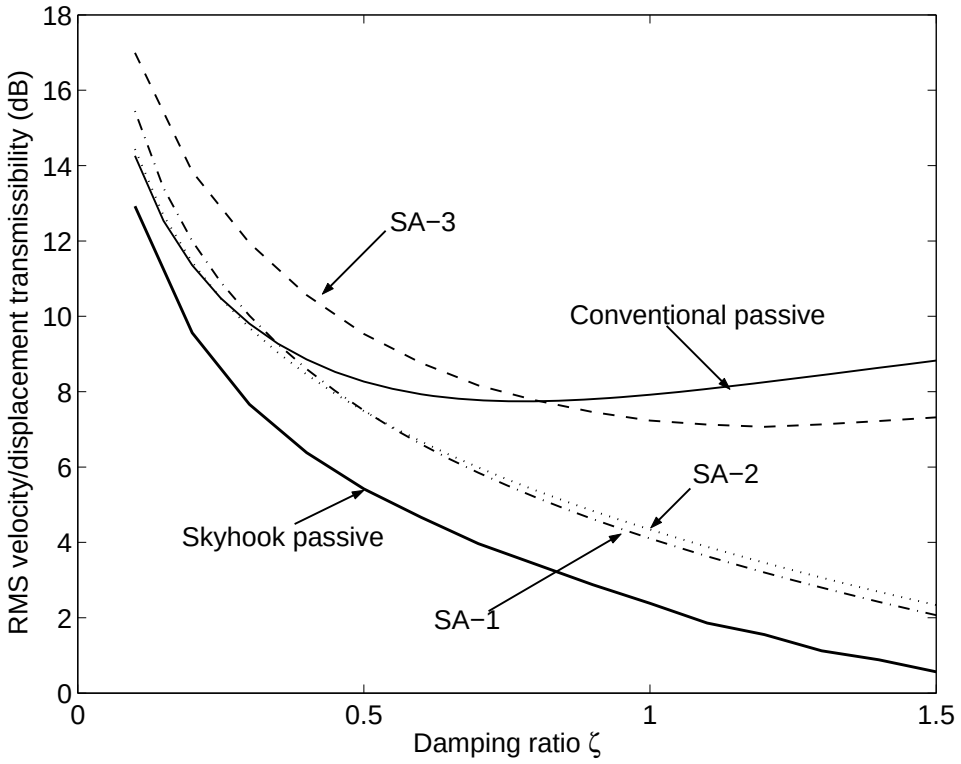

Figure 5.10 RMS velocity transmissibility to random displacement excitation

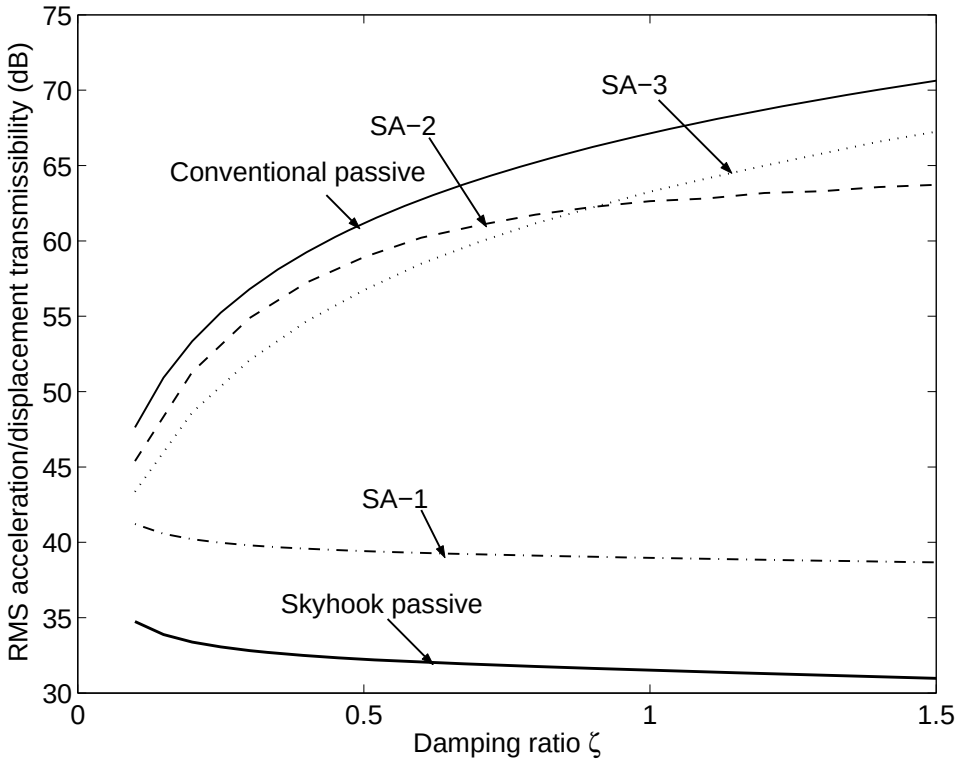

Figure 5.11 RMS acceleration transmissibility to random displacement excitation

5.3.3 EXPERIMENTAL WORK

Experimental work was also carried out to study the vibration isolation performance of the semi-active control algorithm for random disturbances. The experimental set-up used is the same as detailed in Section 3.7. A random acceleration excitation with a flat spectrum within the frequency range 5-100Hz was used for the experiment, and the frequency range 5-60Hz was plotted.

Figure 5.12 shows the time histories of the acceleration response of the system and the random base disturbances. It is obvious that a frequency that is equal to the natural frequency of the system is dominating the acceleration response.

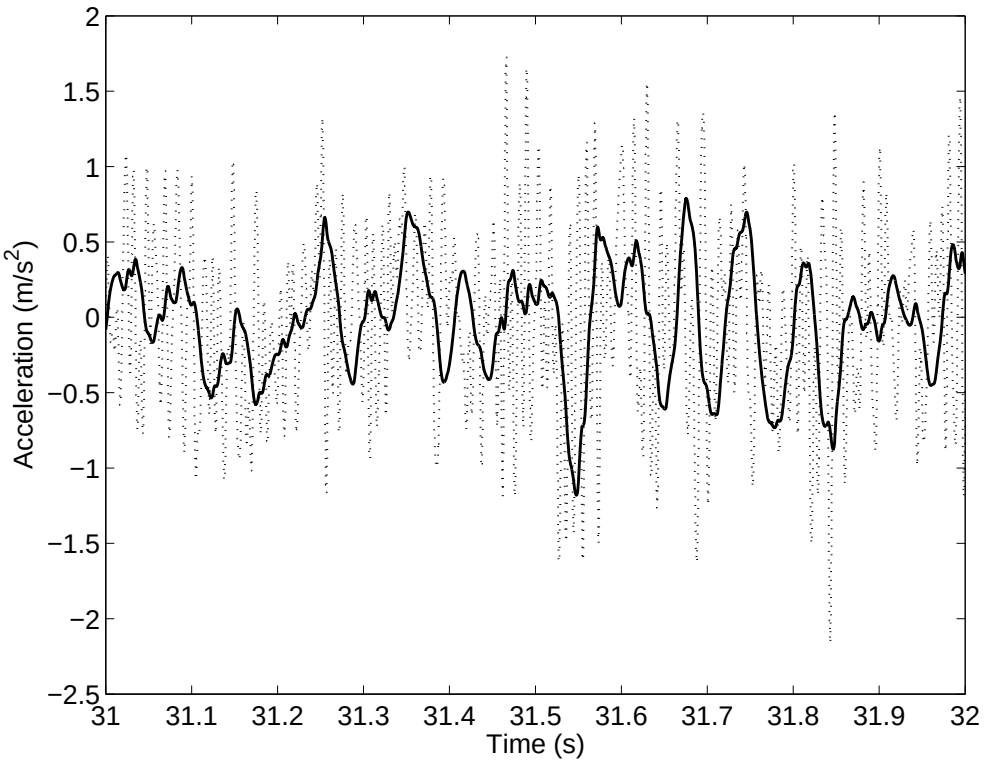

Figure 5.12 Measured time histories of accelerations (− acceleration response of the system; ····· base excitation)

Figure 5.13 shows the measured transmissibility curve of the SDOF system with the on-off skyhook damper in operation. As a comparison, the acceleration transmissibility curve measured under harmonic disturbances is also shown. The figure suggests that the on-off skyhook semi-active control strategy is no worse for random disturbances except in the frequency range close to resonance. However, this

observation is based on the fact that the on-state damping of the system is not big enough, which is limited by the properties of the experimental rig. The difference in the performance of the semi-active damper for random and harmonic disturbances will be much greater if the on-state damping of the system can be made large enough.

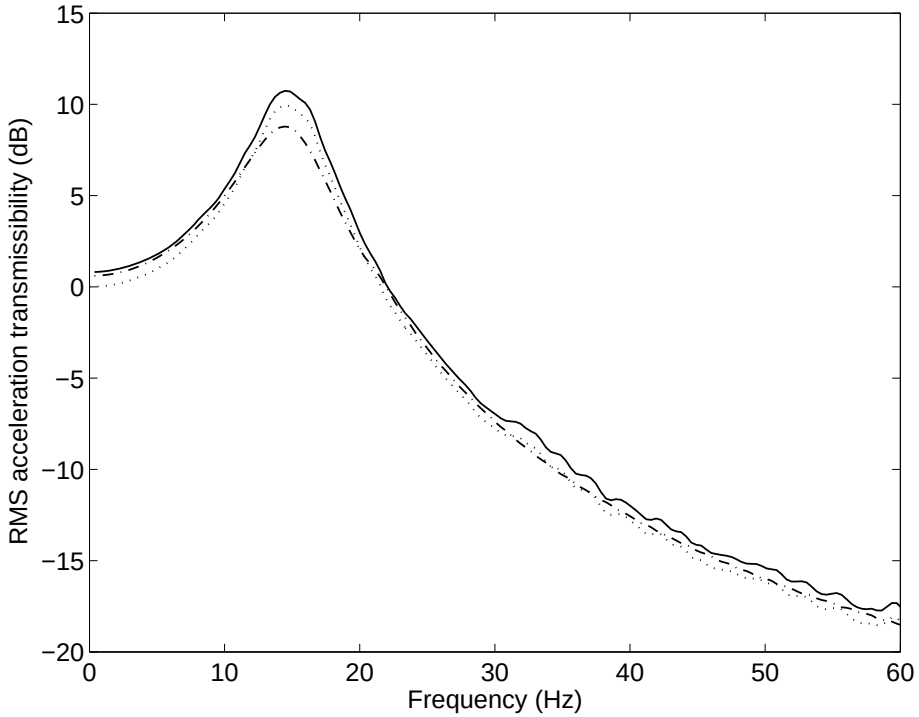

Figure 5.13 Measured acceleration transmissibility to random disturbances (− measured random; ····· simulated random; −·−· measured harmonic)

Figure 5.14 compares the RMS responses of the semi-active damper with those of the passive system with a closed and open circuit. It can be seen from both Figure 5.13 and Figure 5.14 that the performance of the semi-active damper for random disturbance is worse than that for the harmonic disturbances, and it is even worse than the passive case with close circuit. However, there is some advantage if one looks at displacement transmissibility and velocity transmissibility as suggested by Figure 5.7 and Figure 5.9 for larger damping coefficients.

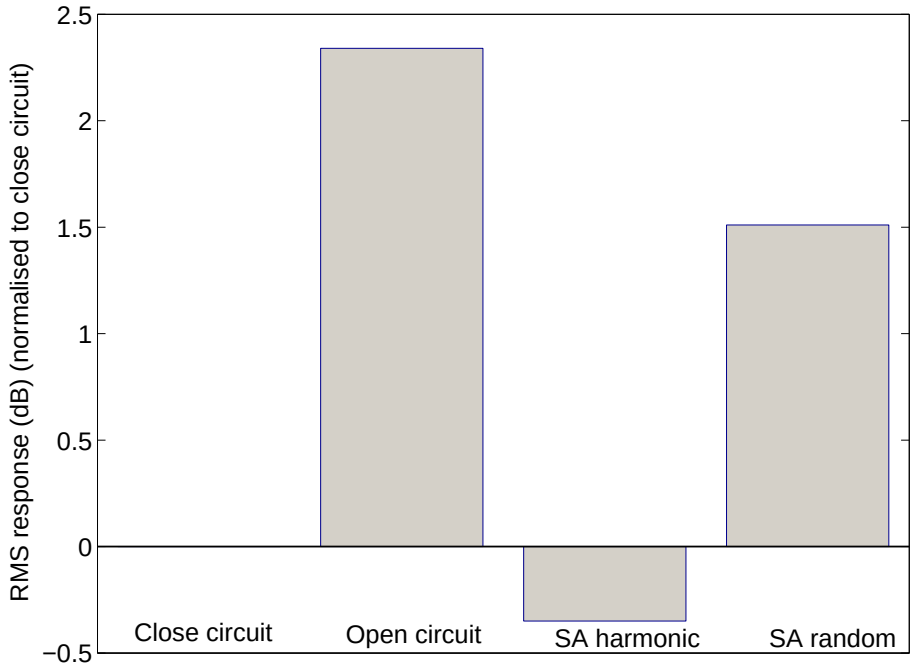

Figure 5.14 Comparison of the RMS responses of the semi-active system

5.4 CONCLUSIONS

This chapter studied the vibration isolation performance of semi-active damping control algorithms for isolation of random disturbances. The performance of three semi-active damping control strategies for isolation of random disturbances has been studied numerically for three special cases when the displacement, velocity and acceleration excitation spectrum are assumed to be flat. An analytical solution to calculate the RMS responses of the conventionally damped SDOF system and the skyhook SDOF system subject to base excitation has been derived. Physical interpretation has been described to explain why semi-active dampers fail to isolate certain types of random excitation using purely passive damping. The simulation results show that the skyhook damper always provides the best performance, and on-off relative control can hardly provide any benefit on isolation of random disturbances. Both on-off and continuously skyhook semi-active control can provide performance improvements over the conventional passive damper for the cases when the inputs are displacement and velocity, i.e. velocity in/velocity out, velocity in/acceleration out, displacement in/displacement out , displacement in/velocity out and displacement in/acceleration out.

CHAPTER 6

6. GENERAL CONCLUSIONS

6.1 CONCLUSIONS

This chapter contains the general conclusions of this thesis. Detailed conclusions are included in each chapter, so only the salient points will be recorded here. Throughout the thesis, the work has covered aspects involving the use of semi-active damping control for vibration isolation of sensitive equipment from various base disturbances.

Following the introduction and literature review in Chapter 1, Chapter 2 detailed the model development of four semi-active control algorithms, which are continuous skyhook control, on-off skyhook control, continuous balance control and on-off balance control. The derivation of these four control algorithms was discussed with clear physical interpretation. A phenomenon often referred to as chatter occurs with semi-active damping control at low excitation frequencies. The conditions for chatter to occur were discussed by studying the dynamics of the system, and a modified control scheme was suggested to avoid the chatter problem. Jerk, which is defined as abrupt changes in the acceleration, was identified as the other problem when using semi-active dampers. Jerk is caused by the abrupt change in the damping force. A shaping function was introduced to smooth the abrupt change in the damping force, and anti-jerk semi-active control strategies were proposed. Both the continuous skyhook control and on-off skyhook control algorithms intend to produce the effect of skyhook damping when the damper is on. The original expression for the continuous skyhook control can provide the same amplitude and phase for damping force in its on-state as those of a skyhook damper. Due to the practical limitation of physical systems, however it can only provide the same amplitude and phase during part of the on-state period. The on-off skyhook control can only ensure that the semi-active damping force is the same sign of the desired skyhook damping force. The magnitude is not representative of the skyhook damper force anymore, although it is shown that it gives similar isolation performance. Both on-off and continuous balance control algorithms require the damping force to oppose the spring force whenever the

damping force and the spring force have the opposite sign. The on-off balance control cannot ensure that the damping force is exactly equal to the spring force since it can only produce a damping force proportional to the relative velocity across the damper in its on-state. Depending on the dynamics of the system and the damping coefficient, the spring force can partly be cancelled or even sometimes the spring force can be over cancelled which may cause the system become unstable. Matlab/Simulink models of the four control algorithms were established. Numerical simulations were carried out in chapters 3-5 using these models.

Chapter 3 investigated the performance of the four semi-active damping control algorithms for isolation of harmonic disturbance through numerical simulations and experimental tests. Numerical simulations were carried out in Matlab/Simulink to study the vibration isolation performance of the semi-active damping control strategies. The isolation performance was evaluated in terms of root-mean-square (RMS) transmissibility of acceleration and relative displacement. The performance of the semi-active damping control algorithms are compared with that of a conventional passive damper and skyhook damper. The results showed that the semi-active damping control strategies can reduce the response at resonance without worsening higher frequency isolation performance. It can be concluded that getting the phase right is the first priority by comparing the isolation performance of the continuous and on-off skyhook control strategies shows that. An experiment was set up to investigate the use of an electromagnetic device as a semi-active damper for vibration isolation. The on-off skyhook control algorithm was chosen to be implemented in the laboratory. A series of tests was conducted to investigate the dynamic characteristics of the electromagnetic damper. The measurement results showed that by opening and closing the circuit of the coil system, the damping of the system can be effectively changed. Thus, it can be used as a semi-active damper for vibration isolation. The measurement results agreed with the theoretical prediction reasonably well. Although the measurement results only showed the semi-active damper gave a marginally better performance than the conventional passive damper, better performance could be achieved if the off-state damping ratio could be made much smaller and on-state damping larger.

Both the theoretical and measurement results in Chapter 3 also showed that percentages of time when the semi-active damper is on are frequency dependent, which means that the switching of the damper may be comprised if more than one frequency is present at the same time. Chapter 4 studied the effects of a secondary frequency which is a harmonic or subharmonic of the fundamental frequency on the switch state of the semi-active damper for the fundamental frequency. It was shown that for a SDOF system with an on-off skyhook semi-active damper, both the velocity switch and the relative velocity switch will be greatly affected due to the addition of the secondary frequency. The secondary frequency which is a harmonic of the fundamental frequency would largely affect the relative velocity switch, and a secondary frequency which is a subharmonic of the fundamental frequency would largely affect the velocity switch. The vibration isolation performance of the semi-active system to periodic excitation was studied numerically and experimentally. For the square and triangular waves studied in chapter 4, the frequency components are integer multiples of the natural frequency of the system, and the first harmonic with the fundamental frequency is dominant in amplitude. The results show that the semi-active damper can provide better isolation performance than the conventional passive damper. Experimental results were limited by achievable damping of the suspension of the loudspeaker.

For random excitations, there are many frequency components present at the same time and since the amplitudes and phases are arbitrary, the semi-active damper might fail to work properly. Chapter 5 discussed the effectiveness of semi-active dampers in isolating random disturbances. An analytical solution is derived for the RMS response of a SDOF system with a conventional passive and a skyhook damper subject to random base excitation with a flat spectrum. The RMS responses of a SDOF system incorporating the semi-active dampers for three special cases when the spectra of displacement, velocity and acceleration are flat are numerically simulated. Physical interpretation has been described to explain why semi-active dampers fail to isolate certain types of random excitation using purely passive dampers. The simulation results show that the skyhook damper always provides the best performance, and on-off relative control can hardly provide any benefit on isolation of random disturbances. Both on-off and continuously skyhook semi-active control can provide

performance improvements over the conventional passive damper for the cases when the inputs are displacement and velocity, i.e. velocity in/velocity out, velocity in/acceleration out, displacement in/displacement out , displacement in/velocity out and displacement in/acceleration out.

Overall, the thesis has demonstrated the benefits and the limitations in using basic semi-active damping control strategies for vibration isolation of various base disturbances. Significant isolation performance could be achieved using semi-active dampers for harmonic and some periodic disturbances. The performance may be not so pronounced for random disturbances with arbitrary spectrum.

6.2 RECOMMENDATIONS FOR FUTURE WORK

This thesis studied the vibration isolation performance of the semi-active control strategies for harmonic, periodic and random disturbances. The work could be extended to study the isolation performance for shock. Shock is normally classified as a transient phenomenon in contrast to vibration that is normally a steady-state phenomenon. Shock differs from vibration as the load can be relatively large but the duration relatively short. For shock disturbances it is normally the maximum acceleration response that can result in damage. The relative displacement may be of concern if the relative motion is expected to exceed the clearance. It would be useful for some practical applications to study the effectiveness of the semi-active control strategies for shock isolation.

Research into implementing the control strategy employed using alternative semi-active devices could prove worthwhile. A device with higher on-state damping and lower off-state damping would work best.

A logical extension of the research into the effectiveness and suitability of the semi-active control strategies in this thesis is an investigation into the performance of the semi-active control strategies in controlling of multimode vibratory systems.

APPENDICES

A1 ISOLATION PROPERTIES OF SEMI-ACTIVE DAMPERS

From the results in chapter 5, it can be seen that semi-active damper is capable of providing better isolation across the whole spectrum as compared to a passive damper. The primary purpose of this appendix is to investigate thoroughly the isolation properties of semi-active systems. Specifically the following question will be answered: Why are semi-active dampers able to isolate at frequencies well below that which is possible with a passive damper, even though, similar to passive dampers, they do not add any energy to the system.

To answer this question, consider a base excited SDOF system. The response of a passive system to a harmonic base-excitation, such as

$$x_0 = X_0 e^{i\omega t} \qquad \text{Equation Section 1}(A.1)$$

is given by

$$x = X_0 \left|H(\omega)\right| e^{i(\omega t+\phi)} \qquad (A1.2)$$

where

$$\left|H(\omega)\right| = \left[\frac{1+\left(2\zeta\frac{\omega}{\omega_n}\right)^2}{\left[1-\left(\frac{\omega}{\omega_n}\right)^2\right]^2+\left(2\zeta\frac{\omega}{\omega_n}\right)^2}\right]^{\frac{1}{2}} \qquad (A1.3)$$

and

$$\phi = -\tan^{-1}\left(\frac{2\zeta\left(\frac{\omega}{\omega_n}\right)^3}{1-\left(\frac{\omega}{\omega_n}\right)^2+\left(2\zeta\frac{\omega}{\omega_n}\right)^2}\right) \qquad (A1.4)$$

The variables $\left|H(\omega)\right|$ and ϕ represent the transmissibility amplitude and phase shift

between the output and input. ζ and ω_n are the damping ratio and natural frequency of the system, respectively.

The behaviour of the system for different damping ratios and input frequencies is shown in Figure A1.1. It can be seen that increasing the damping reduces the resonance response, but it deteriorates the isolation performance in the isolation range where $\omega/\omega_n > \sqrt{2}$. This represents the well-known compromise between better control of resonance and poorer vibration isolation at higher frequencies due to damping. The phase diagram in Figure A1.2 indicates that increasing damping contributes to a lower phase difference between the base and the sprung mass. Further discussions on this subject can be found in most vibration text books, for example [11].

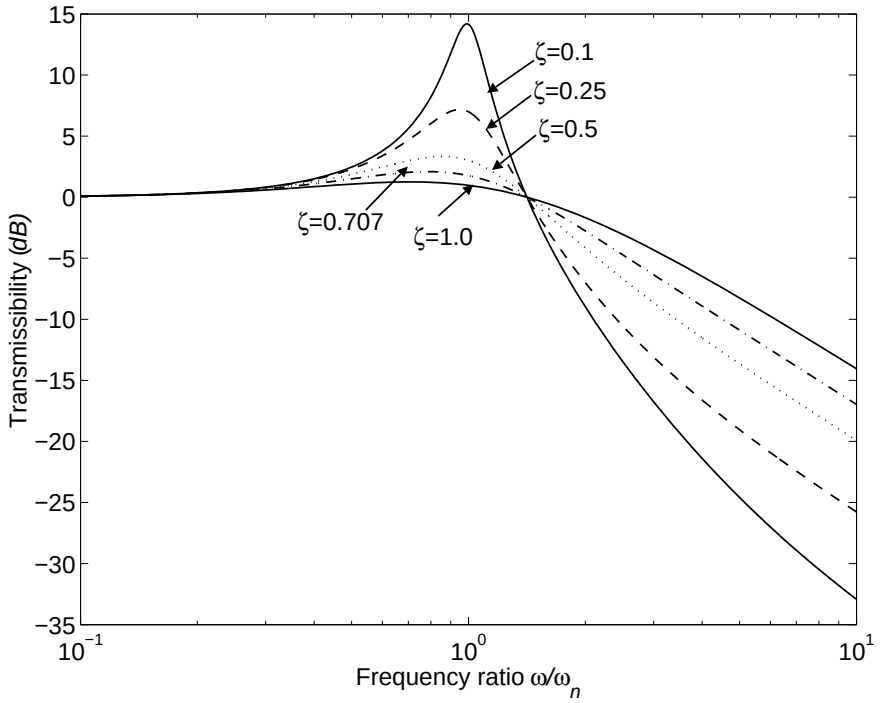

Figure A1.1 Acceleration transmissibility of a passive SDOF system

To determine the reason for the above, and also why semi-active dampers are able to isolate at frequencies far below the fixed frequency of system with passive dampers, the transmissibility equation for the system in Figure A1.6 is derived. Unlike the passive system, it is not possible to derive the transmissibility equation for the semi-active system because the damping coefficient is time dependent. Alternatively, we consider its equivalent where the damper is connected between the mass and an

imaginary sky, as shown in Figure A1.5.

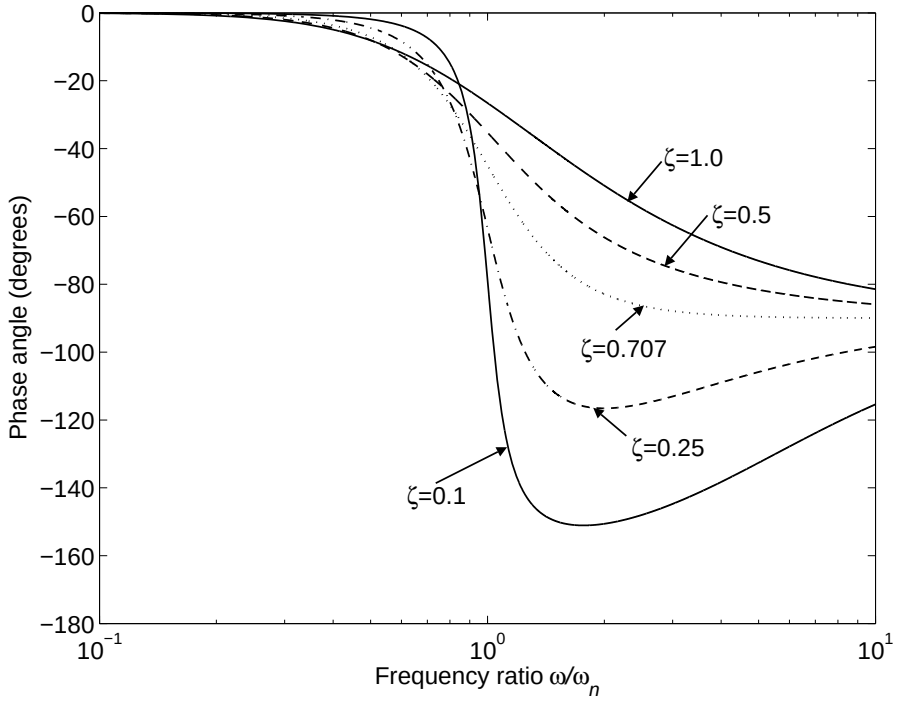

Figure A1.2 Transmissibility phase of a passive SDOF system

For this system, the transmissibility amplitude and phase are:

$$\left|H(\omega)\right| = \frac{1}{\left\{\left[1-\left(\frac{\omega}{\omega_n}\right)^2\right]^2 + \left[2\zeta\left(\frac{\omega}{\omega_n}\right)\right]^2\right\}^{1/2}} \tag{A1.5}$$

$$\phi = -\tan^{-1}\frac{2\zeta\frac{\omega}{\omega_n}}{1-\left(\frac{\omega}{\omega_n}\right)^2} \tag{A1.6}$$

The amplitude and phase of the transmissibility of the skyhook system are shown in Figure A1.3 and Figure A1.4. Comparing equations of (A1.5)and (A1.6) provides the insight as follows. The transmissibility amplitudes have the same denominators but different numerators. For a passive system, the numerator is a function of damping ratio, ζ, where as for a skyhook system, it is a constant. Table A1.1 shows the effect of ζ on transmissibility in different frequency ranges for a conventional passive system. The table is derived from evaluating the numerator and denominator of

equation (A1.3), which shows that the frequency range in which amplification, direct transmission and attenuation occurs is independent of the damping ratio ζ.

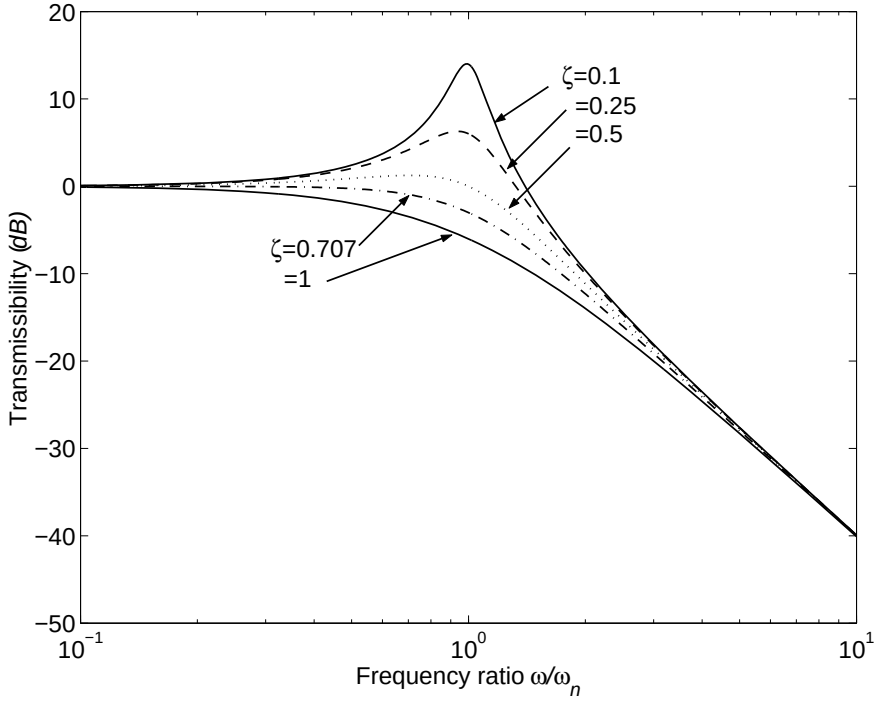

Figure A1.3 Acceleration transmissibility of a skyhook damper system

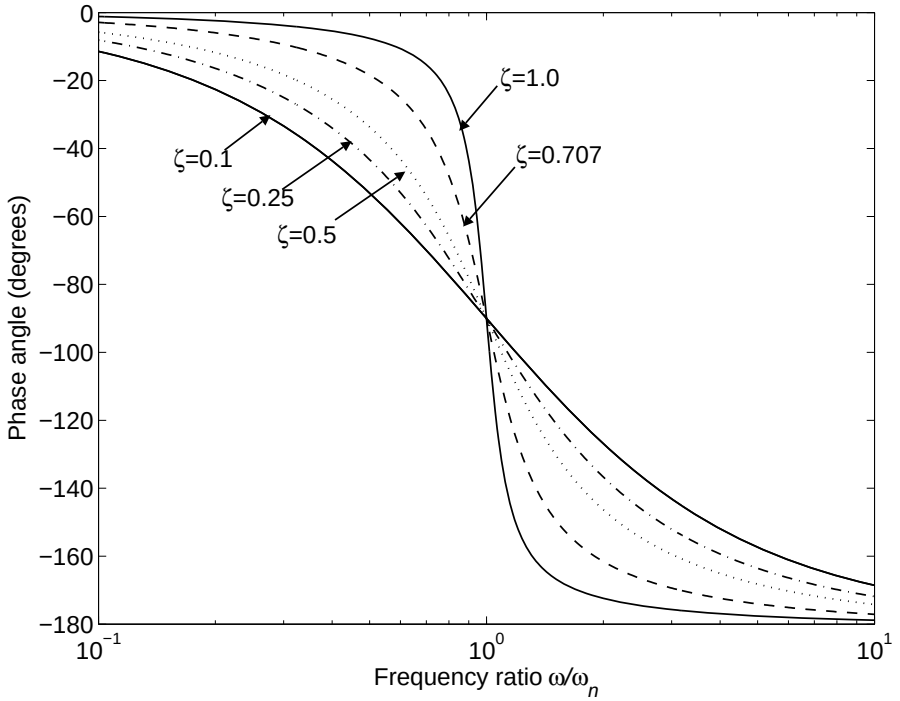

Figure A1.4 Transmissibility phase of a skyhook system

Examining equation (A1.5)-(A1.6) shows that a skyhook damper yields completely

different results. The numerator is a constant, and therefore the transmissibility is relative to unity depends whether the denominator is less than, greater, or equal to 1. Evaluating the denominator for one of the three possibilities will allow us to make conclusions on the effect of ζ on the transmissibility magnitude. Consider the frequency range where some isolation is achieved. For this to happen, the frequency ratio must be such that:

$$\left[1-\left(\frac{\omega}{\omega_n}\right)^2\right]^2+\left[2\zeta\left(\frac{\omega}{\omega_n}\right)\right]^2 \geq 1 \tag{A1.7}$$

which will reduce to

$$\left(\frac{\omega}{\omega_n}\right)^2 \geq 2-4\zeta^2 \tag{A1.8}$$

Table A1.1 Effect of ζ on transmissibility for a passive conventionally damped SDOF system

$\frac{\omega}{\omega_n}$	$\left[1-\left(\frac{\omega}{\omega_n}\right)^2\right]^2$	$\lvert H(\omega)\rvert$	
<1	<1	>1	Amplification
=1	=0	>1	Amplification
$1<\bullet<\sqrt{2}$	<1	>1	Amplification
$=\sqrt{2}$	=1	=1	Direct transmission
$>\sqrt{2}$	>1	<1	Isolation

The above equation shows that for a passive skyhook damper, as ζ increases, attenuation occurs at lower frequencies, unlike a passive system in which the isolation is independent of ζ. Two special cases exist in the equation, the first of which is when $\zeta=0$, the equation reduces to $\omega/\omega_n \geq \sqrt{2}$. This indicates that when no damping is present, isolation stars at $\omega=\sqrt{2}\omega_n$, the fixed frequency of the passive system. For $\zeta>0$, isolation starts at frequencies smaller than $\sqrt{2}\omega_n$, thus we can conclude that for a given ζ, a skyhook system behaving as a skyhook system can always provide better isolation performance than passive ones.

The second case is when

$$2 - 4\zeta^2 = 0 \tag{A1.9}$$

or

$$\zeta = \frac{\sqrt{2}}{2} = 0.707 \tag{A1.10}$$

This is the minimum damping ratio at which the skyhook system provides isolation at all frequencies. Therefore, it is possible to tune a skyhook system such that it can provide isolation across the whole frequency.

The passive representation of the semi-active system assumes that the off-state damping is zero. In practice, however, it is not possible and may not desirable. In most cases, c_{off} is a small portion of the on-state damping. Therefore, in reality, the passive representation of the semi-active system dampers appears as shown in Figure A1.5.

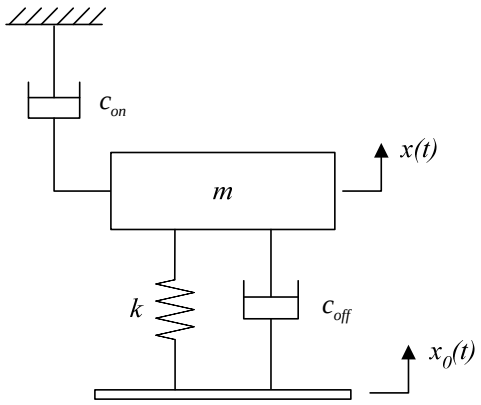

Figure A1.5 Actual representation of a skyhook system

This modifies the transmissibility equation to:

$$\left|H(\omega)\right| = \left[\frac{1+\left[2\zeta_{off}\,\frac{\omega}{\omega_n}\right]^2}{\left[1-\left(\frac{\omega}{\omega_n}\right)^2\right]^2+\left[2(\zeta_{on}+\zeta_{off})\left(\frac{\omega}{\omega_n}\right)\right]^2}\right]^{1/2} \tag{A1.11}$$

$$\phi = -\tan^{-1}\left[\frac{2\left[(\zeta_{on}+\zeta_{off})\frac{\omega}{\omega_n}-\zeta_{off}\frac{\omega}{\omega_n}+\zeta_{off}\left(\frac{\omega}{\omega_n}\right)^3\right]}{1-\left(\frac{\omega}{\omega_n}\right)^2+4(\zeta_{on}+\zeta_{off})\zeta_{off}\left(\frac{\omega}{\omega_n}\right)^2}\right] \tag{A1.12}$$

where

$$\zeta_{on}=\frac{c_{on}}{2m\omega_n};\zeta_{off}=\frac{c_{off}}{2m\omega_n} \tag{A1.13}$$

Figures A1.6 and A1.7 show the transmissibility and phase angle of the skyhook system with non-zero off-state damping. Comparing Figure A1.6 with Figure A1.3 shows that the insertion of off-state damping has two effects compared to the system without off-state damping: (1) it reduces the RMS acceleration ratio at and around the natural frequency; (2) it increases the RMS acceleration ratio at frequencies greater than natural frequency.

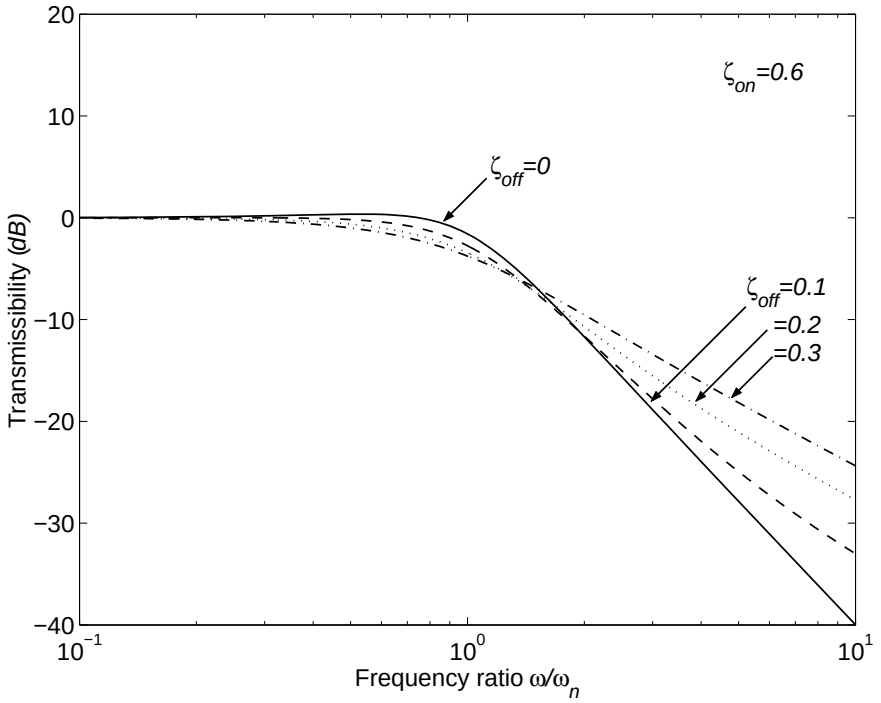

Figure A1.6 Transmissibility magnitude of an actual skyhook damper system

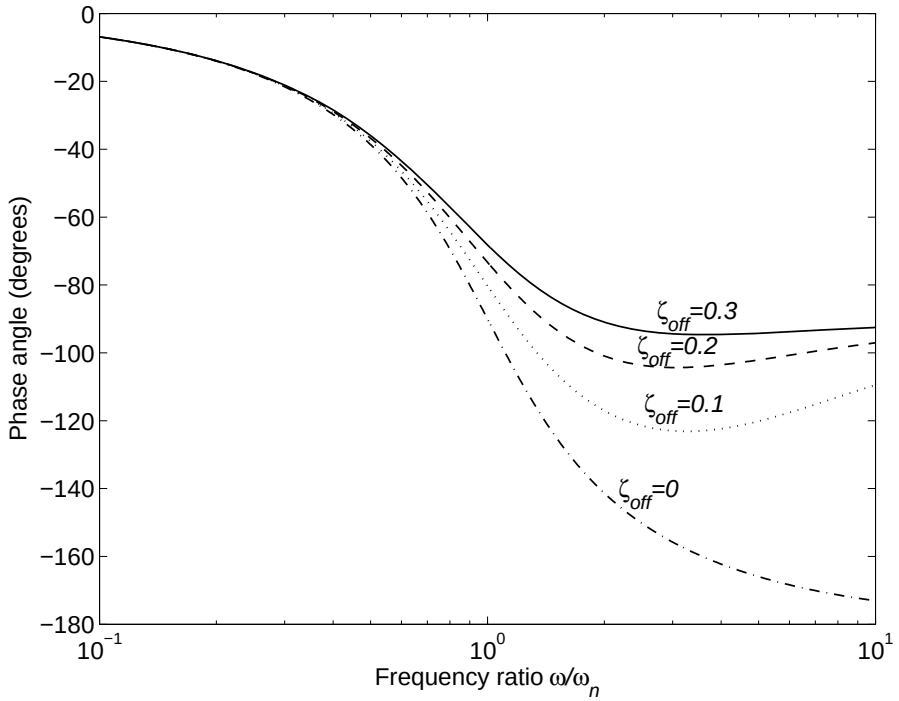

Figure A1.7 Transmissibility phase of an actual skyhook damper system

A2 ANALYSIS OF ELECTROMAGNETIC DAMPING

Figure A2.1 shows a SDOF base isolation system model using an electromechanical damper. In the model, the magnet is arranged to move together with the base and the coil is attached to and moves together with the mass to be controlled. When the coil is moving in the magnetic field, a voltage called the back electromotive force (emf) is induced in the coil, which is governed by Lenz's Law. If the strength of the magnetic field is B, the coil moves with a velocity of $\dot{x}$ and the base velocity is $\dot{x}_0$, then the induced voltage in the coil can be expressed as

$$E_{bemf} = BL(\dot{x} - \dot{x}_0) \qquad \text{Equation Section 12}(A2.1)$$

where $L = ln$ is the effective length of the wire; l is the length of the coil per turn and n is the number of effective coil turns.

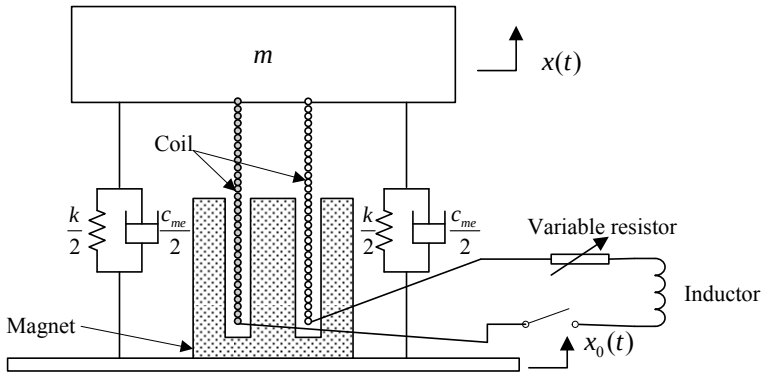

Figure A2.1 Model of a base isolation system using an electromechanical damper

If the circuit is closed, there will be a current flowing in the coil, and there will be an electromechanical force F_{em} on the coil. This force is developed by the interaction between the magnetic field of strength B that exists across the gap and the magnetic field due to current flowing in the coil. The resulting force is

$$F_{em} = BLI \qquad (A2.2)$$

Assuming the resistance of the coil is R_c and is connected to an external resistance R_{ext}, then the current related to the induced *back emf* is given by

$$I = \frac{E_{bemf}}{R_c + R_{ext}} \tag{A2.3}$$

The electromechanical force F_{em} therefore can be written as

$$F_{em} = \frac{(BL)^2}{R_c + R_{ext}}\left(\dot{x} - \dot{x}_0\right) \tag{A2.4}$$

For the SDOF system with an electromechanical damper subject to base excitation, the equation of the motion can be written as

$$m\ddot{x} + c_{me}(\dot{x} - \dot{x}_0) + k\left(x - x_0\right) + F_{em} = 0 \tag{A2.5}$$

where k is a spring constant and c_{me} is the mechanical damping coefficient of the system. Substituting equation (A2.4) into (A2.5), gives

$$m\ddot{x} + (c_{me} + c_{em})(\dot{x} - \dot{x}_0) + k\left(x - x_0\right) = 0 \tag{A2.6}$$

where $c_{em} = \frac{(BL)^2}{R_c + R_{ext}}$ is the electromechanical damping due to the electromechanical damper. It can be seen from equation (A2.6) that the damping of the system consists of two parts, one is the mechanical damping c_{me}, and the other is the electromechanical damping c_{em}. The mechanical damping is fixed for a given system, while the electromechanical damping can be changed by varying the external resistance or simply opening or closing the circuit. The maximum damping coefficient of the system occurs when $R_{ext} = 0$, which is given by

$$c_{\max} = c_{me} + \frac{(BL)^2}{R_c} \tag{A2.7}$$

The damping ratios corresponding to the mechanical damping and electromechanical damping are given by

$$\begin{aligned} \zeta_{me} &= \frac{c_{me}}{2m\omega_n} \\ \zeta_{em} &= \frac{c_{em}}{2m\omega_n} = \frac{(BL)^2}{R_c + R_{ext}}\frac{1}{2m\omega_n} \end{aligned} \tag{A2.8}$$

A3 LIST OF EQUIPMENT USED FOR EXPERIMENTS

Equipment	Serial Number	Quantity
HP 35655A Analyser	2911A01088	1
Derritron Vibrator Type VP.4	325	1
TPA series Professional Power Amplifier	8252	1
Colossus 12 MB Loudspeaker Driver	14314	1
B&K 4393 Accelerometer	1697354 1697154	2
B&K 2635 Charge Amplifier	943130 1474190	2
Wavetek DM25XT Digital Meter	60405182	1
HM 303-6 Analog Oscilloscope	25620	1
Kemo Type VBF8 Dual Variable Filter 0.01Hz-100kHz	56198	1
PCB accelerometers	307A 10302	2
PCB Conditioner	13287	1
Hmeg Signal generator	24953 04110	2
Stabilised power supply LT3-1 2×0-30V 1A	0619	1

A4 THE CONTROLLER CIRCUIT

The on-off skyhook control strategy was chosen to be implemented due to its simplicity and effectiveness. The block diagram of control strategy is shown in Figure A4.1. The measured acceleration signals $\ddot{x}$ and $\ddot{x}_0$ are passed through the integrator blocks 1 and 2 respectively to get the corresponding velocity signal, $\dot{x}$ and $\dot{x}_0$. The relative velocity, $\dot{x} - \dot{x}_0$, is obtained using the sum block 3. The velocity response $\dot{x}$ is multiplied by the relative velocity signal $\dot{x} - \dot{x}_0$ in a multiplier block 4 to form the condition function $\dot{x}(\dot{x} - \dot{x}_0)$ as defined in chapter 2. The velocity product signal is input to a logic test block 5, and the output of the logic test block is used to control the switch. The output of logic block is either unity (or "true") or zero (or "false").

The electrical circuit diagram of the control strategy is shown in Figure A4.2, and a picture of the actual circuit board is shown in Figure A4.3.

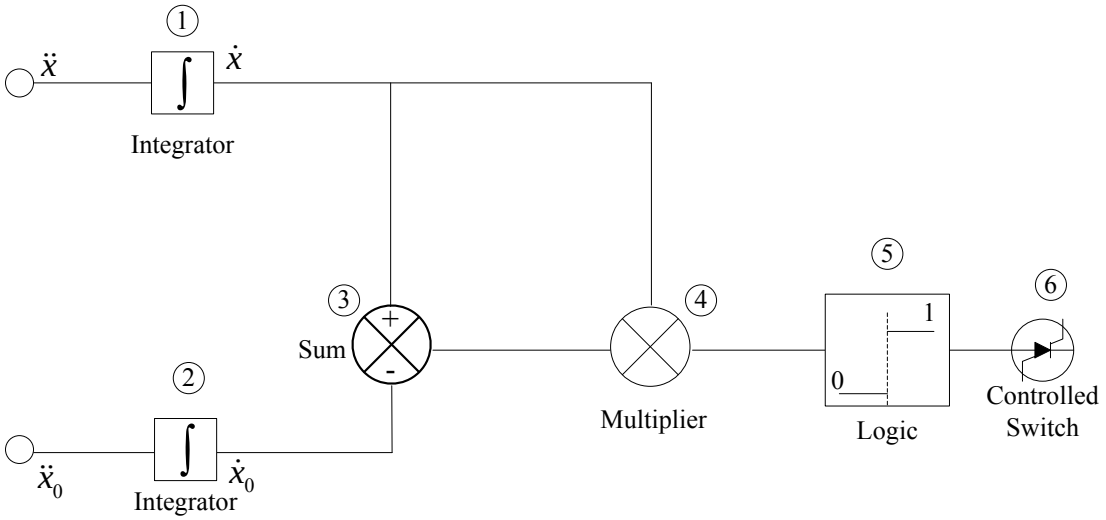

Figure A4.1 Block diagram of on-off skyhook control strategy

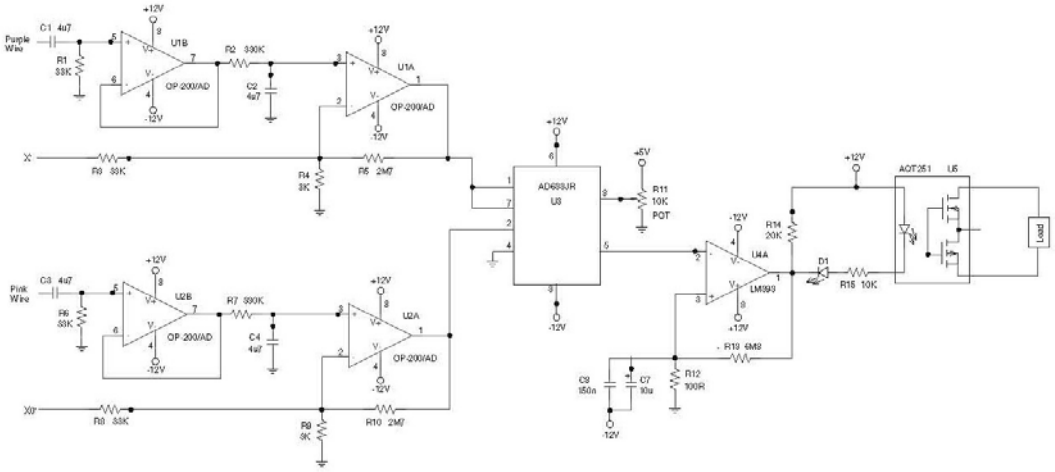

Figure A4.2 Circuit diagram of on-off skyhook control strategy

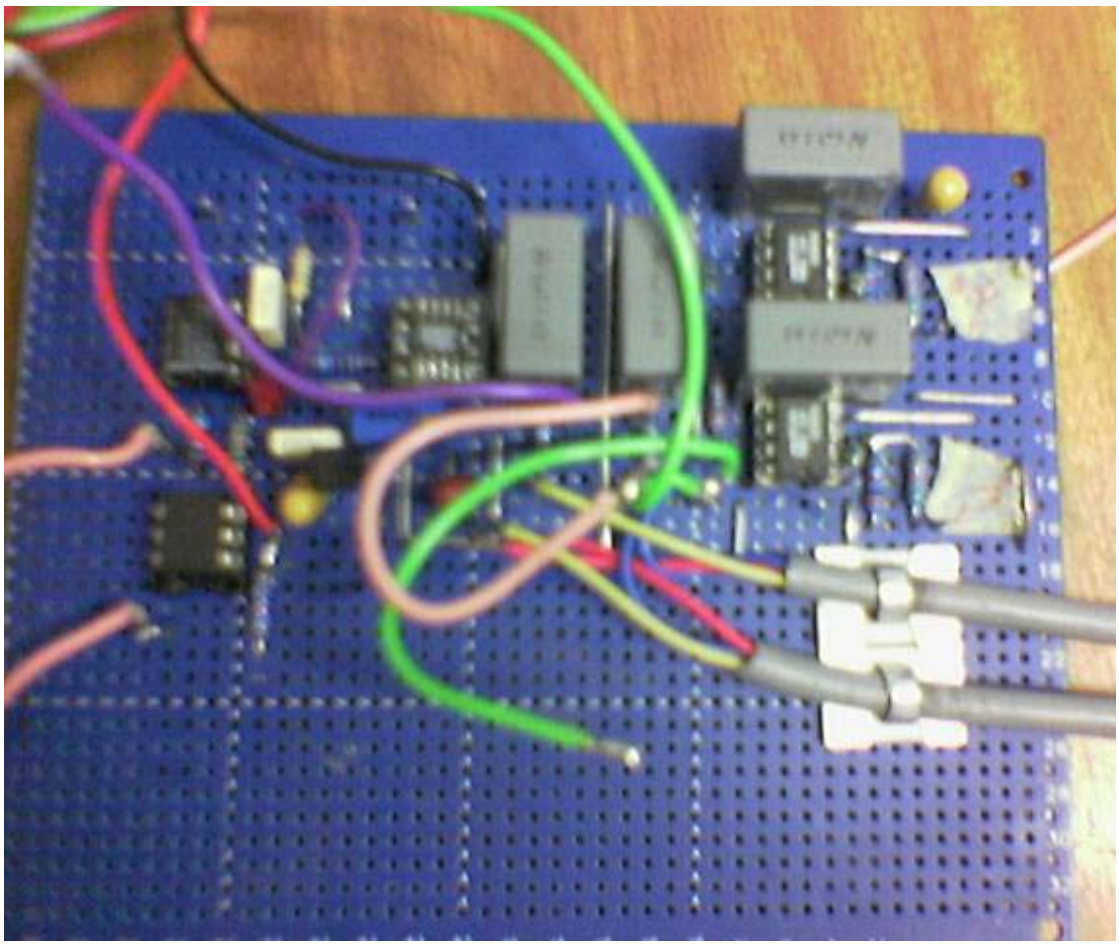

Figure A4.3 Picture of the actual circuit board

GLOSSARY OF TERMS

a_0, a_n, b_n	=	Fourier series constant
c	=	damping coefficient
$c_{\max}$	=	maximum damping coefficient
$c_{\min}$	=	minimum damping coefficient
c_{on}	=	on-state damping coefficient
c_{off}	=	off-state damping coefficient
c_{pass}	=	passive damping coefficient
c_{sky}	=	skyhook damping coefficient
c_{sa}	=	semi-active damping coefficient
$\frac{d}{dt}, \frac{d^2}{dt^2}$	=	first and second derivatives
F_c	=	active control force
F_d	=	damping force
F_k	=	stiffness force
F_{sa}	=	semi-active damping force
F_{sky}	=	skyhook damping force
k	=	stiffness coefficient
H, H_1, H_2	=	transfer function
Im, Re	=	imaginary and real part of complex variable
$\mathbf{K}_1, \mathbf{K}_2, \mathbf{K}_3, \mathbf{K}_4$	=	functions for the fourth Runge-Kutta method
G	=	gain factor
m	=	mass
t_0	=	start time
$S_x(\omega), S_{x_0}(\omega)$	=	power spectral density
Δt	=	time difference
t_s	=	Switching time
τ , T	=	period of vibration
$T_{\ddot{x}}$	=	acceleration transmissibility
T_{x-x_0}	=	relative displacement transmissibility

$\omega, \omega_1, \omega_2$	=	frequency of excitation
ω_n	=	natural frequency
x, x_1, x_2	=	displacement response
$\dot{x}, \dot{x}_1, \dot{x}_2$	=	velocity response
$\ddot{x}, \ddot{x}_1, \ddot{x}_2$	=	acceleration response
x_0, x_{01}, x_{02}	=	base displacement
$\dot{x}_0, \dot{x}_{01}, \dot{x}_{02}$	=	base velocity
$\ddot{x}_0, \ddot{x}_{01}, \ddot{x}_{02}$	=	base acceleration
$x(t), y(t), y_1(t), y_2(t)$	=	time series
$\overline{x^2(t)}$, $\overline{x_T{}^2(t)}$	=	mean square value of $x(t)$ and $x_T(t)$
$x_T(t)$	=	periodic time series
$X(i\omega)$		Fourier transform of $x(t)$
$\ddot{X}_0$	=	amplitude of acceleration of the excitation
ζ	=	damping ratio
$\zeta_{\max}$	=	maximum Damping ratio
$\zeta_{\min}$	=	minimum Damping ratio

REFERENCES

1. Harris, C.M., *Shock and vibration handbook*. 1987: McGRAW-HILL.

2. Karnopp, D.C., *Active and passive isolation of random vibration*, in *Isolation of Mechanical Vibration, Impact, and Noise*, J.C. Snowdon and U.E. E., Editors. 1973, Bolt Beranek and Newman Inc: Cincinnati, Ohio. p. 64-86.

3. Nelson, F.C., *Vibration isolation: a review, I. sinusoidal and random excitations.* Shock and Vibration, 1994. **1**(5): p. 485-493.

4. Snyder, S. and C.H. Hansen, *Active control of noise and vibration*. 1997: Spon Press.

5. Bies, D.A. and C.H. Hansen, *Engineering noise control 2nd Edition*. 1996, UK: E & FN Spon.

6. Beranek, L.L. and I.L. Ver, *Noise and vibration control engineering: principles and applications*. 1992: John Wiley and Sons.

7. Snowdon, J.C., *Vibration and shock in damped mechanical Systems*. 1968: John Wiley & Sons.

8. Mead, D.J., *Passive vibration control*. 1999, London: John Wiley & Sons Ltd.

9. Fuller, C.R., S.J. Elliott, and P.A. Nelson, *Active control of vibration*. 1996, London: Academic Press.

10. Soong, T.T., *Active structural control: theory and practice*. 1990, New York: John Wiley & Sons.

11. Rao, S.S., *Mechanical vibrations*. Third Edition ed. 1995: Addison-Wesley Publishing Company.

12. White, R.G. and J.G. Walker, *Noise and vibration*. 1982, West Sussex, England: Ellis Horwood Limited.

13. Franchek, M.A., M.W. Ryan, and R.J. Bernhard, *Adaptive passive vibration control.* Journal of Sound and Vibration, 1995. **189**(5): p. 565-585.

14. Bernhard, R.J., H.R. Hall, and J.D. Jones. *Adaptive-passive noise control*. in *Inter-Noise*. 1992. Toronto, Ontario, Canada.

15. Karnopp, D.C., M.J. Crosby, and R.A. Harwood, *Vibration control using semi-active force generators.* ASME Journal of Engineering for Industry, 1974. **96**(2): p. 619-626.

16. Krasnicki, E.J., *Comparison of analytical and experimental results for a semi-active vibration isolator.* Shock and Vibration Bulletin, 1980. **50**: p. 69-76.

17. Crosby, M.J. and D.C. Karnopp, *The active damper: a new concept for shock and vibration control.* Shock and Vibration Bulletin, 1973. **43**: p. 119-133.

18. Elliott, S.J., M. Serrand, and P. Gardonio, *Feedback stability limits for active isolation systems with reactive and inertial actuators.* ASME Journal of Vibration and Acoustics, 2001. **123**: p. 250-162.

19. Krasnicki, E.J. *The experimental performance of an "on-off" active damper*. in *Proceedings of the 51st Shock and Vibration Symposium*. 1980. San Diego, USA.

20. Ahmadian, M., R. Brian, and X. Song. *Harmonic analysis of semi-active suspensions*. In *16th Biennial Conference on Mechanical Vibration, ASME Design Technical Conference*. 1997. Sacramento, CA.

21. Yi, K. and B.S. Song, *A new adaptive skyhook control of vehicle semi-active suspensions.* Proceedings of the Institution of Mechanical Engineers Part D-Journal of Automobile Engineering, 1999. **213**: p. 293-303.

22. Sciulli, D., *dynamics and control for vibration isolation design*, in *Department of Engineering Mechanics*. 1997, Virginia Polytechnic Institute and State University: Blacksburg, Virginia.

23. Symans, M.D. and M.C. Constantinou, *Experimental testing and analytical modeling of semi-active fluid dampers for seismic protection.* Journal of Intelligent Systems and Structures, 1997. **8**(8): p. 644-657.

24. Karnopp, D.C., *Active and semi-active vibration isolation.* ASME Journal of Vibration and Acoustics, Special 50th Anniversary Design Issue, 1995. **117**: p. 177-185.

25. Rakheja, S. and S. Sankar, *Vibration and shock isolation performance of a semi-active "on-off" damper.* ASME Journal of Vibration, Acoustics, Stress, and Reliability in Design, 1985. **107**: p. 398-403.

26. Sireteanu, T., D. Stancioiu, and C.W. Stammers. *Use of magnetorheological fluid dampers in semi-active driver seat vibration control*. in *ACTIVE 2002*. 2002. ISVR, Southampton, UK.

27. Alanoly, J. and S. Sankar, *A new concept in semi-active vibration isolation.* ASME Journal of Mechanisms, Transmissions, and Automation in Design, 1987. **109**: p. 242-247.

28. Wu, X. and M.J. Griffin, *A semi-active control policy to reduce the occurrence and severity of end-stop impacts in a suspension seat with an electrorheological fluid damper.* Journal of Sound and Vibration, 1997. **203**(5): p. 781-793.

29. Rakheja, S. and S. Sankar, *Effectiveness of "on-off" damper in isolation dynamical systems.* Shock and Vibration Bulletin, 1986. **57**: p. 147-156.

30. Wu, X., et al., *Simulation and experimental study of a semi-active suspension with an electrorheological damper.* International Journal of Modern Physics, 1994. **B8**: p. 2987-3003.

31. Zhang, Y.F. and W.D. Iwan, *Active interaction control of civil structures. Part 1: SDOF systems.* Earthquake Engineering & Structural Dynamics, 2002. **31**(1): p. 161-178.

32. Yang, J.N. and A.K. Agrawal, *Semi-active hybrid control systems for nonlinear buildings against near-field earthquakes.* Engineering Structures, 2002. **24**(3): p. 271-280.

33. Yoshida, K. and T. Fujio, *Semi-active base isolation for a building structure.* International Journal of Computer Applications in Technology, 2000. **13**(1-2): p. 52-58.

34. Sadek, F. and B. Mohraz, *Semi-Active control algorithms for structures with variable dampers.* ASCE Journal of Engineering Mechanics, 1998. **124**(9): p. 981-990.

35. Sadek, F. and B. Mohraz. *Variable dampers for semi-active control of flexible structures*. in *6th U. S. National Conference in Earthquake Engineering*. 1998. Oakland.

36. Han, S.S. and S.B. Choi, *Control performance of an electrorheological suspension system considering actuator time constant.* International Journal of Vehicle Design, 2002. **29**(3): p. 226-242.

37. Fernando, D.G., *Dynamic analysis of semi-active control techniques for vehicle applications*, in *Mechanical Engineering*. 2001, Virginia Polytechnic Institute and State University: Blachsburg, Virginia.

38. Hrovat, D., P. Barak, and M. Rabins, *Semi-active versus passive or active tuned mass dampers for structural control.* Journal of Engineering Mechanics, 1983. **109**(3): p. 692-705.

39. Holdmann, P. and H. M., *Possibilities to improve the ride and handling performance of delivery trucks by modern mechatronic systems.* JSAE Review, 1999. **20**(4): p. 505-510.

40. Ahmadian, M. *Ride evaluation of a class 8 truck with semiactive suspensions*. in Advanced Automotive Technologies American Society of Mechanical Engineers, 1993. New York USA.

41. Lieh, J., *Effect of bandwidth of semiactive dampers on vehicle ride.* Journal of Dynamic Systems Measurement and Control, 1993. **115**(3): p. 571-575.

42. Giua, A. and A. Sanganta. *Approximation of an Optimal Gain Switching Active Law with a Semiactive Suspension*. in *IEEE Conference on Control Applications*. 1998. Piscataway, Nj, USA.

43. Saxon, N.L., W. Meldrum, and T. Bonte. *Semiactive suspension: a field testing case study*. in *Developments in Tire, Wheel, Steering, and Suspension Technology SAE Special Publications*. 1998. Warrendale, PA, USA.

44. Lieh, J., *Semiactive and active suspensions for vehicle ride control using velocity feedback.* Journal of Vibration and Control, 1997. **3**(2): p. 201-212.

45. Carter, A.K., *Transient motion control of passive and semi-active damping for vehicle suspensions*. 1998, the Virginia Polytechnic Institute and State University: Blacksburg, Virginia.

46. Fang, X. and W. Chen, *Fuzzy control technology and the application to vehicle semi-active suspension.* Chinese Journal of Mechanical Engineering, 1999. **35**(3): p. 98-100.

47. Ursu, I., et al., *Artificial intelligence based synthesis of semi-active suspension systems.* The Shock and Vibration Digest, 2000. **32**(1): p. 3-10.

48. Donald, L.M. and G. Mehrnaz, *The chatter of semi-active on-off suspensions and its cure.* Vehicle System Dynamics, 1984. **13**: p. 129-144.

49. Pan, G., et al. *Adaptive vibration control policy of semi-active "on-off" damper*. in *Proceedings of Pioneering International Symposium on Motion and Vibration Control in Mechatronics*. 1999. Tokyo.

50. Pan, G., H. Matsuhisa, and Y. Honda, *Smoothing of on-off damper force with the variable damping coefficient.* Transaction of Japanese Society of Mechanical Engenderers (C), 2000. **66**(644): p. 1158-1164.

51. Ahmadian, M., R. Brian, and X. Song, *No-jerk semi-active skyhook control method and apparatus*, in *United States patent*. 2000: USA.

52. Miller, L.R. and C.M. Nobles, *Methods for Eliminating jerk and noise in semi-active suspensions.* Journal of Commercial Vehicles, 1990. **Section 2**(99).

53. Ursu, I., U. Felicia, and T. Sireteanu. *On anti-chattering synthesis for active and semi-active suspension systems*. in *3rd IFAC International Workshop on Motion Control*. 1998. Grenoble, France.

54. Miller, L.R. *Tuning Passive, semi-active, and fully active suspension systems*. in *Proceeding of the 27th Conference on Decision and Control*. 1988. Austin, Texas, US.

55. Oueslati, F. and S. Sankar, *A class of semi-active suspension schemes for vehicle vibration control.* Journal of Sound and Vibration, 1994. **172**(3): p. 391-411.

56. Mehdi, A. and X. Song. *Effects of system delays on semi-active suspension performance*. in *Proceedings of the Sixth International Conference on Recent Advances in Structural Dynamics*. 1997. ISVR, University of Southampton, UK.

57. Jeon, D., C. Park, and K. Park. *Vibration Suppression by controlling an MR damper*. in *6th International Conference on Electrotheological and Magnetortheological Suspensions and Their Applications*. 1997. Yonezawa, Japan.

58. Patten, W.N., J. Mo., Kuehn, and J. Lee, *A primer on design of semi-active vibration absorbers.* Journal of Engineering Mechanics, 1998. **124**(1): p. 61-68.

59. Karnopp, D.C., *Design principles for vibration control systems using semi-active dampers.* ASME Journal of Dynamic Systems, Measurement, and Control, 1990. **112**: p. 448-455.

60. Neil, D.S., R. Stanway, and A.R. Johnson, *Vibration control using smart fluids: a state-of-the-art review.* The Shock and Vibration Digest, 1999. **31**(3): p. 195-203.

61. Symans, M.D. and M.C. Constantinou, *Semi-active control systems for seismic protection of structures: a state-of-the-art review.* Engineering Structures, 1999. **21**(6): p. 469-487.

62. Roger, S., J.L. Sproston, and A.K. El-Wahed, *Applications of electrorheological fluids in vibration control: a survey.* Smart Materials and Structures, 1996(5): p. 464-482.

63. Feng, M.Q., *Application of hybrid sliding isolation system to buildings.* Journal of Engineering Mechanics, 1993. **119**: p. 2090-2108.

64. Karnopp, D., *Permanent-magnet linear motors used as variable mechanical dampers for vehicle suspensions.* Vehicle System Dynamics, 1989. **18**(4): p. 187-200.

65. Kanamori, M. and Y. Ishihara, *Finite-element analysis of an electromagnetic damper taking into account the reaction of the magnetic-field.* JSME International Journal Series Iii-Vibration Control Engineering for Industry, 1989. **32**(1): p. 36-43.

66. Liu, Y., T.P. Waters, and M.J. Brennan, *A comparison of semi-active damping control strategies for vibration isolation of harmonic disturbances.* Journal of Sound and Vibration, 2005. **280**(1): p. 21-39.

67. Choi, S.-B. and W.-K. Kim, *Vibration control of a semi-active suspension featuring electrorheological fluid dampers.* Journal of Sound and Vibration, 2001. **234**(3): p. 537-546.

68. Donald, L.M., *Semi-Active heave and pitch control for ground vehicles.* Vehicle System Dynamics, 1982. **11**: p. 31-42.

69. Newland, D.E., *An introduction to random vibrations, spectral and wavelet analysis*. 1994, Essex, England: Longman Scientific & Technical.

70. Crandall, S.H. and W.D. Mark, *Random vibration in mechanical systems*. 1963: Academic Press.